354/4/11n/79

H. 2431

NL-78-94

ANL-78-94

MASTER

HIGH-PERFORMANCE BATTERIES FOR ELECTRIC-VEHICLE PROPULSION AND STATIONARY ENERGY STORAGE

Progress Report for the Period October 1977—September 1978

ARGONNE NATIONAL LABORATORY, ARGONNE, ILLINOIS

Prepared for the U. S. DEPARTMENT OF ENERGY
under Contract W-31-109-Eng-38

DISTRIBUTION OF THIS DOCUMENT IS UNLIMITED

DISCLAIMER

This report was prepared as an account of work sponsored by an agency of the United States Government. Neither the United States Government nor any agency Thereof, nor any of their employees, makes any warranty, express or implied, or assumes any legal liability or responsibility for the accuracy, completeness, or usefulness of any information, apparatus, product, or process disclosed, or represents that its use would not infringe privately owned rights. Reference herein to any specific commercial product, process, or service by trade name, trademark, manufacturer, or otherwise does not necessarily constitute or imply its endorsement, recommendation, or favoring by the United States Government or any agency thereof. The views and opinions of authors expressed herein do not necessarily state or reflect those of the United States Government or any agency thereof.

DISCLAIMER

Portions of this document may be illegible in electronic image products. Images are produced from the best available original document.

The facilities of Argonne National Laboratory are owned by the United States Government. Under the terms of a contract (W-31-109-Eng-38) between the U. S. Department of Energy, Argonne Universities Association and The University of Chicago, the University employs the staff and operates the Laboratory in accordance with policies and programs formulated, approved and reviewed by the Association.

MEMBERS OF ARGONNE UNIVERSITIES ASSOCIATION

The University of Arizona
Carnegie-Mellon University
Case Western Reserve University
The University of Chicago
University of Cincinnati
Illinois Institute of Technology
University of Illinois
Indiana University
Iowa State University
The University of Iowa
Kansas State University
The University of Kansas
Loyola University
Marquette University
Michigan State University
The University of Michigan
University of Minnesota
University of Missouri
Northwestern University
University of Notre Dame
The Ohio State University
Ohio University
The Pennsylvania State University
Purdue University
Saint Louis University
Southern Illinois University
The University of Texas at Austin
Washington University
Wayne State University
The University of Wisconsin

NOTICE

This report was prepared as an account of work sponsored by the United States Government. Neither the United States nor the United States Department of Energy, nor any of their employees, nor any of their contractors, subcontractors, or their employees, makes any warranty, express or implied, or assumes any legal liability or responsibility for the accuracy, completeness or usefulness of any information, apparatus, product or process disclosed, or represents that its use would not infringe privately-owned rights. Mention of commercial products, their manufacturers, or their suppliers in this publication does not imply or connote approval or disapproval of the product by Argonne National Laboratory or the U. S. Department of Energy.

Printed in the United States of America
Available from
National Technical Information Service
U. S. Department of Commerce
5285 Port Royal Road
Springfield, Virginia 22161
Price: Printed Copy $9.50; Microfiche $3.00

Distribution Category:
Energy Storage--Electrochemical--
Advanced Batteries (UC-94cb)

ANL-78-94

ARGONNE NATIONAL LABORATORY
9700 South Cass Avenue
Argonne, Illinois 60439

NOTICE
This report was prepared as an account of work sponsored by the United States Government. Neither the United States nor the United States Department of Energy, nor any of their employees, nor any of their contractors, subcontractors, or their employees, makes any warranty, express or implied, or assumes any legal liability or responsibility for the accuracy, completeness or usefulness of any information, apparatus, product or process disclosed, or represents that its use would not infringe privately owned rights.

HIGH-PERFORMANCE BATTERIES FOR ELECTRIC-VEHICLE PROPULSION AND STATIONARY ENERGY STORAGE

Progress Report for the Period
October 1977—September 1978

P. A. Nelson — Director, Chemical and Electrical Systems
D. L. Barney — Director, Advanced Battery Projects
R. K. Steunenberg — Manager, Lithium/Metal Sulfide Battery Program
A. A. Chilenskas — Manager, Advanced Battery Technology Development
E. C. Gay — Section Manager, Battery Engineering
J. E. Battles — Group Leader, Materials Development
F. Hornstra — Group Leader, Battery Charging Systems
W. E. Miller — Group Leader, Industrial Cell and Battery Testing
M. F. Roche — Group Leader, Cell Chemistry
H. Shimotake — Group Leader, Cell Development and Engineering
R. Hudson — Program Manager, Eagle-Picher Industries, Inc.
R. J. Rubischko — Program Manager, Gould Inc.
S. Sudar — Program Manager, Rockwell International

November 1978

Previous Quarterly Reports in This Program

ANL-77-35	January—March 1977
ANL-77-68	April—June 1977
ANL-77-75	July—September 1977
ANL-78-21	October—December 1977
ANL-78-45	January—March 1978

DISTRIBUTION OF THIS DOCUMENT IS UNLIMITED

PREFACE

This program on high-temperature secondary batteries consists of an in-house research and development effort at Argonne National Laboratory and subcontracted work by industrial laboratories. The work at Argonne is carried out primarily in the Chemical Engineering Division, with assistance on specific problems being given by the Materials Science Division and, from time to time, by other Argonne divisions.

Progress on this program through March 1978 has been covered by quarterly reports that apply largely to Argonne in-house work. This report covers the period of October 1977-September 1978 and contains individual contributions from the major subcontractors, as well as an account of the in-house work at Argonne.

The individual efforts of many engineers, scientists, and technicians are essential to the success of the program; recognition of these efforts is given by the individual authors that are cited throughout the report.

TABLE OF CONTENTS

TABLE OF CONTENTS (cont'd)

TABLE OF CONTENTS (contd)

TABLE OF CONTENTS (contd)

HIGH-PERFORMANCE BATTERIES FOR ELECTRIC-VEHICLE PROPULSION AND STATIONARY ENERGY STORAGE

Progress Report for the Period
October 1977—September 1978

ABSTRACT

This report covers the research, development, and management activities of the programs at Argonne National Laboratory (ANL) and at industrial subcontractors' laboratories on high-temperature batteries during the period October 1977—September 1978. These batteries are being developed for electric-vehicle propulsion and for stationary-energy-storage applications. The present cells, which operate at 400-500°C, are of a vertically oriented, prismatic design with one or more inner positive electrodes of FeS or FeS_2, facing electrodes of lithium-aluminum alloy, and molten LiCl-KCl electrolyte.

During this fiscal year, cell and battery development work has continued at ANL, Eagle-Picher Industries, Inc., the Energy Systems Group of Rockwell International, and Gould Inc. Related work has also been in progress at the Carborundum Co., General Motors Research Laboratories, and various other organizations. A major event was the initiation of a subcontract with Eagle-Picher Industries to develop, design, and fabricate a 40 kW-hr battery (Mark IA) for testing in an electric van. Conceptual design studies on a 100 MW-hr stationary-energy-storage module were conducted as a joint effort between ANL and Rockwell International. A significant technical advance was the development of multiplate cells, which are capable of higher performance than bicells.

SUMMARY

Commercial Development

To achieve successful commercialization of the lithium/metal sulfide battery, industry must be convinced that this battery is technically feasible, marketable, and capable of meeting governmental requirements. A report has been prepared on these three commercialization factors.

The first commercial production of lithium/metal sulfide batteries will probably be for limited markets (*i.e.*, low volume and high cost) such as postal vans, buses, mining vehicles, and submarines. In these near-term markets the relatively high price of the batteries should be offset by their favorable performance characteristics. The market size of the pilot markets at different battery costs has been estimated.

With respect to resource utilization, questions of cost and availability of lithium have been discussed with lithium producers, and studies based on their projections have indicated that an adequate supply will be available for at least the next twenty years at an acceptable cost.

Industrial Subcontracts

The goal of the program at ANL is to foster the development of a competitive, self-sustaining industry for the production of electric-vehicle and stationary-energy-storage batteries. To this end, industrial firms were invited to participate in the program, with about 50% of the current funding directed to industrial subcontractors. The three major subcontractors--Eagle-Picher Industries, Inc., Gould Inc., and Rockwell International's Energy Systems Group--are developing manufacturing procedures as well as testing and fabricating test cells. Other subcontractors are developing materials and components.

Eagle-Picher Industries, Inc. Eagle-Picher has been awarded the Mark IA battery contract, which entails the development, design and fabrication of a 40 kW-hr battery by early 1979. This battery will undergo stationary and in-vehicle testing at ANL.

Eagle-Picher selected the Li-Al/FeS multiplate cell for use in the Mark IA battery. Over the last year, about 50 multiplate cells have been fabricated, and a majority of these cells have been or are being tested by either Eagle-Picher or ANL. Some cells have achieved very high specific energies--greater than 100 W-hr/kg at the 4-hr rate. However, several problems with the operation of this type of cell have been discovered: a gradual loss of cell capacity beyond 60 cycles, high resistance (>1 mΩ), and poor wetting of the separator by the electrolyte. In each of the above areas, the necessary improvement can probably be achieved through changes in the design or fabrication technique. Promising approaches are under investigation in each area as a result of an intensive development program. To date, the test results indicate that the performance goals for the Mark IA can be met within the scheduled time.

Mark IA hardware other than cells is also being designed and fabricated by Eagle-Picher. This hardware includes a cell tray, temperature-control and fail-safe equipment, electrical/electronic components, and an insulated battery case. Great care has been taken to minimize hardware weight without otherwise affecting battery performance. To assure the lifetime requirements of the battery, lifetime tests were performed on materials at operating temperature.

In addition to the development of the Mark IA, a 6-V lithium/metal sulfide battery is being fabricated by Eagle-Picher. Testing of this battery will aid in developing the final design for the Mark IA.

Vibrational tests of Li-Al/FeS_2 bicells are proceeding at Eagle-Picher. Results indicate that the lithium/metal sulfide cell will withstand the vibrations due to road usage of test vehicles.

Gould Inc. During the past year, Gould fabricated nearly 50 upper-plateau Li-Al/FeS_2 bicells. Testing of these cells is currently being conducted at ANL. Gould also fabricated two Li-Al/FeS multiplate cells, one of which operated for 43 cycles and attained a specific energy of ~90 W-hr/kg at a 40-A discharge current. The performance of this multiplate cell was nearly identical to that of a similar bicell. Gould Inc. has also fabricated and tested about

forty Li-Al/FeS bicells. These cells were tested to evaluate electrode composition and porosity as well as separator form and configuration. The following conclusions were reached from testing these cells: the room-temperature resistance of cells can be significantly reduced by the use of BN-felt instead of BN-cloth separators; cell resistance at operating temperature can be reduced by the use of a thin nickel sheet (instead of iron sheet) topped with a busbar as the positive current collector; and the positive-electrode utilization can be significantly improved by adding either carbon, cobalt, or excess iron to the positive electrode or by using a LiCl-KCl electrolyte with a high LiCl content (61 mol % LiCl-39 mol % KCl). The test data indicate that the near-term (1979-1981) performance goals for the electric-vehicle battery can be met or exceeded with the Li-Al/FeS system.

Using the Li-Al/FeS bicells, Gould also evaluated various electrode fabrication techniques. In some of the bicells, 5.25 wt % Li-Al alloy was extruded and sheets of this material were used as negative electrodes. The capacity of cells with negative electrodes fabricated by this method was found to be limited by the negative electrode, and development of this method was temporarily discontinued. Tests have been conducted on cells with positive electrodes fabricated by a hot-extrusion method. The preliminary results have been encouraging. Finally, Gould Inc. is conducting a design and cost analysis of the lithium/metal sulfide battery.

Rockwell International The Energy Systems Group at Rockwell International (RI) is developing Li-Si/FeS_x cells for electric-vehicle and stationary-energy-storage applications.

Over the past year, work was performed at RI on positive electrode structures (rib and split-rib designs) that are amenable to high-volume, low-cost productions. Studies were also done on separators made of corrosion-resistant ceramic materials--AlN, Si_3N_4, CaO, Li_4SiO_4, and Li_4SiO_4 plus Li_3PO_4. The results obtained with a 1:1 mole ratio of Li_3PO_4 and Li_4SiO_4 are believed to be sufficiently promising to warrant further study of this system.

During this year, a 2.5-kW-hr stationary-energy-storage cell was fabricated by RI. Although the cell lifetime was short, useful information was obtained during the operation of this cell. Another 2.5-kW-hr cell is under construction. Testing of sixteen Li-Si/FeS bicells for electric-vehicle applications was also completed during this year. These tests indicated that (1) particle retainers of nickel screen are superior to porous nickel sheets, (2) negative current collectors made of Type 430 stainless steel are superior to collectors of low carbon steel, (3) operation of the cells at temperatures above 450° improves positive-electrode utilization, and (4) the use of a LiCl-rich electrolyte improves positive-electrode utilization. Although substantial progress has been made in the development of the electric-vehicle cell, further work is needed to attain the required cost and performance goals.

Over the past year, conceptual design studies of a 100 MW-hr energy-storage plant have been under way both at ANL and RI. These two conceptual designs have been recently merged into one. A preliminary design has been prepared of a 4 MW-hr module to be tested in the Battery Energy Storage Test (BEST) facility.

Other Contracts. In the area of materials and components, the Carborundum Co. is developing BN-felt electrode separators, the Illinois Institute of Technology is investigating the electrochemical desposition of molybdenum for joining and plating current-collector structures, and ILC Technology is developing insulated electrical feedthroughs. In addition, General Motors Corp. is undertaking an experimental investigation of lithium-alloy/FeS_2 cells with molten LiCl-KCl electrolyte.

Industrial Cell and Battery Testing

A facility for testing up to 50 industrial cells is currently being constructed at ANL; to be included as an integral part of this facility is a computer system for monitoring of cell performance and data acquisition. This facility will be used primarily for lifetime testing of industrial cells. A facility is also being constructed for laboratory tests of large (up to 60 kW-hr) batteries that will precede in-vehicle tests. This facility will have the capability for computer-controlled operation and data acquisition.

Two industrial firms under contract with ANL--Eagle-Picher Industries, Inc. and Gould Inc.--have fabricated Li-Al/FeS and Li-Al/FeS_2 bicells. These cells have been qualification tested, either at ANL or their own laboratories, to determine the optimum design features of this type of cell. In addition, other tests have been performed on Eagle-Picher cells to determine the optimum operating conditions.

The results obtained from the qualification tests of Eagle-Picher Li-Al/FeS_x bicells indicate that the specific energy of a bicell can be increased more effectively by maximizing the electrode capacity density than by maximizing the utilization alone, and that the higher utilization of thin-electrode (<4 mm) cells does not compensate adequately for the lower ratio of active material to cell weight. In all cases, the cell resistance was the dominant factor in the power capability.

Two conclusions were reached with regard to the operating mode of Eagle-Picher cells: the cell capacity is significantly higher at 500°C than at 450°C, and increasing the temperature decreased the open-circuit voltage of the cell at various stages of discharge.

Some general conclusions were reached from the results of tests on the Gould Li-Al/FeS_2 bicells. For optimum operation of the FeS_2 electrode, the cell should be designed to have 50 at. % lithium in the negative electrode and to utilize less than 70% of the lithium. The use of more than 30 vol % electrolyte (discharged state) in the FeS_2 electrode does not appear to offer any benefit in cell performance. In cells with positive-electrode thickness of 5.6 to 10.4 mm, the cells with a thicker positive electrode had lower utilization of the active material. For FeS_2 electrodes that are more than 5.6-mm thick, the effect of electrode thickness on utilization should be considered in the cell design.

Eagle-Picher Industries was contracted by ANL to develop, design and fabricate a 40 kW-hr battery (Mark IA) by early 1979. This battery will undergo stationary and in-vehicle testing at ANL.

Battery Design

In the battery design effort for the electric-vehicle battery, measurements were made of the heat generated by a cell during operation, and the calculated and measured values were found to be in agreement. This information will be used in the design of a heating/cooling system for an electric-vehicle battery. In other design work, an assessment was made of the rectangular versus the cylindrical configuration for a 50 kW-hr battery; the cylindrical configuration appears to be superior to the rectangular one.

Over the past year, conceptual design studies of a 100 MW-hr energy-storage plant have been under way at ANL and Rockwell International. These two conceptual designs have been recently merged into one. The following technical areas have dominated the design efforts: (1) the determination of the cell size and configuration; (2) the selection of materials for conductors and structures; (3) the creation of module designs that are amenable to factory fabrication, transport by truck, and on-site assembly with a minimum of labor; and (4) the achievement of a high packing density. During the next year, efforts will be made to reduce the battery plant cost for this design.

Cell Development and Engineering

This part of the program is directed toward improving the performance of lithium/metal sulfide cells. Over the past year, about 35 engineering-scale bicells were built and tested at ANL.

During this report period, an attempt was made to improve the performance of engineering-scale FeS bicells (electrodes fabricated by pressing techniques) by either of two methods--the use of a LiCl-rich electrolyte (61 mol % LiCl-39 mol % KCl) or the addition of 16 mol % Cu_2S to the positive electrode. Cell tests indicated that both of these methods improve electrode utilization by 10 to 40%. Subsequently, tests were conducted to determine the effect of positive capacity density (0.7 to 1.6 A-hr/cm^3) on the performance of engineering-scale FeS bicells with either LiCl-rich electrolyte and no Cu_2S additive, or eutectic electrolyte and 16 mol % Cu_2S additive, or eutectic electrolyte and no Cu_2S additive. Tests results showed that, without the use of Cu_2S additive or LiCl-rich electrolyte in these FeS cells, the positive-electrode utilization is poor. In addition, the bicell with Cu_2S additive and a positive loading density of 1.6 A-hr/cm^3 and the bicell with LiCl-rich electrolyte and a loading density of 1.4 A-hr/cm^3 exhibited the best performance characteristics for electric-vehicle applications.

In order to further increase the specific energy of the Li-Al/FeS cell, the use of multiplate cells has been proposed. This cell design consists of three negative electrodes of Li-Al alloy, two positive electrodes of metal sulfide, a BN-felt separator, and a molten LiCl-KCl electrolyte. Calculations indicate that the multiplate FeS cell should achieve a specific energy of 131 W-hr/kg at the 4-hr rate.

Investigations are continuing on Li-Al/FeS_2 cells in which part or all of the iron sulfide in the positive electrode is replaced by nickel sulfide. In general, the cells with nickel sulfide in the positive electrode have shown better capacity retention and longer lifetimes than cells with FeS_2 positive

electrodes. The results of these studies also suggested that the use of sulfur-to-metal ratios that are somewhat less than 2.0 in Li-Al/MS_x cells tends to improve the stability of the cell capacity for at least a few hundred cycles.

Carbon-bonded positive electrodes are being developed as an alternative to those made by pressing techniques. In the development of the carbon-bonded electrode, an effort has been made to maximize the deliverable energy per unit volume of positive electrode by optimizing the type, amount, and degree of dispersion of the carbonaceous filler material. Tests using small-scale FeS cells indicated that 8-10 vol % carbon with dense carbon powder or fibers as the filler results in greater than 70% positive-electrode utilization at a current density of 100 mA/cm^2. In the investigation of potential manufacturing methods for carbon-bonded electrodes, the use of a heat-treated catalyst (1 wt % maleic anhydride) to polymerize the furan resin reduced the curing time to about 15 min at 200°C. Tests were conducted on four engineering scale bicells with carbon-bonded electrodes. The carbon-bonded electrodes were composed of either FeS_2, NiS_2-CoS_2, FeS-Cu_2S, or FeS. These tests showed that carbon-bonded positive electrodes are a viable alternative to cold- or hot-pressing techniques for the fabrication of electrodes and that they have good electrical-performance characteristics. A choice between carbon-bonding and pressing probably will depend primarily on relative costs and adaptability to mass production.

Earlier work at ANL had indicated that non-conductive ceramic powders are a possible low-cost alternative to the BN fabric and felt currently used as electrode separators in lithium/metal sulfide cells. During this past year, eight engineering-scale bicells with MgO powder separators were tested. The results indicate that powder separators may be an alternative to BN felt or fabric. At the present time, however, further work is needed to demonstrate the long-term stability of powder separators, particularly under vibration, and to develop multiplate cell designs that can accommodate powder separators.

Materials Development

A series of static corrosion tests on representative current-collector materials was conducted at 450°C in either $CuFeS_2$, NiS, NiS_2, or TiS_2 and LiCl-KCl electrolyte. These results were combined with those of previous experiments on FeS, Cu_2S, FeS, and CoS_2 and yielded the following order for increasing corrosiveness of the metal sulfide environments: FeS, Cu_2S, $CuFeS_2$, NiS, FeS_2, TiS_2, NiS_2, and CoS_2. Tests on BeO feedthrough insulators showed that these components have excellent corrosion resistance to the negative-electrode environment.

The oxidation potentials of seven nickel-base alloys in electrolyte at 425°C were determined. All of these alloys had breakdown potentials between that of nickel (2.48 V) and molybdenum (2.70 V). The alloys with high molybdenum concentrations had the highest values, whereas those alloys with high iron concentrations had the lowest values.

Testing has been completed for three Li-Al/FeS cells with nickel components in the positive electrode. The corrosion attack was minimal over most of the component surfaces, but localized regions exhibited extensive corrosion due to intergranular attack. The mean corrosion rate after nearly three months of

operation was 110 μm/yr. Hastelloy B components in the positive electrodes of two Li-Al/FeS_2 cells showed uniform surface attack, and a gradient in the rate of reaction (the highest rates near the edges of the collector). Both of these cells were operated for one month periods, and the components had high corrosion rates, >600 μm/yr.

Metallic substrates coated with electrically conductive ceramic are being considered as substitutes for the expensive molybdenum current collectors presently used in Li-Al/FeS_2 cells. Thus far, low-carbon steel specimens coated with TiB_2, TiN and FeB-FeB_2 have been obtained from vendors. Preliminary static corrosion tests indicate that TiN has good potential as a coating material.

Felt and powder separators are being developed as an alternative to the expensive BN fabric currently used in lithium/metal sulfide cells. During the past year Carborundum Co. has fabricated approximately 20 m^2 (200 ft^2) of BN felt. Tests on this material have shown that it possesses sufficient strength and flexibility for use in cells. In-cell tests on BN felt and MgO powder have been conducted during this year. At low current densities (<60 mA/cm^2) the utilization of active material was the same for cells using both types of separators; however, at high current densities, cells with MgO-powder separators had a lower utilization than that of cells with BN-felt separators. This latter effect is believed to be due to the lower porosity of the powder separator (∿50 *vs.* 90%). Porous, sintered Y_2O_3 and MgO separators are being fabricated and evaluated. Processing techniques have been developed to fabricate Y_2O_3 plates that are thin (∿1-2 mm), porous (50-60%), and flat. Two Li-Al/FeS cells using this type of separator have been assembled so far. One of these cells has operated for 83 days (283 cycles) at current densities up to 100 mA/cm^2. The performance of these cells has been comparable to that of cells using BN-felt or MgO-powder separators.

The following conclusions were reached from flowability studies of FeS and MgO powder: an MgO powder separator (70 vol % solid) will hold its shape after some initial degree of compaction; cold-pressed or hot-pressed FeS electrodes will easily flow or extrude at stresses as low as 200 kPa; and the extrusion of FeS and salt mixture is possible above stresses of 200 kPa at 350-450°C.

Contact angle measurements have been made of molten LiCl-KCl on various cell materials. The only material instantaneously wet by the salt was Li-Al alloy. Type 304 stainless steel and Y_2O_3 had easy-to-wet behavior, whereas FeS_2, FeS, Li_2S, Fe, BN, MgO, and Fe had difficult-to-wet behavior. Pretreatment of some of the difficult-to-wet materials (*e.g.*, BN felt and MgO powder) with $LiAlCl_4$ has been found to improve material wettability. Contact angle measurements were also used to estimate the height to which a porous cell component can maintain electrolyte infiltration; for structures formed from powders with particle sizes of 100 μm or less, no problem is expected with electrolyte drainage.

Over the past year, 52 engineering cells have undergone post-test examinations. The major causes of cell failure were the honeycomb current collector cutting the separator and cell assembly problems. Most of the causes of cell failure have been mechanical in origin and can be corrected by modifications in the cell design.

The following conclusions were drawn from studies of some of the post-test cells: (1) a significant lithium concentration gradient can occur in charged negative electrodes; (2) Y_2O_3-felt or powder separators used in both FeS and FeS_2 cells react with sulfur to form Y_2O_2S; (3) the corrosion of the molybdenum current collector used in FeS_2 cells is minimal; (4) the lifetime of low-carbon steel current collectors is ∿800 days in Li-Al electrodes but only ∿225 days in FeS-Cu_2S electrodes; and (5) when used in the positive electrode, carbon migrates to the negative electrode.

Cell Chemistry

In the cell chemistry studies, the properties of the metal disulfide electrodes were investigated through cyclic voltammetry, small-scale cell tests, and metallographic studies.

The current status of the Li-Fe-S phase diagram is presented. The important phases are FeS_2, $Fe_{1-x}S$, $Li_3Fe_2S_4$, Li_2FeS_2, Fe, and a solid-solution field which is connected with Li_2FeS_2. This phase diagram was used to describe the discharge mechanism of the FeS_2 electrode in LiCl-KCl electrolyte. The charge mechanism of this electrode is more complicated than the discharge mechanism, and is still under investigation.

Studies were conducted on the behavior of FeS_2 electrodes in LiCl-KCl electrolyte of varying composition (eutectic, KCl-rich, and LiCl-rich). Cyclic voltammetry showed that the electrochemical reversibility of FeS_2 electrodes in either LiCl-rich or eutectic electrolyte was poor at high electrode utilization. Cyclic voltammetry, cell tests, and metallographic studies showed that $KFeS_2$ formed during the charging of FeS_2 electrodes in KCl-rich electrolyte; however, the reversibility problem of FeS_2 in either LiCl-rich or eutectic electrolyte was found not to be caused by this potassium-containing phase. Cell tests indicated that the phases involved in the reaction with poor reversibility were $Li_3Fe_2S_4$ and FeS_2.

Metallographic studies were performed on the use of CoS_2 as an additive to FeS_2 electrodes. These studies indicated that Li-Co-S analogs of Li-Fe-S compounds do not exist at cell operating temperature. Thus cobalt and iron sulfides follow independent charge-discharge paths, with cobalt present as its binary Co-S compounds. It was recommended that a reassessment of the effects of this additive on cell performance should be undertaken.

Over the past year, studies were conducted on FeS electrodes to determine the limits of J-phase ($LiK_6Fe_{24}S_{26}Cl$) formation, which has been shown to have an adverse effect on electrode kinetics. Cells tests and voltammetry studies of Li-Al/FeS cells confirmed earlier studies which had indicated that the conversion of J phase to FeS requires a potential of about 1.6 V *vs.* LiAl. Out-of-cell tests indicated that J-phase formation should be reduced in FeS cells by increasing the LiCl concentration in the eutectic electrolyte or by using a high operating temperature (>450°C). Tests in small-scale FeS cells showed that a LiCl concentration of 67 mol % in the LiCl-KCl electrolyte and an operating temperature of 450°C result in a satisfactory positive-electrode utilization (91% at a current density of 50 mA/cm^2).

Exploratory studies were undertaken on FeS-NiS electrodes and FeSe electrodes. In tests on small-scale Li-Al/$Fe_{0.5}Ni_{0.5}S$ cells, J phase (probably with nickel substituted for a portion of the iron) was found. In tests on small-scale Li-Al/FeSe cells, a selenium analog of J phase was found.

Studies of the properties of lithium negative electrodes were also undertaken. Operation of Li-Al electrodes containing various additives (In, Sn, Pb, Cu, Ag, Sb, Zn, or Mg) showed that indium is the only one that significantly improves capacity retention.

Advanced Battery Research

The objective of this program is to devise new combinations of electrode materials and electrolytes that will provide a basis for the development of inexpensive, high-performance batteries. Over the previous year, studies were conducted of cells having negative electrodes of either calcium alloy or magnesium alloy, positive electrodes of metal sulfide or metal oxide, and a molten-salt electrolyte.

A 70 A-hr prismatic Ca(Mg_2Si)/LiCl-KCl-$CaCl_2$/NiS_2 cell (assembled in the uncharged state) was tested to evaluate the behavior of calcium electrodes in a practical configuration. This cell, although not optimized for specific energy, achieved 42 W-hr/kg at the 6-hr rate. Operation was terminated after 120 cycles due to declining coulombic efficiency. The results of this cell test were very encouraging.

Since the electrolyte in the above cell is relatively expensive because of its high lithium content (54 mol % LiCl), a search was made for alternative electrolytes for calcium/metal sulfide cells. The salt that was discovered to be the most promising is 29 mol % LiCl-20 mol % NaCl-35 mol % $CaCl_2$-16 mol % $BaCl_2$.

Cyclic voltammetry studies were initiated on metal disulfide (FeS_2 and NiS_2) electrodes *vs.* $CaAl_4$ in either LiCl-KCl-$CaCl_2$ or LiCl-NaCl-$CaCl_2$-$BaCl_2$ electrolyte. In these studies, the high-voltage (1.8 V) reactions of FeS_2 and NiS_2 exhibited poor electrochemical reversibility; however, this reversibility problem may be the result of minor overpotentials for the calcium-ion reactions rather than a problem of a more serious nature. The cause of the poor reversibility and methods of eliminating it will be sought in future experiments.

Studies were conducted on alternative negative electrodes to the Ca-Mg-Si system used in the engineering-scale cell. Negative electrodes evaluated during the past year included Ca-Si, Ca-Al-Zn, and Ca-Pb. The Ca-Si electrode was the only one found to have acceptable utilization for electric-vehicle applications. Both the Ca-Mg-Si and Ca-Si systems will be evaluated in future cell tests.

The investigation of cells having magnesium negative electrodes was prompted by the promising properties of magnesium. The performance of the following small-scale cells was studied: Mg_2Al_3/NiS_2, Mg_2Al_3/TiS_2, Mg_2Cu/TiS_2, Mg_2Cu/Ni-MgO, and Mg_2Cu/Fe-MgO. None of the above cell systems showed promise for further cell development. Owing to the unfavorable results obtained with the magnesium cells, it was decided to concentrate future efforts on calcium cells.

I. INTRODUCTION

(D. L. Barney, R. K. Steunenberg)

Lithium/metal sulfide batteries are being developed by Argonne National Laboratory (ANL) and its industrial subcontractors for use as (1) power sources for electric-vehicle propulsion, and (2) stationary-energy-storage applications such as load leveling on electric utility systems or storage of energy produced by solar, wind or other intermittent sources. In general terms, the major requirements for an electric-vehicle battery are high specific energy (W-hr/kg), high volumetric energy density (W-hr/L), and high specific power (W/kg). Economic considerations indicate that the battery should have a minimum lifetime of three years (~1000 deep discharge cycles or equivalent) and a maximum cost of about $35-40/kW-hr. The specific energy and specific power requirements are somewhat less stringent for the stationary-energy-storage battery, but this application requires a longer lifetime (~10 years and 3000 cycles) and a lower cost (~$20/kW-hr). The approaches that are being taken in the designs of cells and batteries for these two applications differ significantly as a result of these requirements.

The strategy that has been adopted for the electric-vehicle battery involves the development, design, and fabrication of a series of lithium/metal sulfide batteries by industrial subcontractors. Each of the batteries in this series, designated Mark I, II, and III, has a specific set of objectives. The main purpose of the Mark I battery is to evaluate the technical feasibility of the lithium/metal sulfide system for electric-vehicle batteries and to resolve interfacing problems between the battery and the vehicle and charger. The Mark II battery has somewhat higher performance goals than Mark I, but the main emphasis is on the development of designs and materials that will permit low-cost manufacturing techniques. The Mark III battery is planned as a high-performance prototype suitable for evaluation and demonstration in a passenger car. The performance and lifetime goals for the Mark I, II, and III batteries are presented in Table I-1.

In August 1977, a decision was made to proceed with a Mark I battery, which is designated Mark IA. A request for proposals was issued in November, and a contract was awarded to Eagle-Picher Industries, Inc. at Joplin, Missouri. This contract, which went into effect February 1978, calls for the development, design, and fabrication of a 40 kW-hr battery package consisting of two 20 kW-hr modules to be delivered to ANL in 12 months. The technical goals for the Mark IA battery are presented in Table I-2. In the statement of work for the Mark IA contract, the goals are listed in the following order of preference: (1) operability, (2) energy output, (3) power output, (4) specific energy, (5) specific power, and (6) lifetime. When the Mark IA battery is delivered to ANL, it will be tested in the laboratory and then in an electric van. The performance and lifetime goals for the Mark IA battery are somewhat lower than those listed in Table I-1 for the Mark I battery. The present plan is to design and fabricate a group of cells, designated Mark IB, to achieve the full Mark I cell goals.

An effort has been initiated on a Mark II battery development program that is expected to extend over a period of four or five years and result in the delivery of prototype electric-vehicle batteries that would be commercially viable and manufacturable at moderate cost. The first phase of

Table I-1. Program Goals for the Lithium/Metal Sulfide Electric-Vehicle Battery

Goal	Mark I	Mark II	Mark III
Specific Energy, W-hr/kg			
Cell (average)[a]	100	125	160
Battery	75	100	130
Energy Density, W-hr/liter			
Cell (average)	320	400	525
Battery	100	200	300
Peak Power, W/kg[b]			
Cell (average)[a]	100	125	200
Battery	75	100	160
Battery Heat Loss, W[c]	300	150	125
Lifetime			
Deep discharges	400	500	1000
Equivalent kilometers	65,000	95,000	240,000
Equivalent miles	40,000	60,000	150,000

[a] Individual cells for the Mark I battery will have about 10% excess specific energy and power above those shown to allow for possible cell failures and mismatching; a 4% excess is planned for the individual Mark II cells.

[b] Peak power sustainable for 15 sec at 0 to 50% state of discharge; at 80% discharge, the peak power is 70% of the value shown.

[c] The values shown represent the heat loss of the battery through the insulated jacket; under some operating conditions, additional heat removal may be required.

this program includes three cost and design studies at Gould Inc., Eagle-Picher Industries, Inc., and the Energy Systems Group of Rockwell International. These three studies were started in July 1978 and are scheduled for completion by the end of October. The next phase of the Mark II program will involve the initiation of two development contracts about January 1, 1979. These contracts will be directed toward the development of battery designs and fabrication methods, and will each result in the fabrication of a 50-kW-hr battery.

For stationary-energy-storage applications, assessment studies have indicated that batteries having a life of 8 to 12 years and a capital cost of about $20 to $30/kW-hr would be competitive with other methods of storing energy or producing supplemental power. Program goals for the stationary-energy storage battery are given in Table I-3. The present plan is to develop a battery module of about 5-6 MW-hr capacity, which will be tested in the BEST (Battery Energy Storage Test) Facility. This facility is the result of a joint undertaking by the U.S. Department of Energy, the Electric Power

Table I-2. Technical Goals for the Mark IA Battery

Battery Characteristics	Goals
Energy Output, kW-hr[a]	40
Power Output, kW[b]	30
Maximum Weight, kg	680
Maximum Volume, liters	400
Specific Energy, W-hr/kg[a]	60
Energy Density, W-hr/liter[a]	100
Operating Temperature, °C	400-500
Maximum Heat Loss, W	400
Battery Voltage, V	144
Cycle Life[c]	200

[a]Discharge to 1.00 V/cell at the 4-hr rate.

[b]Sustained through a 15-sec pulse at 50% state of discharge.

[c]To 20% loss of the design capacity.

Table I-3. Program Goals for the Stationary-Energy-Storage Battery

Program Goal	BEST Module	Demonstration
Energy Output, MW-hr	5	100
Power, MW		
Peak	1.5	25
Sustained	1.0	10
Specific Energy,[a] W-hr/kg	80	60-150
Cycle Life	500-1000	3000
Discharge Time, hr	5-10	5-10
Charge Time, hr	10	10

[a]Based on cell weight only.

Research Institute, and the Public Service Company of New Jersey to provide for the testing of various types of batteries on an electric-utility system.

The battery cells that are being considered for stationary energy storage have lithium-silicon or lithium-aluminum negative electrodes and FeS positive electrodes. Conceptual design studies of a 100 MW-hr energy-storage plant that were being conducted independently at ANL and at the Energy Systems Group of Rockwell International have been merged into a joint effort by these two organizations under an ANL subcontract with Rockwell. In the present concept, the 100-MW-hr plant will consist of 5- to 6-MW-hr modules. These

modules are made up of 35 kW-hr submodules in a container that is weatherproof and thermally insulated. Each submodule consists of a stack of eight multiplate cells. In the present conceptual design, the cells are in the form of an approximately 25-cm cube, and the electrode plates are oriented horizontally.

The lithium/metal sulfide battery program consists of an in-house research and development effort at ANL and work performed under subcontracts with various industrial or academic organizations. The ANL effort includes cell chemistry studies, materials development and evaluation, cell and battery development, industrial cell and battery testing, battery design, and commercialization studies. Preparations are also being made for laboratory and in-vehicle tests of the Mark IA battery and for statistical lifetime testing of cells. Another small effort at ANL is directed toward the development of calcium alloy/metal sulfide cells, which have a low cost potential.

Among the industrial subcontractors, nearly all of the cell development, design and fabrication work is performed by Eagle-Picher Industries, Inc., Gould Inc., and the Energy Systems Group of Rockwell International. The Carborundum Co. is involved in the preparation of boron nitride separator materials and the development of production processes for these materials. The General Motors Research Laboratories are conducting a systematic investigation of the characteristics of FeS_2 electrodes. Other subcontractors participating in the program during the period covered by this report are Budd Co., Catalyst Research Corp., Electric Technology Corp., ESB, Inc., ETA, Inc., ILC Technology Inc., Illinois Institute of Technology, Sigma Research, Inc., Thermo Electron Corp., TRW, Inc., and United Technologies Corporation.

As a result of the cell development effort, significant improvements have occurred in the lifetime and performance of Li-Al/FeS and Li-Al/FeS_2 bicells* during the past few years, as shown by Figs. I-1 through I-6. The M-, R-, KK-, and CB-series cells shown in these figures were designed and fabricated at ANL; the others were built by industrial subcontractors. Also shown in these figures are the projected performance and lifetime goals for the cells of electric-vehicle batteries. In general, the Li-Al/FeS cells have shown long cycle life (Fig. I-1), but they are limited in specific energy (Fig. I-2) and specific power (I-3). The life of the Li-Al/FeS_2 cells that have been tested to date has not exceeded about 500 cycles (Fig. I-4), but these cells have achieved higher specific energy (Fig. I-5) and specific power (Fig. I-6) than the Li-Al/FeS cells. A major improvement in performance has resulted from the development of multiplate cell designs (see Fig. I-2). It appears that the Mark I and II performance goals for electric-vehicle batteries can be met by Li-Al/FeS cells, using the multiplate design. The Mark III goals, however, will require the use of Li-Al/FeS_2 cells.

*These cells contain a single positive electrode and two facing negative electrodes.

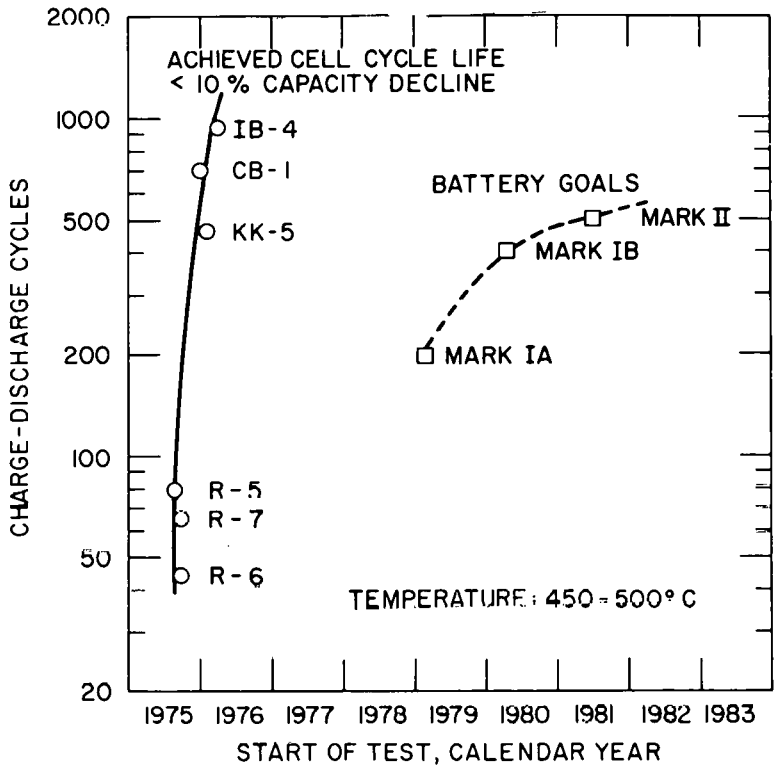

Fig. I-1. Cycle Life of Li-Al/FeS Cells.
(ANL Neg. No. 308-78-174)

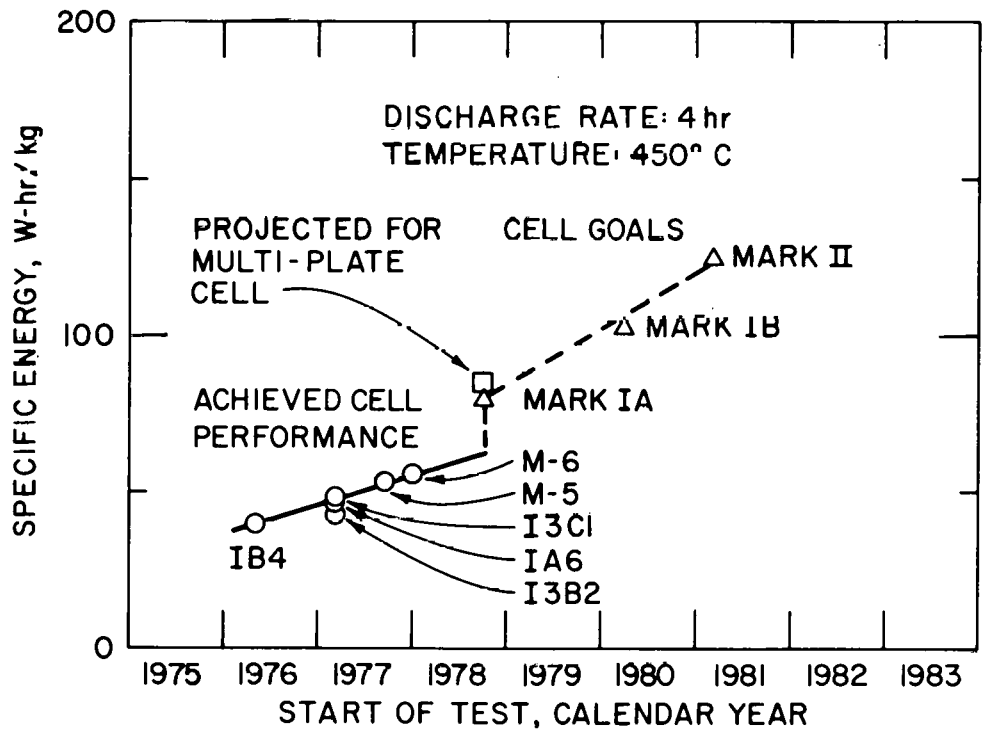

Fig. I-2. Specific Energy of Li-Al/FeS Cells.
(ANL Neg. No. 308-78-169)

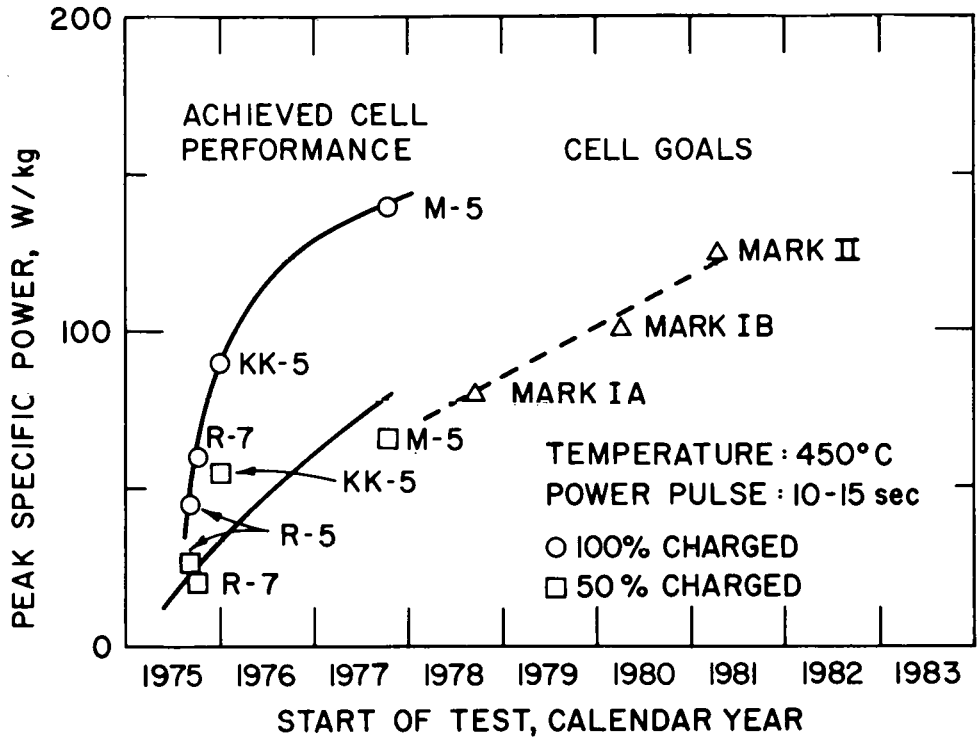

Fig. I-3. Peak Specific Power of Li-Al/FeS Cells. (ANL Neg. No. 308-78-176)

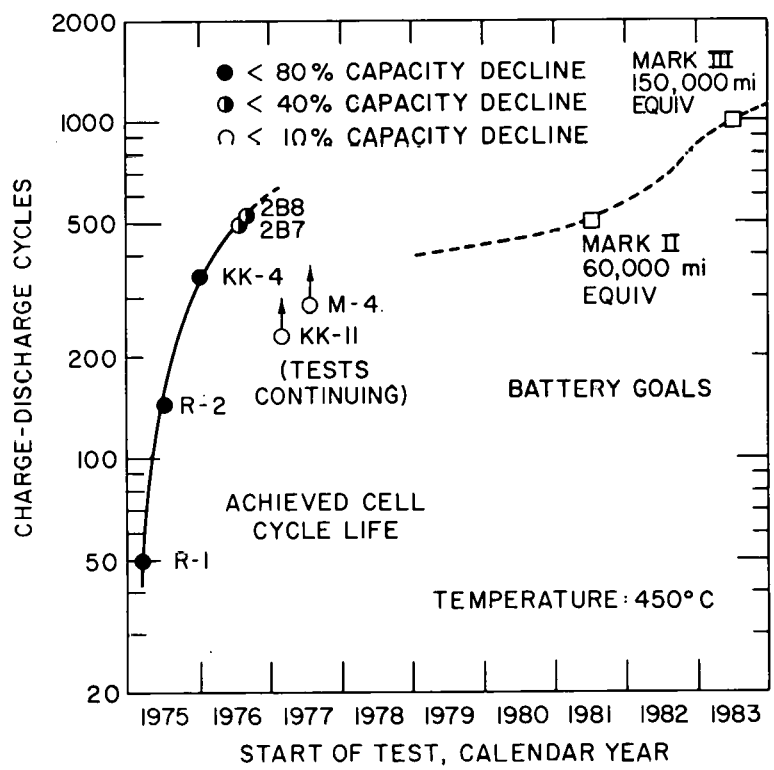

Fig. I-4. Cycle Life of Li-Al/FeS_2 Cells. (ANL Neg. No. 308-78-173)

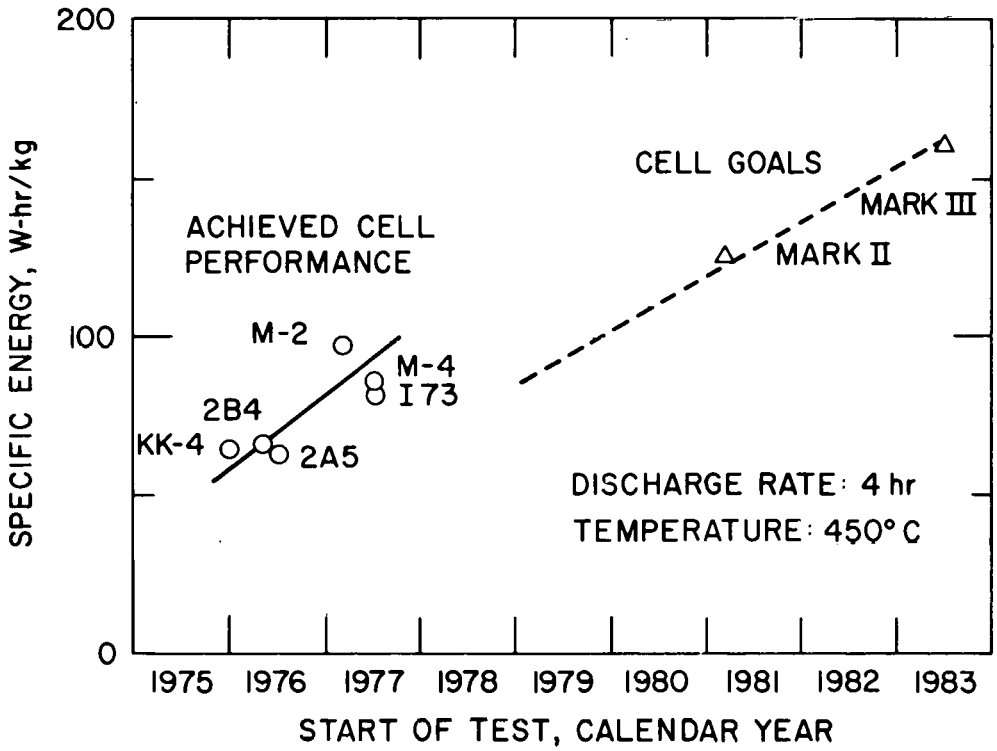

Fig. I-5. Specific Energy of Li-Al/FeS_2 Cells. (ANL Neg. No. 308-78-175)

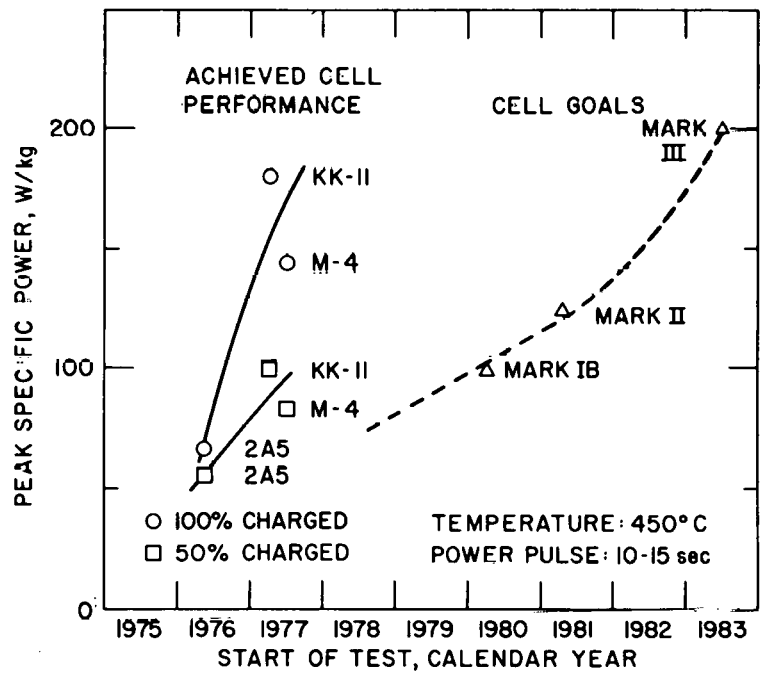

Fig. I-6. Peak Specific Power of Li-Al/FeS_2 Cells. (ANL Neg. No. 308-78-170)

II. COMMERCIAL DEVELOPMENT
(A. A. Chilenskas)

The objective of the commercialization studies at ANL is to provide data on the manufacturing cost and market requirements for the lithium/metal sulfide battery. The commercialization studies are conducted at ANL with assistance from industrial subcontractors and consultants. These studies involve the identification of potential markets, manufacturing cost analyses, financial plans, and evaluations of competing technologies.

To achieve successful commercialization of the lithium/metal sulfide battery, industry must be convinced that the battery is (1) technically feasible, (2) marketable, and (3) capable of meeting governmental requirements. In regard to the first condition, the Mark I tests of the electric-vehicle battery and the BEST facility tests of the stationary-energy-storage battery are expected to establish the technical feasibility of the system. The second condition involves marketability of the battery at an acceptable cost. The first commercial production will probably be for limited markets (*i.e.*, low volume and high cost), and these pilot markets are discussed below. The third condition involves the safety aspects of the battery, environmental and health considerations, and resource utilization. A preliminary assessment of the safety aspects of the lithium/metal sulfide battery has been conducted by Budd Co. Their results are highly encouraging with respect to the safe deployment of lithium/metal sulfide batteries in electric vehicles (ANL-77-75, pp. 12-13). A brief discussion of the cost and availability of lithium is presented below.

A. A. Chilenskas and W. L. Towle[1] have prepared a paper on the above three conditions, and, based on their findings, have developed a schedule for the commercialization of lithium/metal sulfide batteries. According to this schedule, van tests with a 60-kW-hr battery will be done in 1981-1983, and pilot-plant production and full-scale automated production of lithium/metal sulfide cells will occur by 1982 and 1987, respectively. These dates are based on present and projected funding for the battery program, and are considered to be the earliest possible dates.

A. Pilot Markets

The first commercial production of lithium/metal sulfide batteries will probably be for limited (low volume and high cost) markets such as postal vans, buses, mining vehicles, and submarines. In these near-term (1982-1990) markets the relatively high price of the batteries should be offset by their favorable performance characteristics. A study of these near-term markets gave the results shown in Table II-1, where the projected market size for various applications is given for different battery costs.

The bus market is of special interest to potential electric vehicle manufacturers, both in the U.S. and throughout the world, because the cost of purchasing buses is very often subsidized by national or local governments. In the U.S. the Urban Mass Transportation Authority (UMTA) provides an 80% federal subsidy for bus purchases. An analysis[2] has shown that a significant market size of about 40 MW-hr/yr could be achieved by 1982; this 1982 market could then rapidly expand to about 580 MW-hr/yr in 1985 and to about 934 MW-hr in 1990, which is enough to support the output from one automated battery plant.

Table II-1. Pilot Markets for the Lithium/Metal Sulfide Battery

Price, $/kW-hr	Market Size,[a] MW-hr/yr	Markets	Year Initiated
300	85	Submersibles	1982
200	119	Postal vans	1982
170	197	Postal vans	1982
150	441	Postal vans, buses, mining vehicles	1982
50	580	Buses	1987
50	18,900	Vans	1987
50	934	Buses	1990

[a]The market size shown assumes that the Li/MS battery captures the entire market. The effect of market-sharing because of competition from other advanced batteries will need to be considered as part of an overall business plan.

The van market after 1987 (assuming that automated battery plants produce Li/MS batteries at about $50/kW-hr) can be very large. An estimate has been made that this market could support 300,000 battery-powered vans per year, which would require 18,900 MW-hr/yr of plant capacity. This market alone would require the output from about 17 automated battery plants rated at 1,100 MW-hr/yr.

A near-term market of interest for the Li/MS battery is a high-performance battery for use in fork-lift trucks for the U.S. Army. Eagle-Picher Industries, Inc. has been contracted to deliver several cells and a 6-V battery module to Fort Belvoir (MERADCOM) for test evaluation.

B. Lithium Supply and Demand

Institutional agencies with responsibilities in resource surveillance and management are, of course, interested in the effect of the mass-production of lithium/metal sulfide batteries on the world lithium resources. The projected lithium requirements for the use of the lithium/metal sulfide battery for the electric-vehicle and stationary-energy-storage applications are shown in Table II-2. To achieve a significant production of utility and electric-vehicle batteries will require a substantial fraction of the known lithium reserves. The lithium production by the year 2000 would require about 15% of U.S. reserves (Class A, B, and C) and about 5% of the world reserves (Class A, B, and C). Although adequate domestic and world-wide reserves appear to be available up until the year 2000, the cost of the resource as a function of large-volume production remains in question, and appears to be resolvable only as part of an actual commercialization effort.

Table II-2. Projected Lithium Requirements

	Yearly Production			
	1982-87	1987-91	1991-95	1995-2000
Batteries Produced, MW-hr	400	10,000	30,000	70,000
Number of 100 MW-hr Utility Plants	1	33	100	230
Number of 4-kW-hr Electric-Vehicle Batteries	7,500	1.7×10^5	5×10^5	1.1×10^6
Lithium in Batteries, metric tons	280	7,000	21,500	49,000
Conventional Uses metric tons	5,000	6,000	7,500	10,000
Annual Lithium Production,[a] metric tons	5,300	13,000	29,000	59,000
Capital for Lithium Production,[b] $ × 10^6	--	240	480	900

[a]The cumulative lithium production up until the year 2000 is estimated to be 489,000 metric tons.

[b]Based on $30 million for 1,000 metric tons/yr.

REFERENCES

1. A. A. Chilenskas and W. L. Towle, *A Commercialization Scenario for the Lithium/Metal Sulfide Battery*, unpublished (November 1977).

2. S. Nelson and A. A. Chilenskas, *A Preliminary Evaluation of Near-Term (1980-1985) Markets for Lithium/Iron Sulfide Batteries*, unpublished (1977).

III. INDUSTRIAL SUBCONTRACTS

The ultimate goal of the program at ANL is to foster the development of a competitive, self-sustaining industry for the production of electric-vehicle and stationary-energy-storage batteries. To this end, industrial firms were invited to participate in the program, with approximately 50% of the current funding directed to industrial subcontracts. Three firms--Eagle-Picher Industries Inc., Gould Inc., and the Energy Systems Group of Rockwell International--are developing manufacturing procedures and fabricating test cells. Carborundum Co., the Illinois Institute of Technology, and ILC Technology Inc. are developing cell materials and components.

A. Eagle-Picher Industries, Inc.
(R. Hudson)

Eagle-Picher Industries, Inc. entered into the lithium/metal sulfide battery program in May, 1975 as one of the first industrial contractors to associate themselves with Argonne National Laboratory in the battery program. Initial efforts in the program were directed toward developing prismatic cells suitable for use in electric vehicles and stationary-energy-storage applications. The effort for the last year has been directed primarily toward development of electric-vehicle cells. These efforts to date have proved very successful. Some of the FeS cells have operated in excess of 1,000 cycles in the laboratory. Innovative designs and fabrication techniques have been developed at Eagle-Picher, and the fabrication of the initial demonstration battery is now feasible. In February 1978, Eagle-Picher was awarded the Mark IA contract for the design, development and fabrication of a 40-kW-hr battery. This battery will demonstrate the technical feasibility of the Li/MS battery for electric-vehicle use. Delivery of the battery is currently scheduled for February 1979. As a part of the development program at Eagle-Picher, lithium/metal sulfide cells have been vibrated at levels which can be expected under normal vehicle use. These tests have shown no problems to exist within the system.

Eagle-Picher management is firmly committed to the development of the Li/MS battery. This is exemplified by Eagle-Picher establishing a pre-pilot plant facility which has the capability to produce 3 to 4 MW-hr/yr.

1. Cell Development for the Mark IA Battery
(E. Cupp, J. Buchanan, L. Aupperly, and J. Whitford)

In February 1978 Eagle-Picher was awarded a contract to design, develop, fabricate, and deliver a 40-kW-hr battery to Argonne National Laboratory. The contracted program is for a year, with the battery to be delivered to Argonne in February 1979. The battery will be initially tested at ANL and then will be tested in a demonstration electric van. The van will be fully instrumented to monitor the performance of the battery while operating under road-load conditions. The technical goals for the Mark IA battery are presented in Table I-2. The battery will contain two modules (20-kW-hr capacity) connected in series. Specific areas which are being addressed in the program are cell development, battery hardware development, cell testing, test equipment for cells and batteries, and assembly techniques for batteries.

a. Multiplate Cell Development

In order to meet the battery criteria set forth in Table I-2, the multiplate FeS cell was chosen. The basic weight and volume restraints for the Mark IA battery precluded the use of bicell assemblies. The multiplate cell construction selected, while not the optimum configuration in all respects, is a compromise among weight, energy, volume, and power considerations. A cell concept design review was held at Eagle-Picher in February 1978 at which time this design was reviewed with ANL. The first multiplate cell design had its inception in the cylindrical battery configuration of the Mark "O" battery design. These proposed cells utilized 12.7 × 17.8 cm electrodes (four positive and five negative). This cell configuration allows cells with a capacity of 450 A-hr theoretical and about 320 A-hr nominal at the 4-hr rate to be fabricated. The cell configuration, however, was such that 120 cells could not be fitted in the two modules required for the Mark IA battery; therefore, the Mark O cell design was abandoned. However, tooling for the 12.7 × 17.8 cm electrode was under fabrication at the time of the award of the Mark IA contract, and thus the first series of multiplate cells (a total of 20 cells) was constructed using 12.7 × 17.8 cm electrodes.

The final cell design for the Mark IA battery has as its conceptual basis an effort to get the most capacity in the allowed volume. The major restraints are the physical dimensions of the battery compartment of the electric vehicle and the volume required for thermal insulation, *etc.* An electrode dimension of 17.8 × 17.8 cm was selected for this cell. The cell consists of three positive and four negative electrodes. All of the multiplate cells fabricated after the first 20 had this design. This cell design is shown in Fig. III-1.

The electrodes for the multiplate cells are cold pressed into a honeycomb-type plate, as shown in Fig. III-2. Utilizing a 500 ton (5×10^5 kg) press, we compressed the active powders, weighed to ±0.1 g, into plates at pressures of from 1,350 to 1,450 kg/cm^2. These pressures yield positive electrodes having approximately 50% porosity and negative electrodes having 20-25% porosity. The electrodes assembled by this method are strong and easily handled during cell fabrication.

The separator utilized in the multiplate cells is BN cloth. This material is soaked in a solution of absolute methyl alcohol and LiCl-KCl eutectic before cell assembly. The separator is then formed on a die and dried, to form an open-ended box. One such box fits over the open face of each positive electrode, and physically separates the positive and negative electrodes. Further separation in the form of particle barriers made up of fine pore-size materials such as Y_2O_3 and ZrO_2 felts are also utilized. In addition to the above separation, a stainless steel screen forms a particle retainer around each electrode.

Considerable design effort has been expended to develop a light-weight terminal assembly for the Mark IA cell. A trade-off has been made between peak power capability and weight. Calculated values indicated that a 0.47-cm copper-cored iron terminal should give resistances in the area of 1 mΩ. In practice, resistances have been approximately 2.0 mΩ at the cell operating temperature. The size of the terminal has been increased from 0.47 to 0.78 cm, and the resistance to date appears to have been reduced to the desired range.

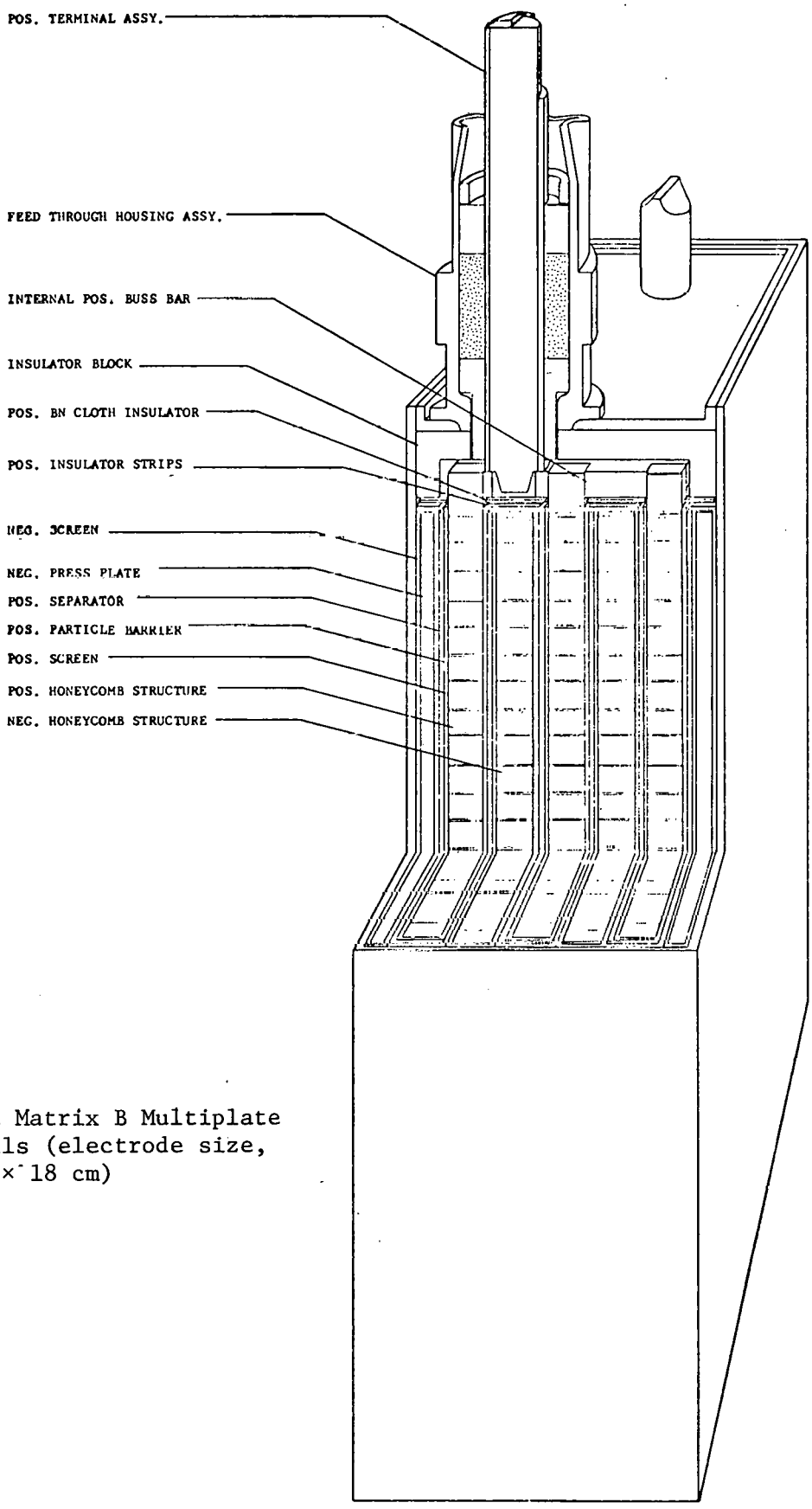

Fig. III-1. The Matrix B Multiplate Cells (electrode size, 18 × 18 cm)

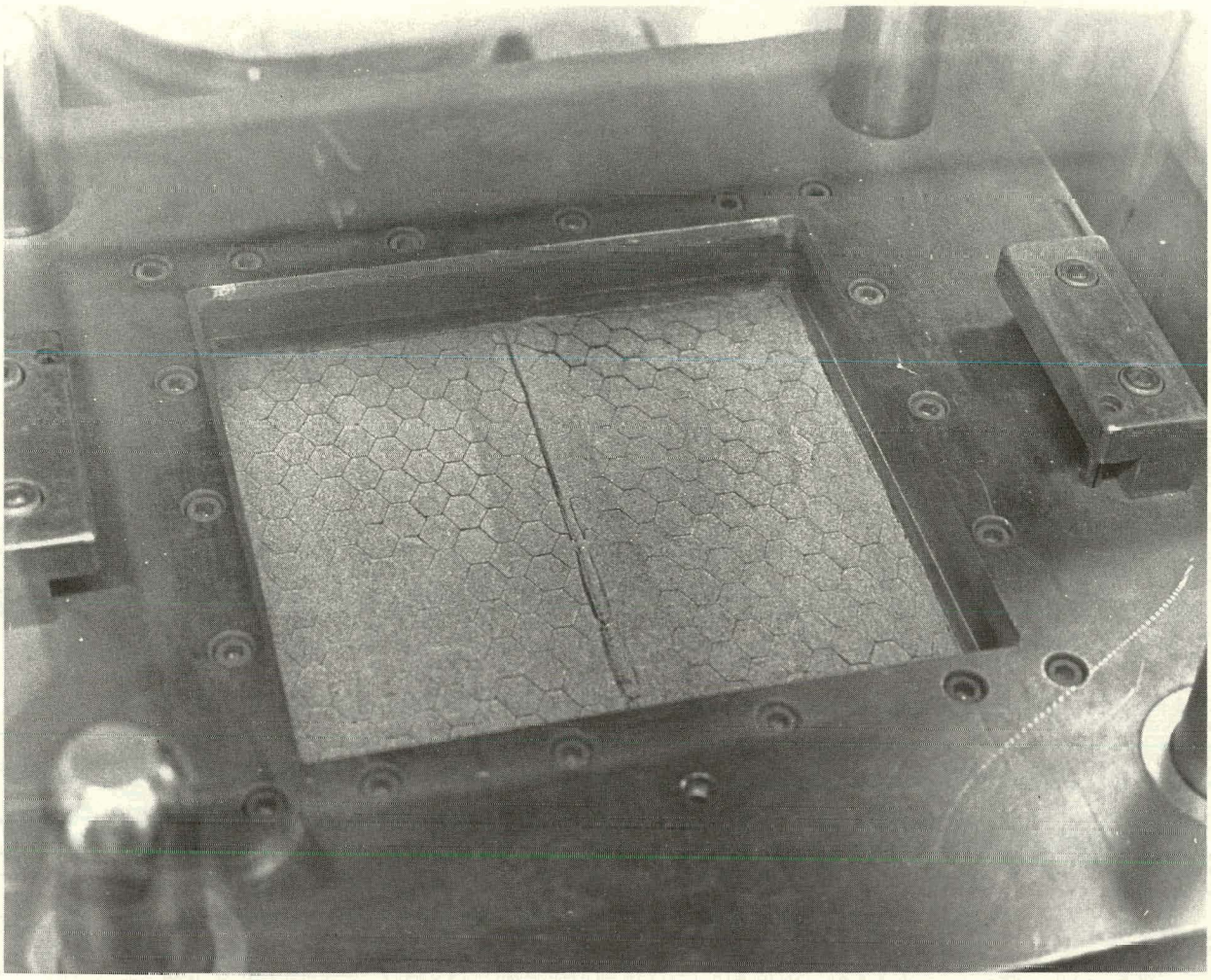

Fig. III-2. Pressed Positive Electrode

The raw materials are received, sampled, and accepted on the basis of specifications which were prepared especially for this project. Lithium-aluminum alloy, Cu_2S, FeS, and electrolyte materials must meet particle-size requirements.

The final assembly of the cell consists of stacking the appropriate electrodes and separators together, as shown in Fig. III-3, and then pushing the complete assembly into the cell container. At this point, the terminal assemblies are welded to the electrode leads, and the cover and feedthrough housing are welded in place (Fig. III-4). The feedthrough insulators are placed into the housing around the terminal, compacted, and crimped into place. The cells are then leak-checked and then filled with electrolyte.

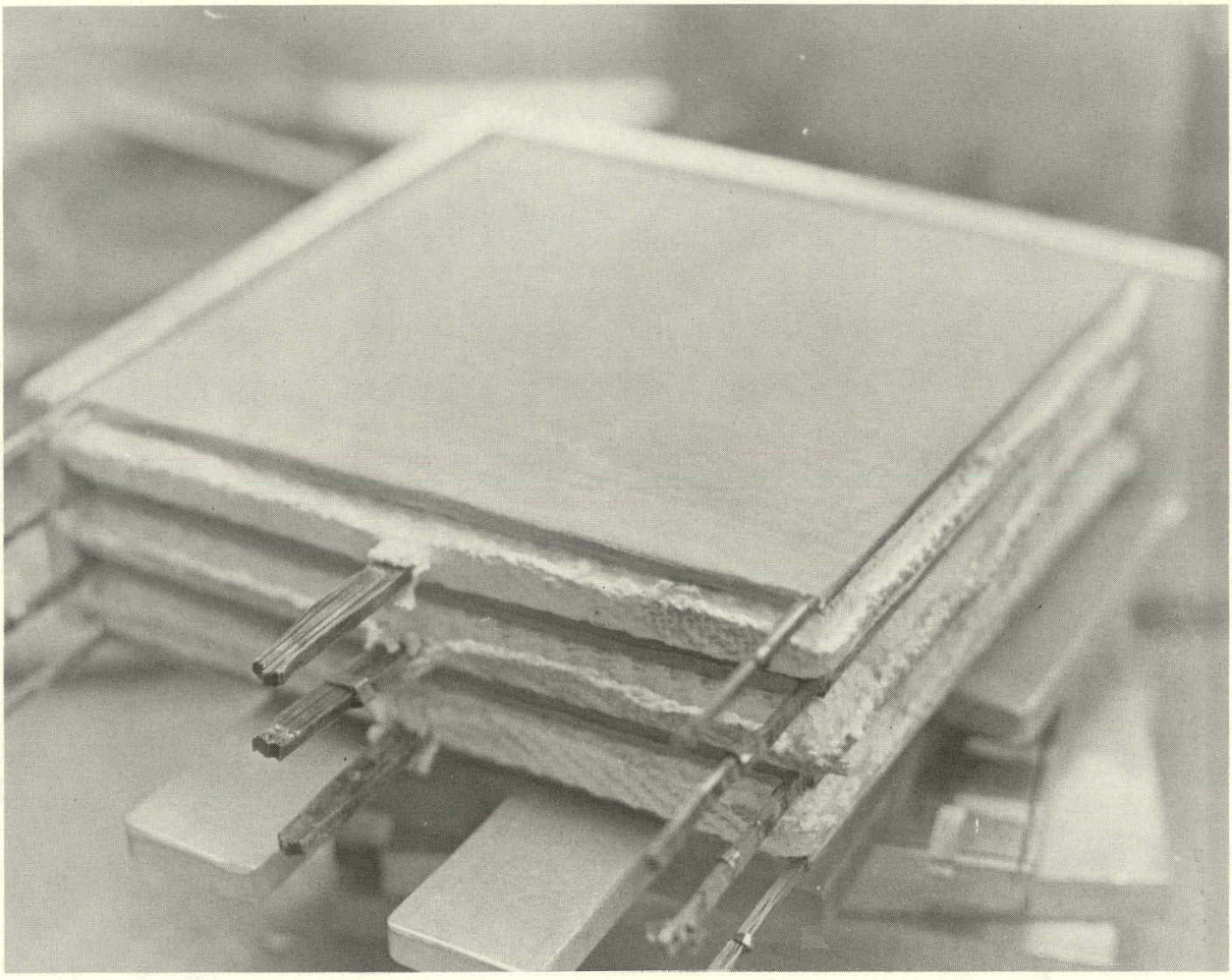

Fig. III-3. Electrodes Prior to Installation into Containers

b. Test Results of Multiplate Cells

i. Matrix A Cells

As mentioned previously, the Matrix A cells had electrode sizes of 13 × 18 cm. In general, these cells were built and tested to explore the design strengths and weaknesses of multiplate cells. In addition, various types of particle retainers and additives to the positive electrode were to be evaluated. In the Matrix A cells, the type of particle barrier and the positive active material were varied. Three types of particle barriers were used: a stainless steel screen, a stainless steel screen and ZrO_2 felt, and a stainless steel screen and Y_2O_3 felt. In addition, three types of additives to the positive electrode were tested: Cu_2S (either 10, 15, or 20 wt %), Cu powder, and $CuFeS_2$ (either 17, 24, or 31 wt %). Table III-1 lists the design variables for each Matrix A cell.

Table III-1. The Variables for Matrix A Cells

Cell No.	Capacity, A-hr		Particle Retainer[a]	Pos. Elect. Additive[b]
	Pos.	Neg.		
EPMP-5-001	405	453	--	--
EPMP-5-002	405	453	--	--
EPMP-5-003	405	453	Y_2O_3	--
EPMP-5-004	405	453	Y_2O_3	--
EPMP-5-005	405	453	--	Cu_2S(10)
EPMP-5-006	405	453	ZrO_2	Cu_2S(10)
EPMP-5-007	405	453	ZrO_2	Cu_2S(15) + Fe
EPMP-5-008	405	453	Y_2O_3	Cu_2S(15) + Fe
EPMP-5-009	354	453	Y_2O_3	Cu_2S(15) + C
EPMP-5-010	354	453	ZrO_2	Cu_2S(15)
EPMP-5-011	405	453	Y_2O_3	Cu_2S(15)
EPMP-5-012	405	453	--	Cu_2S(20)
EPMP-5-013	405	453	Y_2O_3	Cu_2S(20)
EPMP-5-014	405	453	Y_2O_3	Cu_2S(20)
EPMP-5-015	405	453	ZrO_2	Cu_2S(20)
EPMP-5-016	405	453	Y_2O_3	Cu(17)
EPMP-5-017	405	453	Y_2O_3	$CuFeS_2$(17)
EPMP-5-018	405	453	Y_2O_3	$CuFeS_2$(24)
EPMP-5-019	405	453	Y_2O_3	$CuFeS_2$(31)

[a] All particle retainers in felt form; in addition, 200-mesh SS screen was used on all electrodes.

[b] Number in parentheses indicates wt % of additive.

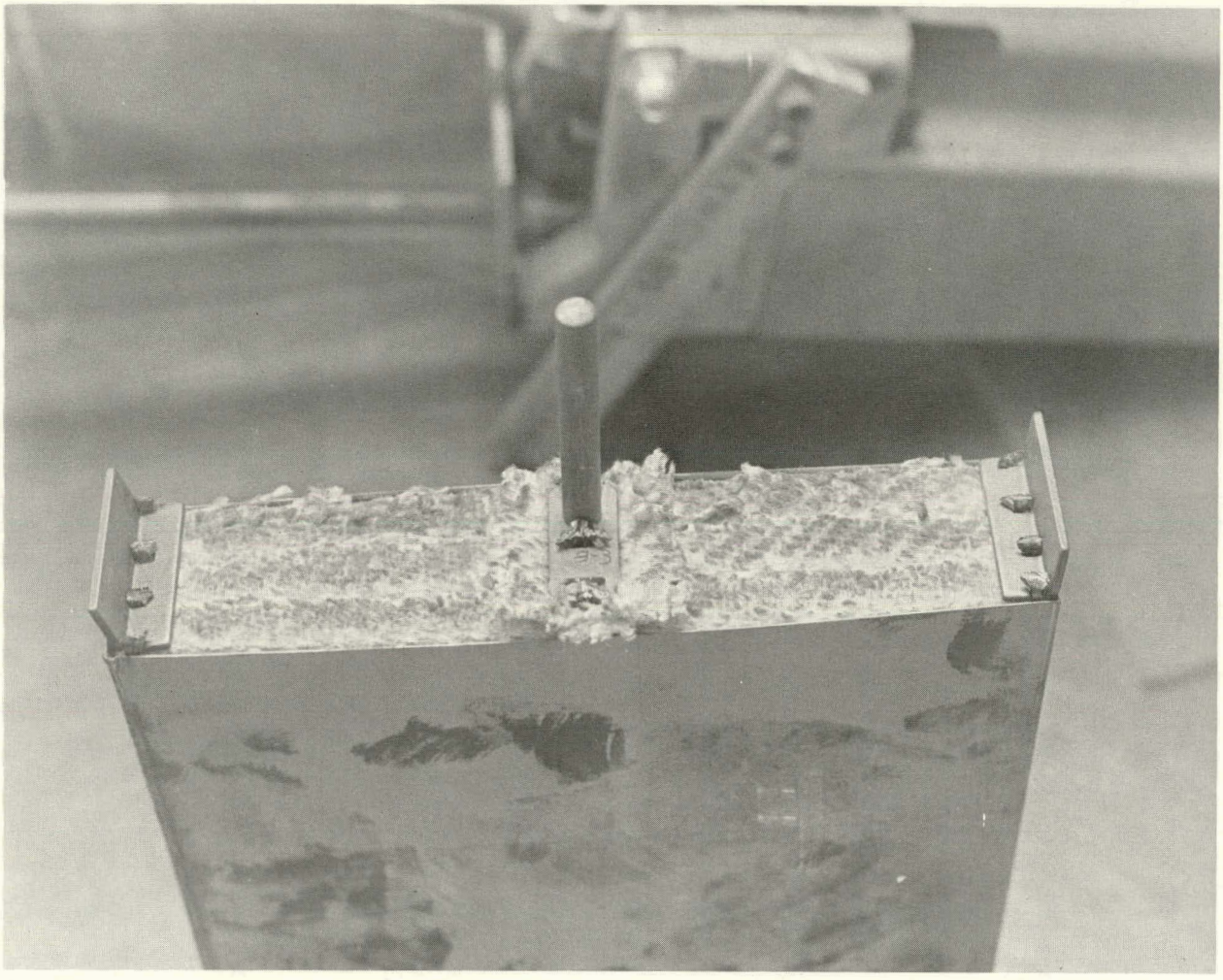

Fig. III-4. Positive and Negative Bus Welded in Place

Table III-2 presents performance data for the Matrix A cells. Due to a high failure rate on these cells caused by equipment malfunctions and other defects, a complete analysis of the test data was not possible. However, the following inferences can be drawn from the data.

For cells with no additive in the positive electrode, the utilization of the active material was very low after the initial discharge. The addition of 10 wt % Cu_2S to the positive electrode increased the utilization. These cells had stable performance for about 40 to 50 cycles, and a utilization of 60-65% after 60 cycles. The addition of 15 wt % Cu_2S to the positive electrode increased the utilization to 80% at 40 cycles. The utilization of cells with 20 wt % Cu_2S additive did not differ from that of cells with 15 wt % Cu_2S. Finally, the $CuFeS_2$ additive did not seem to have the same beneficial effect as that of Cu_2S.

Cells EPMP-5-009 and EPMP-5-010 showed high performance levels after 75 cycles, which appears to be connected with the higher negative-to-positive capacity ratios for these cells. The type of particle barrier used appears to have little significance.

Table III-2. Performance Data for Matrix A Cells

Cell No.	Max. Capacity,[a] A-hr	No. Cycles	Capacity Decline per Cycle, %
EPMP-5-001[b]	275	7	0.53
EPMP-5-002[b]	293	4	--
EPMP-5-003	257	60	0.30
EPMP-5-004	269	47	0.70
EPMP-5-005	323	94	0.29
EPMP-5-006	312	100	0.25
EPMP-5-007	340	40	0.038
EPMP-5-008	344	68	0.40
EPMP-5-009	302	75	0.133
EPMP-5-010	307	74	0.135
EPMP-5-011[b]	--	--	--
EPMP-5-012	312	8	--
EPMP-5-013[b]	--	--	--
EPMP-5-014[b]	--	--	--
EPMP-5-015[b]	321	11	0.19
EPMP-5-016	327	56	0.35
EPMP-5-017	310	125	0.20
EPMP-5-018	320	68	0.28
EPMP-5-019	310	34	0.65

[a]Measured at the 4-hr rate.

[b]Failed after only a few cycles due to equipment malfunction.

ii. Matrix B Cells

As mentioned previously, the Matrix B cells were built using the 18 × 18 cm electrodes. The Li-Al electrodes for these cells were found to warp after the cold-pressing operation; this of course causes problems with cell assembly. However, all the cells were fabricated as listed in Table III-3. These cells were constructed to assess different types of honeycomb current collectors (nickel or iron), the addition of Cu_2S (15 and 20 wt %) to the positive electrode mixture, the use of LiCl-rich electrolyte (67 mol % LiCl-33 mol % KCl), and the use of a Y_2O_3 particle retainer in addition to the stainless steel screen.

Table III-3. Variables for the Matrix B Cells

Cell No.	Theoretical Capacity, A-hr Pos.	Neg.	Positive Current Collector[a]	Terminal Rod[b]	Particle Retainer
EPMP-7-020	449	400	Fe (0.008 cm)	Fe (0.47 cm)	--
EPMP-7-021	449	400	Fe (0.013 cm)	Fe (0.78 cm)	--
EPMP-7-022	398	402	Fe (0.013 cm)	Fe (0.78 cm)	Y_2O_3[c]
EPMP-7-023	398	402	Fe (0.013 cm)	Fe (0.78 cm)	Y_2O_3[c]
EPMP-7-024	405	409	Fe (0.008 cm)	Fe (0.47 cm)	Y_2O_3[c]
EPMP-7-025	405	409	Ni (0.008 cm)	Ni	--
EPMP-7-026	405	409	Ni (0.008 cm)	Ni	Y_2O_3[c]
EPMP-7-027	405	409	Ni (0.008 cm)	Ni	Y_2O_3[c]
EPMP-7-028	405	409	Fe (0.013 cm)	Fe (0.78 cm)	Y_2O_3[c]
EPMP-7-029	405	409	Fe (0.013 cm)	Fe (0.47 cm)	Y_2O_3[c]
EPMP-7-030	405	409	Fe (0.013 cm)	Fe (0.78 cm)	Y_2O_3[d]
EPMP-7-031[e]	402	440	Fe (0.013 cm)	Fe (0.47 cm)	Y_2O_3[d]
EPMP-7-032	402	440	Fe (0.013 cm)	Fe (0.47 cm)	Y_2O_3[d]
EPMP-7-033	402	440	Fe (0.013 cm)	Fe (0.47 cm)	Y_2O_3[d]
EPMP-7-034	402	440	Ni (0.008 cm)	Fe (0.47 cm)	Y_2O_3[d]
EPMP-7-035	402	440	Ni (0.008 cm)	Fe (0.47 cm)	Y_2O_3[d]
EPMP-7-036	402	440	Ni (0.008 cm)	Fe (0.47 cm)	Y_2O_3[d]

[a]Numbers in parentheses are thicknesses of honeycomb ribbon.

[b]Numbers in parentheses are diameters.

[c]Only on positive electrode.

[d]On positive and negative electrodes.

[e]Used LiCl-rich electrolyte.

Seventeen cells were built for this test matrix. The data to date are inconclusive. Some problems with cell wetting have occurred and it is felt that many of these cells were tested in the electrolyte-starved state. However, the preliminary results from some of these cells are promising. Early data indicate the desirability of 0.013-cm iron current collectors and 0.78-cm iron terminal rods for the positive electrodes. Some indication of higher utilization of positive material has been noted in conjunction with the 20 wt % Cu_2S additive in the positive electrode and the LiCl-rich electrolyte. Table III-4 presents capacity and cycle data for Matrix B cells.

Table III-4. Cell Performance Data for Matrix B Cells

Cell No.[a]	Max. Capacity, A-hr	Capacity on Last Cycle, A-hr	No. Cycles
EPMP-5-020	295	290	>35
EPMP-7-021	331	325	>36
EPMP-7-022	315	295	>39
EPMP-7-023	313	320	>30
EPMP-7-025	320	285	>43
EPMP-7-026	301	275	>56
EPMP-5-028	320	303	>26
EPMP-7-030	358	287	>37
EPMP-7-032	--	342	>19
EPMP-7-034[b]	--	--	--
EPMP-7-035	265	265	>12

[a]Cells not listed have not yet been put into operation.

[b]Short-circuited during electrolyte filling operation.

[c]Tested at 425-430°C.

iii. Matrix C Cells

The Matrix C cells are under construction. This cell matrix contains cells having refinements over the Matrix B cells. The negative electrode has been made smaller to allow for electrode expansion after pressing the Li-Al alloy. These cells were tested to determine the effect on performance of the following design features: Cu_2S additive in the positive electrode, LiCl-rich electrolyte, Y_2O_3 particle retainers, and nickel current collectors for the positive electrode.

One of the Matrix C cells has been used in an attempt to increase separator wettability by pretreating the BN separator with lithium tetra chloro aluminate (ANL-78-21, p. 48). Although the electrolyte filling operation was successful, the cell short-circuited through the separator after being placed in operation. The remaining cells in this matrix, 24 cells in all, have not as yet been placed under test.

The last matrix of Mark IA cells will be built shortly; these cells will establish the final configuration of the Mark IA cell.

2. Development of Hardware for the Mark IA Battery
(K. Gentry, J. Miller, M. McGinty)

The objective of this portion of the Mark IA program effort at Eagle-Picher is to design, develop, and fabricate all battery-associated hardware (other than cells) for the Mark IA battery.

The goals of the Mark IA program (Table I-2) have the following order of preference: (1) operability, (2) energy storage, (3) power, (4) weight, (5) and lifetime. First and foremost, operability should be achieved. The energy storage is determined by the capacity of the cells, but the battery hardware must supply a thermally efficient, insulated container with a uniform temperature to assure optimum stored energy. The power delivered by the cells must be efficiently transferred from one cell to another and from the cells to the battery terminals; therefore, much design effort was expended to optimize the inter-cell connectors and power bus. Weight is always an important concern when trying to maximize energy storage devices in which mobility is required. The utmost care has been taken to minimize hardware weight without otherwise affecting the performance of the battery. To assure the lifetime required of the battery hardware, tests were performed on materials at operating temperature; and simulated abrasive tests were performed on the electrical insulation, a potential failure mode. High reliability materials and commercially available parts are used in the design whenever possible. Every choice of material and fabrication technique is closely analyzed.

In addition to the development program for the Mark IA battery, a 6-V battery with similar design characteristics was developed and is currently being fabricated. This battery will aid in determining battery-type controls and monitoring that will be required for the Mark IA. The information obtained in the design, development, and fabrication of the 6-V battery has been of great help in preventing major problems with the Mark IA.

a. Conceptual Design of Battery Hardware

i. Battery Case for the Mark IA Battery

To attain maximum thermal efficiency and yet minimize weight and volume, a very efficient insulation for the battery case was required. A survey of available insulations was made, and the only candidate available that would meet the thermal loss goal (300 W) was a multilayered vacuum insulation. This required a vacuum-bottle approach in which metal foil layers are placed within the vacuum space. Two available sources were solicited for the multilayered foil-insulation material, and MULTIFOIL®* was chosen. Various geometries were considered for the vacuum container design, and calculations determining weight, volume, and ease of fabrication were performed to determine the optimum configuration. Other battery case designs that were considered included: honeycomb walls, structural support (truss and membrane), and massive thick-wall single-sheet containers. These designs were all discarded for various reasons, and the final design utilized a thin-wall corrugation approach (see ANL-78-45, pp. 12-13). This resulted in a rectangular container with optimum efficiency as a battery case. Figure III-5 is a sketch of the battery case for one of the 20 kW-hr modules.

*MULTIFOIL is a registered trademark of Thermo Electron Corp., Waltham, Massachusetts.

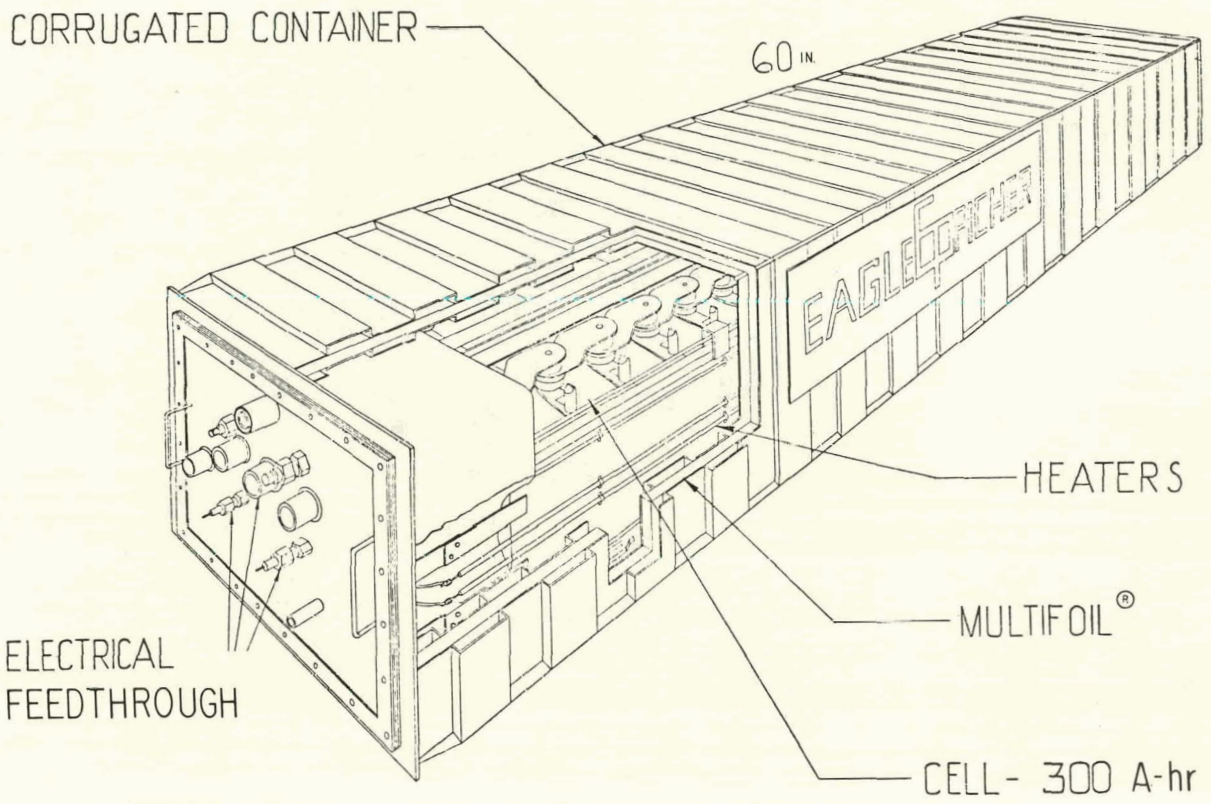

Fig. III-5. Battery Case for a 20-kW-hr Battery Module

ii. Ancillary Hardware for the Mark IA Battery

After the basic cell requirements were determined, a method of assembling and packaging 60 cells per 20 kW-hr module was determined. For a dynamic environment, the cell block must be considered as a unit to determine overall operating characteristics.

To assure adequate performance of the battery, the 60 cells must be electrically isolated from one another, yet react as a "lumped mass" for environmental (vibration and shock) inputs. This task was accomplished by assembling the cells into a tray with high-temperature electrical insulation completely surrounding each cell. Figure III-6 is a photograph of a prototype cell tray loaded with aluminum blocks to simulate the actual cell weight. This cell tray will be assembled with a prototype battery case and exposed to simulated vibrations expected in the vehicle; this test will assure mechanical structural capability.

Additional hardware development consists of selecting and testing commercially available parts for specific applications. Some of the major items are: temperature controllers, cooling fans, heaters, thermocouples, and appropriate electrical feedthroughs for battery current and voltage monitoring.

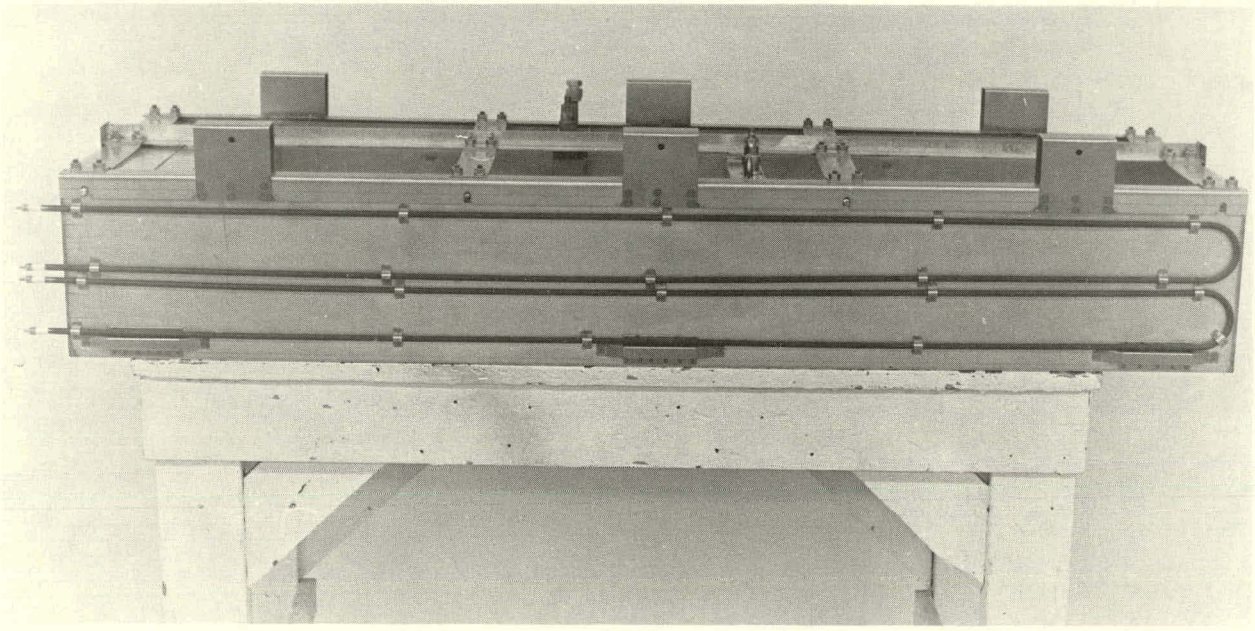

Fig. III-6. Cell Tray for the 20-kW-hr Battery Module

b. Testing of Battery Materials

Both wire insulation and cell insulation had previously been tested under separate ANL contracts. From these test data, the most suitable insulation for the Mark IA was chosen. These insulation materials were chosen based on hundreds of hours of tests at operating temperature, and were determined to be the best choice for their required application. Once the materials were received at Eagle-Picher, they were used in actual cell testing. These materials have now accumulated over a thousand hours of test, and appear to be adequate as presently designed.

Adhesive ceramics have also been tested and a candidate chosen for use in battery assembly of electrical insulation parts.

For the application of temperature control and monitoring, the K-type thermocouple was chosen for its superior performance and expected life at battery operating temperature and under possible oxidizing atmospheres. Even though the battery compartment is to be maintained under an inert atmosphere, the K-type thermocouple was determined to be superior to other types of thermocouples. Thermocouple penetration feedthroughs were also studied, and tests comparing the accuracy of temperature measurement by various approaches were performed. The tested approaches include straight K-type thermocouple wire, K-type thermocouple-feedthrough conductors, and hermetic gold-plated copper terminals. The results of these tests indicated that a temperature fluctuation of a maximum of 2°C existed under the worst-case conditions tested. The hermetic feedthrough copper conductor, with an expected accuracy within ±1°C, was chosen for thermocouple wires. This accuracy is well within the allowable limits.

c. Testing of Battery Hardware

To support various design requirements, it was necessary to conduct tests of battery hardware, including cell trays, temperature control and fail-safe equipment and heat-exchanger equipment.

To aid in the design of cell tray and cell end-plate restraints, a test was constructed to determine forces exerted by a restrained cell. Data obtained were used in stress calculations for materials of the cell tray.

As the need for support equipment became necessary, various temperature controlling devices and fail-safe equipment became a system requirement. The temperature control within the battery requires both heating and cooling depending upon the load (*i.e.*, driving profile imposed on the battery). After the necessary equipment had been designed and fabricated, equipment check-out was performed. A test oven was used to simulate the battery operating environment and various driving profiles. In every case tested, the equipment performed as designed. This equipment may be used in the 6-V battery and the 40-kW-hr battery.

To aid in design of the heat exchanger within the battery, a thermal test station was fabricated to determine various efficiencies of the heat exchanger. Both smooth-tube and finned-tube applications were tested, and data were obtained for use in final hardware design. Figure III-7 is a photograph of the thermal test oven.

A major requirement of operability of the battery lies in the ability to control the temperature within each individual battery module during all phases of the charge/discharge cycle. A thermal management scheme was initiated to determine the thermal effects on the battery hardware of various cell reactions. From information obtained on reversible heating ($T\Delta S$) and cooling effects and calculations made for irreversible heating (I^2R), along with anticipated ambient losses of the system, a mathematical model was constructed to determine the temperature profile due to these heating and cooling effects (see ANL-78-45, pp. 14-15). The program was structured with battery current *vs.* time as the variable input, and the response is the battery mean temperature *vs.* time. This design tool has been and will continue to be used for design of various components of the battery hardware.

d. Support Contracts

Two industrial firms, Budd Co. and Thermo Electron Corp., were contracted by Eagle-Picher to aid in the completion of the tasks required for the development of the 40-kW-hr battery. The contract with Budd Co. involves design analysis and vibrational testing of a 20-kW-hr module. The contract with Thermo Electron Corp. involved the design and fabrication of the insulated battery case for the Mark IA.

3. Six-Volt Battery

A 6-V battery was also included in the statement of work for the Mark IA battery program. This battery design and fabrication program has aided in defining fabrication techniques for all battery-associated hardware in the Mark IA. Fabrication of the 6-V battery hardware preceded fabrication of the hardware for the prototype 20-kW-hr module; and valuable fabrication experience was gained in container welding and thermal-insulation wrapping.

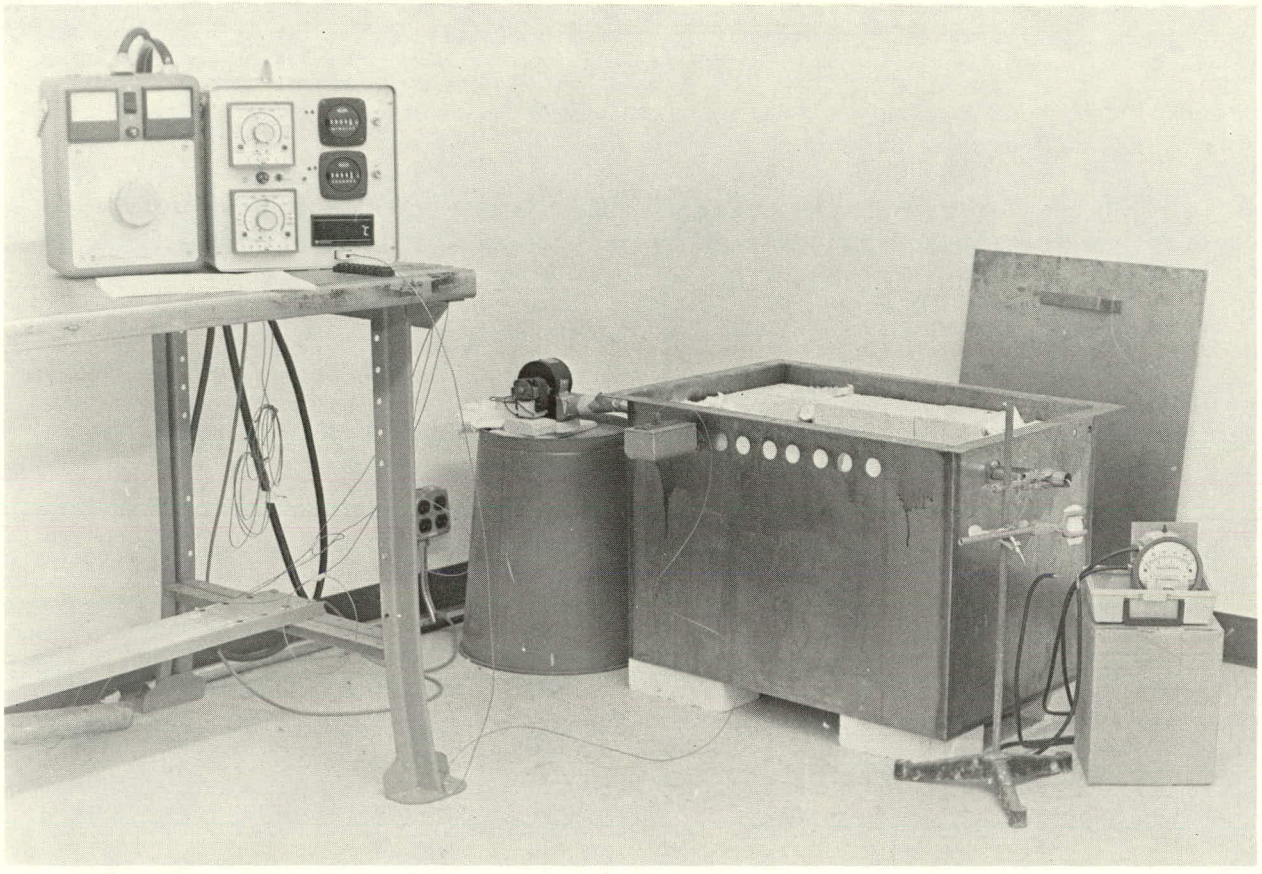

Fig. III-7. Thermal Test Station

Tests of this battery planned at Eagle-Picher include battery thermal and electrical performance, as well as response to vibrations. Testing of the hardware for the 6-V battery will be completed by the end of October 1978, with delivery to ANL scheduled for early in November 1978.

4. Cell Vibration Testing
(C. Farris, J. Miller, R. Grimm)

One of the major goals of the cell development effort at Eagle-Picher is to test the ability of lithium/metal sulfide cells to withstand road vibrations. Goals of this effort included testing cells, analyzing data, and making adjustments to cell design as required to survive expected vibrations in electric-vehicle applications.

Test results indicated no harmful or undesirable effects to the cell's electrochemical reactions. The cell hardware was able to withstand the vibration levels imposed upon the cell, and much information was obtained on the necessity of and effects on electrical insulation, both on the cell and on the electrical wires.

a. Cell Design Characteristics and Manufacturing Techniques

The cell chosen for initial vibration tests was a Li-Al/FeS_2 bicell (Type I8 series cells, ANL-78-21, p. 21). This cell configuration, suggested for test by ANL, was chosen to determine the effects of vibrations on the molybdenum to molybdenum weld joints of the electrodes. Other design features of the Type I8 cells included the following: continuous molybdenum ribbon from the bottom of the honeycomb current collector to the top of the tab bundle, 100-mesh molybdenum screen on positive electrode, no ZrO_2 cloth particle retainers, no BN insulator electrode, and a particle barrier of stainless steel 165-mesh screen.

These cells were constructed primarily to reduce the ratio of hardware to active material and thereby increase the specific energy.

A low activated resistance was found to exist in a number of these Type I8 cells. Table III-5 lists the activated resistance of the cells in this series. Various cells with low activated resistances (both cells that had been cycled and cells that had not been cycled) were sectioned, and in all cases positive active material was found to have migrated through the particle retainer screen. Tests were then conducted on Type I8 electrodes in electrolyte baths, and it was determined that active material was being washed out of the electrodes by the electrolyte during the electrolyte-filling operation. This effect was more pronounced in positive electrodes than in negative electrodes.

Table III-5. Activated Resistances of Type I8 Cells

Type I8 Cell No.	Electrolyte Weight, g	Activated Resistance,[a] Ω
EP-021	198	160
EP-022	170	320
EP-023	189	0.4
EP-024	174	40
EP-025	245	0.1
EP-026	247	20,500
EP-027	255	5,000,000
EP-032	364	2.6
EP-033	369	0.4
EP-028	299	1.0
EP-029	219	3.2
EP-030	306	0.6
EP-031	372	100
EP-034	309	3,000,000

[a]The unactivated resistance of all these cells was infinity.

Subsequently, replacement cells for the defective Type I8 cells were built with the following design features to prevent the escape of active material from the positive electrode: a positive particle barrier of 150-mesh molybdenum screen, FeS_2 sieved to -40 to +150 mesh, Y_2O_3-felt particle barriers on both positive and negative electrodes, BN insulator electrodes, and particle barriers of 115-mesh stainless steel screen. Figure III-8 shows a schematic drawing of these replacement cells.

b. Vibration Testing and Equipment

Vibration testing was completed at Eagle-Picher's Environmental Laboratory. Equipment used is shown in Fig. III-9, and includes a Ling Model 275A Exciter, a Ling Model PP60/80 power supply, and an instrumentation console for controlling and monitoring the vibration levels. The cells were under constant surveillance with a charge/discharge cycler and voltage and current recorder during vibration testing.

The cell was placed in the test fixture and bolted to a mounting plate (see Fig. III-10). Under the mounting plate are three layers of Transite for heat insulation between the oven and the shaker head. The Transite is cut so as to fill as much of the oven as feasible. A cell mounting plate was bolted through the Transite to the aluminum vibration plate, and the aluminum plate was then bolted to the shaker head in such a way as not to allow a direct heat path from the oven area to the shaker head.

The power leads for the cell were four-gauge asbestos insulated wire, and the voltage monitoring leads were sixteen-gauge high-temperature insulation wires being considered for battery usage. A braze joint was utilized at the cell terminals to minimize contact resistance (see Figs. III-11 and -12).

The cells were vibrated at a level of 0.63-cm (0.25 in.) displacement amplitude (5-16 Hz) and 1.5 g (16-50 Hz), with a sweep time of 7.5 min. This level was continued until 1.37×10^6 vibrational cycles were accumulated on the test specimen. This fulfilled the minimal requirement of 1×10^6 cycles. Vibration was performed on a schedule of approximately a 4-hr cell discharge (17 A) and no vibration during the approximately 8-hr charging mode (9 A). Table III-6 shows the cell cycling schedule during vibration. This table summarizes the vibration/electrical sequencing of the cells.

c. Results of Vibrational Tests

A total of 1.37×10^6 vibrational cycles were accumulated on the cells; this is equivalent to over 12 years of expected road life. Several problems were encountered during the vibration cycles, but none were related to cell operation. Failures experienced during the vibrations were all in the lead wires on the shaker. The problems were attributed to oxidation of the copper conductors, insulation being torn away, or brittleness of the wire due to braze material wicking. These problems were solved and the last three runs were without failures.

Results of this testing indicate that the lithium/metal sulfide cell will withstand the vibrations due to road usage of the test vehicles. As noted above, the failures experienced were in the lead wires, and much design effort has been expended to assure that the battery will not have wires attached or supported in the same manner. The brazed wire joints and the routing of the wires have been designed to eliminate problem areas.

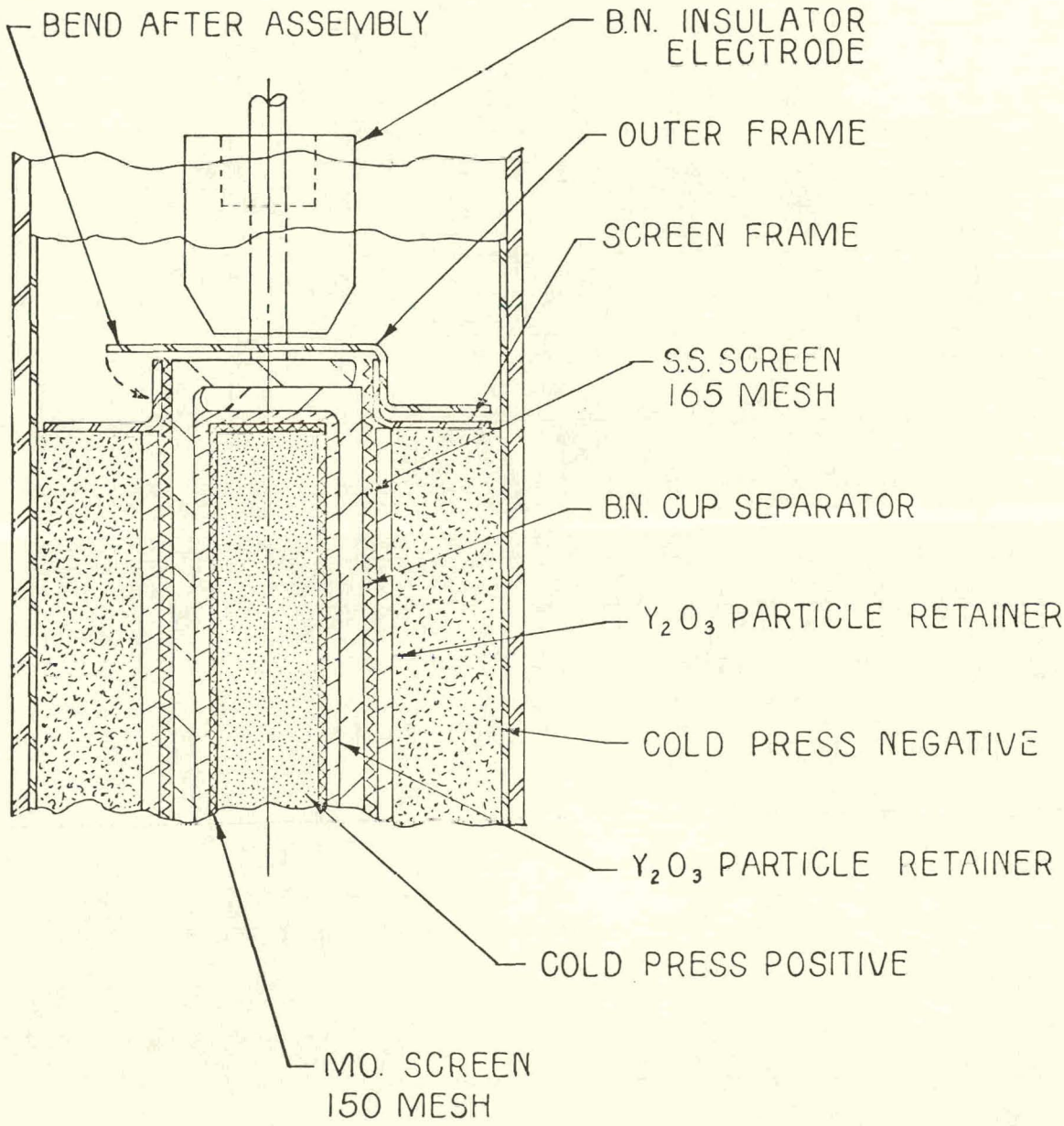

Fig. III-8. The Type-I8 Replacement Cell Design

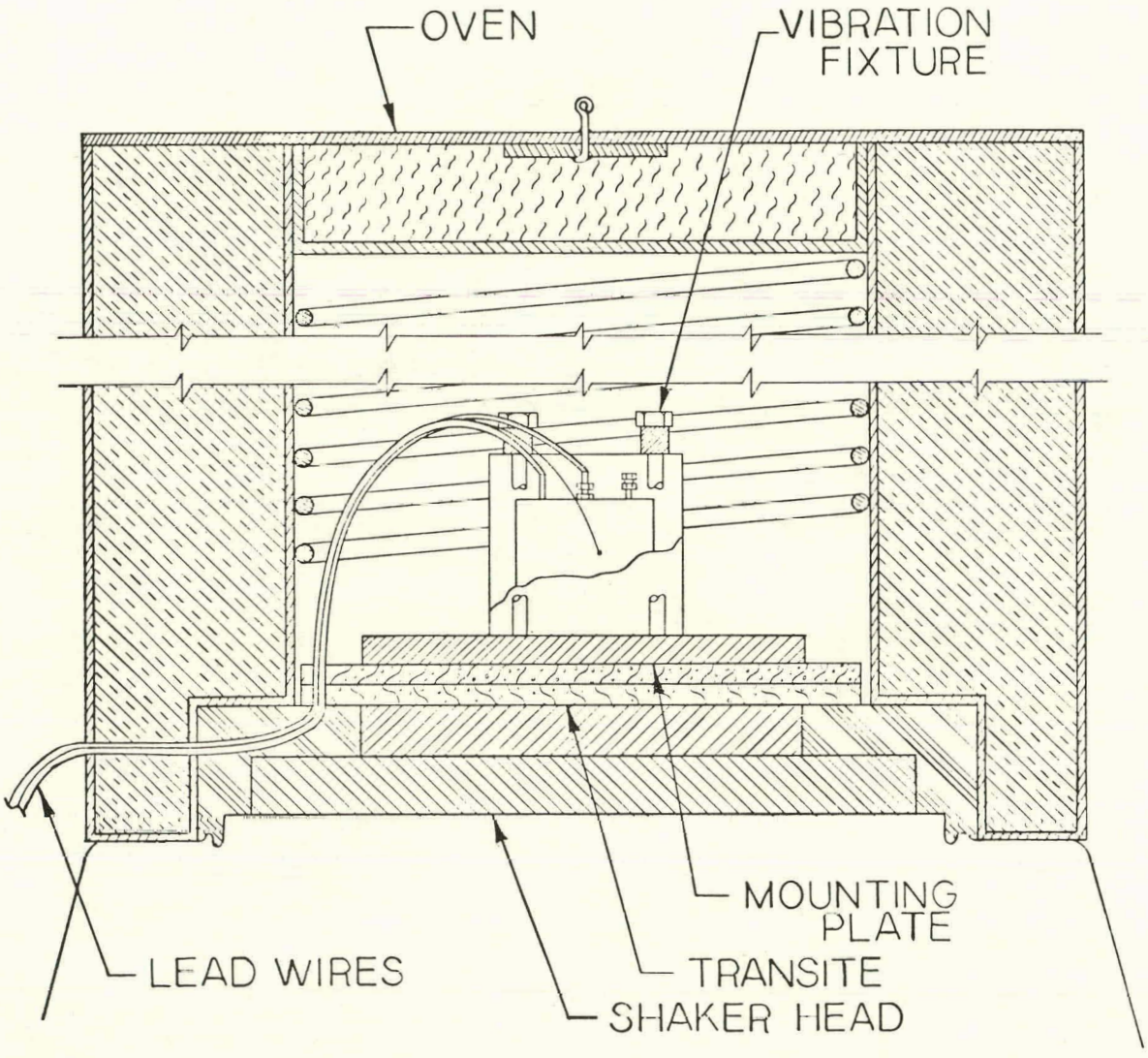

Fig. III-9. Equipment for Cell Vibration Tests

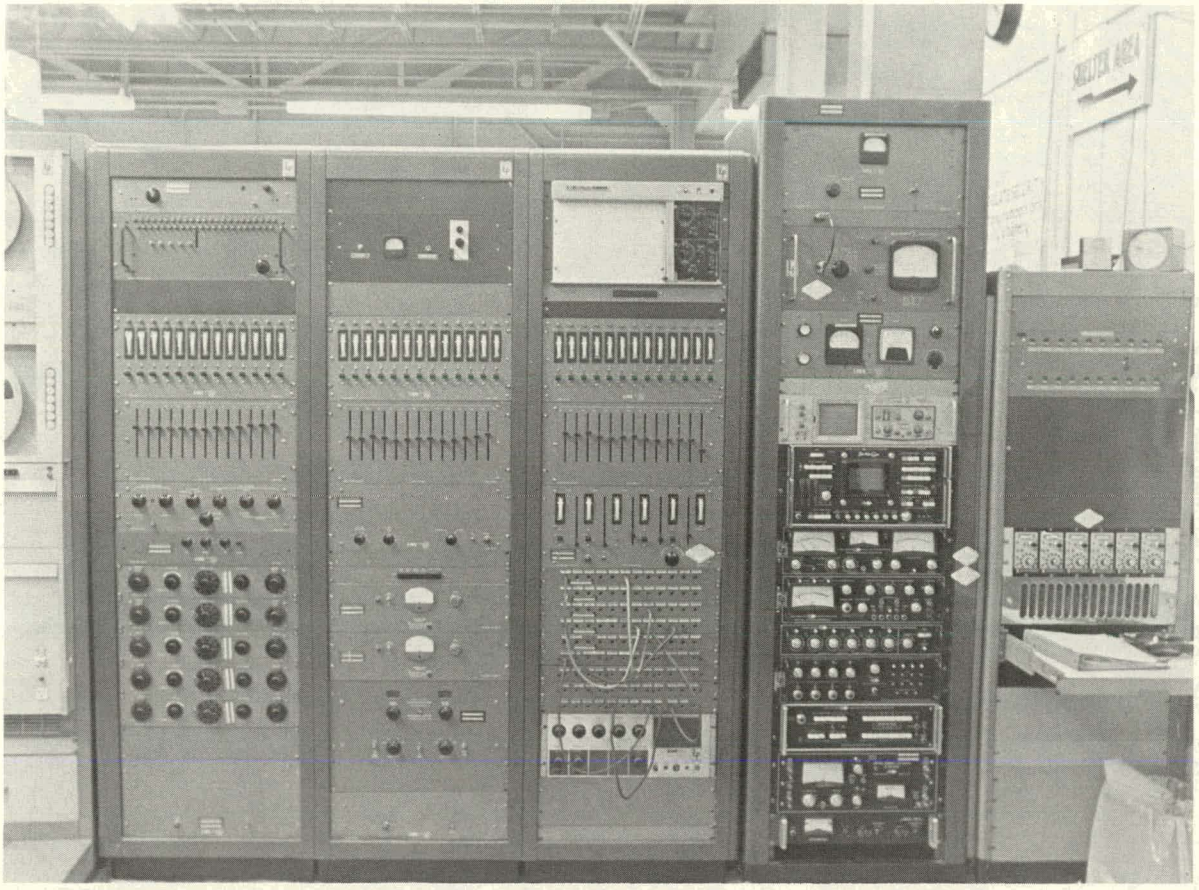

Fig. III-10. Vibration Test Control Equipment

Fig. III-11. Vibration Cell Electrical Connections

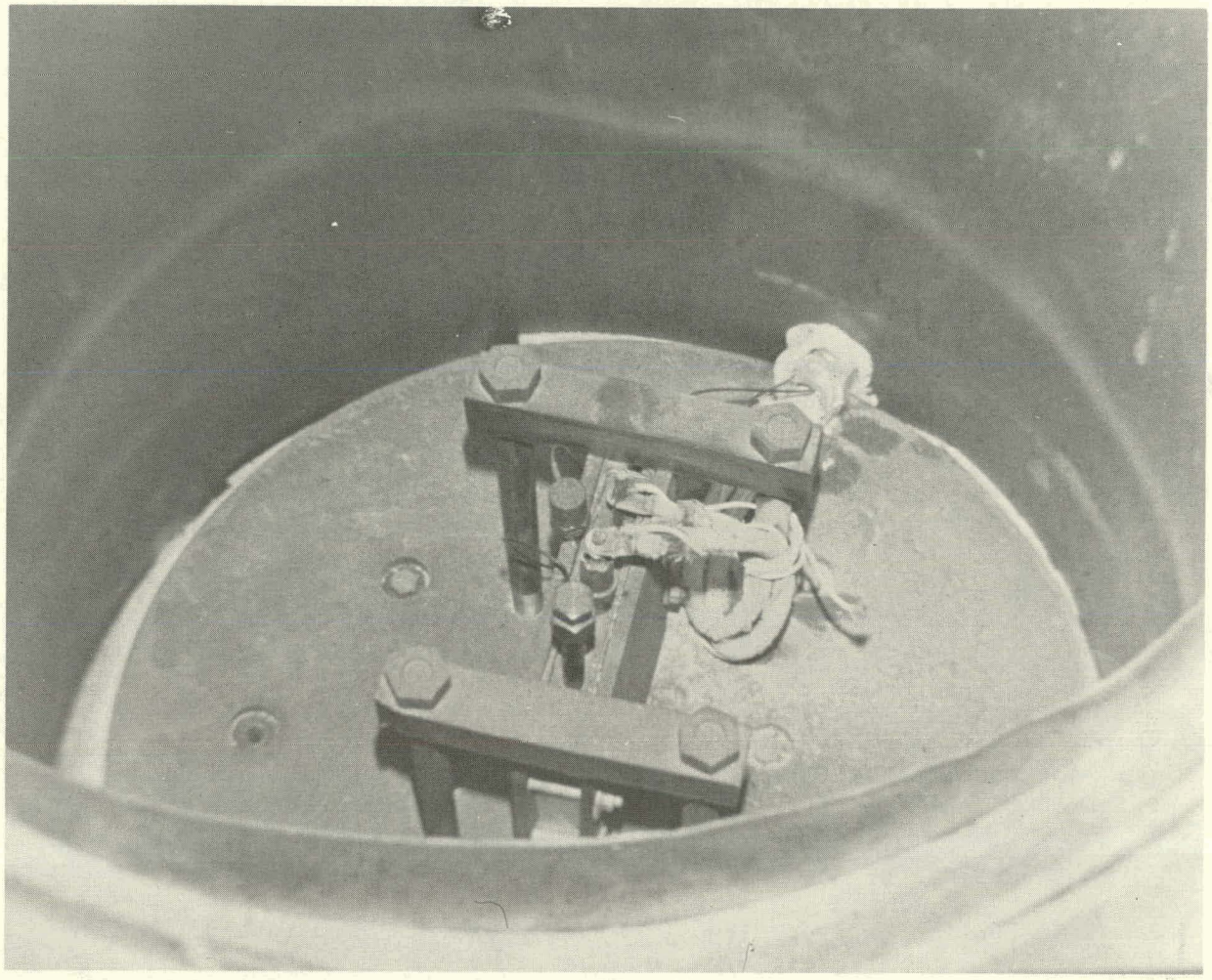

Fig. III-12. Vibration Cell in Test Oven on Ling 275A Exciter

Table III-6. Cycling Schedule during Vibrations

Type I8 Cell No.	Cycle No.	Capacity on Last Cycle, A-hr	Vibration
EP-035	1-34	67.75	No
	35-36	66.6	Yes
	37-89	55.9	No
	90-92	57.6	Yes
	93-100	65.3	No
EP-036	1-15	86.89	No
	16-18	61.80	Yes
	19-148	46.6	No

B. Gould Inc.

The development effort at Gould has been directed toward (1) the fabrication and delivery of upper-plateau* Li-Al/FeS_2 bicells, (2) development of Li-Al/FeS multiplate cell designs, (3) development of improved Li-Al/FeS cell designs, cell components, and performance characteristics, (4) development of electrode fabrication processes suitable for mass manufacturing, and (5) the expansion and improvement of cell test facilities.

The lithium/metal sulfide battery program at Gould Inc. has been managed by Mr. R. J. Rubischko since mid-1975. A total of nine professionals and technicians have been assigned to the program. The program is supported by various analytical and shop service groups. The Li/MS Program is organized to function as a team on major tasks with the primary responsibilities for specific items assigned to the individuals. Mr. L. W. Eaton, Project Engineer, is responsible for overall cell design and fabrication, tooling, and positive electrode development. Mr. E. J. Chaney is responsible for separator fabrication and development, seal development, facilities, and special cell testing. Dr. F. Marikar is responsible for the post operative analysis of cells, materials evaluation, and negative electrode development. Mr. R. E. Thompson is responsible for cell life-testing, data analysis, and computer modeling. Mr. Y. B. Assaf is responsible for quality assurance, documentation, and material procurement and control. Mr. T. E. Hickman is responsible for test facility design and installation. Mr. H. Kramer, Mr. S. Lockwood, and Mr. N. Luna are technicians who have the responsibility for fabrication, assembly, inspection and testing of components and cells.

1. Upper-Plateau Li-Al/FeS2 Test Cells

About 55 upper-plateau Li-Al/FeS_2 bicells were fabricated from September 1977 to December 1977. At that time they represented the largest single set of lithium alloy/metal sulfide cells fabricated. The Gould cells were assembled in accordance with previously defined specifications, helium-leak checked, filled with electrolyte, electrochemically formed through two cycles of charge and discharge, coated with high-temperature paint, and delivered to ANL for testing. The primary problem encountered in the assembly of these cells was the welding of molybdenum current-collector components. Several design modifications were required to improve the quality of the welds which were failing due to embrittlement of molybdenum during welding. Problems were also encountered during the electrolyte filling operation. These problems were related to the heating system of the fill-formation facility and were not associated with the cells. This equipment has since been modified and improved. The final upper-plateau FeS_2 cells were delivered to ANL by early-February 1978. The testing of these cells is being carried out at ANL (see Section IV.A.3).

2. Development of Li-Al/FeS Multiplate Cells

As a part of the Li-Al/FeS development effort, a multiplate cell design was developed during September-October 1977. Detailed drawings and specifications were delivered to ANL at that time. The multiplate cell configuration is shown in Fig. III-13. Two prototype multiplate cells were

*These cells are operated only on the upper of two voltage plateaus that are characteristic of FeS_2 cells.

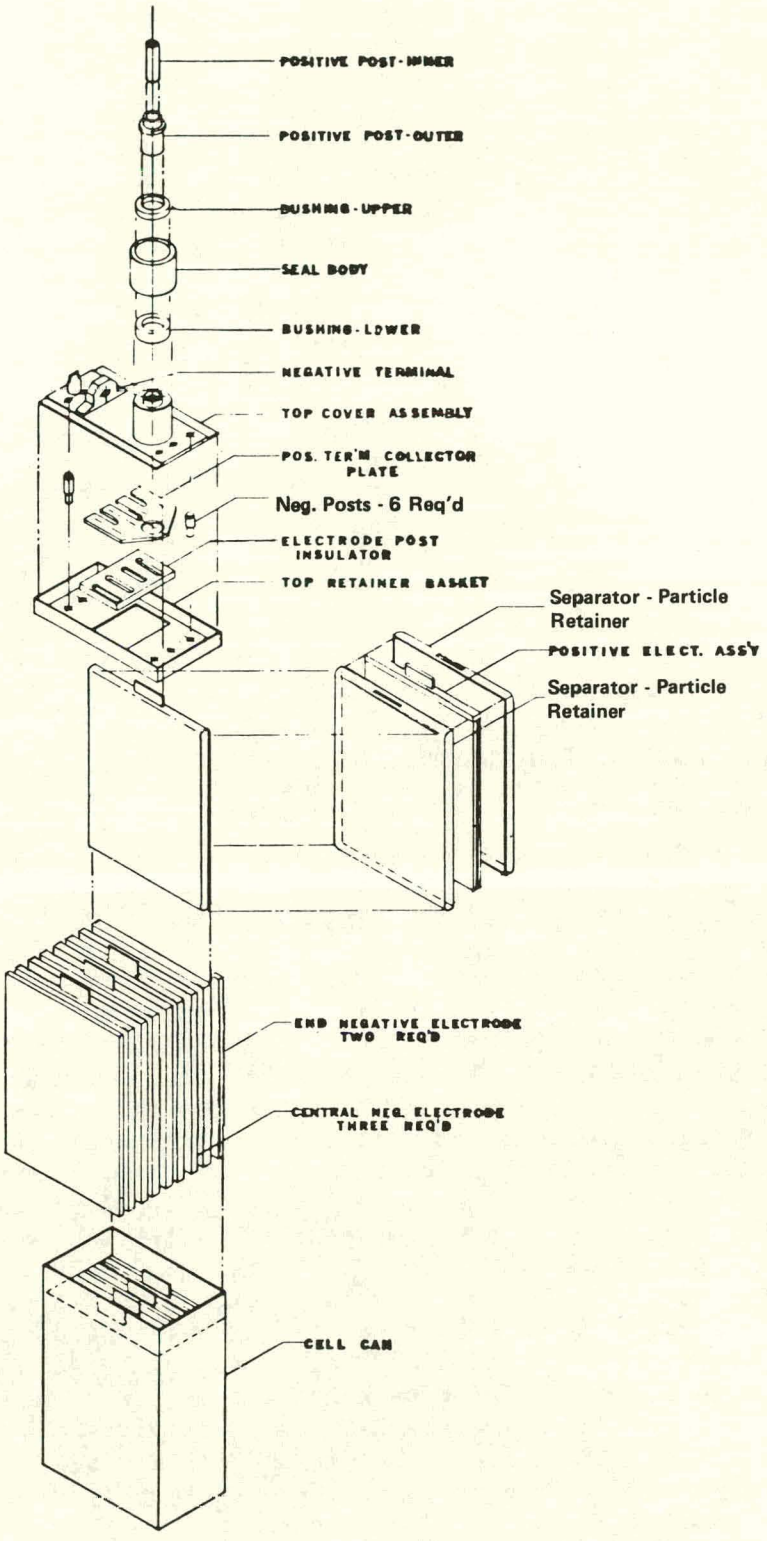

Fig. III-13. Multiplate Cell Design

fabricated after a design review held at ANL in November 1977. The first cell failed during the formation cycles due to the insufficiency of added electrolyte. A second cell was assembled and placed on test at Gould early in March 1978. This is the first multiplate Li-Al/FeS electric-vehicle cell operated successfully at Gould. The cell weighed 6.5 kg and had a theoretical capacity of 535 A-hr. It was tested through 43 cycles (over 1150 hours) until a faulty container weld caused about one third of the electrolyte to drain away from the cell. The cell was discharged at various currents, the highest current being 100 A (58 mA/cm^2). The specific energy was ∿52 W-hr/kg at 100-A discharge and ∿90 W-hr/kg at 40-A discharge currents. The performance characteristics were essentially identical to those of a similar bicell, X-9. The resistance of the multiplate cell, based upon current interruptions, was 0.8 mΩ at t = 0 sec and 1.1 mΩ at t = 15 sec. Further development of multiplate cell designs will follow the demonstration of reliable performance in bicells using BN-felt separators.

3. Development of Li-Al/FeS Bicells

The Gould effort for Li-Al/FeS cell development has been directed toward (1) the design of cell components and development of fabrication techniques that will enable a high rate of production at low cost while maintaining technical reliability, and (2) the evaluation of electrode composition and porosity as well as separator form and configuration. The effects on cell operation of electrode and separator operating characteristics need to be identified to optimize cell performance. Rigorous evaluation of the effects of varying positive electrode formulation, negative electrode fabrication and composition, and fiber density of separator material requires a formidable number of cells. Within the scope of the current project, considerable care had to be devoted to untangling the cross effects of modifications in the cell design.

The initial FeS cells (see Fig. III-14) consisted of a single positive electrode compacted with a current collector consisting of 100 g of expanded metal in 24 layers, a 125-μm (5 mil)-thick iron sheet, and a 0.6-cm (0.25 in.)-dia iron rod. These cells also had two hot-pressed Li-Al negative electrodes containing iron current collectors. The electrode separator and particle retainer were made of BN cloth and ZrO_2 cloth, respectively. The cell can was made of 0.058-cm (0.023 in.)-thick 1010 steel and had a heavy, bulky seal. The recent cells have two positive half-slabs of active materials sandwiched between a current collector of 0.0325-cm (0.013 in.) nickel sheet topped with a bus bar. This electrode is wrapped with a 250-mesh stainless steel screen. A shoebox-type screen basket holds a separator of nonwoven BN-felt face sheets and side strips around the positive electrode; the two negative electrodes, which were hot pressed from alloy powder, have no current collector. The cell uses Li-rich electrolyte and the cell can is made of either 304 stainless steel or 1010 steel. The seal is small, simple, and weighs only 60 g. The logic behind the evolutionary process in cell design, as well as the problems encountered and the solutions that emerged are all discussed in the following section.

Appendix A presents the engineering characteristics of the forty Li-Al/FeS bicells (the X series) built to date. The table summarizes the important design parameters along with information on positive material utilization, cell resistance, specific energy, and cycle life.

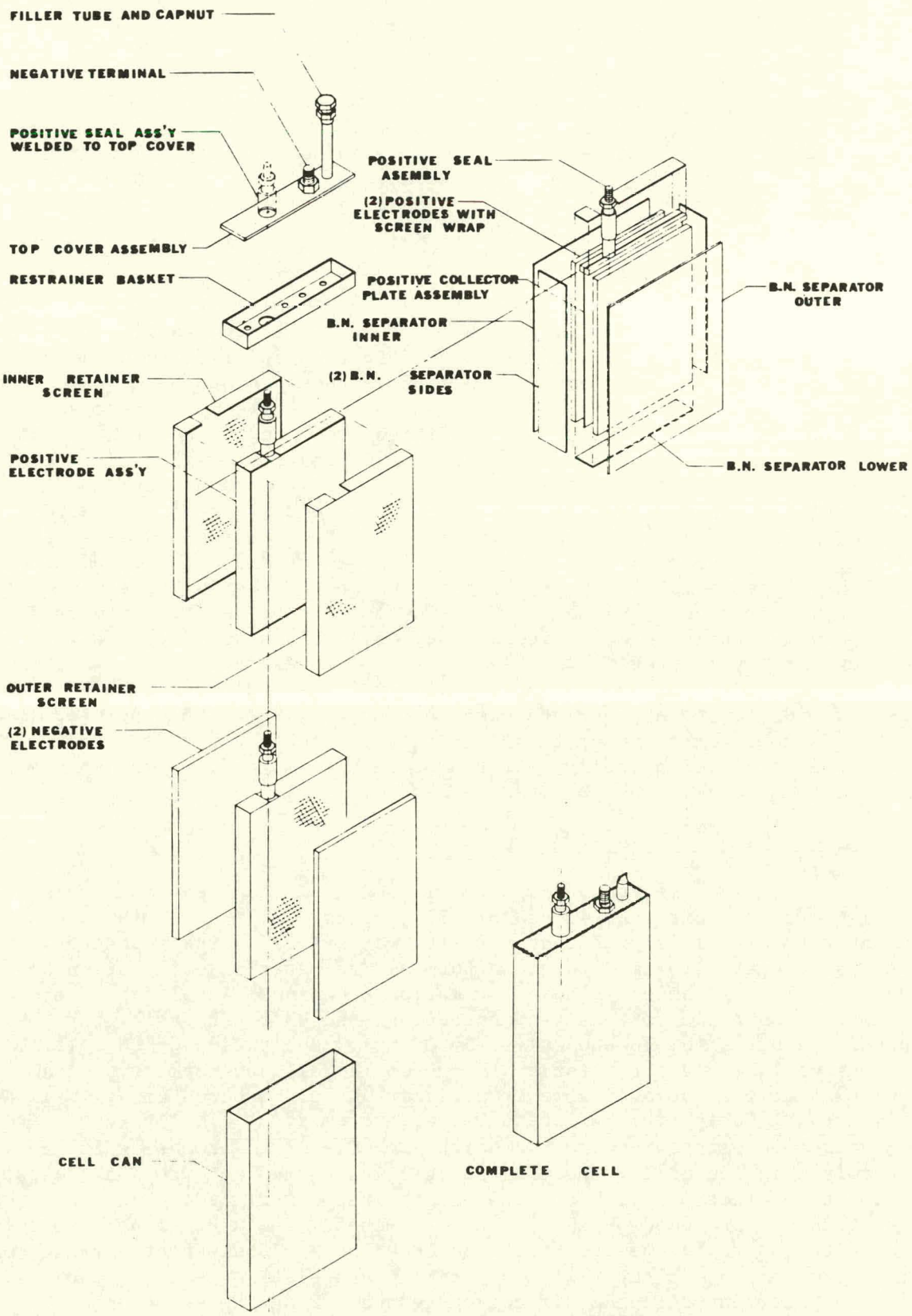

Fig. III-14. Schematic Drawing of a Li-Al/FeS Bicell

a. Cell Design and Separator Development

The objective of this effort is (1) the development of improved cell hardware configurations which result in increased cell specific energy, reduced cell impedance and low cost, and (2) the development of improved fabrication techniques which lead to increased reproducibility and reliability, increased productivity (reduced labor input), and low cost. In the evolutionary process towards these goals, four chronological phases of development were identified.

i. Phase I

It was realized early in the first phase of cell development that the several layers of X-met used in the positive and negative electrodes constituted an underestimate of the conductance of the electrode active materials. The removal of the expanded metal greatly simplified electrode fabrication and cell assembly, and permitted the sandwiching of a 0.0058 cm-thick-1010 steel sheet between the hot-pressed positive half slabs. Cells assembled in this manner showed a decrease in resistance measured by current interruption (at t = 0 and t = 15 seconds). Attempts were also made during this period to replace the expensive ($250/m^2) ZrO_2 cloth used as a particle retainer with low-cost carbon felt. These attempts did not succeed since the electrolyte would not wet the carbon felt even after pretreatment with electrolyte solutions. Since the hot pressing of the negative electrode is not amenable to high rates of production, discussions were begun with the Aluminum Company of America (ALCOA) to attempt to extrude a 5 wt % Li-Al alloy. As a test of this approach, slabs of 4.56 wt % Li-Al alloy with nine machined ribs (to provide the appropriate electrode spacing) were incorporated in cell X-7. This represents one of the first attempts to incorporate a solid lithium alloy in an engineering cell. After a dozen cycles, cell operation was terminated, and the cell was examined.

ii. Phase II

Separator cups fabricated from BN woven cloth were used in all the experimental Li-Al/FeS bicells, up to X-9. The use of a cloth separator results in significant porosity variations in the separator, and this was suspected to lead to nonuniform active-material utilization and increased cell resistance. Also, fabrication techniques involving BN cloth cups were unsuitable for mass manufacturing, and BN cloth was by far the most expensive single item in the cells ($5900/m^2). Evaluation of BN felt configurations was the highest priority in the Gould cell development program. Since BN felt was not available from either ANL or Carborundum Co.,* it was fabricated at Gould from BN fibers salvaged from scrap cloth pieces. The felt was pretreated with an aqueous solution of LiCl-KCl to promote wetting by electrolyte in the cell. The treated felt was formed into two half cups, and the positive electrode with the ZrO_2 cloth wrap was placed in the shoe box-type structure produced by mating the half-cups. The use of these felt cups along with the replacement of the iron sheet by a nickel-sheet current collector (selected for its superior conductivity and electrochemical stability) was the most important design modification tested during the second phase.

---

*Contracted by ANL to fabricate BN felt (see Section VII.B).

The fabrication of the felt cups is an extremely difficult process and was not satisfactory even as a temporary measure. (The first multiplate cell, GIII-2, assembled during this period was built using the more familiar cloth cups.) The next step in separator development was to evaluate the potentially less expensive sheet separators. Cell X-11 which employed 5.25 wt % Li-Al alloy extrusions purchased from ALCOA limited the capacity of the negative electrode on discharge (determined by a LiAl reference electrode). Metallographic examination of the extruded material indicated that the distribution of the lithium-ion-conducting β-LiAl phase was in the form of isolated island-like platelets rather than as an interconnected network in the α-matrix as observed in the cast material. Under these circumstances, a multiplate cell was constructed using negative electrodes of compacted 8.18 wt % alloy powder, the only innovation being hot pressing without electrolyte. This fabrication technique has produced reliable negative electrodes which have never shown any discharge limitation, even against the best of the positive electrodes.

Concurrent with these design changes in negative electrodes and separators were experiments to improve positive-material utilization, an important parameter in achieving high specific energy. Increasing the iron content in the positive electrode to twice the stoichiometric amount in Cell X-21 resulted in a significant increase in utilization at high rates of discharge. The performance improvements seen in X-21 were surpassed significantly in Cell X-22 where the excess iron, carbon and cobalt additives were employed in conjunction with the use of a LiCl-rich electrolyte* (49 wt % LiCl). Cell X-22 was the first engineering cell to demonstrate nearly 100% positive utilization at up to a 30-mA/cm^2 current density. Some of the performance characteristics of this cell are listed in Table III-7. Cell X-22 had a typical resistance of 2.8 mΩ at t = 0 sec and 3.3 mΩ at t = 15 sec. Cell X-22 had, in addition to the 100% excess iron, 5 wt % cobalt

Table III-7. Performance Data on Cell X-22

Current, A		Coulometric	Sulfur	Specific
Charge	Discharge[a]	Eff., %	Utilization, %	Energy, W-hr/kg
3	3 (7.0)	100	100	89
10	10 (23.3)	99	100	87
10	15 (34.9)	--	99	84
10	20 (46.5)	--	97	82
10	25 (58.1)	--	88	73
10	25 (58.1)	100	86	70

[a]Number in parentheses indicates discharge current density in milliamperes per centimeter squared.

*Recommended by ANL investigators as a means of limiting the formation of the utilization-restricting "J-phase" ($LiK_6Fe_{24}S_{26}Cl$).

and 5 vol % carbon; the importance of these additives will be discussed in a later section. In addition to attaining high electrochemical efficiency, X-22 also was the first cell to employ felt-sheet separators. These felts were fabricated at Gould and pre-treated with LiCl-KCl in the manner previously described. After some 30 cycles of operation (about 750 hr) the cell developed a short circuit. Post-operational analysis revealed that migration of active material in one of the BN junctions at the bottom of the cell was the cause of the failure.

iii. Phase III

A closer examination of the feasibility of using dense, solid negative electrodes was undertaken during this phase. The experience gained earlier pointed to the possibility of using sliced slabs of cast material, and five cells were made with 6 wt % Li-Al in the slab form. In these cells, the negative electrode limited discharge capacity, and the low lithium content of the alloy was thought to be responsible for this behavior. Slabs machined from an 8 wt % alloy were used in the next five cells, but the problem persisted. It is now surmised that a blocking layer of some sort at the negative/electrolyte interface is responsible for impeding ion transport. A study of this phenomenon has been deferred until the positive-electrode felt separator has been optimized.

In order to contain the active material at the positive electrode edge, we used a thin metal "U" channel around the electrode. Positive electrodes framed with edge channels prefabricated from a 1010 steel strip (1.25-cm wide and 0.023-cm thick) were used in Cells X-26 through X-40. None of these cells operated for more than ten cycles. Post-operative analysis revealed that the most frequent mode of failure was the crushing of the separator between the shoe-box screen basket and the rigid, inflexible edge channels, probably during cell assembly. Other solutions had to be sought for the edge-containment problem.

Cell X-25 was built to assess Y_2O_3 felt as a separator. The cell had a very short life and post-test examination revealed partial penetration of the separator by the screen basket in several locations and a short circuit on the separator face wider than 2.54 cm. Such extensive penetration of the separator has never been encountered with Gould-fabricated felt or Carborundum-fabricated BN cloth. The Y_2O_3 felt was found to have poor compressive strength (the nominally 0.1-cm and 0.2-cm thick felts required typically 94.5 and 161 kPa, respectively, to be compressed to half their thickness) and practically no resilience. When compressed to their half thicknesses, the Y_2O_3 felts crumbled, and it is questionable whether the material can be handled successfully in any cell.

iv. Phase IV

In the current stage of the development program we are evaluating the effectiveness of a 250-mesh stainless steel wrap around the positive electrode; this wrap serves as a particle retainer and edge container. In addition, BN felt* is being evaluated as separators. Initial experiments have shown that the sprinkling of $LiAlCl_4$ on these felts, as

*Fabricated by Carborundum Co. (fiber density, 30-60 mg/cm^2).

recommended by ANL (see ANL-77-68, p. 42), promotes wetting by electrolyte in the cell. Cell X-34 had a separator fabricated of BN felt (45-mg/cm^2 fiber density). A single layer of felt was used for each electrode face, without any supporting ZrO_2 cloth. Post-operational analysis of this cell identified a short circuit caused by loss of separator in at least one region. The separator thickness was typically 0.05 to 0.075 cm as compared to the usual thickness of 0.1 cm used with Gould felts of 60-mg/cm^2 density.

A priority of the fourth phase is the reduction of the excess iron used in the positive electrode of Cells X-22 and X-21. It is possible that the ideal amount of excess iron is above 10 wt %, far below the 100 wt % used in X-21 and X-22. A reduction of the excess iron will result in significant improvements in specific energy. Cells are currently being assembled or tested to evaluate BN-felt separators treated with $LiAlCl_4$, and limited excesses of iron powder in the positive electrode.

b. Positive Electrode Development

Analysis of the effect of positive electrode design on cell specific energy led to the recognition of the importance of attaining high positive-material utilization at high current densities. The improvement of positive utilization was allocated a priority second only to the separator development. Figure III-15 shows the positive utilization achieved in some of the Gould cells as a function of current density, and Table III-8 describes the positive electrode design.

Cell G-II-03-003, one of the first Gould-fabricated FeS bicells, used considerable amounts of copper sulfide. This additional metal sulfide in the positive electrode resulted in an increase in utilization, but it was feared that the fairly soluble, readily reducible copper ions might have a detrimental effect on cell life. Testing of the later cells (X-9, -21, and -22) showed that small quantities of cobalt and carbon (XC-72 Cabot Black) when present together in the positive mix are even more effective than copper in improving the utilization. The curve for Cell X-9 in Fig. III-15 clearly shows this improvement. The multiplate cell, GIII-2, which also had cobalt and carbon added to the positive electrode, showed essentially identical utilization to the bicells with this additive.

Another important finding was that an excess of iron in the positive electrode raised the utilization even further. Cell X-21 shows the benefits gained by preparing the discharged positive electrode with twice the stoichiometric amount of iron powder. The best results obtained thus far have been in Cell X-22. In this cell, the addition of cobalt, carbon, and excess iron to the positive electrode was supplemented with the use of LiCl-rich electrolyte. The utilizations achieved in this cell are the highest for Li-Al/FeS engineering cells operated at Gould to date.

Cells are being built at present to optimize the composition of the electrolyte and to minimize the excess iron, or to substitute it with other elements in limited amounts to escape the weight penalty suffered in using large excesses of iron.

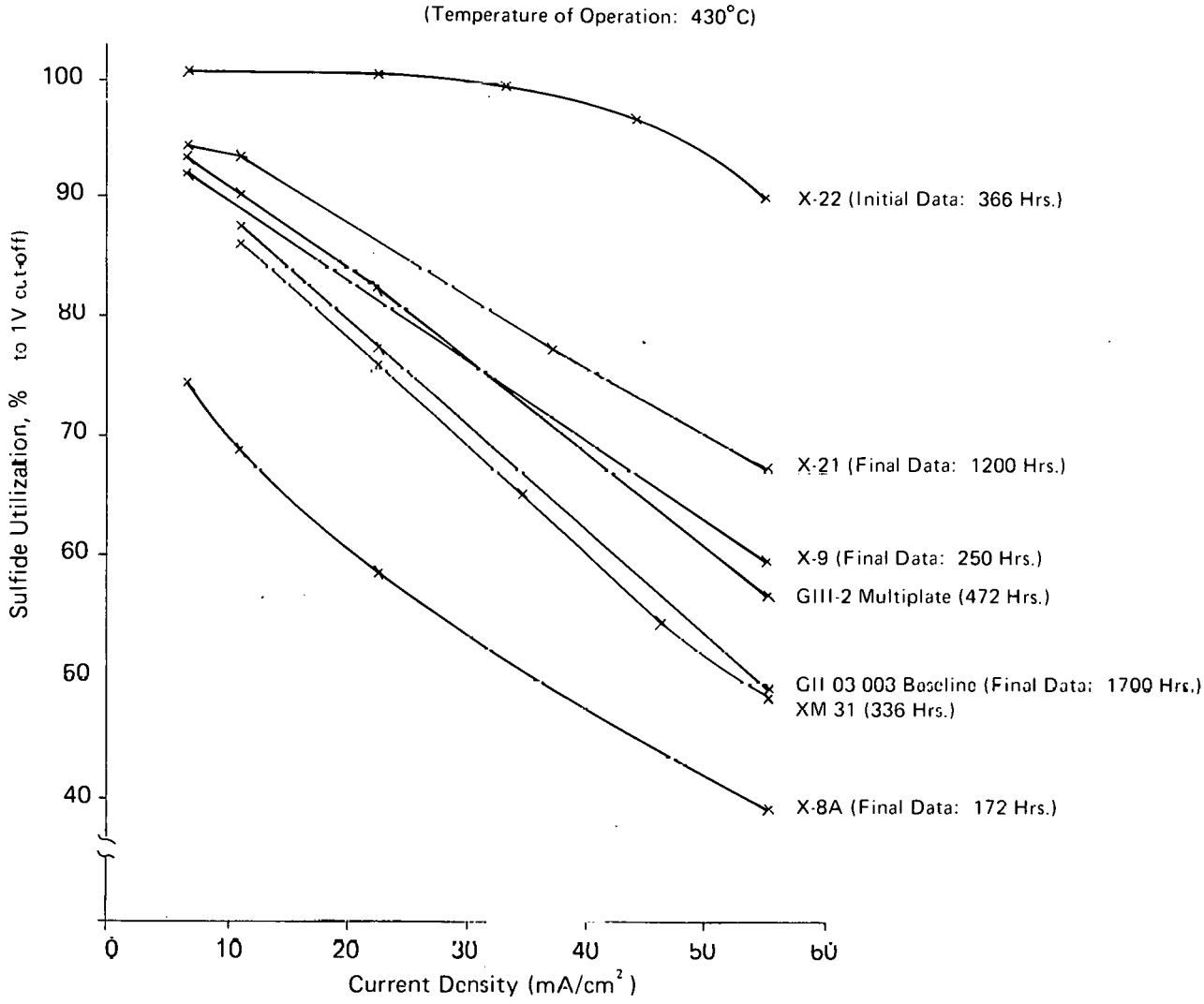

Fig. III-15. Positive Utilization as a Function of Current Density for Seven Gould Cells

Table III-8. Positive Additive Optimization of Li-Al/FeS Cells

Cell	Electrolyte, wt % LiCl	Additives[a] C, vol %	Co, wt %	Excess Fe, wt %	Cu, wt %	Pos. Util.,[b] %
X-8A	44.2	--	5	10	--	39.5
X-31	53.3	3	--	100	--	48.4
GII-03-03	44.2	--	--	10	11.2	50.0
GIII-2	44.2	5	5	10	--	57.2
X-9	44.2	5	5	10	--	60.0
X-21	44.2	5	5	100	--	67.9
X-22	49.5	5	5	100	--	89.5

[a]Volume percent of active mix minus salt; wt % of stoichiometric amount of active iron.

[b]Measured at 59 mA/cm^2.

c. Negative Electrode Development

As in several other battery systems, the negative electrode is associated with lower material weight per unit capacity and is logically the source of excess capacity. In view of the importance of improving positive utilization, the Gould effort has avoided building FeS cells in which the capacity is likely to be limited by the negative electrode.

The focus of negative-electrode improvement under these circumstances has been on the use of dense, solid negative structures ultimately aimed at production by extrusion of Li-Al. Sliced slabs of cast Li-Al alloy with machined ribs, ALCOA extruded sheet, and sawed slabs of cast material (compositions ranging from 4.6 to 8.2 wt % lithium) were employed as negative electrodes in engineering cells. Using Li-Al wire reference electrodes, solid structures in this composition range suffered serious polarization on discharge. No such limitation was found with negative electrodes of hot-pressed powder. In the early Gould cells, 4.6 wt % Li-Al powder electrodes compacted with electrolyte performed satisfactorily. However, as the utilization of the positive electrode increased, greater utilization of the negative electrodes was required. Evidence from the ANL testing of Gould upper-plateau FeS_2 cells (see Section IV.A.3) has indicated that negative-electrode limitation occurs at 8 wt % lithium. Thus, it was decided that compacted negative electrodes of 8 wt % Li-Al powder be used in experimental cells. The charged composition of these negative electrodes is set at 17 to 18 wt % Li by design. Since it is believed that the upper limit for extrusion of LiAl is about 5 wt % Li, the solid-extrusion approach has been abandoned. Powder rolling is now being considered as a technique for mass manufacturing.

d. Current Collector Development

The baseline cell GII-03-003 had several layers of X-met embedded in both the electrodes for the purpose of current collection. The conductance of the negative electrode was not improved by the X-met and negative current collectors were eliminated in the early X-series cells. No increase in cell resistance was found when the X-met in the negative electrodes was removed. The X-met current collectors in the positive electrodes were also removed, and a central iron sheet (0.058-cm thick) sandwiched between simple slabs of positive material was substituted. This substitution led to a decrease in cell resistance.

The improvement in the cell resistance characteristics caused by lighter, more efficient current collector systems is shown in Table III-9.

Table III-9. Development of the Current-Collector System for Li-Al/FeS Cells

Cell	Current Collector System		Resistance,[b] mΩ	
	Material[a]	g/A-hr	t = 0 sec	t = 15 sec
GII-03-003	Fe (0.0125)	1.89	4.5	5.4
X-8A	Fe (0.058)	1.06	3.2	3.9
X-20	Ni (0.032)	0.61	2.7	3.3
X-21	Ni (0.032)	0.63	3.0	3.5
X-24	Ni (0.032)	0.44	3.4	4.2
X-40	Ni (0.032)	0.69	2.5	3.0
GIII-2[c]	Ni (0.032)	0.77	0.8	1.1

[a]Numbers in parentheses indicate thickness of sheets in centimeters.

[b]Measured at a 50% depth of discharge.

[c]Multiplate cell design.

The measurements of the cell resistance are made utilizing well defined current-interruption measurements of the cell impedance. The cell resistance diagram in Fig. III-16 was constructed on the basis of such data for a cell with a BN-felt separator (0.15-cm thick, 60 mg/cm^2), and at 50% charge. Measurements of the resistance at cell-operating temperature of the inactive metallic components are also included in this figure. Studies of this nature indicated that a considerable saving in weight is possible by substituting 0.032-cm thick nickel sheet for 0.058-cm thick iron sheet, thereby exploiting the higher conductivity of nickel. Bicells currently being made employ a nickel sheet topped with a bus bar as the positive current collector; the cell can provides negative current collection. Bicell X-40 demonstrated the best resistance characteristics achieved thus far, the measured resistance in the half-charged state being 2.5 mΩ at current interruption and 3.0 mΩ 15 sec later.

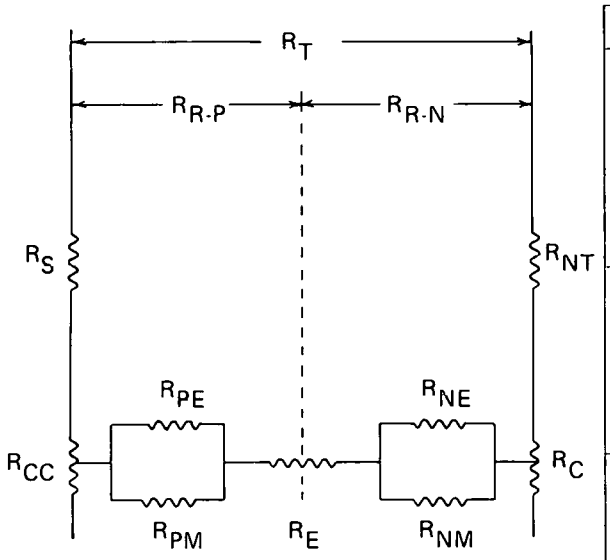

	Resistance of	Symbol	Value
Measured	Total Cell	R_T	2.7 mΩ
	Reference - Positive	R_{R-P}	2.5 mΩ
	Reference - Negative	R_{R-N}	0.2 mΩ
	Seal	R_S	0.86 mΩ
	Current Collector	R_{CC}	0.4 mΩ
Calculated	Electrolyte	R_E	0.29 mΩ
	Negative Material	R_{NM}	<0.05 μΩ
	Negative Electrolyte	R_{NE}	∿ 2mΩ
	Positive Electrolyte	R_{PE}	2.1 mΩ
By Difference	Positive Material	R_{PM}	2.31 mΩ
	Container + Negative Terminal	$R_C + R_{NT}$	∿ 0.05 mΩ

Fig. III-16. Gould LiAl/FeS Bicell Resistance Diagram

e. Post-Operative Analysis

Efficient communication of the results of post-operative analysis is a crucial part of the cell development program. For this analysis, the cell is sectioned at room temperature and these sections are carefully examined by photomicrography. Other relevant details recorded during post-test analysis include the average thickness of the separator, the extent of wetting by the electrolyte, and the presence or absence of electrolyte in various parts of the cell.

A post-operative cell diagram is shown in Fig. III-17 for bicell X-34. The resistance of the cell at room temperature as well as that of the sawed sections provides information on the effectiveness of material containment. The location in the cell and approximate areas that are the subject of low-magnification photomicrography are indicated by P_x. The photographs, usually obtained at 10X magnification, are of immense value in documenting design faults and other peculiarities.

Figure III-18 presents some of the common modes of cell failure determined by the post-operative analysis at Gould. These include rupture of the separator causing a short circuit, penetration of the separator by the negative screen, crushing of the separator between the positive edge channel and the negative screen, and escape of positive active material through the separator.

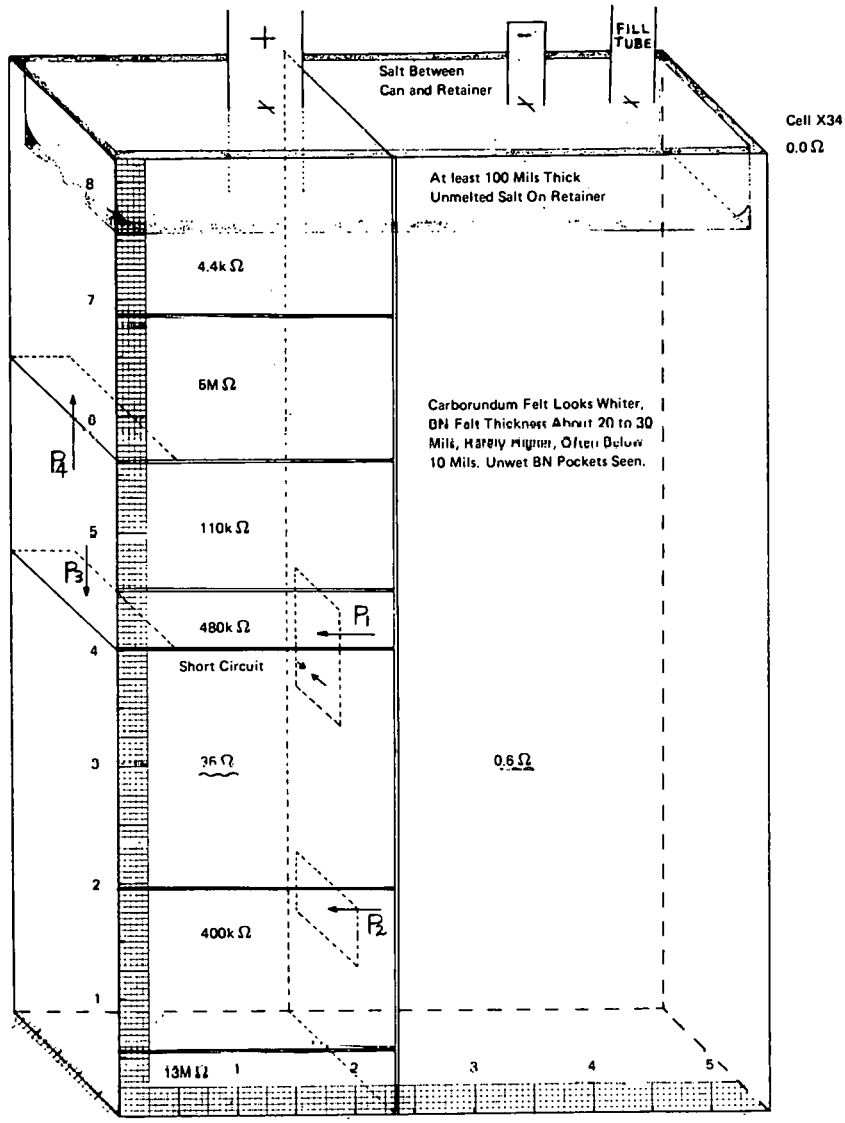

Fig. III-17. Diagram of a Post-Operative Cell (P_x indicates the location of available photographic record)

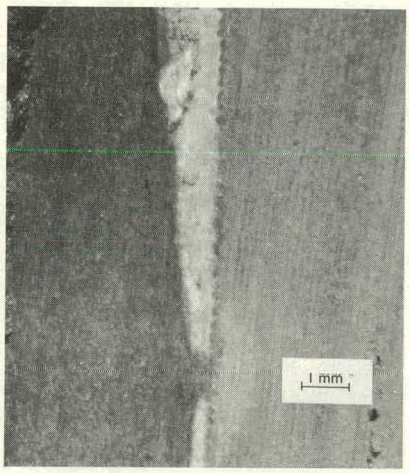

a. Separator discontinuity.

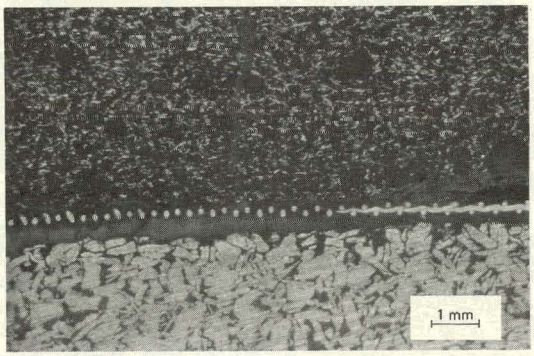

b. Negative screen migration to positive electrode.

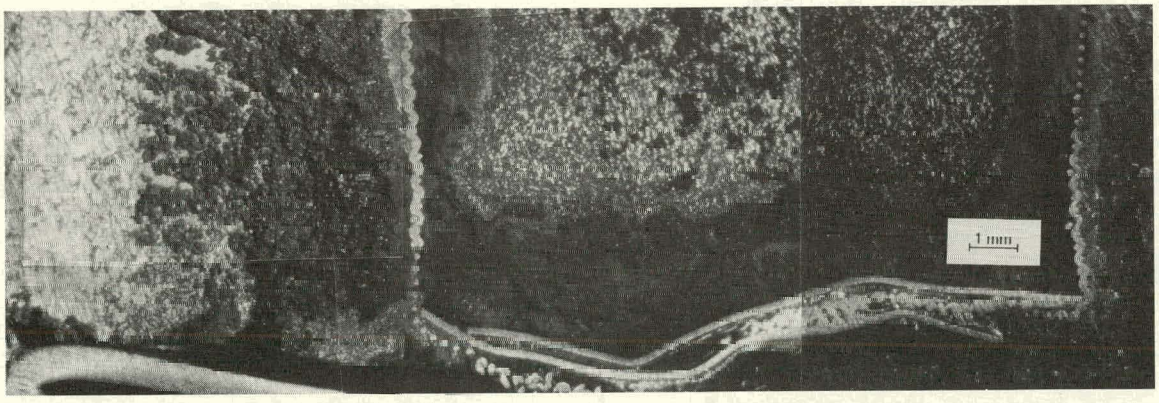

c. Migration of positive active material.

Fig. III-18. Photomicrographs of Cell Sections Illustrating Common Mode of Failure in Gould Cells

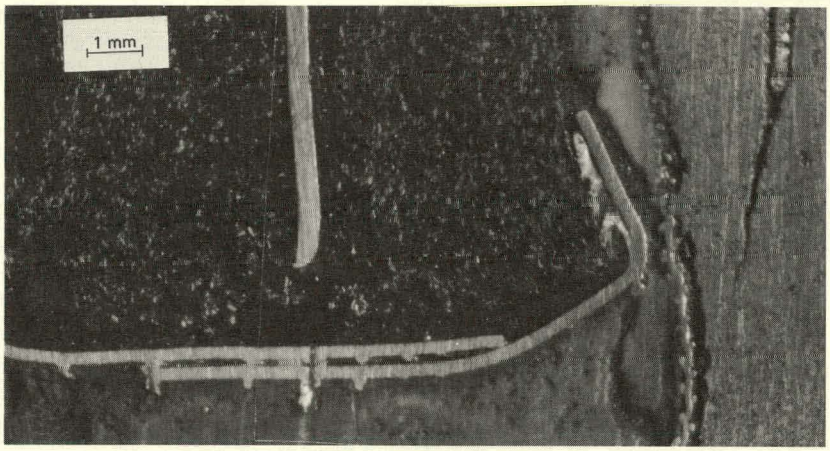

d. Separator crushed between edge channel and screen.

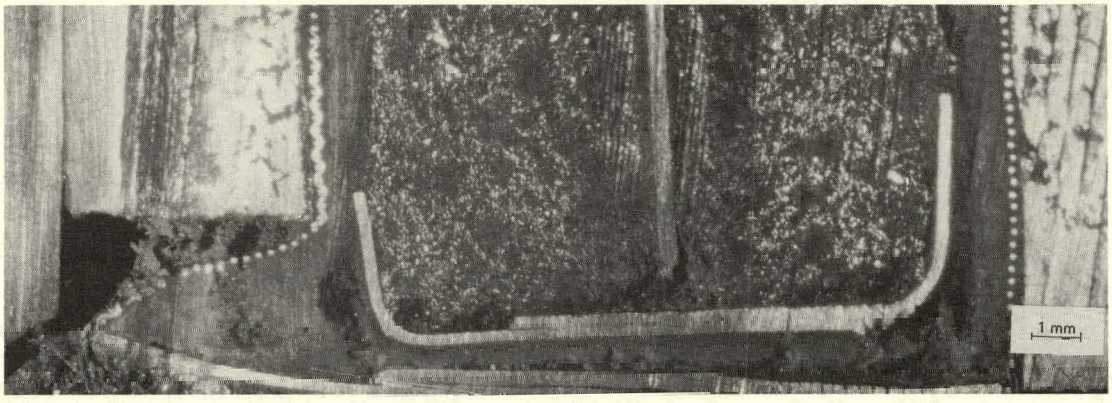

e. Mechanical damage of screen basket caused by negative electrode.

Fig. III-18. (contd)

Photomicrographs of Cell Sections Illustrating Common Mode of Failure in Gould Cells

4. Process Development

A requirement of the cell development program is that the fabrication procedures be capable of mass producing cell materials at a high rate and low cost. Much effort has been expended on (1) developing extrusion processes to produce electrodes, and (2) modifying the cell design to utilize nonwoven separators. In addition, the program is using more industrially fabricated hardware in order to reduce development cost and increase material reliability.

a. Negative Electrode Extrusion

Due to the high electronic and Li^+ conductivity of the negative electrode, we decided to test dense, solid forms of the material; the mechanical properties of lithium-aluminum alloys also indicated that they were suitable candidates for hot extrusion. The first experimental extrusions were produced by the Aluminum Company of America from 5.25 wt % Li-Al ingots supplied by Kawecki Berylco Industries. Ten billets ($\sim$180 kg) of this material were extruded at temperatures between 370 and 480°C into flat as well as ribbed sheet forms. The sheets (12.8-cm wide, 0.375-cm thick) were extruded at 25 to 50 cm/min of billet length. This process can provide sufficient negative material for 1.75 kW-hr of LiAl/FeS cells based on the GIII design in one minute. However, the material when used as a negative electrode in an engineering cell (X-11) severely limited capacity on discharge. This could be due to the distribution of the highly Li^+ conducting β-LiAl phase in the form of isolated platelets in the extruded material, rather than as an interconnected network of veins as has been observed in the as-cast material.

Sawed slabs of cast material of the same composition also exhibited negative discharge limitation, although not as severe as with the extruded alloy. Sawed slabs of cast material containing up to 8.18 wt % Li have been evaluated as negative electrodes, and all of them were found to polarize on discharge; no such limitation occurs with powders of the same composition. While this phenomenon is being investigated, the hot-rolling of alloy powders is being considered as an alternative to the abandoned extrusion method.

b. Positive Electrode Extrusion

The positive electrodes in the Gould experimental cells have been fabricated by hot pressing a mixture of lithium sulfide, iron powder, and electrolyte at temperatures close to the melting point of the electrolyte. By this method, it has been possible to prepare electrodes with porosities (electrolyte + void volume) in the range of 35 to 40%, but the temperature and pressure during electrode fabrication have to be maintained in a rather narrow range to ensure reproducibility.

An extruder capable of producing positive half-electrode slabs was designed in November 1977 and an experimental extruder capable of producing strips (2.54-cm wide, 0.33-cm thick) was designed and constructed soon afterwards. This extruder unit consists of a stainless-steel pressure tube closed at one end by the ram of a hydraulic cylinder and provided with an

appropriate opening at the other end. The tube is surrounded by electrical heaters capable of raising the temperature to 400-500°C. The ram is capable of exerting up to 14 MPa (2000 psi) pressure. The unit can handle about 500 g of active material, sufficient for the positive electrode in one experimental bicell.

The experimental extruder has been plagued with heater burnout problems. However, the small chunks of material extruded in early operation seem to be void-free, and this is encouraging. A part of the heater problem is due to the adverse surface-to-volume ratio of the small experimental unit. Thus, it is desirable to switch to a full-size, larger unit as soon as the feasibility of the technique is established. The experimental unit is now fully operational, and the effects of variation in the electrolyte portion of the positive material are being evaluated.

c. Fabrication of Cell Hardware

Although the ultimate reduction in cost of cell hardware has to wait until the components are manufactured by the thousands, significant savings in the ongoing program can be achieved by using industrially supplied hardware. The Gould development program has advanced to the stage at which the only hardware-related operations performed in-house are the assembly of the seal which is then welded to the current collector and can top, and the final assembly of the entire cell. The cost of hardware in an experimental bicell is about $40.15 at present. The prices, in lots of 100 units, of the individual metallic components are listed in Table III-10.

Table III-10. Cost of Metallic Hardware in Gould Cells

Component	Quantity	Average Price, $
Seal Body	100	2.42
Seal Positive Post Inner	100	3.79
Seal Positive Post Outer	100	4.11
Cell Top Cover	100	1.10
Cell Can		
Steel (0.058-cm thick)	65	10.00
Steel (0.045-cm thick)	25	12.49
SS (0.037-cm thick)	10	22.00
Top Retainer Basket	100	3.00
Assembly Current Collector	79	2.00
Current Collector Plate	79	3.71
Current Collector Bar	79	8.72
Side Cell Shims	100	1.30

The reduction in cost of metallic hardware per cell during the past year is probably over an order of magnitude. Similar reductions in cost have been achieved for the ceramic parts used in the seals. Whereas the Y_2O_3 and Al_2O_3 bushings in the seals for earlier cells cost $113 per cell (excluding tooling costs), the corresponding parts in the seals for more recent cells cost $11.30 per cell.

5. Facilities to Assemble and Test Cells

Gould has a facility for fabricating and assembling cells in an argon atmosphere. This facility is schematically represented in Fig. III-19, and includes furnace wells, a hydraulic press (35 ton), and welding equipment. A plasma arc welder was acquired and installed recently. The argon atmosphere is purified and conditioned by two independent systems, each of which is capable of operating the entire glove-box system if required. The purification systems reduce the concentration of water to 0.5 ppm, the concentration of nitrogen to 50 ppb, the concentration of oxygen to 200 ppb, and the concentration of hydrogen to 500 ppb. Also the argon gas-circulation system contains heat exchangers to maintain the glove-box temperature at 20-24°C, and a pressure-control system to maintain the gas pressure in the system to ±0.5 cm of water at pressures slightly over an atmosphere.

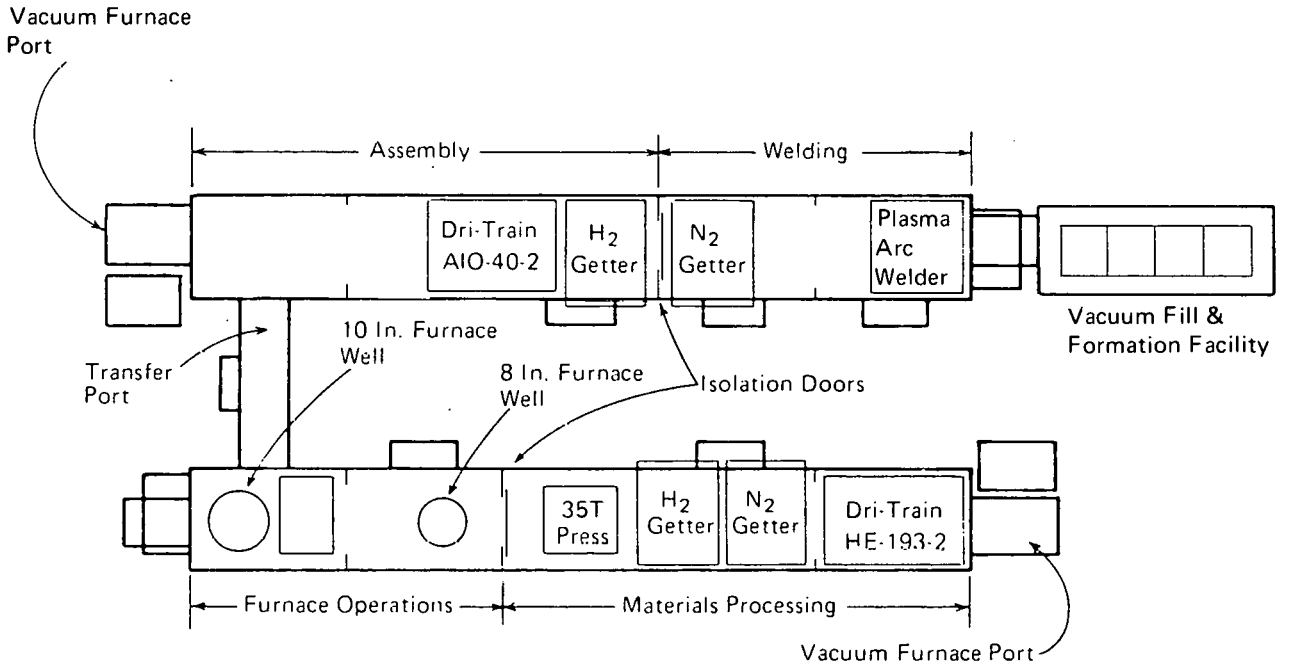

Fig. III-19. Gould Glove-Box Facility for Assembling Cells

Connected to the argon-atmosphere facility, and also shown in Fig. III-19, is the fill-formation facility. This facility is used to fill cells with electrolyte and then electrochemically form the electrodes. Originally designed to handle 10 bicells, this facility was modified during 1978 to handle four large multiplate cells.

Gould also has a dry room, which operates at moisture levels of ≤150 ppm H_2O. This room is used for conducting post-test analysis and handling solid forms of Li-Al alloy.

A 10-cell test facility was built that is capable of automatically cycling and gathering data from 10 cells or batteries with a total series voltage under 38 V. A block diagram of this facility is shown in Fig. III-20. The cells can be charged/discharged at currents up to 125 A and power tested (one cell at a time) at currents up to 1000 A. The system is capable of constant-power discharging a cell or a 10-cell string up to 20 kW. An Analog Devices MacSym One computer with 32 K memory and supporting BASIC language acts as cycler logic, data acquisition, and backup temperature control. Three floppy disk drives, a teletype, a lockable keyboard, and a 32-character display are parts of the system. A full complement of I/O and peripheral capability is available. All control systems have manual backup. Lights and displays show the status of all the cells continuously. In addition the MacSym One unit has emergency battery power to control an orderly shutdown upon power failure; it will also disconnect short-circuited cells from the battery.

The above test facility is supplemented with five manual single cell cyclers modeled along the lines indicated in Fig. III-21. These cyclers were built during 1978.

In addition to these major facilities, the program has a number of subsidiary monitoring and quality-control facilities, including a helium leak detector, various analytical equipment to ensure the purity of the glove-box atmosphere, a transmission radiograph, and a surface area analyzer. Access also exists to a P.A.R. potentiostat-galvanostat-universal-programmer electrochemical system.

6. Design and Cost Study

Work is in progress on the following four aspects of a design and cost study:

(i) definition of the optimum configuration and performance characteristics of lithium alloy/metal sulfide cells and batteries for electric vehicles and other near-term potential markets;

(ii) comparison and selection of the most cost-effective and reliable manufacturing techniques for producing components, cells, and batteries;

(iii) definition of the near-term development efforts necessary to achieve the Mark II goals (see Table I-2);

(iv) estimation of the installation cost of pilot facilities and manufacturing facilities and the cost of electric-vehicle batteries produced in those facilities.

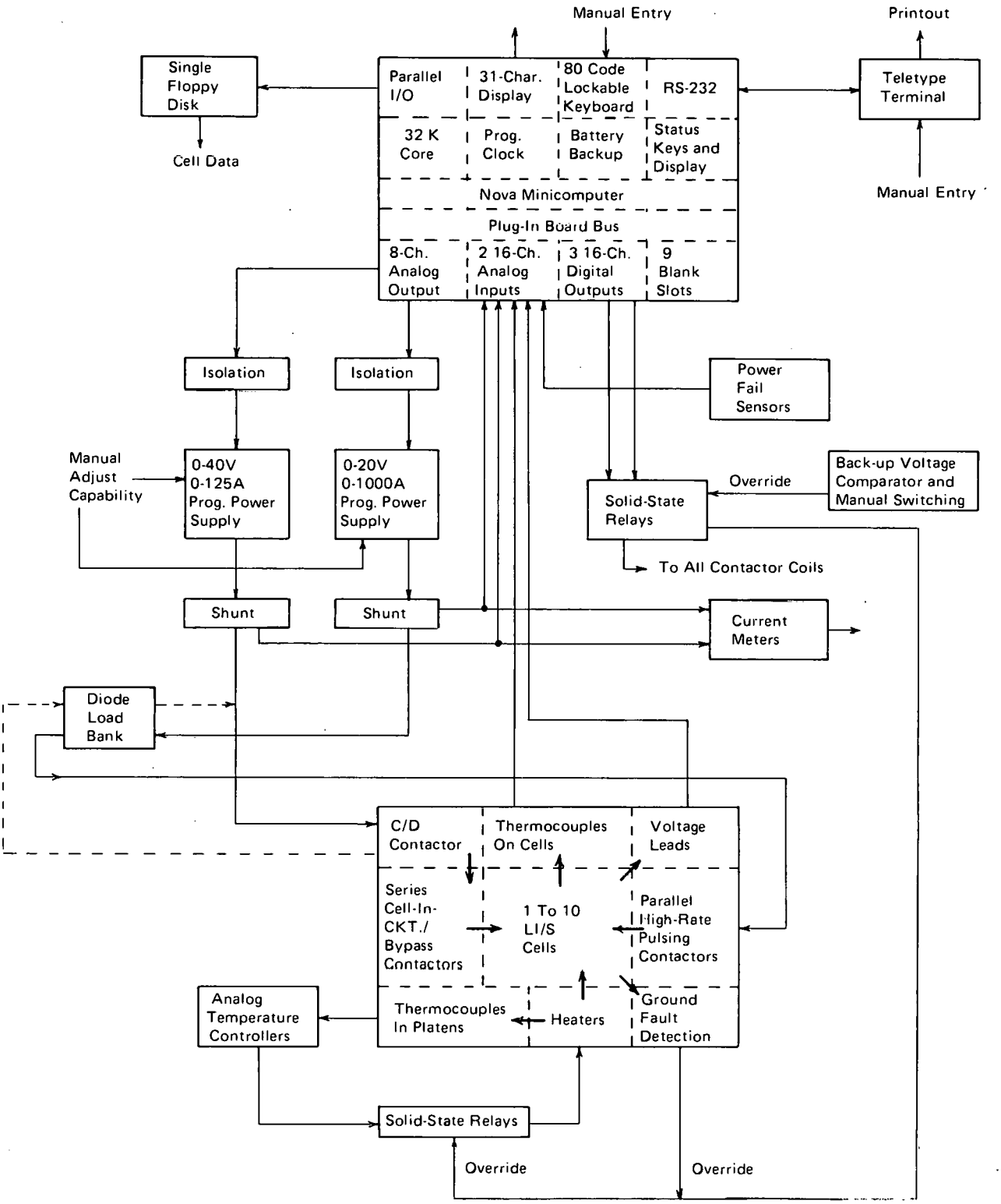

Fig. III-20. Gould Ten-Cell Test Facility

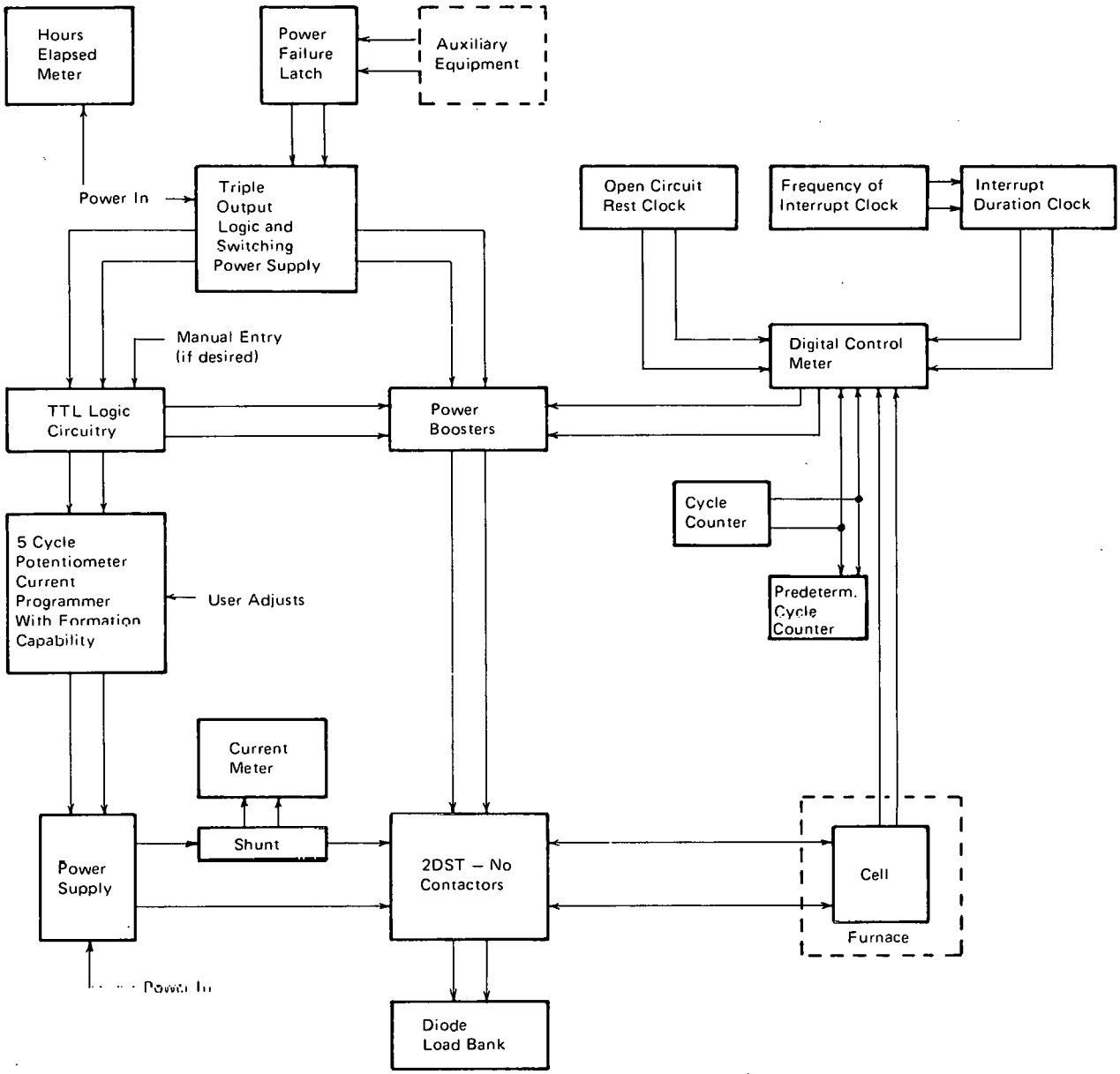

Fig. III-21. Block Diagram of Cell Cycler

The first phase of the study involved an analysis of cell and battery designs to identify the effect of variations in cell design on performance. A mathematical cell model for prismatic cells was developed and programmed for a Tektronix computer. More than 500 cell design alternatives have been evaluated, and the significant factors have been identified. A summary of this analysis is shown in Table III-10. Figures III-22 and -23 depict the cell gravimetric and volumetric specific energies, respectively, which will result from implementing these design features.

Table III-10. Matrix of Design Performance Levels

Cell Component	Range	Design No.[a] 550	552	554	553	555	556	557	551
Pos. Electrode									
Utilization	80-95%	-	0	+	+	+	+	+	+
Current Density	60-100 mA/cm^2	-	0	+	+	+	+	+	+
Voltage	1.15-1.25 V	-	0	+	+	+	+	+	+
Excess Fe	100-10%	-	0	+	+	+	+	+	+
Dis. Porosity	35-25%	-	0	+	+	+	+	+	+
Curr. Coll. Thick.	0.032-0.02 cm	-	0	+	+	+	+	+	+
Neg. Electrode									
Charge Porosity	30-5%	-	-	-	0	+	+	+	+
Li Utilization	50-70%	-	-	-	0	+	+	+	+
Separator									
Thickness	0.011-0.062 cm	-	-	-	-	-	0	+	+
Fiber Density	70-35 mg/cm^2	-	-	-	-	-	0	+	+
Electrolyte									
Starvation	0-100%	-	-	-	-	-	-	-	+

[a]The minus symbol represents a low level; the zero represents a medium level; and the plus indicates a high level.

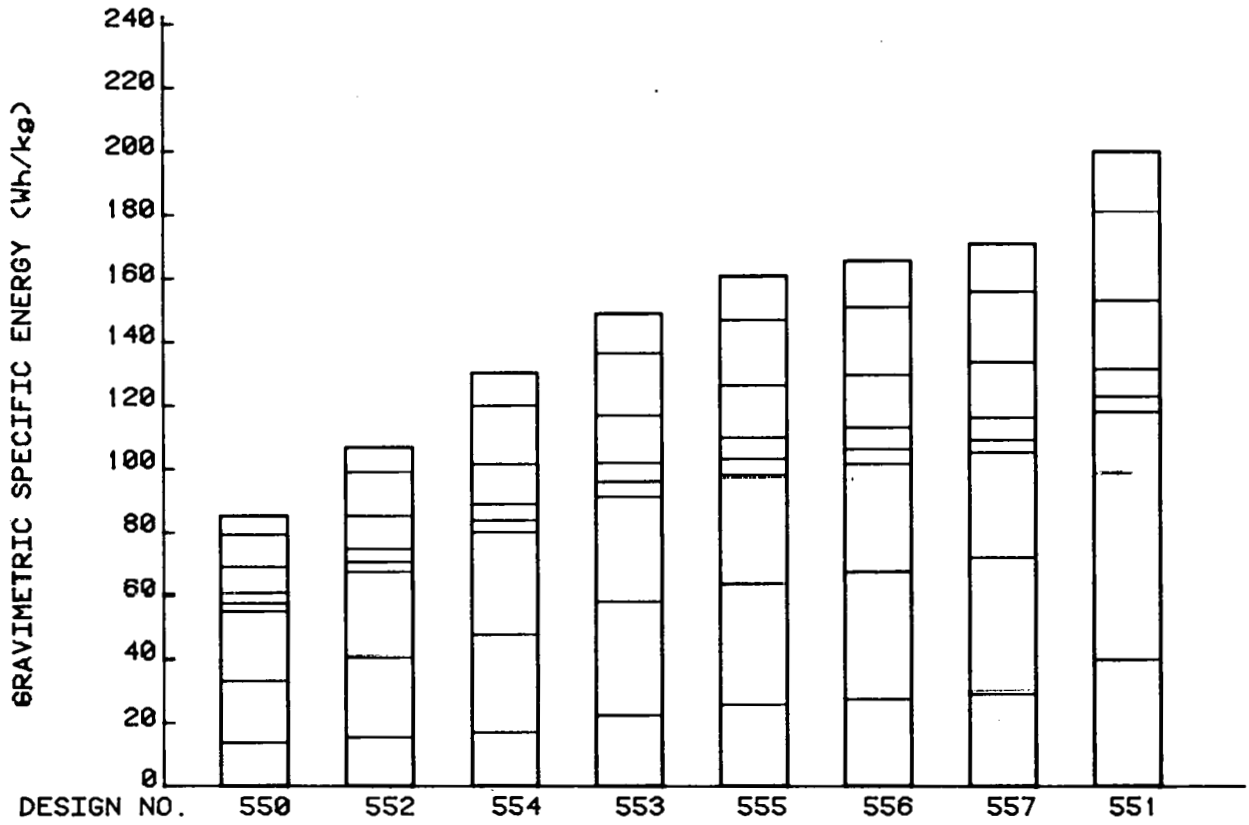

Fig. III-22. Gravimetric Specific Energy Levels for 725 W-hr Cell Designs

Cost estimates of materials and components are being obtained from mass manufacturers and potential suppliers. These data will serve as the basis for a cost analysis of the materials of construction. Also, the alternatives in manufacturing and assembly techniques are being evaluated with respect to their cost and technical feasibility.

The information gained from the above exercise is being applied to identify the most cost-effective direction for the near-term development of cells, batteries, and manufacturing processes. Alternatives are being appraised in terms of their cost and technical risk, and priorities are being established for these alternatives.

In the final stage of the design and cost study, an estimate of the cost of pilot and manufacturing facilities, based upon the alternatives that appear most promising at that time, will be prepared.

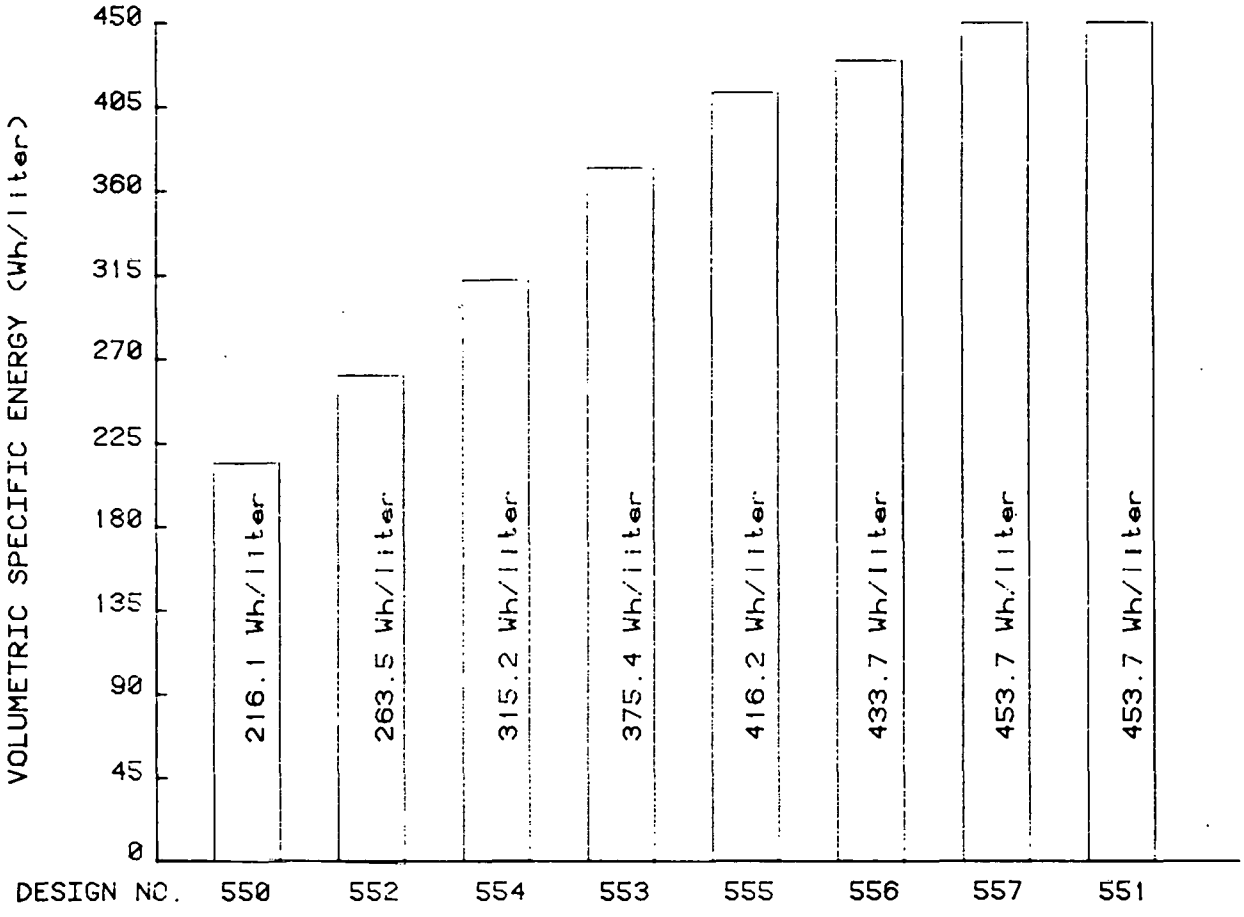

Fig. III-23. Volumetric Specific Energy Levels for 725 W-hr Cell Designs

C. Rockwell International

(S. Sudar)

1. Cell Development Program

The cell design now under development at Rockwell International consists of Li-Si negative electrodes and FeS_x positive electrodes housed within a prismatic case. Since the BN cloth or felt separators used successfully by ANL and others with LiAl electrodes is attacked by Li_xSi alloys, the more stable AlN in powder form has been used as the separator in most cells built during the reporting period. Work has been restricted to the use of FeS positive electrodes to avoid the more severe corrosion problems encountered with FeS_2. Although the eutectic salt composition of LiCl-KCl was used as the electrolyte in most of the work reported here, limited use of LiCl-rich electrolyte was also investigated.

The development of cells for both stationary-energy-storage and electric-vehicle applications was continued in this period. The technology is complementary in both cases, the principal differences residing in the size and capacity of the cells and the goals for cost, life, and specific energy for the two applications. The utility application requires larger cells, ~2.5 kW-hr capacity, with more stringent requirements for cost (~$30/kW-hr) and life (2,000 cycles). The vehicle batteries will use smaller capacity cells (150 to 450 W-hr) and require higher specific power (>100 W/kg) and specific energy (>100 W-hr/kg). The cell cost goal for the electric vehicle application is ~$45/kW-hr.

During this period, a 2.5 kW-hr cell for the utility application was built and tested. Although the life of this cell was short, much useful information was obtained during the design and operation. Work on electric-vehicle cells was performed with bicells having capacities of ~150 W-hr. Over 20 cells were fabricated and tested. Although substantial progress has been made in the development of cells for this application, further work will be necessary to attain the economic and performance goals required to bring this cell to the market place.

The more significant developments of the portions of this program funded by ANL are discussed herein. Reference to portions of the program funded by Rockwell, notably development of Li-Si negative electrodes, has been made where applicable.

a. Positive Electrode Development

(J. Hall, L. McCoy)

Cycling of lithium/metal sulfide cells is attended by the expansion and contraction of the active materials, which impose significant stresses on the cell case. Efforts have been made to devise electrode structures capable of containing the swelling forces generated by the positive electrode during discharge by physically bonding a particle-retaining member (*e.g.*, screen or porous nickel) to internal electrode structural members. These are, in turn, bonded to a current-collecting back plate. In general, nickel has been used as the structural material with the objective of obtaining greater protection from anodic dissolution than can be provided by lower-cost steel. If this approach proves successful, nickel-coated steel will be

substituted for the nickel structure. A similar approach has been taken in developing the negative electrode, except that swelling forces are greatest during the charge cycle and corrosion problems differ in their fundamental nature.

In previous years, both electrode structures have been based on a metal honeycomb to contain the active materials. The work performed during this period was directed to the investigation of electrode structures which could provide the dimensional stability of the honeycomb-cored electrode but could be produced at a lower cost and weight. Positive electrode development was concentrated on two different electrode types. Both were designed to permit all of the high-temperature assembly operations, *i.e.*, brazing or bonding, to be done before loading of the active material. The two types of electrode structures are shown in Fig. III-24. Both are constructed of nickel except that the split-rib design has a central copper current conductor. The major physical parameters varied in the investigation included (1) the spacing between the ribs, (2) the rib material thickness, and (3) the physical form of the particle retainer, screen, or porous nickel.

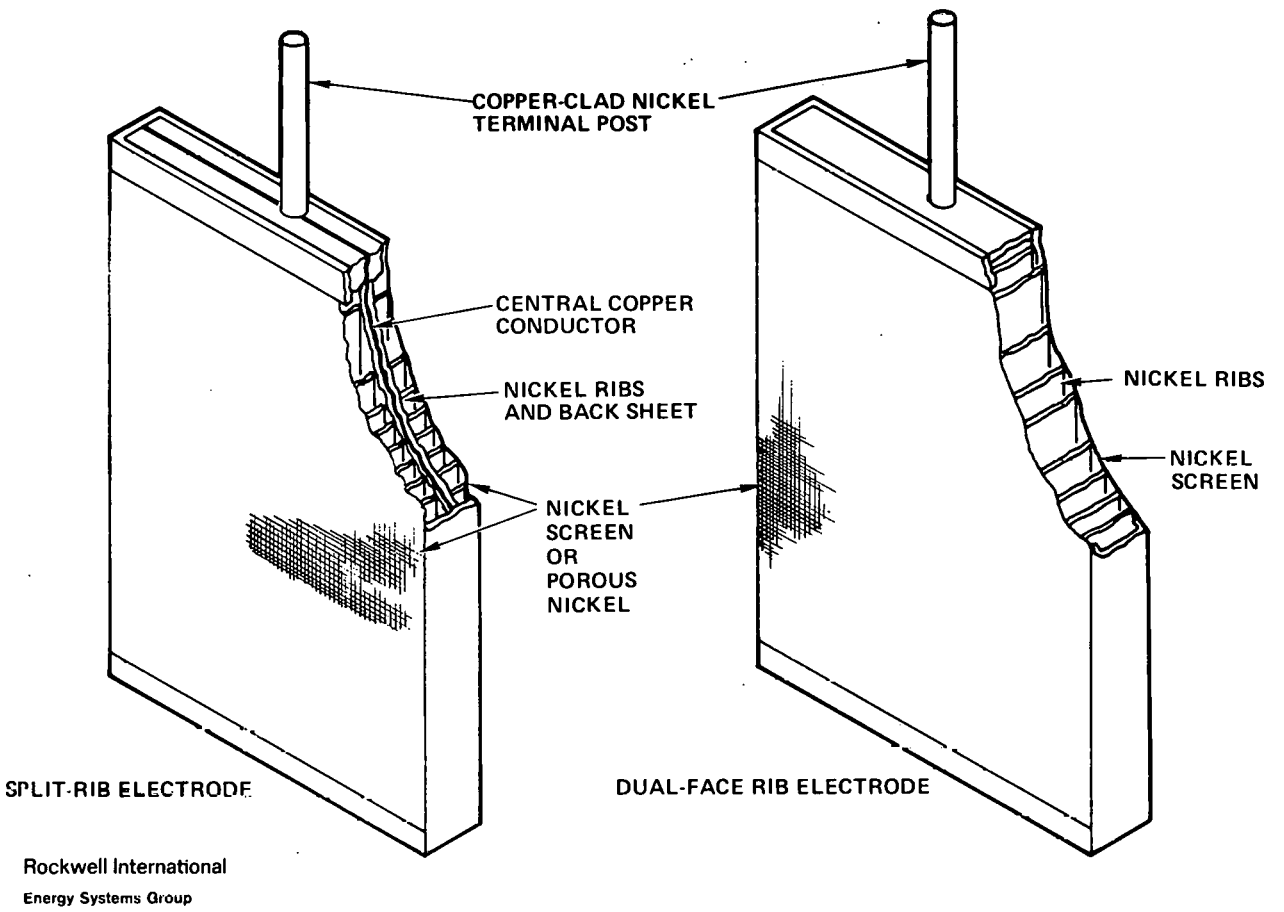

Fig. III-24. Two Designs for the Positive Electrode

The two basic types of positive electrode structures (rib and split-rib) were tested with the variables shown in Table III-11. The positive electrodes measured approximately 13 × 17 cm. This electrode size is similar to that of the electric-vehicle cell and is an intermediate state of scale-up for stationary-energy-storage cells (23 × 23 cm). The close rib spacing (3.2 mm) combined with the thin rib (0.3 mm) was found to give the best strength-to-weight ratio for containment of positive-electrode active materials.

Cells with positive electrode structures covered with screen generally had specific resistances of 1.3 to 1.6 Ω-cm^2, while those cells using positive electrodes covered with 0.25-mm porous nickel sheet had specific resistances ranging from 2.3 to 2.6 Ω-cm^2. Also, the screen proved to be physically stronger than the porous nickel. This fact, together with a lower electrolyte resistance, led to the selection of screen as the material for future development work. No significant difference in cell internal resistance could be detected between the rib and the split-rib designs.

b. Ceramic Separator Development
(H. M. Lee)

Work was performed to evaluate corrosion-resistant ceramic materials for their potential value as separators in both vehicle and utility energy storage cells. Earlier work had identified a number of materials, including AlN, β-Si_3N_4, and Y_2O_3, as resistant to attack by lithium and lithium alloys. Boron nitride, which has been shown to possess good resistance to attack by lithium-aluminum alloy, is not stable in contact with the more lithium-active, lithium-silicon alloys (*e.g.*, Li_5Si) and was, therefore, not included in this study. Additional candidate materials were sought, and methods of fabricating selected ceramic materials in various forms at low cost were investigated. Emphasis was placed on development of powder separators.

Because the suitability of a ceramic material for a cell separator depends on its physical properties as well as its resistance to attack in the cell environment, most of the evaluation work was conducted using a small Li-Si/FeS cell equipped with a single positive and negative electrode, each measuring 5 × 5 cm, as shown in Fig. III-25. Each type of electrode was, except for size, similar to those used in the full-scale test cells. The positive electrode was 0.48-cm thick and was loaded with 0.9 A-hr/cm^3 of Li_2S and Fe powder. A 200-mesh screen was used as a particle barrier. The negative electrodes were 0.32-cm thick and were loaded with $FeSi_2$ to provide a capacity matching that of the positive electrode (when charged to Li_9FeSi_2). An 80-mesh screen was used as the particle barrier in this case. A 1.5-mm thick cavity was created between the electrodes by the use of dense, narrow BN spacer bars when powder separators were to be evaluated. In this case, the ceramic powder was compacted into the cavity to a density of ~50 vol %. When sintered plates were used, the spacer bars were omitted. The results of the tests on these cells are listed in Table III-12. Although most ceramic powders used were in fine particle form (≤200 mesh), two particle sizes of AlN were tested, as shown in this table. In some instances, *e.g.*, CaO and Li_4SiO_4, instability of the material was evident by the appearance of extra negative electrode plateaus and rapid loss of cell capacity.

Table III-11. Major Positive Electrode Variables in Full-Scale Test Cells

Electrode Type	Rib Thickness, mm	Rib Spacing, mm	Copper Current Conductor Thickness, mm	Design of Nickel Particle Retainer	Initial Utilization at 30 mA/cm^2, %	Cell Operating Resistance, Ω-cm^2
Rib	0.25	3.2	0	Porous Nickel	54	4.0
Rib	0.25	3.2	0	Porous Nickel	83	2.3
Rib	0.30	3.2	0	200-Mesh Screen	83	1.3
Rib	0.30	3.2	0	200-Mesh Screen	76	1.6
Rib	0.50	3.2	0	100-Mesh Screen	88	1.2
Rib	0.50	6.4	0	Porous Nickel	79	2.4
Split-Rib	0.25	3.2	1.0	Reinforced Porous Ni	79	2.6
Split-Rib	0.25	3.2	1.0	Reinforced Porous Ni	79	2.5
Split-Rib	0.25	3.2	0.25	100-Mesh Screen	74	1.0
Split-Rib	0.25	3.2	0.25	100-Mesh Screen	83	2.0
Split-Rib	0.25	3.2	0.25	25- by 500-Mesh Screen	75	1.5

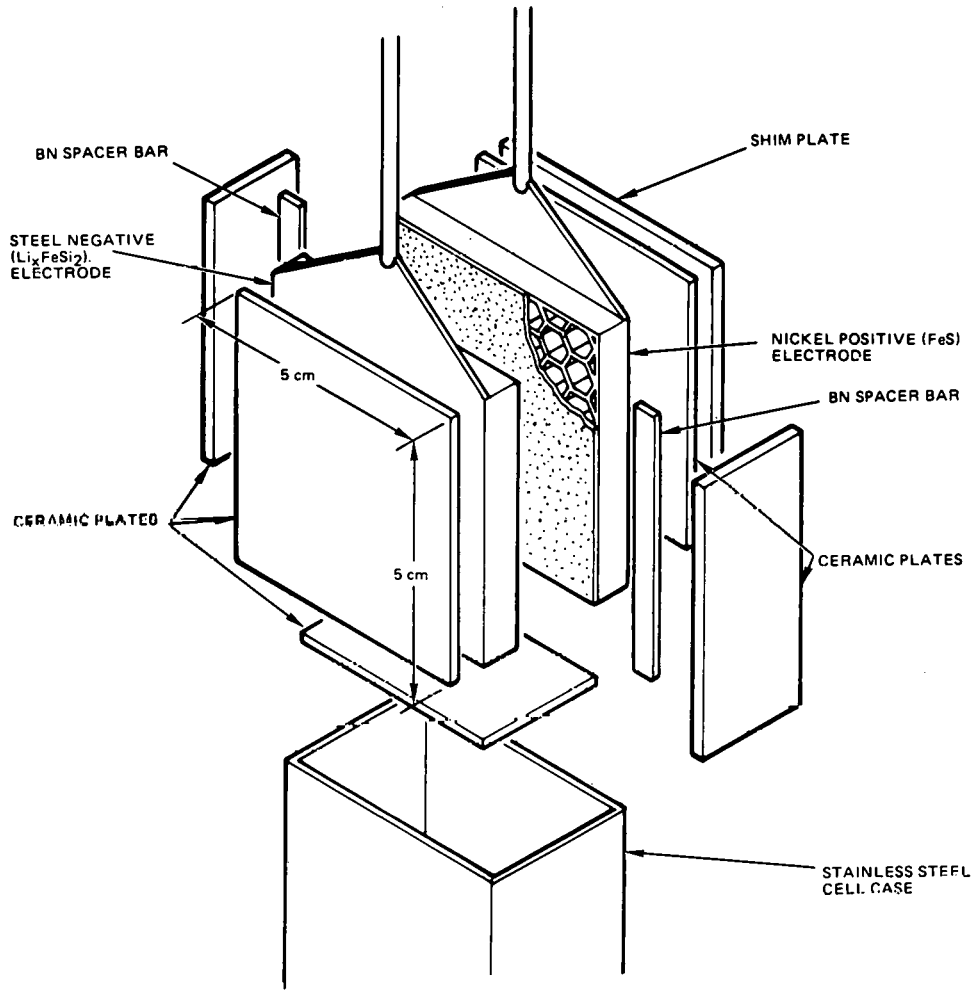

Fig. III-25. Powder Separator Test Cell

Considerable investigatory work was done on separator material with compositions containing varying ratios of lithium orthosilicate (Li_3SiO_4) and lithium orthophosphate (Li_3PO_4). These materials have been described by Hu, Raistrict, and Huggins[2] as lithium-ion conductive materials. This property may provide some practical benefit by reducing internal cell resistance even when used as a porous material. Superior results were obtained when this type of material was used in sintered plate form rather than as a powder. Although this class of material has potential value as a relatively low-cost separator, further work is required to determine its long-term stability and to assess the quantitative advantage to ion-conductivity in porous separators. Calculations using a theoretical model suggest the separator resistance decreases by 20-30%, depending on particle size, packing density, *etc.*, when this material is used in a cell.

The development of a powder separator has been pursued because it is potentially less expensive then fiber separators. (Several of the fabrication steps, necessary for fiber formation, are eliminated.) Fine AlN powder can be fabricated by direct nitriding of aluminum powder. However, fabrication of coarse powder or porous plates increase fabrication costs by

Table III-12. Performance of Test Cells

Materials	Forms and Ion Conductivity	Particle Size, Mesh	Source and Purity	Coul. Eff., %	Utiliz., %	Cycles	Remarks
AlN	Powder Nonconductive	-200	Cerac/Pure, Inc., 99%	100	40	30	Little change in capacity
AlN	Powder Nonconductive	-40 to +80	Cerac/Pure, Inc., 99%	98	80	40	Slow decrease in capacity
Si_3N_4	Powder Nonconductive	-325	Cerac/Pure, Inc., 99.9%	93	60	25	May be impure, loss in capacity
CaO	Powder Nonconductive	-325	Cerac/Pure, Inc., 99.8%	93	45	30	Extra plateaus, loss in capacity
Li_4SiO_4	Powder Ion-Conductive	-200	ESG, Sintered at 1000°C	100	60	40	Extra plateaus, rapid decrease in capacity
Li_4SiO_4 (75%) Li_3PO_4 (25%)	Powder Ion-Conductive	-200	ESG, Sintered at 1000°C	100	65	15	Loss in capacity
Li_4SiO_4 (50%) Li_3PO_4 (50%)	Powder Ion-Conductive	-200	ESG, Sintered at 1000°C	100	65	60	Loss in capacity
Li_4SiO_4 (25%) Li_3PO_4 (75%)	Powder Ion-Conductive	-200	ESG, Sintered at 1000°C	95	80	15	Loss in capacity
Li_4SiO_4 (25%) Li_3PO_4 (75%)	Plate Ion-Conductive	Porosity = 45% Thick = 0.175 cm	ESG, Sintered at 1000°C	100	73	20	No loss in capacity
Li_3PO_4	Powder Nonconductive	-200	Alpha Product, 98%	100	70	60	Slow loss in capacity

factors of 3 to 10. Ceramic fibers of AlN and Si_3N_4 can be produced only under highly specialized conditions, and the yield would be so small that mass production would not be economically feasible. Mixtures of Li_4SiO_4-Li_3PO_4 can be produced relatively inexpensively by a solid-state reaction from a mixture of Li_2CO_3, SiO_2, and Li_3PO_4.

c. Development and Life Testing of Stationary-Energy-Storage Cells (R. C. Saunders, J. Hall)

A 2.5-kW-hr cell was placed in operation. Figure III-26 is a picture of the assembled cell. This cell contained 16 electrode pairs (23 × 23 cm) and is believed to be the largest Li/MS cell ever put on test.

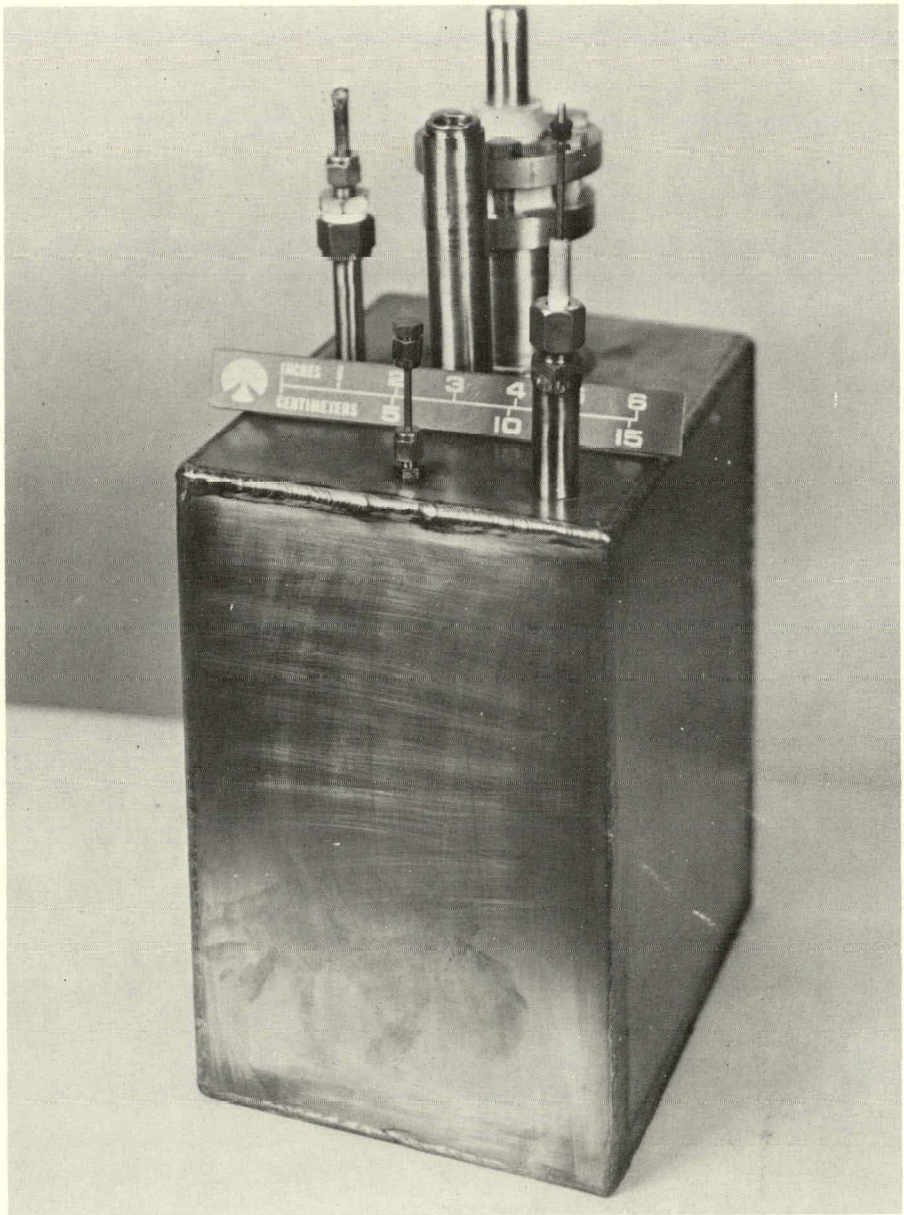

Fig. III-26. Load-Leveling Cell (2.5 kW-hr)

The cell was designed with a capacity for use in stationary-energy-storage systems. The electrode designs reflect the state of the art at the time the design was initiated. The design of other components (*e.g.*, current conducting members, case, and feedthrough) presented problems unique to the fabrication of large cells of this type.

The design features of the positive and negative electrodes are summarized in Table III-13. The weights of the principal cell components are shown in Table III-14. The cell consists of vertically oriented electrodes, eight positive and nine negative, arranged in a rectangular metal case equipped with a sealed, insulated feedthrough for the positive electrodes. The current conductor post for the negative-electrode assembly was grounded to the case. The positive-electrode feedthrough was a commercial Conax unit sized to accommodate the nickel-clad copper conductor post (1.91-cm dia). Excess metal was machined from the feedthrough to reduce its weight.

Table III-13. Design Features of the Discharged State of a LiSi/FeS Cell (nominal capacity, 2.5 kW-hr at 4-hr rate)

	Cathode	Anode
Theoretical Loading Density	0.80 A-hr/cm^3	1.20 A-hr/cm^3
Active Material	Li_2S + Fe	$FeSi_2$ Union Carbide
Structure	Vertical Nickel Rib	Type 430 Stainless Steel Honeycomb
Containment	Porous Nickel	80 Mesh, Type 430 Stainless Steel Screen
Current Collector	Nickel Sheet	Copper, 0.25-mm thick
Nominal Size	22.5 × 21.6 × 0.48 cm	22.9 × 22.9 × 0.32 cm
Electrode Design	Floating	Case-Grounded
Required Number	16	16

In the negative electrodes (23 × 23 × 0.32 cm), shown in Fig. III-27, the metal honeycomb core was diffusion bonded to the back current conductor sheet. The particle retainer, 80-mesh screen, was spot-welded to the honeycomb after the electrode was loaded with $FeSi_2$. Except for the end electrodes, these electrodes were brazed back-to-back with an intervening layer of copper (0.25-mm thick) to reduce IR losses and to improve the uniformity of current distribution. The positive electrodes (22.5 × 21.6 × 0.48 cm), depicted in Fig. III-28, had a dual-faced rib construction. The particle retainer, a porous nickel sheet 65% dense and 0.25-mm thick, was brazed to the ribs. The active material, Li_2S and Fe powder, was loaded in a ratio to produce FeS when charged, and the top current-conductor bar was welded in place.

Table III-14. Weight Breakdown of 2.5-kW-hr Cell

Component	Weight, g
Cathode	
Nickel Rib Structures (8)	4,992
Nickel Screens (16)	262
Nickel Tabs (8)	193
Active Material Li_2S and Fe (70% utilization)	5,614
	11,061
Anode	
Type 430 Stainless Steel Honeycomb Structures (16)	1,102
Type 430 Stainless Steel Screens (16)	704
Type 430 Stainless Steel Backplates (16)	862
Copper Current Collectors (16)	946
Nickel Tabs (16)	425
Active Material $FeSi_2$ (charged to Li_9FeSi_2)	2,171
	6,210
Ceramics	
Spacers (BN)	494
AlN Powder Separator	1,910
	2,304
Electrolyte	
Cathode: Active Material	2,321
Screen	124
Anode: Active Material	3,004
Screen	214
Separator	979
	6,642
Feedthrough	1,645
Conductors	
Positive	762
Negative	789
	1,551
Case	3,959
Total	33,472[a]

[a]The calculated specific energy at the 5-hr rate is 75 W-hr/kg.

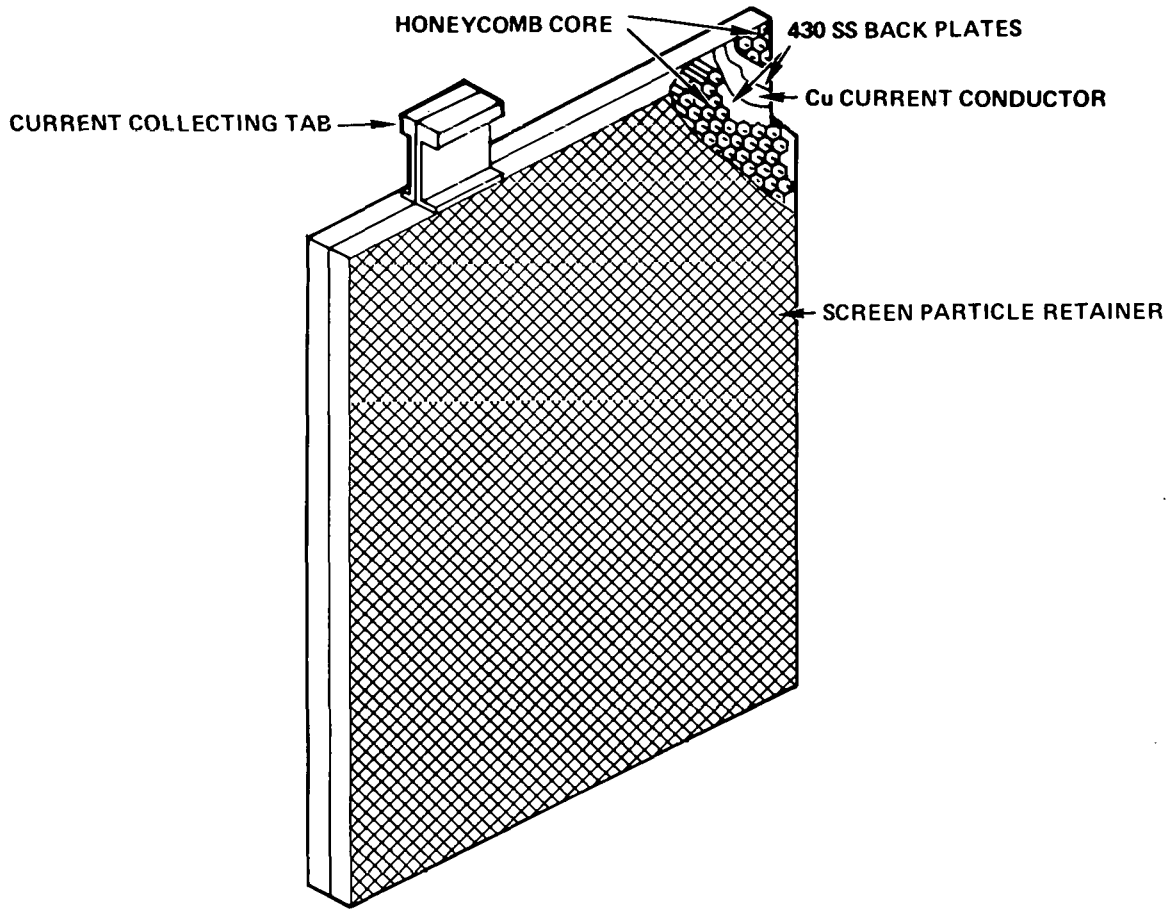

Fig. III-27. Negative Electrode Design

The insulating ceramic separators consisted of fine AlN powder (Cerac/Pure Inc., 99% purity and 200 mesh or finer). The thickness, 1.5 mm, was defined by dense BN spacer bars of this thickness, placed at the edges of the electrodes. Boron nitride bars of a similar thickness were used to insulate the positive electrodes from the case. The nickel bus bars were welded to the current conducting tabs of each set of electrodes. The cell was filled at atmospheric pressure in an inert-atmosphere glove box with eutectic LiCl-KCl electrolyte purchased from the Lithium Corporation of America. Operation of the cell was at 460 ± 10°C in a furnace well of a glove box. Additions of electrolyte were made during the break-in cycling period of the cell.

The initial performance of the cell appeared satisfactory except that the design capacity (75 W-hr/kg at the 5-hr rate) was not obtained. The performance data obtained in cycles 3 through 15 are shown in Table III-15. A sudden short circuit was observed during discharge in cycle 16, an unusual occurrence with cells of this type. As the short circuit was permanent (*i.e.*, the cell could not be recharged) the cell operation was terminated and the top removed. The bus bars were removed and the short circuit was located between two sets of electrodes. These were electrically isolated and the bus bars were again welded to the remaining electrodes.

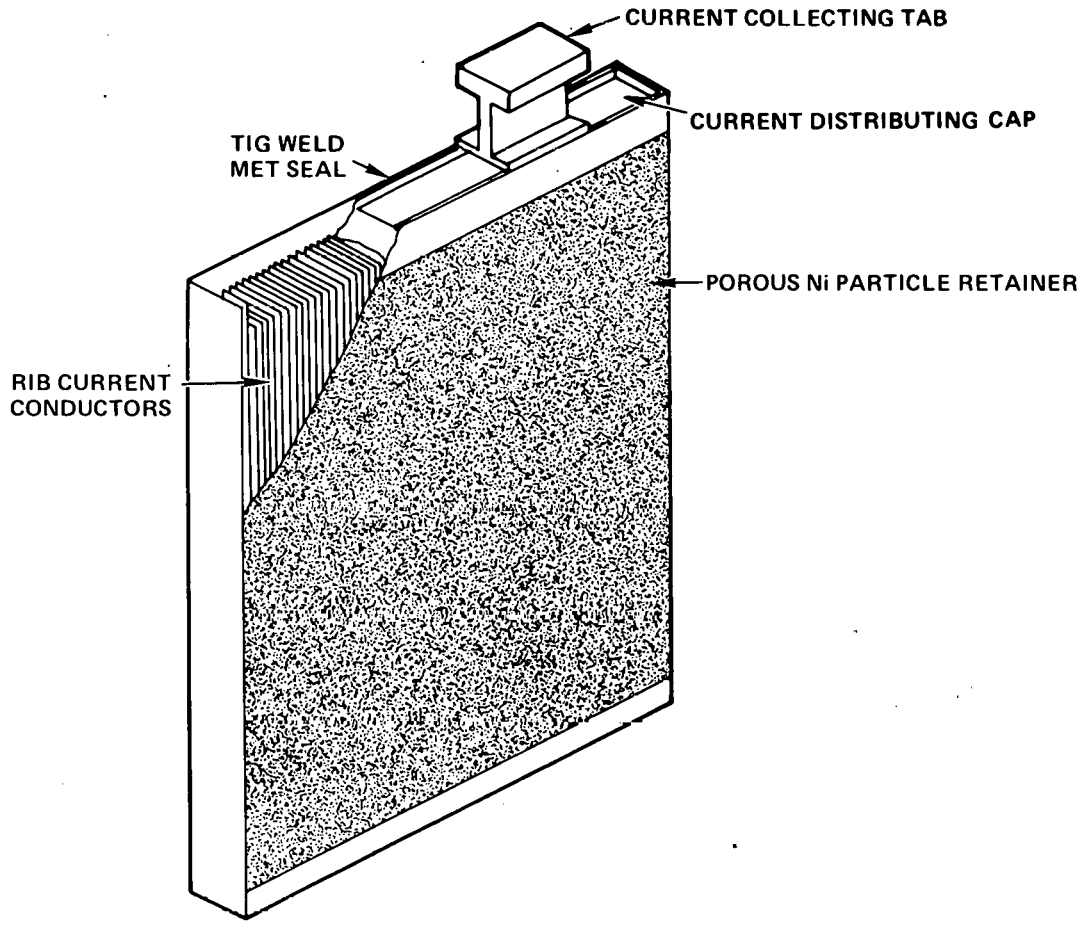

Fig. III-28. Positive Electrode Design

Table III-15. Performance Data for the 2.5 kW-hr Cell

Cycles	3-15
Time, hr	300
Current, A	200
Current Density, mA/cm^2	25
Rate of Charge and Discharge, hr	9.5
Resistance, Ω-cm^2	2.9
Utilization, %	75.9
Coulombic Efficiency, %	99.2
Energy Efficiency, %	74.8
Average Discharge Voltage, V	1.19
Energy Storage Capacity, kW-hr	2.243

Thereafter, the cell was operated for 35 cycles when short circuiting was again observed. At this point, the cell operation was terminated and the cell examined. Voids (no electrolyte or AlN powder) were found in the upper areas of all electrodes. In the absence of physical support, the porous nickel ruptured in many places, thereby creating metal-to-metal shorting paths.

As a result of this experience, we concluded that the porous nickel is physically too weak for practical use as a particle-retaining member. This component has been replaced with a nickel screen on subsequent cells. The method of electrolyte filling used in this cell did not provide proper wetting and an adequate amount of electrolyte. Electrolyte filling in a vacuum is now used to avoid this problem. The absence of AlN powder in the upper portion of the separator space is believed to be caused by penetration of fine AlN powder through the 80-mesh screen covering on the negative electrode. Several means of avoiding this problem are being considered. Despite the short life of this cell, valuable experience has been gained in the design of large cells, and the problems encountered are being solved.

A second 2.5 kW-hr cell is now under development. This cell, called the Mark LL-1 test cell, will be representative of the basic building block cell for commercial-scale energy-storage plants. While the construction of this cell is scheduled for later this fiscal year, the cell design, assembly procedures, and specifications have been completed, and a design review has been held with ANL.

The Mark LL-1 cell will be similar to the cell described above, except that design improvements have been added that should result in a more reliable operating life. The porous nickel particle retainer that failed in the earlier 2.5-kW-hr cell has been replaced with nickel screen. The nickel screen has been shown to be substantially stronger than the porous nickel sheet and has a lower electrolyte tortuosity. The use of the screen replacement for porous nickel has demonstrated a marked reduction in cell resistance.

The calculated energy density for the Mark LL-1 cell is 75 W-hr/kg. The expected operating resistance will be lower than the 2.9 Ω-cm^2 exhibited by the earlier cell because of improvements in bus-bar attachment methods and the use of a screen for the positive-electrode particle barrier.

d. Development of Li_x-Si/FeS Electric Vehicle (EV) Cells
(J. Hall, L. R. McCoy, W. Friske)

Development of Li_xSi/FeS electric-vehicle cells was initiated with the objective of transferring stationary-energy-storage cell technology to the design and fabrication of cells for electric-vehicle application. Sixteen FeS bicells, designated Rockwell Electric Vehicle Cells (REVC), were built and tested.

The bicells had electrodes measuring 12.7 × 17.8 cm. The positive material thickness was 0.48 cm (split-rib design), or twice that thickness (dual-face rib design).* The current collector of the positive

*See Fig. III-24 for depiction of this design.

electrode was made of nickel and had one of three designs--honeycomb, vertical rib, or shelf. The active material in the uncharged state was Li_2S and Fe in a 1:1 ratio. The face of the electrode was covered by either porous nickel (early cell tests) or nickel screen (later cell tests). The negative electrodes employed a honeycomb core similar to that shown in Fig. III-27 and were 0.32-cm thick; all components were made of Type 430 stainless steel. The honeycomb was diffusion-bonded to the current-conductor plate; the electrode was filled uniformly with $FeSi_2$; and an 80-mesh screen was spot-welded to the honeycomb surface to seal the electrode. All cells were assembled with dense BN spacer bars to confine the ceramic powder separator as described in the preceding section. Figure III-29 shows the components of this type of cell.

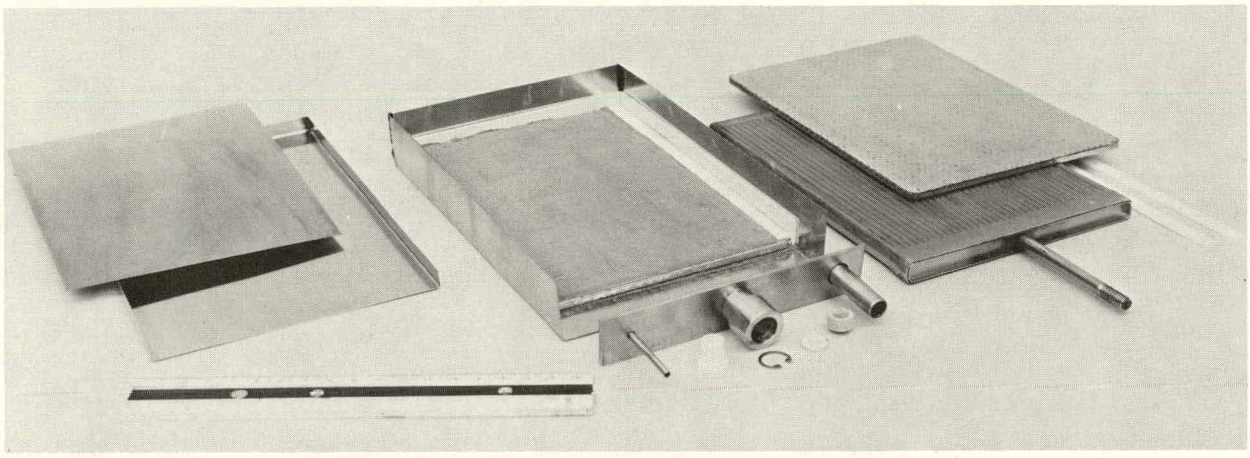

Fig. III-29. Electric-Vehicle Cell Components

Experience to date with these cells is summarized in Appendix B. The porous nickel sheet in the positive electrode was free of apparent attack, but rupture of this member by internal swelling or bond failure was the frequent cause of cell failure by short circuiting. The tortuosity of the porous nickel contributed significantly to internal cell resistance, and the high-rate discharge properties of this type of electrode were generally poor. The use of a nickel screen, particularly with shelf- or vertical-rib positive electrodes, avoided these problems and good performance was attained at high discharge-charge rates. In addition, the use of Type 430 stainless steel rather than low-carbon steel for negative current-collector material extends the life of this negative electrode, but further improvement is needed.

Studies[2-3] had indicated that the formation of J phase ($LiK_6Fe_{24}S_{26}Cl$) in FeS electrodes has an adverse effect on electrode kinetics. Previous results (ANL-78-45, p. 57) also suggested that J-phase formation can be avoided or minimized by operating the cell at high temperatures (>450°C) or by increasing the LiCl content of the electrolyte. For the REVC cells, significant improvements were achieved both by cell operation at temperatures above 450°C and by use of Li-rich (55 wt % LiCl-45 wt % KCl) electrolytes.

The above statements can be illustrated by a comparison of the performance of three cells--REVC-7, -9, and -10. Table III-16 illustrates the differences in a number of cell performance parameters when nickel screen (REVC-10) was substituted for porous nickel (REVC-7) and when an LiCl-rich electrolyte (REVC-9) was substituted for LiCl-KCl eutectic (REVC-10). The beneficial effects of both substitutions are apparent in an increased watt-hour recovery.

Table III-16. Performance Data for Li-Si/FeS Electric-Vehicle Cells

	Current Density, mA/cm^2		
	30	60	90
REVC-7[a]			
Percent Utilization (FeS)	61	38	21
Coulombic Efficiency, %	96	98	99
Discharge Voltage (average), V	1.21	1.10	0.95
Capacity Recovered, W-hr	114	64	31
REVC-9[b]			
Percent Utilization (FeS)	82	77	--
Coulombic Efficiency, %	97	96	--
Discharge Voltage (average), V	1.22	1.18	--
Capacity Recovered, W-hr	149	135	--
REVC-10[c]			
Percent Utilization (FeS)	82	59	51
Coulombic Efficiency, %	97	98	98
Discharge Voltage (average), V	1.26	1.22	1.17
Capacity Recovered, W-hr	156	103	89

[a] Porous nickel on positive electrode.

[b] 100-mesh nickel screen on positive electrode.

[c] Electrolyte; 55 wt % LiCl and 45 wt % KCl.

In comparison with the cells listed in Appendix B, Cell REVC-10 operated for a relatively long period (152 cycles), and its performance was remarkably stable. The active-material (FeS) utilization remained at about 85% at the 8-hr rate, and the coulombic efficiency at ~99% over its entire life. Figure III-30 shows the voltage-capacity curves of this cell at cycles 8 and 150. The minor changes in the voltage-capacity curves are due to a slow loss of capacity of the negative electrode with continued cycling at the cell operating temperature (average about 460°C). The specific power and voltage of REVC-10 at various discharge currents for full and 65% charge are shown in Fig. III-31. (A current of 100 A represents a current density of about 180 mA/cm^2.) These tests were performed by sequentially applying higher currents in steps of 20 A with a duration of 15 sec at each step.

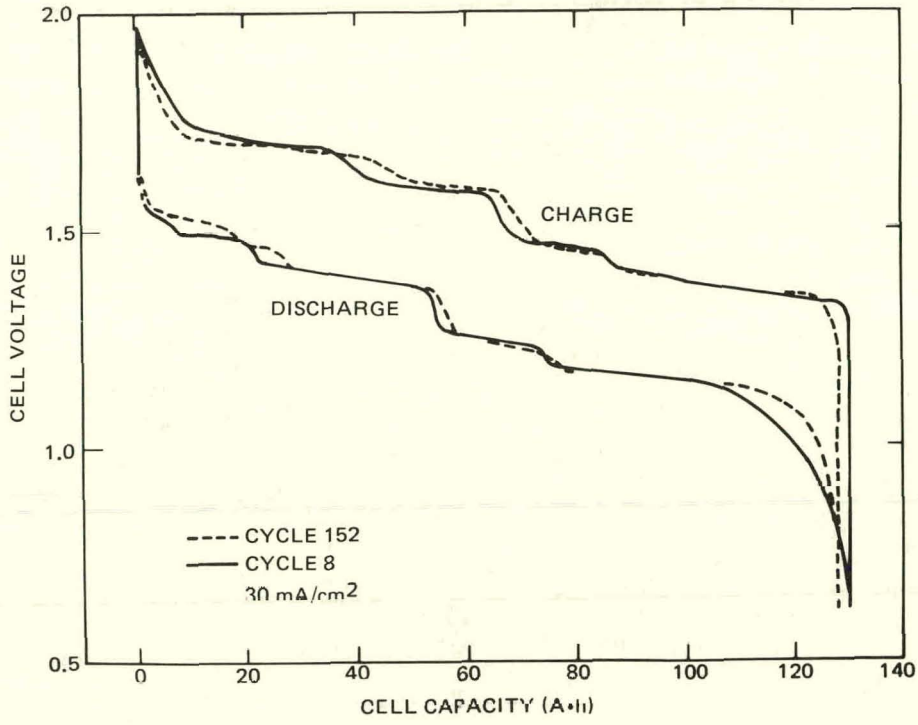

Fig. III-30. Voltage *vs.* Capacity of Cell REVC-10 at Cycles 8 and 152

Experience with another series of cells (REVC-A series, see Fig. III-32) indicates that the fine AlN powder separator used in many of these cells can enter voids in the negative electrodes, thereby causing "slumping" of the powder separator in the manner observed with the 2.5 kW-hr cell. This slumping is greater if the cells are filled with electrolyte in a vacuum, as is the present procedure. Finely pored Y_2O_3 ceramic cloth over the negative electrode appears to minimize this problem; other materials and material combinations are being evaluated. A cell with Y_2O_3 cloth over the negative electrode screen and with a fine AlN powder separator is scheduled to be tested at ANL.

Two other cells have been built to test different types of particle retainers with coarse AlN powder separators. REVC-8A1 was built using coarse AlN powder (-40 +80 mesh) for the separator, ZrO_2 cloth over the positive electrode, and Y_2O_3 cloth over the negative electrodes. The use of ZrO_2 cloth was based on the assumption that the coarse ceramic powder would be a less effective particle barrier for positive active material than the fine AlN powder used in the past. REVC-9A1 was built with coarse AlN powder and ZrO_2 cloth over the positive electrode screen.

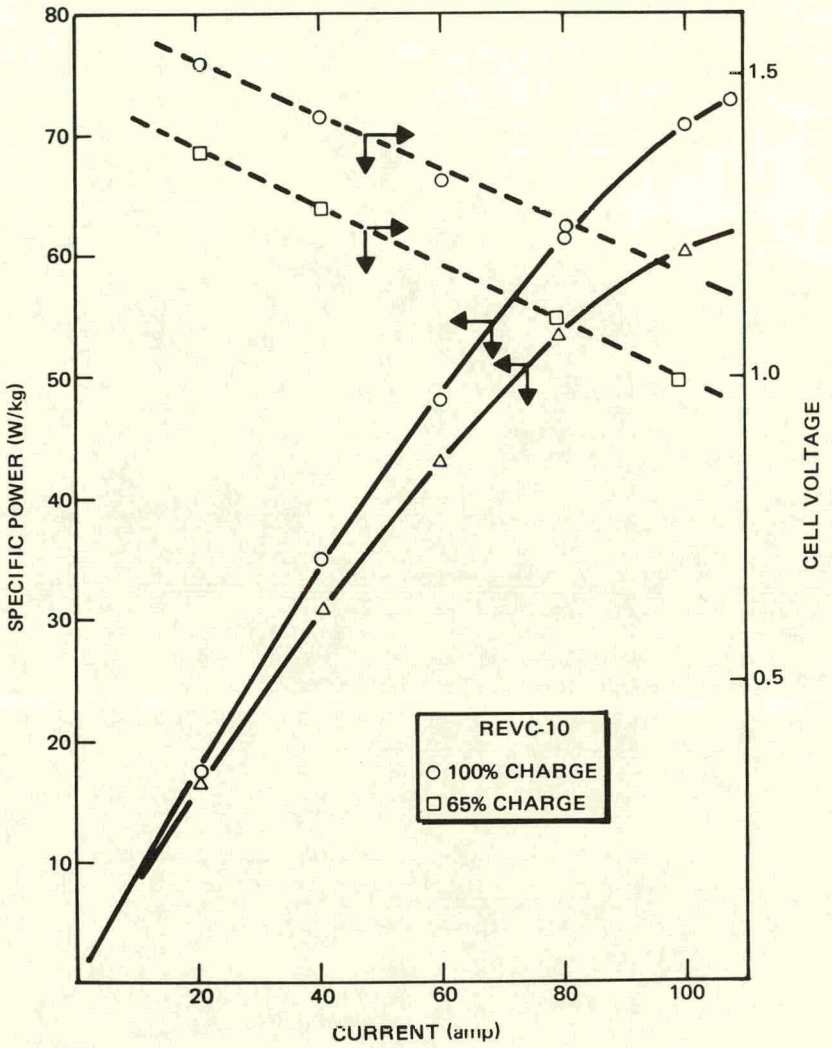

Fig. III-31. Specific Energy and Cell Voltage of REVC-10 as a Function of Discharge Current

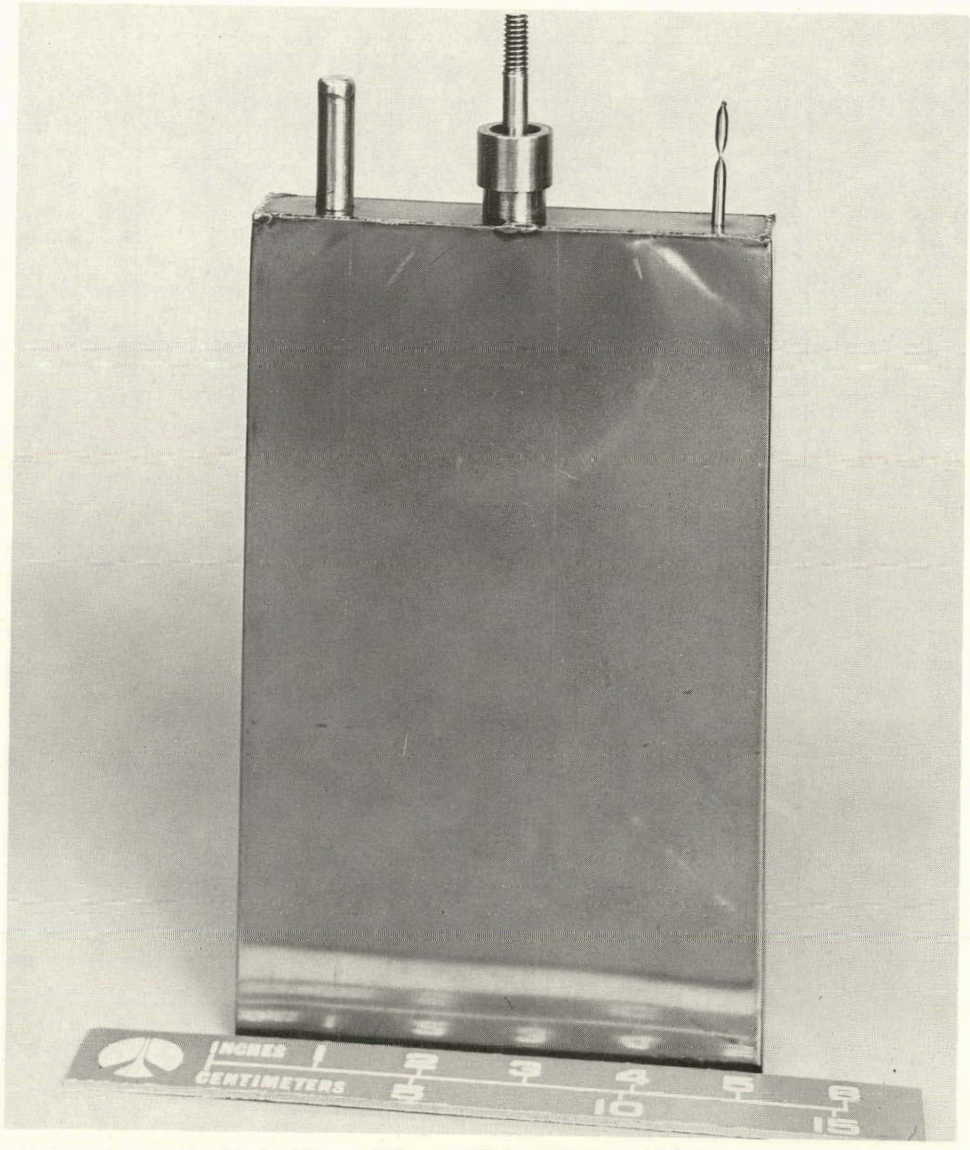

Fig. III-32. Electric-Vehicle Cell

2. Conceptual Design of a Stationary-Energy-Storage System
(E. Adler, I. Goldstein, W. Grieve, R. Talbot, T. Shimazaki, K. Yun, W. Wood)

Stationary energy storage offers an economic method for electric utilities to meet increasing peak demands and to improve their base generation load factor. Rockwell Energy Systems in conjunction with the Argonne National Laboratory (ANL) and the Electric Power Research Institute (EPRI), is developing the lithium alloy/iron sulfide battery for utility use.

The specific objectives of this work are three-fold:

1) to provide a conceptual design and cost estimate for a 100-MW-hr energy-storage plant,

2) to provide a design concept and cost estimate for a 240 kW-hr submodule for this 100 MW-hr plant,

3) to provide a preliminary reference design and cost estimate for a 4 MW-hr module which will be tested in the Battery Energy Storage Test (BEST) Facility.

The conceptual design for the 100-MW-hr energy-storage plant is discussed later (Section V.B).

A preliminary reference design for a stationary-energy-storage module using Li alloy/FeS cells to be tested in the Battery Storage Test (BEST) Facility has been prepared by Rockwell International. The BEST facility is designed to test electrochemical energy storage devices at a utility site during the 1980's. The test module will have a capacity of 4 MW-hr and will be operated at a nominal voltage level of 1000 V (dc), the limitation of the BEST facility converter. The battery module will comply with site specific environmental and safety regulations as well as dimensional constraints associated with the facility itself. The dimensional constraints are related to the test bay dimensions, 20 × 24 m, and the 6.3 m hook height of the building crane.

Figure III-33 shows a module as it would appear within the BEST facility. The only substantial difference between this module design and the one described for the 100 MW-hr plant is that one of the structural frames was eliminated to allow for smaller submodules. The height of air distribution manifolds for heat management was also reduced.

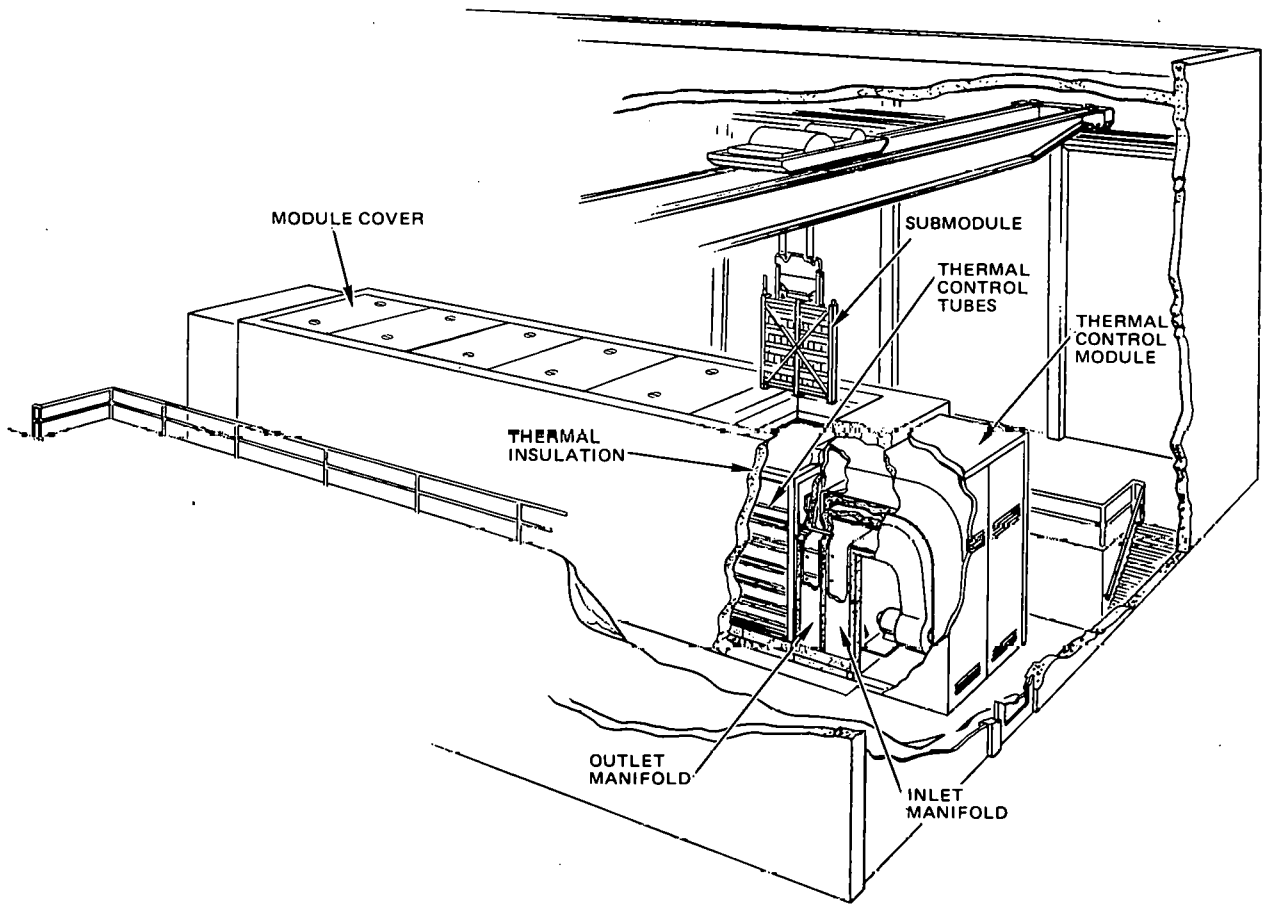

Fig. III-33. A 4-MW-hr Battery Module in the BEST Facility

3. Mark II Cost and Design Studies
(B. McFarland, T. Cowell)

The objective of this study is to provide information to the Argonne National Laboratory and the Department of Energy (DOE) concerning the feasibility of designing and manufacturing a cost-effective lithium/metal sulfide battery in the near term (1981-1986) for an electric vehicle (EV). The following events are projected during this period:

1980 - Demonstration of a 50 kW-hr EV battery that meets the Mark II goals (defined in Table I-1).

1983 - Initiate battery pilot production in a plant of about 250 MW-hr/yr capacity with a target selling price* of $60-100/kW-hr.

1986 - Initiate battery production in a plant of about 2000 MW-hr/yr with a target selling price* in the range of $40-60/kW-hr.

*Battery manufacturer's wholesale selling price in 1978 dollars.

The plant capacities and selling price goals listed above are based upon a preliminary market and cost analysis carried out at Argonne National Laboratory (ANL). The current study provides an opportunity for comment on the suitability of this schedule and to suggest alternatives.

The Energy Systems Group of Rockwell is performing a cost and design study prior to receipt of the contract. The contract work will not exceed three calendar months, and consists of three tasks:

1) Battery Manufacturing Cost and Design Study

2) Manufacturing Facilities Study

3) Mark II Development Program Definition

The effort is aimed at defining a Mark II battery which will meet the goals listed in Table I-1.

The company funded effort at Energy Systems Group has concentrated on concept selection trade studies for the Mark II battery, considering bi-, quad-, and hex-cell designs in conjunction with cylindrical and rectangular battery case designs. These trade studies have indicated that the battery output voltage should be the maximum allowed by the vehicle motor to minimize lead and cell resistance losses. Minimum system weight seems to occur when power losses due to lead and cell resistances are 6 to 8%. In addition, the trade studies indicated that a single battery case is desirable, and that a bicell design will be required in order to obtain a single battery case design capable of fitting in the envelope expected for the electric vehicles. The preliminary Mark II battery configuration being evaluated consists of 125 bicells connected in series in a cylindrical case insulated by aluminum vacuum foil. This study is scheduled for completion in late November 1978.

D. Other Contracts

1. Carborundum Co.

Late in 1976 the Carborundum Company conceived a process for the economical production of BN-felt separators. Equipment for three of the major process steps was designed, purchased, and installed in 1978. One of the process steps is the formation of 2-3-μm-diameter B_2O_3 fiber, which is the precursor to the BN fiber. The currently used BN fiber is 7-8 μm in diameter. The new, finer BN fiber is expected to provide a stronger, denser, more flexible BN-bonded BN-felt separator.

Felt forming and bonding equipment was also installed. Optimization of this equipment, which is designed to produce BN felt in continuous strips, will result in the production of samples of felt separator fabricated from 3-μm-diameter BN fiber. In 1979 and 1980, work is planned on the high-rate conversion of B_2O_3 fiber to BN fiber.

The production of about 275 kg of BN roving was completed in March 1978, and an additional 50 kg was added to the stockpile in September 1978. The laboratory facilities for producing sheets (30-cm square) of BN-felt

separators were expanded to the 25 m^2/month level from the previous level of 10 m^2/month. The production of 60 m^2 of BN felt was completed in September 1978 and added to the ANL stockpile. This felt was fabricated with a thickness of 2 mm and a weight of about 300 g/m^2.

2. General Motors Corporation

A contract has been negotiated with the Research Laboratories of the General Motors Corporation to undertake an experimental investigation of lithium-alloy/FeS_2 cells with molten LiCl-KCl electrolyte. A small test cell with an FeS_2 working electrode, a large Li-Si or Li-Al counter electrode, and a Li-Al reference electrode has been constructed. This cell is being used to evaluate the performance of the FeS_2 electrode as a function of the electrode thickness, porosity, and current collector. Tests are also planned on the effect of the LiCl concentration in the electrolyte on the electrode performance. The results of these studies will be used in developing a comprehensive mathematical model of the FeS_2 electrode in cooperation with personnel at Lawrence Berkeley Laboratory, the Illinois Institute of Technology, and ANL.

Since this work at General Motors Corporation was initiated late in FY 1978, most of the effort to date has consisted of a review of existing General Motors and ANL data on cells having FeS_2 electrodes and on the development of suitable cell designs and cycling equipment.

3. Illinois Institute of Technology

In the development of cells having FeS_2 electrodes, molybdenum is the only material that has been found suitable for use as a current collector in the positive electrode. Work is in progress at the Illinois Institute of Technology on the electrochemical deposition of molybdenum for joining and plating current-collector structures. The electrolyte selected for the high-temperature electroplating studies is the LiCl-KCl eutectic containing K_3MoCl_6.

The initial experiments in this study involved the electroplating of molybdenum on a nickel rod both in a static system and in a dynamic system (rod rotating). The results of the static and dynamic tests were essentially the same; in both cases a very thin (0.5 μm) layer of molybdenum had been deposited and a 2-5-μm-thick diffusion layer was observed in the nickel substrate. In some cases there was evidence of a thicker (5 μm) deposit of molybdenum, most of which had spalled off. Another feature that was observed was a region of cracks and voids between the diffusion layer in the nickel and the nickel substrate.

It is suspected that the difficulty in obtaining adherent deposits of molybdenum may be related to traces of moisture in the molten-salt electrolyte. Future work is planned with molten-fluoride electrolytes in which the presence of moisture is less critical.

4. ILC Technology, Inc.

In the present lithium/metal sulfide cell designs, an insulating electrical feedthrough is used to connect the positive electrode to the positive terminal outside the cell. Mechanical feedthroughs in which the seal is formed by compressing BN powder are currently in use. ILC Technology, Inc. has been developing an alternative feedthrough design in which a ceramic material serves as the electrical insulator and a hermetic seal is formed by brazing the ceramic to the metal housing.

The brazed feedthrough design lends itself to the use of light-weight, inexpensive stamped-metal parts instead of the machined parts used in the mechanical designs. The potential cost advantage and the pretested hermetic seal are desirable features of the brazed design.

The principal problem with the brazed feedthrough is the lack of compatibility between available braze materials and the molten LiCl-KCl electrolyte in the cell. The two feedthrough designs, shown in Fig. III-34, make use of a long, restrictive path to minimize access of the electrolyte to the brazed region. Feedthroughs of this type have been tested in partial cells at typical battery temperatures with the maximum charging voltage applied to the terminal. Although preliminary tests have given somewhat encouraging results, additional development work and testing will be required before brazed feedthroughs can be incorporated into prototype cell designs.

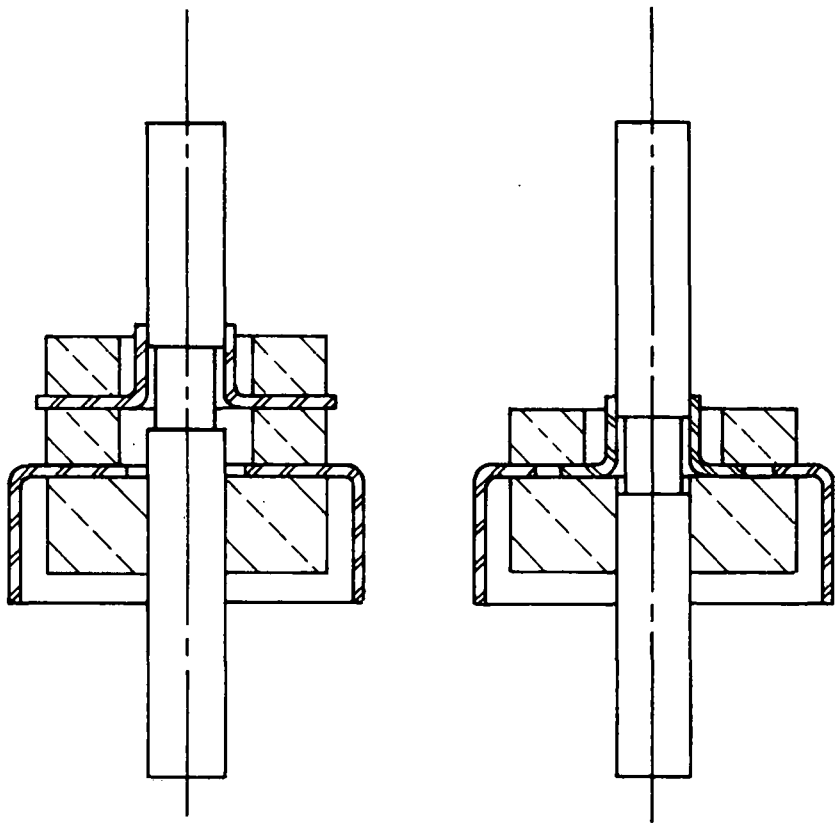

Fig. III-34. Brazed Ceramic to Metal Feedthrough Design

REFERENCES

1. Y-W. Hu, I. D. Raistrict, and R. A. Huggins, *Ionic Conductivity of Lithium Orthosilicate-Lithium Phosphate Solid Solutions*, J. Electrochem. Soc., *124*(8), 1240 (August 1977).

2. B. Tani, *X-Ray Study of $K_6LiFe_{24}S_{26}Cl$, a Djerfisherite-Like Compound*, Am. Minerologist, *62*, 819-823 (1977).

3. F. C. Mrazek and J. E. Battles, *Electrochemical Formation and Chemical Characterization of a Djerfisherite-Like Compound*, J. Electrochem. Soc., *10*, 124 (October 1977).

IV. INDUSTRIAL CELL AND BATTERY TESTING
(W. E. Miller and E. C. Gay)

During this report period, fabrication of equipment for testing cells and batteries was conducted. This equipment includes a facility to test large-scale (up to 60 kW-hr) batteries and another facility to test up to 50 industrial cells. Testing of lithium-aluminum/metal sulfide cells fabricated by industrial subcontractors (Eagle-Picher Industries, Inc. and Gould Inc.) was done at ANL. The improvements in cell designs that are demonstrated by this testing will be incorporated into future cells.

A. Equipment for Cell and Battery Testing

A facility for testing up to 50 industrial cells is currently being constructed at ANL; to be included as an integral part of this facility is a computer system for monitoring of cell performance and data acquisition. This facility will be used primarily for lifetime testing of industrial cells. A facility is also being constructed for laboratory tests of large-scale (up to 60 kW-hr) electric-vehicle batteries that will precede in-vehicle tests. This facility will have the capability for computer-controlled operation and data acquisition.

1. Electric-Vehicle Battery Test Facility
(V. M. Kolba, G. L. Chapman)

A laboratory is being prepared and equipped for static testing of two 60-kW-hr batteries. Batteries will be tested under a variety of modes, *e.g.*, discharges and charges at constant current or constant power; discharges that follow a driving profile such as a SAE J-227 profile;[1] or charges at constant voltage and cell equalization after bulk charging. These tests will employ computer-controlled power supplies. The same computer will be used with peripheral data-acquisition equipment to obtain and integrate the data and to display results either on a cathode-ray tube (CRT) or on hard copy. A block diagram of the system is shown in Fig. IV-1.

Robicon* power supplies (Fig. IV-2) provide the means for discharging and charging the battery. Their capability allows discharge currents of up to 1200 A and charge currents of up to 300 A; the maximum voltage is 250 V. Computer control of the current, by a microcomputer (Plessey, Micro-1), permits operation in various modes. The computer also provides safety monitoring of the battery under test and switching of modes of operation.

Figure IV-3 depicts the computer system and a segment of the CAMAC†-compatible data-acquisition system. Battery and cell voltages, battery current and battery temperatures are monitored on a periodic basis via multiplexers and analog to digital (A/D) converters coupled to a CAMAC system. Data from this system enter the computer for comparison, integration and

*Manufactured by Robicon Corp., Pittsburg, PA.

†The CAMAC System is an international, modular data-acquisition and control standard which, when interfaced to a computer, allows the use of remote stations to gather data and control various types of equipment used in industrial and specialized research projects.

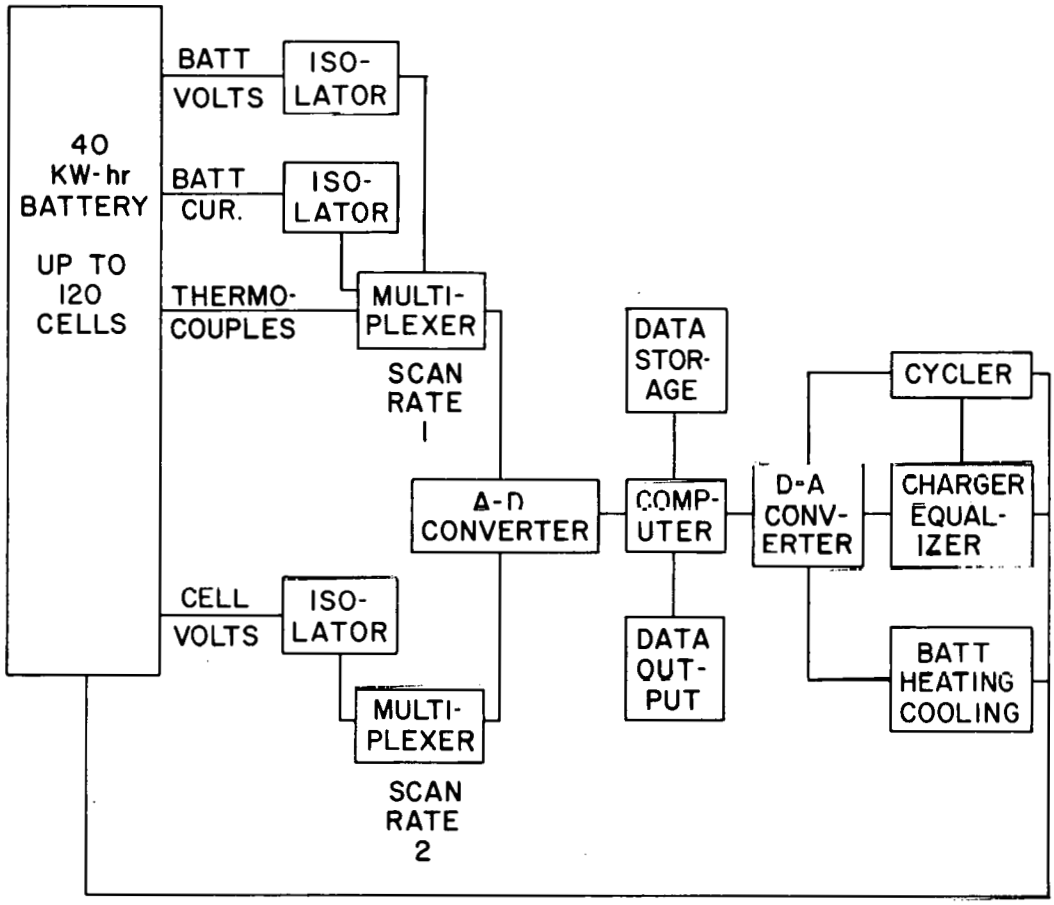

Fig. IV-1. Computer Control and Data-Acquisition System for Testing of Electric-Vehicle Batteries

processing. Memories of 20 K in the core and 5 megabytes on a disc provide storage for the programs, data acquisition and data reduction. A Decscope* provides the visual display, and a Decwriter provides the hard copy.

Equalization charging of the cells is provided by an individual Power-One power supply for each cell. The power supplies have been modified to have a current limit of 10 A at a constant voltage (adjustable) of ∿1.62 V. Each supply has its own voltage sensing leads. The power supplies have been assembled in two modules, each containing 60 power supplies. Provision has been made to control the modules independently or together as a complete system.

2. Fifty-Cell Lifetime Test Facility
(J. D. Arntzen, G. W. Redding, C. L. Chapman)

Construction of a facility capable of testing large numbers of cells for the electric-vehicle program is nearing completion. The emphasis will be on the testing of cells fabricated by industrial contractors to acquire

*Manufactured by Digital Equipment Corp., Maynard, Mass.

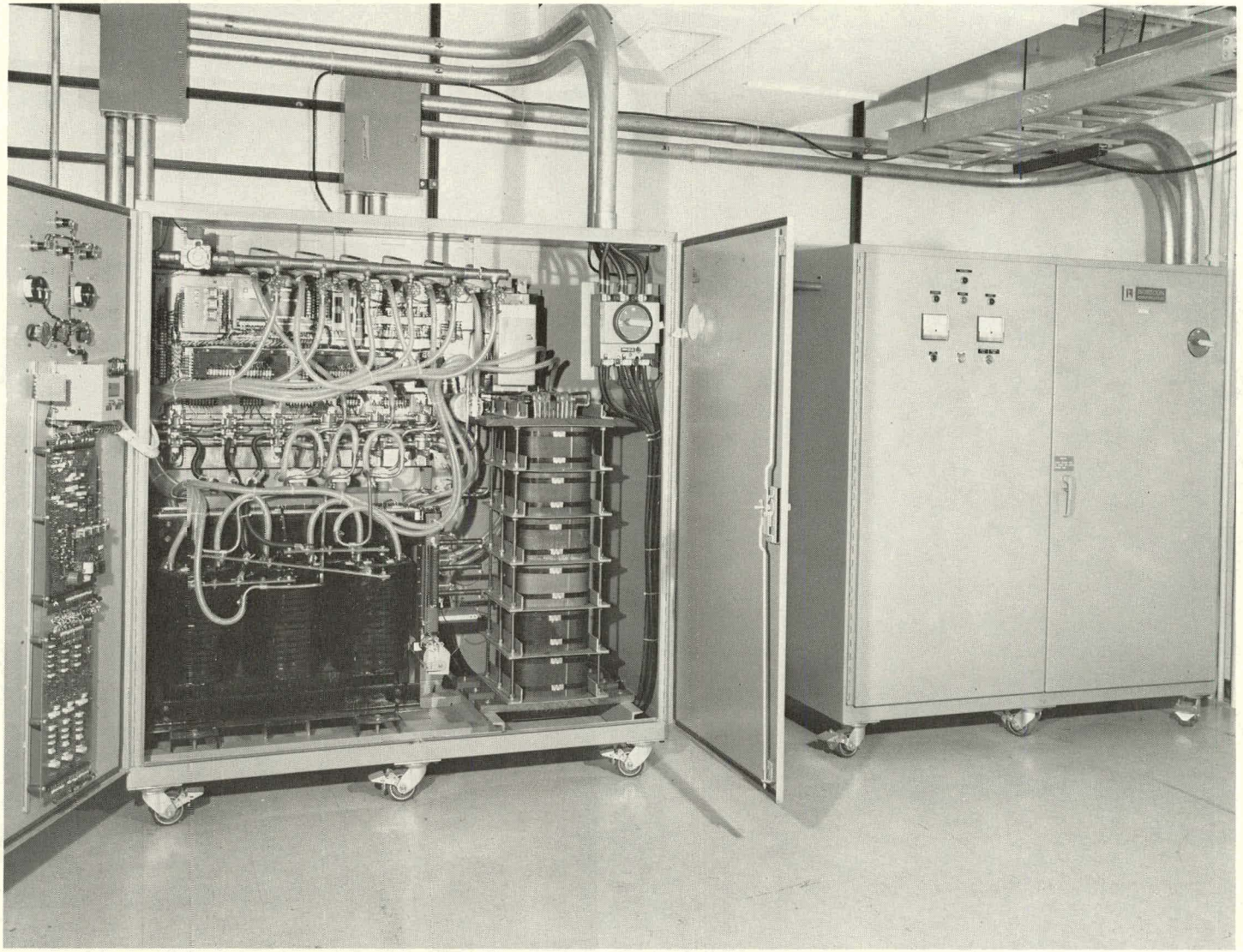

Fig. IV-2. Robicon Power Supplies for Battery Cycling
(ANL Neg. No. 308-78-491)

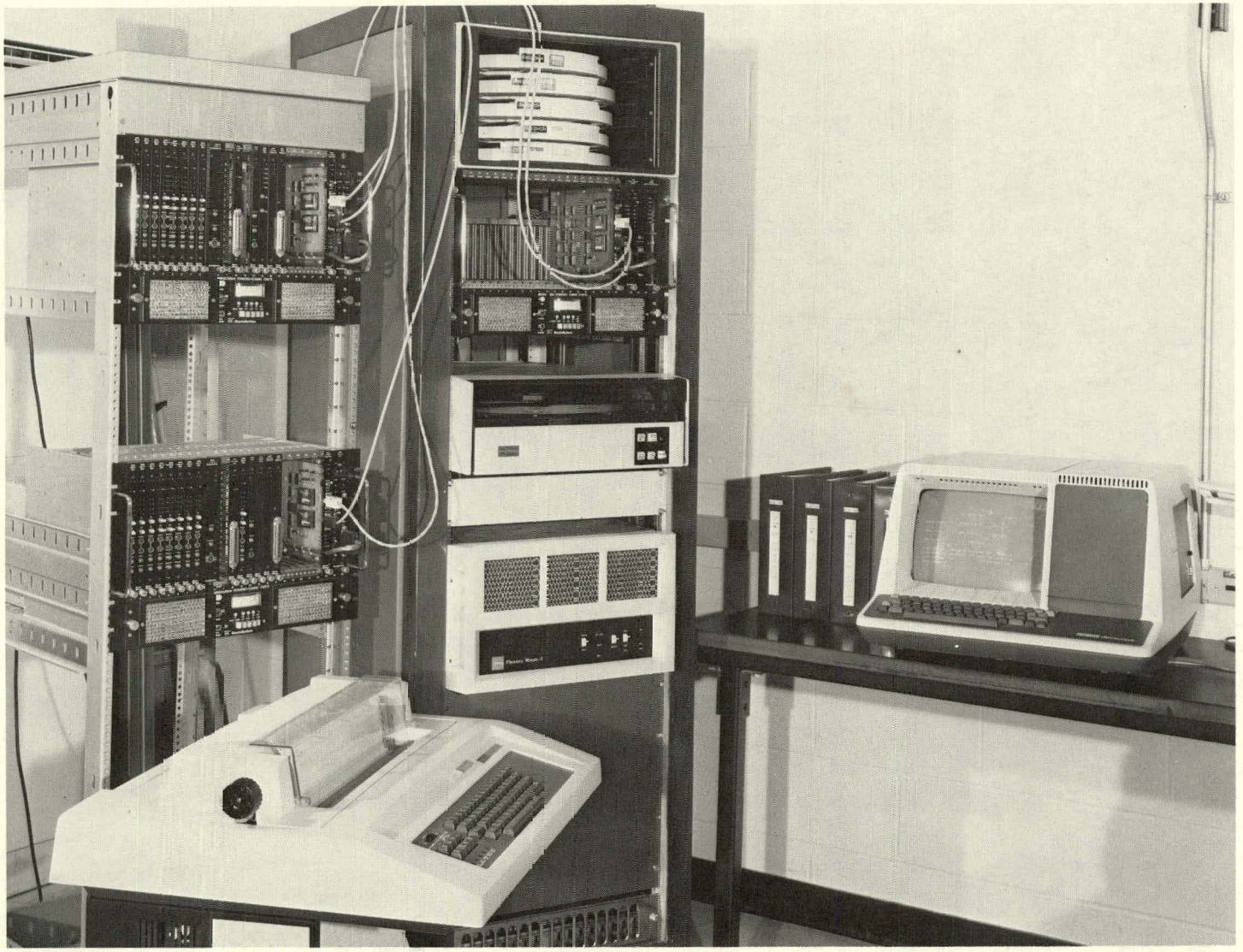

Fig. IV-3. Computer System for Battery Cycling
(ANL Neg. Nc. 308-78-464)

statistical data on the performance of these cells. Figure IV-4 is an overall view of the facility and shows the arrangement of the testing modules in the laboratory.

Each module consists of an open relay rack which contains the furnace unit, furnace temperature control panel, cell cycler, and power supply. Figure IV-5 is a view of a completed module. The furnaces are 114-L (30-gal) drums containing a rigid insulating material and heating elements. The cell being tested will be suspended from the lid of the drum along with heat shields and insulating material. Cell voltage and current leads and a thermocouple enter the drum through feedthroughs in the furnace lid; heater power enters through the side of the drum. All of the furnaces are connected to a low-pressure argon manifold which will provide a positive-pressure argon blanket to reduce atmospheric corrosion. Figure IV-6 shows the furnace configuration.

A prototype cell cycler for use in the test facility was designed and built by the ANL Electronics Division. After the unit had been tested and debugged, bids were solicited and a contract was signed with a commercial vendor (Paraplegics Inc.) for the fabrication of 50 cyclers.

A computer-based data-acquisition system has been purchased to process the information generated by the cell testing facility. The terminals and part of the data-acquisition equipment will be housed in an air-conditioned enclosure adjacent to the facility; the computer will be located remotely.

All data from the 50-cell test facility will be fed to a data-acquisition computer system that will store and compute all desired information on cell performance. Signal leads for voltage, current, and temperature from the individual modules will be fed to a CAMAC crate in the adjacent data-acquisition enclosure. In the CAMAC crate, the signals will be converted from analog to digital, amplified, and multiplexed before being sent to the computer room in another part of the building.

In the computer enclosure the signals are received in another CAMAC crate which contains the computer interface. Data will be sent to a PDP 1134 computer which will process the data into the required form. Data will be available for the following cell parameters: capacity (A-hr), energy (W-hr), elapsed time (hr), average voltage (V), average current (A), and average temperature (°C).

The above data will be displayed in the data-acquisition-system enclosure and the computer room on CRT terminals, and can be printed out on Decwriter terminals. In addition, hard-copy plots can be obtained in the computer room on a Versatek printer-plotter. The computer will utilize disc and magnetic tape for short- and long-term storage, respectively. The displays will include information coded to cell number, cycle number, and time of start and finish of each half cycle. The computer will also store data in the event of power failure, and bootstrap up upon return of power (see Fig. IV-7).

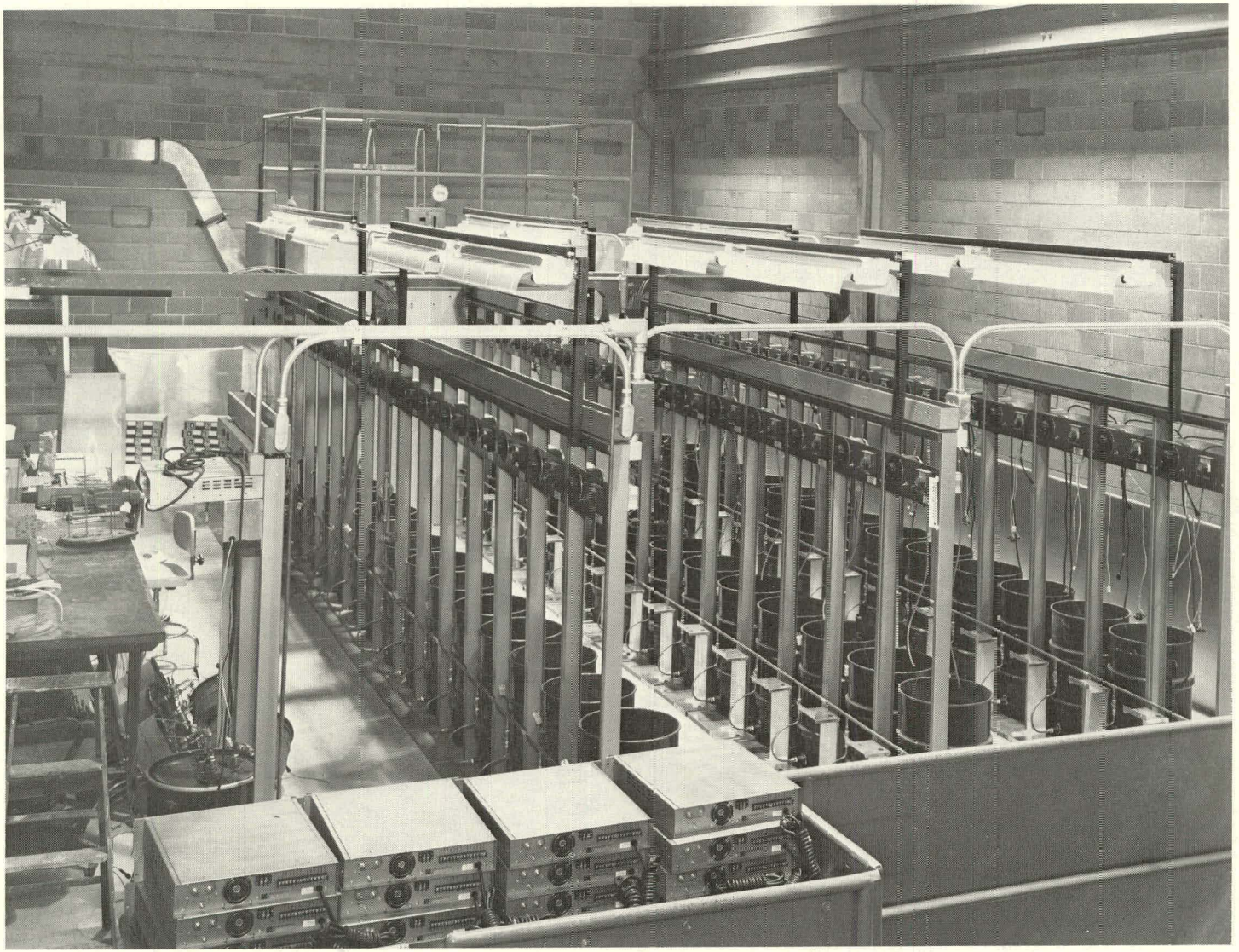

Fig. IV-4. Overall View of 50-Cell Test Facility (ANL Neg. No. 308-78-463)

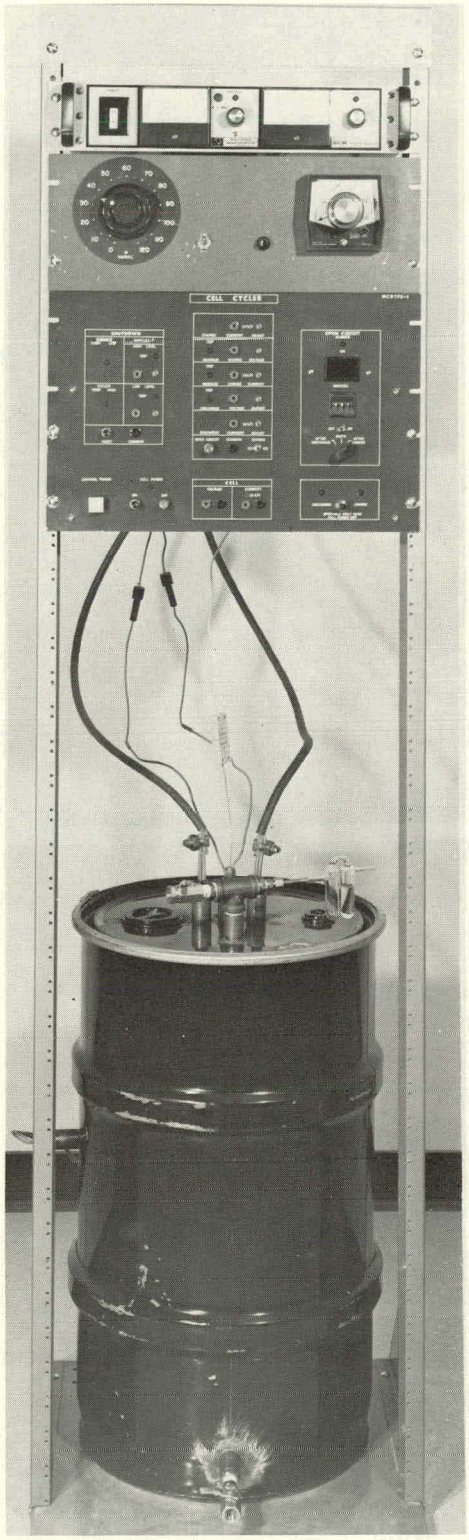

Fig. IV-5. Individual Cell Testing Module (ANL Neg. No. 308-78-178)

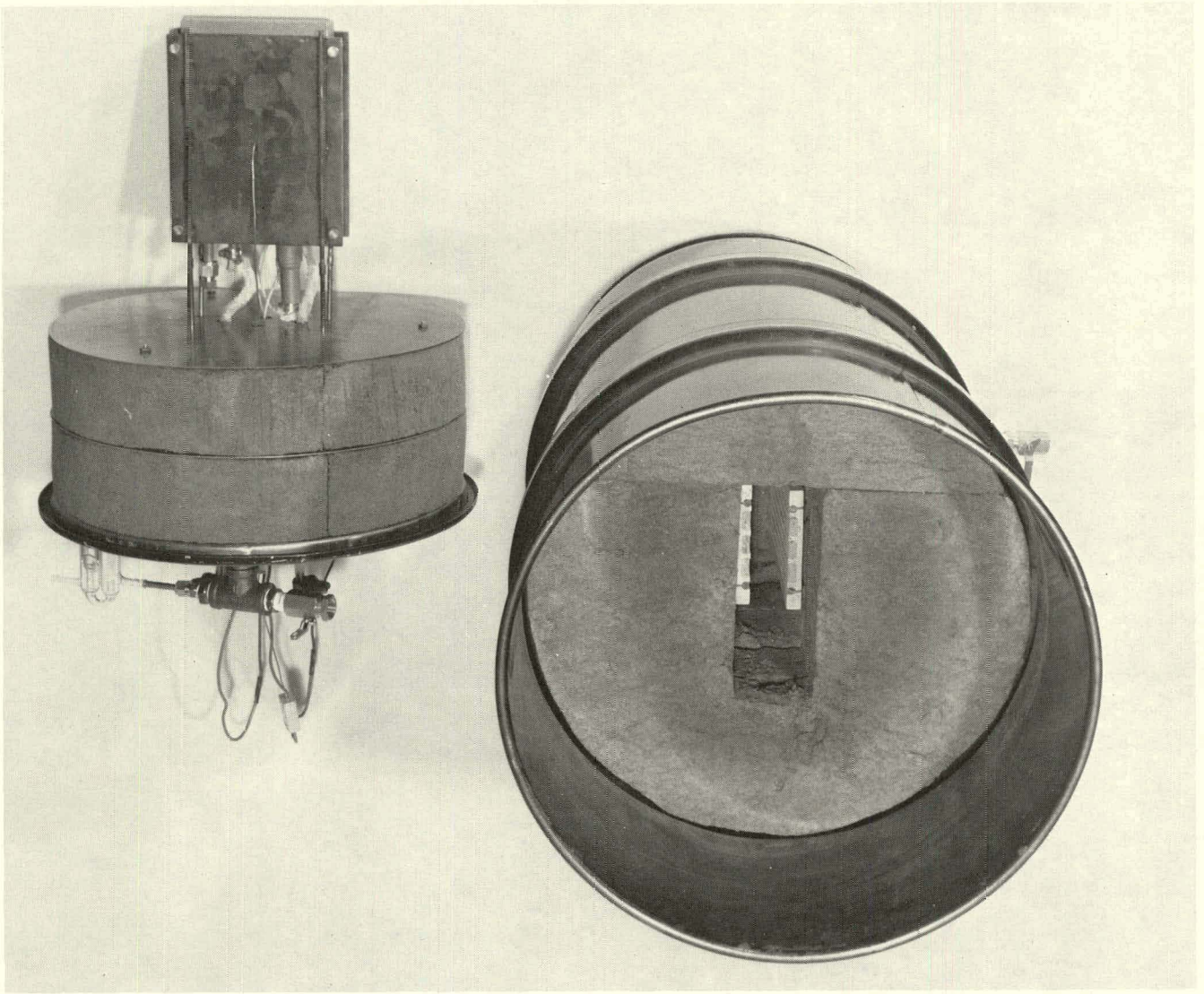

Fig. IV-6. Furnace for 50-Cell Test Facility Module (ANL Neg. No. 308-78-179)

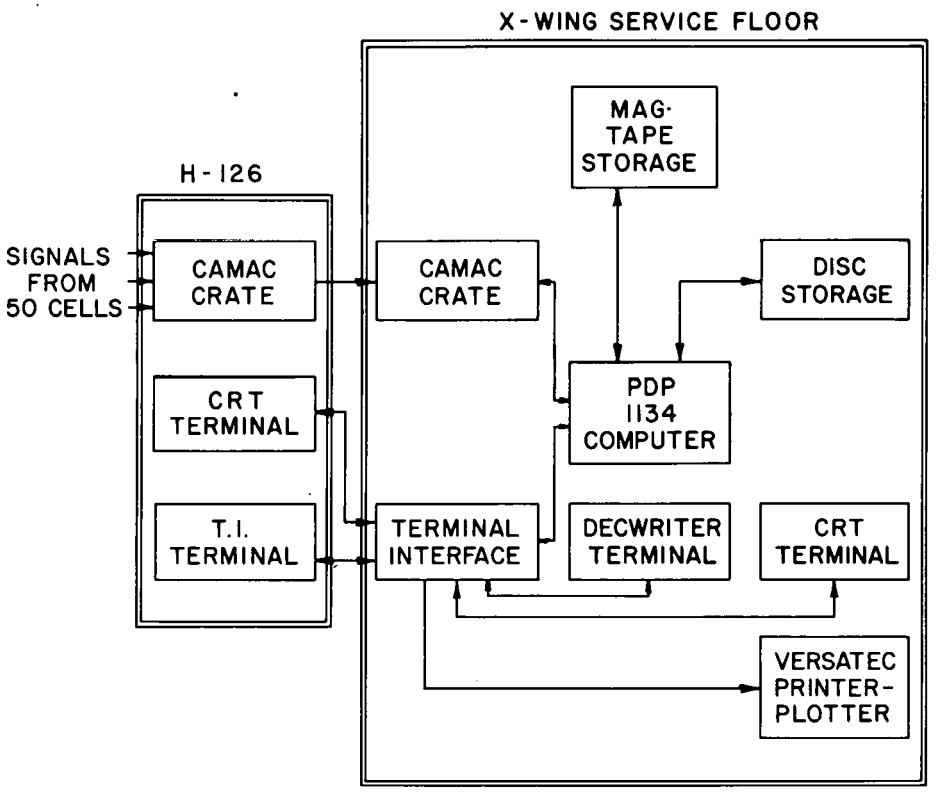

Fig. IV-7. Data-Acquisition System for 50-Cell Test Facility

Currently, all of the furnace control panels are installed in the modules and wired. The power supplies have arrived and 46 out of 50 have been modified to be compatible with the cell cyclers. The enclosure for the data acquisition system has been completed with lights, power, and air conditioning. Data cables have been run and wired to the modules and all data cables between the enclosure and the remote computer facility have been installed. All wiring harnesses for the components in the modules have been fabricated and will be installed upon receipt of the cyclers. The first batch of ten cyclers is due to arrive at ANL late in the year. The argon manifold and connections to the individual furnaces have been completed. Final assembly of the furnace lids is currently under way.

To expedite the testing of some Eagle-Picher multiplate cells, three modules were completed and placed in operation. Operation of the modules has been very satisfactory. The furnaces can operate at 455°C with a heating power input of only 120 W.

B. Testing of Contractor-Produced Cells

Two industrial firms under contract with ANL--Eagle-Picher Industries, Inc., and Gould Inc.--have fabricated Li-Al/FeS and Li-Al/FeS_2 bicells.*

*This type of cell consists of a central positive electrode and two facing negative electrodes.

These cells have been qualification tested, either at ANL or the contractor's laboratories, to determine the optimum design features for this type of cell. In addition, other tests have been performed on these cells to determine optimum operating conditions.

1. Qualification Testing of Eagle-Picher Cells
(T. K. Kaun, P. F. Eshman, W. A. Kremsner)

Eagle-Picher has delivered about 55 bicells during the period covered by this report. The designs of these cells were basically the same as those of the baseline FeS and FeS_2 cells (ANL-76-98, pp. 14-15), but with carefully selected variations (ANL-77-75, pp. 17-18). The baseline cells contained FeS_2 thin (Type 2A) and thick (Type 2B) electrodes as well as FeS thin (Type 1A) and thick (Type 1B) electrodes. The baseline variations included electrode thickness, electrode loading (A-hr/cm^3), separator material, position and diameter of positive terminal rod, and design of the positive current collector. The modifications are evaluated by computer-controlled testing that permits a comparison of specific energy and power characteristics of the various cells. Nearly thirty-two Eagle-Picher bicells were tested at ANL during this report period. Performance data for these cells are presented in Appendix C.

Figure IV-8 shows the utilization of active material in the positive electrodes of the FeS cells as a function of discharge current density. The

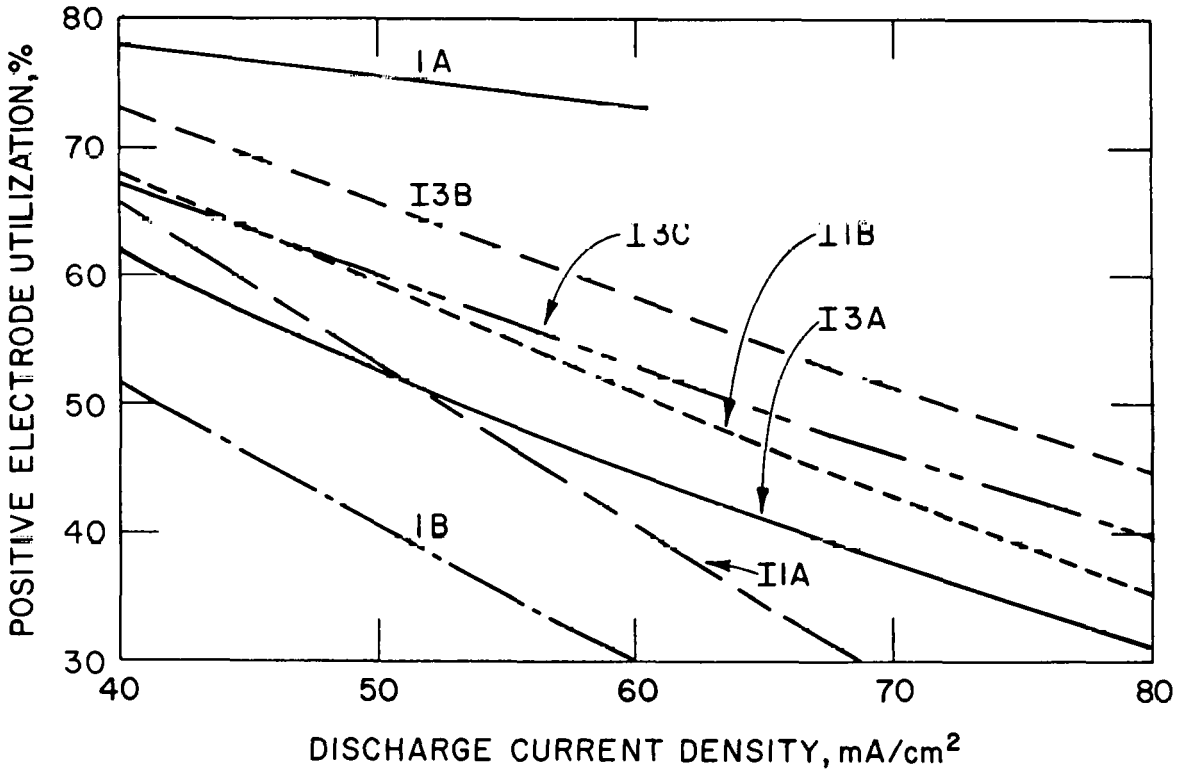

Fig. IV-8. Utilization of Active Material in Eagle-Picher Charged FeS Cells (at least two cells of each type were operated)

utilization of the baseline thin-electrode cells (Type 1A) was much higher than that of the thick-electrode cells (Type 1B) . However, the specific energies of both cells (about 48 W-hr/kg at an 8-hr rate) were lower than those of more recent cells (Type I1A, I1B, I3A, I3B, I3C); this result is partially due to the lower electrode loading (0.77 A-hr/cm^3) and correspondingly higher electrolyte fraction of the baseline cells. The negative electrodes were essentially the same thickness in the Type I3A and I3B cells; however, a thinner positive electrode was used in the 13B cells to obtain higher utilization. With the lowered ratio of active material to cell weight for I3B, the two types of cells had equal specific energies of 52 W-hr/kg. In the Type I3C cell, the negative electrodes were essentially the same thickness as that of the Type I3A and I3B cells, but the capacity loading density of the electrode was increased 13% by decreasing its electrolyte volume. The positive electrode of the Type I3C cell had the same capacity loading volume density as the positive electrode in I3A but was 73% as thick. These design changes reduced the utilization but increased the specific energy to 68 W-hr/kg at the 8-hr rate. Specific energy was influenced more by the loading density than by the utilization.

Investigations by the Cell Chemistry Group (ANL-78-45, pp. 55) and others [2-4] indicated that FeS cell performance can be improved by the addition of LiCl to LiCl-KCl eutectic electrolyte. Thus an Eagle-Picher FeS-Cu_2S cell, 1A5, was operated to assess the effect of LiCl-rich electrolyte (67 mol % LiCl-33 mol % KCl) on performance. This cell had the same design as Cell 1A6 (75 A-hr theoretical capacity), which operated for 96 cycles (66 days) without a decline in performance. Operation of Cell 1A5 was terminated after 43 cycles (19 days) due to a short circuit in the electrical feedthrough. The specific energies and the peak specific powers of these cells were nearly identical--47 W-hr/kg at the 4-hr rate and 45 W/kg, respectively. Positive-electrode utilizations of the theoretical capacity (75 A-hr) were 70% at a current density of 40 mA/cm^2, 66% at 65 mA/cm^2, and 47% at 130 mA/cm^2. The LiCl-rich electrolyte changed the shape of the discharge voltage *vs.* capacity curve; two distinct voltage plateaus were exhibited instead of one. However, the average voltage was unchanged. This alteration of the voltage curve may be associated with suppression of J-phase formation. No overall improvement in cell performance could be attributed to the use of a LiCl-rich electrolyte in a Li-Al/FeS-Cu_2S additive cell; however, the use of LiCl-rich electrolyte in an engineering-scale FeS cell with no Cu_2S additive has been found to improve performance of recent cells.

Performance data for Eagle-Picher Li-Al/FeS_2 cells are presented in Table IV-1. In addition, the positive-electrode utilizations, the specific energies, and the specific powers for these cells are plotted as a function of discharge current density in Figs. IV-9, -10, and -11, respectively. The positive-electrode utilizations for the Type 2A cells are considerably higher than those for Type 2B cells (thick electrode), but the specific energies are lower. The Type I4 cells were built and tested to evaluate the effect of an off-center positive terminal rod; both the utilization and the specific energy of the Type I4 cells were reduced by this change. Electrode loading densities were increased in the I6A-series cells. Although the utilization was reduced in the Type I6 cells, the specific energy and power were improved as shown in Figs. IV-10 and IV-11. Cell I73 had an even higher electrode

Table IV-1. Data and Test Results from Eagle-Picher Two-Plateau Li-Al/FeS_2 Cells

Cell No.	2A5	2B7	I6A	I73	I8L-034	I8H-041
Electrode Thickness, mm						
Positive[a]	3.4	6.3	4.0	5.2	5.1	2.8
Negative	3.3	6.8	6.5	6.6	7.6	4.2
Cell Capacity, A-hr						
Positive Electrode	70	155	155	222	220	117
Negative Electrode	70	155	200	227	290	148
Electrode Loading, A-hr/cm^3						
Positive	0.67	0.79	1.29	1.36	1.39	1.35
Negative	0.67	0.73	0.98	0.99	1.21	1.10
Positive-Electrode Utilization, %						
Current Density, 40 mA/cm^2	77.4	72.7	62.5	55.0	66.4	71.0
Current Density, 80 mA/cm^2	66.7	55.7	51.3	50.7	56.4	63.0
Product of Utilization and Electrode Loading, A-hr/cm^3						
Current Density, 40 mA/cm^2	0.52	0.57	0.81	0.75	0.92	0.96
Current Density, 80 mA/cm^2	0.45	0.44	0.66	0.69	0.78	0.85
Specific Energy, W-hr/kg						
Current Density, 40 mA/cm^2	64.1	79.8	82.5	91.0	120.1	98.0
Current Density, 80 mA/cm^2	44.0	54.5	67.0	79.0	99.1	83.8
Peak Power, W	84.5	97.5	94.3	126	106	136
Peak Power Flux, W/cm^2						
Fully Charged	0.27	0.31	0.30	0.40	0.34	0.43
50% Discharged	0.22	0.21	0.19	0.28	0.19	0.25
Cell Resistance	8.5	7.5	9.0	6.9	6.6	5.3

[a]Because the cells have two negative electrodes and one positive electrode, the positive electrode is considered to consist of two halves, each having the thickness given here.

loading density than the Type I6 cell, and this change resulted in an even higher specific energy. Cell I73 was also used to test the effect of a modified positive current-collector design on cell resistance. This modified current collector reduced cell resistance and consequently increased specific power (see Table IV-1 and Fig. IV-11).

The Type-I8 cells were used to test options for the cell separator/retainer. Boron-nitride felt separators were used in six thick-electrode cells. All six cells developed short-circuits or exhibited poor coulombic efficiency within the first 20 cycles. The primary cause of short-circuiting may have been the poor quality of the BN felt used in these cells. Some modifications of the cell design may be necessary to achieve acceptable lifetimes. Problems in wetting of the BN felt by electrolyte were also encountered. One test of a sufficiently wetted BN felt indicated that the felt

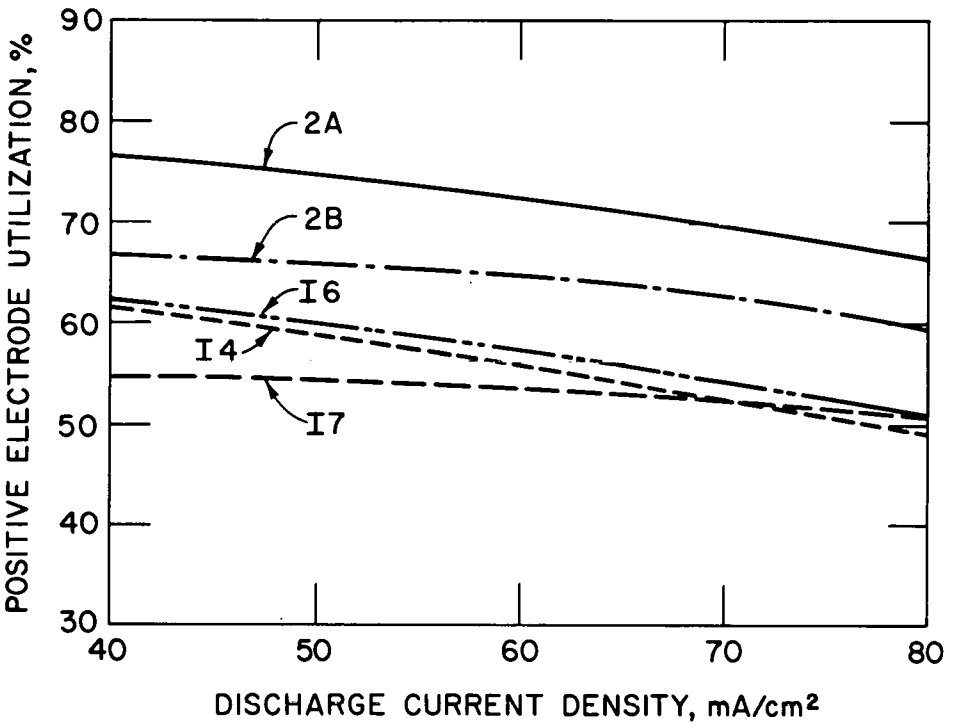

Fig. IV-9. Utilization of Active Material in Eagle-Picher Charged FeS_2 Cells (at least two cells of each type were operated)

results in lower cell resistance than that obtained with BN fabric (9 *vs.* 11 mΩ). A lower resistance improves the capability of the cell. Cell I8L-034 was built with no particle-retaining screens or cloths at all on the electrodes; BN fabric was used as the separator. The positive-electrode current collector had an open molybdenum honeycomb (no center plate) design similar to that in Cell I7A. The initial resistance of the cell at room temperature (electrolyte frozen) was fairly high, about 3 MΩ. The cell was cycled at very low currents (3-A charge and 3-A discharge) for two cycles. Under these cycling conditions, 95% utilization of the positive electrode was attained. During cycling, the specific energy and peak specific power of this cell were very high, 90 W-hr/kg at the 4-hr rate and 65 W/kg, respectively, and a low cell resistance was achieved (6.5-7.5 mΩ). Although the cell developed a short circuit within 20 cycles, it indicated improved performance for the Eagle-Picher cell design.

The Li-Al/FeS_2-CoS_2 cell, I8H-041, had thin electrodes (<3 mm), a BN-fabric separator, and molybdenum screen and Y_2O_3-felt particle retainers. The positive-electrode current collector was a modified open-molybdenum honeycomb structure having an offset terminal rod. This cell demonstrated good specific power characteristics. The low cell resistance of 5.4 mΩ resulted in peak specific power levels of 112 W/kg and 65 W/kg, respectively, at 95% and 50% states of charge. The specific energy was >85 W/kg at the 4-hr rate. A light-weight crimped feedthrough permitted a reduction of the cell weight to 1.22 kg. The cell was life-tested at a current density of

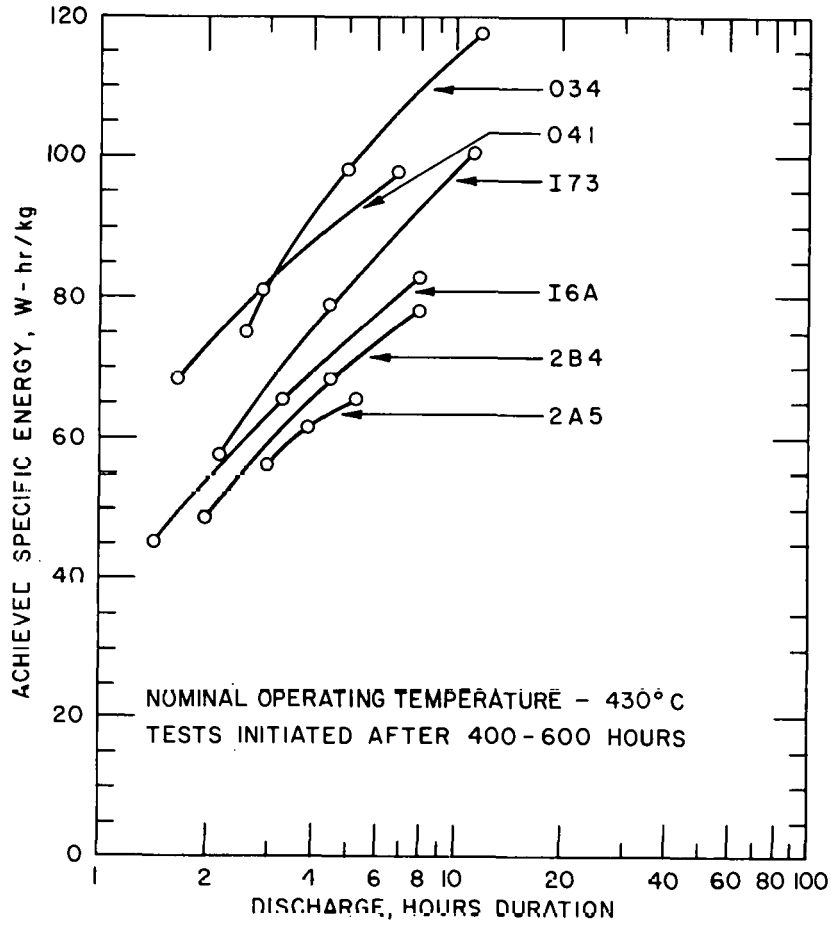

Fig. IV-10. Specific Energies of Eagle-Picher Li-Al/FeS_2 Cells

33 mA/cm^2. The test was terminated at 54 cycles (1000 hr) due to a decline of the coulombic efficiency to <70%.

The results obtained from the above tests of Eagle-Picher cells indicate that the specific energy of a bicell can be increased more effectively by maximizing the electrode capacity density (the product of electrode loading in A-hr/cm^3 and the utilization) than by maximizing the utilization alone. Also, the higher utilization of thin-electrode cells does not compensate adequately for the lower ratio of active material to cell weight. A comparison of Fig. IV-8 with Fig. IV-9 shows that the utilization for Li-Al/FeS cells decreases much more rapidly with increasing current density than that for Li-Al/FeS_2 cells (except in the case of the Type 1A cells). The utilization *vs.* current density curves for cells having thin FeS and thin FeS_2 electrodes (Types 1A and 2A, respectively) were similar. In all cases the cell resistance was the dominant factor in the power capability.

2. Testing of Eagle-Picher Cells

Tests were conducted on Eagle-Picher cells to determine the effect on performance operation at an elevated temperature (>450°C) and to determine the open-circuit voltage as a function of state of charge at 450 and 500°C.

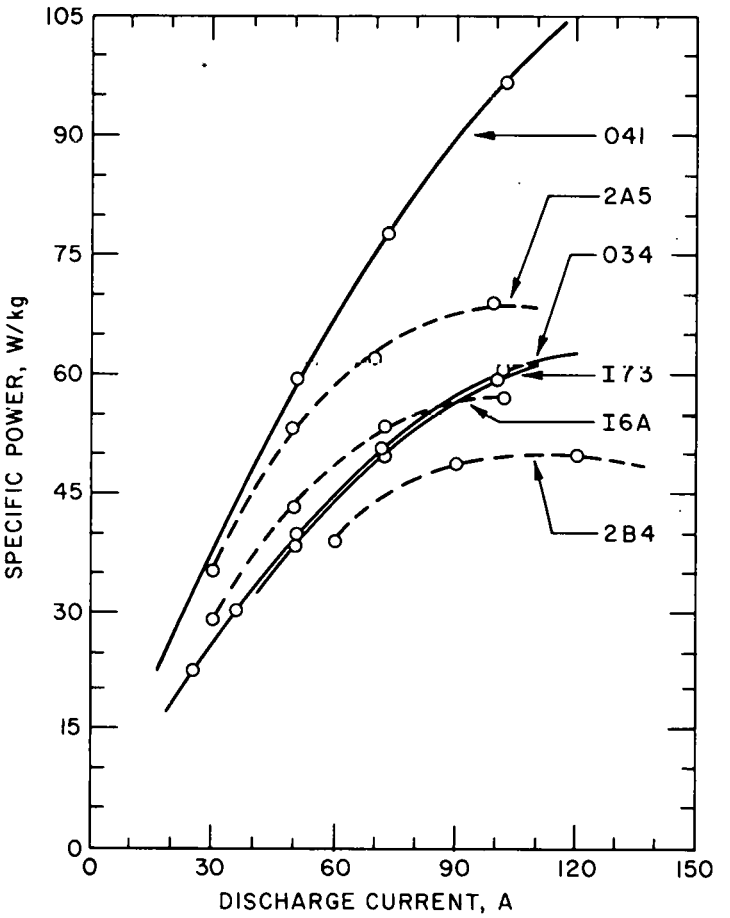

Fig. IV-11. Specific Power Data for Eagle-Picher Li-Al/FeS_2 Cells

a. Open-Circuit Voltages of a Partially Discharged Li-Al/FeS Cell (V. M. Kolba, G. W. Redding, J. L. Hamilton)

Tests were conducted to determine the open-circuit voltage of a Li-Al/FeS-Cu_2S cell as a function of its state of charge. Cell I3C1, which had about 16 mol % Cu_2S in the FeS electrode, was used for these tests. Five preliminary discharges to 0.90 V followed by charges to 1.65 V were conducted to establish capacity ratings for the cell, which were 62.5 A-hr at 450°C and 102 A-hr at 500°C.* The cell was then discharged in increments of 25% of the rated capacities to arrive at 25, 50, 75, and 100% states of discharge at the two temperatures. After each partial discharge, the cell was placed on open circuit for one hour before the voltage was measured. The open-circuit voltage values, which are presented in Table IV-2, are averages of up to four sets of measurements at each temperature and state of discharge.

*In ANL-78-45, p. 55, cell operation at elevated temperature (>450°C) was suspected to inhibit the formation of "J phase" ($LiK_6Fe_{24}S_{26}Cl$) and thereby to increase cell capacity.

Table IV-2. Open-Circuit Voltage of a Li-Al/FeS-Cu_2S Cell as a Function of State of Discharge

Temp., °C	Capacity Discharged %	Capacity Discharged A-hr	Open-Circuit Voltage, V
450	∿0	1.3	1.453
500	∿0	2.0	1.451
450	25	15.6	1.432
500	25	26.0	1.419
450	50	31.2	1.333
500	50	51.0	1.288
450	75	46.9	1.297
500	75	77.0	1.270
450	100	62.5	1.274
500	100	102.0	1.250

Two conclusions can be drawn from these data. (1) The cell capacity is significantly higher at 500°C than at 450°C, and (2) increasing the temperature decreases the open-circuit voltage of the cell at various states of discharge.

b. Effect of Operating Temperature on FeS Cell Capacity
(V. M. Kolba, G. W. Redding, J. L. Hamilton)

The effect of operating temperature (425°C $\leq$ T $\leq$ 525°C) on cell capacity has been investigated in tests of five FeS cells. Design features of these cells are presented in Table IV-3. All cells exhibited a decline in achievable capacity with cycling; however, the coulombic and energy

Table IV-3. Design Features of Cells

Cell No.	Theoretical Capacity, A-hr	Electrode Loading, A-hr/cm^3 Negative	Electrode Loading, A-hr/cm^3 Positive	Cu_2S in FeS Electrode, mol %
1B4	149	0.65	0.76	16
I3B2	127	0.80	0.70	16
I3C1	145	0.85	1.05	16
I3C2	145	0.85	1.05	16
EMP-5-017[a]	406	0.90	1.17	10

[a]Multiplate cell design (see Section III.A.1).

efficiencies remained high for all cells except 1B4. As can be seen in Table IV-4, capacity increases when the temperature is raised from 425 to 525°C. The degree of capacity improvement appears to vary with the total

Table IV-4. Cell Performance at Various Temperatures

Cell No.	Cycle No. Prior to Test	Discharge Current, A	Capacity, A-hr 425°C	450°C	475°C	500°C	525°C
1B4	1130	10	38	-	-	91	-
		15	27	-	-	72	-
I3B2	117	10	95	-	-	105	-
		15	-	-	-	92	-
I3C1	430	10	47	70	-	91	-
I3C2	399	10	65	94	103	103	104
EMP-5-017	78	70	-	229	264	282	-

number of cycles prior to raising the temperature, and was greatest for Cell 1B4 at a 10-A discharge rate. The increased capacity, however, was not permanent. When the temperature was returned to 425°C, all cells returned to their previous capacity within about three cycles.

Although significant improvement was obtained at temperatures of 450 to 475°C (see Cell I3C2, Table IV-4), operation at temperatures approaching 500°C for long periods of time has been shown to increase the corrosion rates of the cell materials (ANL-76-9, p. 45). Based on the test data from Cells I3C1 and I3C2, a nominal temperature of 450°C was selected for Li-Al/FeS batteries, with a maximum of 500°C for short periods of time.

3. Testing of Gould Upper-Plateau FeS_2 Cells
(T. D. Kaun, W. A. Kremsner, P. F. Eshman)

Gould Inc. delivered 55 upper-plateau* Li-Al/FeS_2 bicells to ANL during this reporting period. Performance data on these cells are presented in Appendix C. The Gould cells consist of hot-pressed, 13 x 18 cm (5 x 7 in.) electrodes that are assembled in the uncharged state. These cells are being tested to determine the effect on performance of the following design features: current-collector design, lithium content of the negative electrode, electrolyte volume, thickness of the positive electrode, and method of particle retention. The following seven-day cycling schedule (computer controlled) for testing these cells was established by ANL and Gould: discharge current densities of 33, 66, 100 and 133 mA/cm^2 with a discharge-cut-off voltage of 1.30 V (IR-free), and a current-limited (33 mA/cm^2), constant-voltage (2.15 V) charge. This cycling mode provided consistent data necessary for evaluation of subtle changes in performance from cell to cell; variability due to inconsistent cell resistances was also diminished. The seven-day cycling schedule also included 15-second discharge power pulse sequences at 97% and 50% states of charge. Graphs of cell voltage *vs.* capacity at dis-

*These cells are operated only on the upper of two voltage plateaus that are characteristics of FeS_2 cells.

charge current densities up to 133 mA/cm^2, specific energy *vs.* discharge rate, and specific power *vs.* current were computer-generated for most of the cells.

Performance data on 17 Gould cells are presented in Table IV-5. Higher cell capacity was found for cells of similar design when the charged negative electrode contained 50 at.% rather than 45 at.% lithium. At the fully discharged state, four cells with 5.6-mm thick positive electrodes (namely, Cells G04-03A, -005, -11A, and -017) had 27-29 at.% lithium in the negative electrodes, and four cells with 10.4-mm-thick positive electrodes (namely, Cells G04-09A, -13A, -14B, and -19A) had about 30 at.% lithium regardless of the fully charged composition or the assumed utilization of the negative electrodes. This common composition in the discharged negative electrode indicates that the capacity of the cells with the high assumed negative utilizations (*i.e.*, 75-85%) was limited by the negative electrode.

Since the negative electrode appears to limit capacity in some of the Gould cells, an assessment of the upper-plateau FeS_2 electrode is difficult. Nonetheless, high utilizations of upper-plateau capacity have been achieved. Cell G04-010 showed greater than 85% utilization of the theoretical capacity of the upper-plateau FeS_2 electrode at a current density of 100 mA/cm^2 (45 A), and low electrode polarization. Although not optimized for specific energy, Cell G04-010 achieved 75 W-hr/kg at the 4-hr rate. A thin-electrode Cell, G04-03A, achieved a peak specific power of 75 W/kg.

Figure IV-12 illustrates typical improvement in cell performance using 50 at.% (Cell G04-009) *vs.* 45 at.% (Cell G04-13A) lithium. The two cells are otherwise identical. The capacity of Cell G04-009 is 10-20% greater than that of Cell G04-13A, and it exhibits less decrease with increased discharge rate.

The effect of variations in positive-electrode porosity was evaluated by comparing Cells G04-012 (30% porosity*) and G04-014B (40% porosity*). The positive theoretical capacities of the two cells are similar; Cell G04-014B has a thicker positive electrode to accommodate the increased porosity. These modifications resulted in a somewhat lower capacity utilization (74% compared to 83% for Cell G04-012). The voltage *vs.* capacity curves for these two cells showed similar electrode polarization characteristics. Cell G04-25, which has a positive electrode porosity of 25%, exhibited very stable capacity at current densities up to 100 mA/cm^2. No meaningful evaluation of this cell's utilization can be made, however, because of a change in the current-collector design. With the available data, no case can be made for increasing positive electrode porosity above 30%.

As can be seen in Table IV-5, Cells G04-001, -002, and -09A have positive electrode thicknesses of 5.6, 8.0, and 10.4 mm, respectively, and 50 at.% lithium in the charged negative electrode. In general, the cell with the thicker positive electrode had a predictably lower utilization. This effect is illustrated in Fig. IV-13. Thus the capacities of these cells appear to be limited by the positive electrode. For the thick-electrode

---

*Measured with cell in discharged state.

Table IV-5. Performance Data on Gould Li-Al/FeS_2 Cells

Gould Cell No.	Positive Electrode Thickness, mm	Positive Electrode Theor. Capacity,[a] A-hr	Assumed Negative Electrode Utilization,[b] %	Lithium Content of Li-Al Electrode, at.% Charged	Lithium Content of Li-Al Electrode, at.% Discharged	Cell Capacity, A-hr, at Indicated Current Density 33 mA/cm^2	67 mA/cm^2	100 mA/cm^2	133 mA/cm^2	Cell Resistance, mΩ
G04-001	5.6	95.4	65	50.0	29.8	86	86	86	87	6.3
G04-03A	5.6	96.1	75	50.0	28.6	82	81	81	81	5.5
G04-005	5.6	96.1	85	50.0	28.6	71	71	71	70	5.0
G04-002	8.0	138.6	65	50.0	31.1	121	114	110	102	5.0
G04-09A	10.4	181.1	65	50.0	30.2	164	139	126	c	6.0
G04-010	10.4	186.1	75	50.0	25.5	165	159	152	c	7.5
G04-11A	5.6	96.1	65	45.2	28.0	81	80	80	c	6.6
G04-012	8.0	138.6	65	45.2	28.2	116	113	113	c	8.5
G04-13A	10.4	181.1	65	45.2	30.6	134	128	126	c	8.0
G04-014	10.4[d]	154.8	65	45.2	c	125	117	107	105	7.5
G04-14A	10.4[d]	146.1	65	45.2	30.2	112	110	106	c	6.0
G04-017	5.6	96.1	65	45.2	26.8	86	86	87	86	5.6
G04-19A	10.4	181.1	65	45.2	30.6	129	135	137	c	8.5
G04-022	10.4[d]	149.8	65	45.2	c	136	135	135	134	12.0
G04-023	5.6	97.5	65	45.2	c	77	71	69	c	13.5
G04-025	10.4	178.0	65	45.2	c	130	130	133	c	10.0
G04-25A	7.4	114.0	65	45.2	c	67	65	64	62	7.3

[a] Upper-plateau capacity.

[b] Negative-to-positive capacity ratio increases as assumed negative utilization decreases.

[c] No data available.

[d] The porosities of these electrodes are 35%; all other cells have positive electrode porosities of 30%.

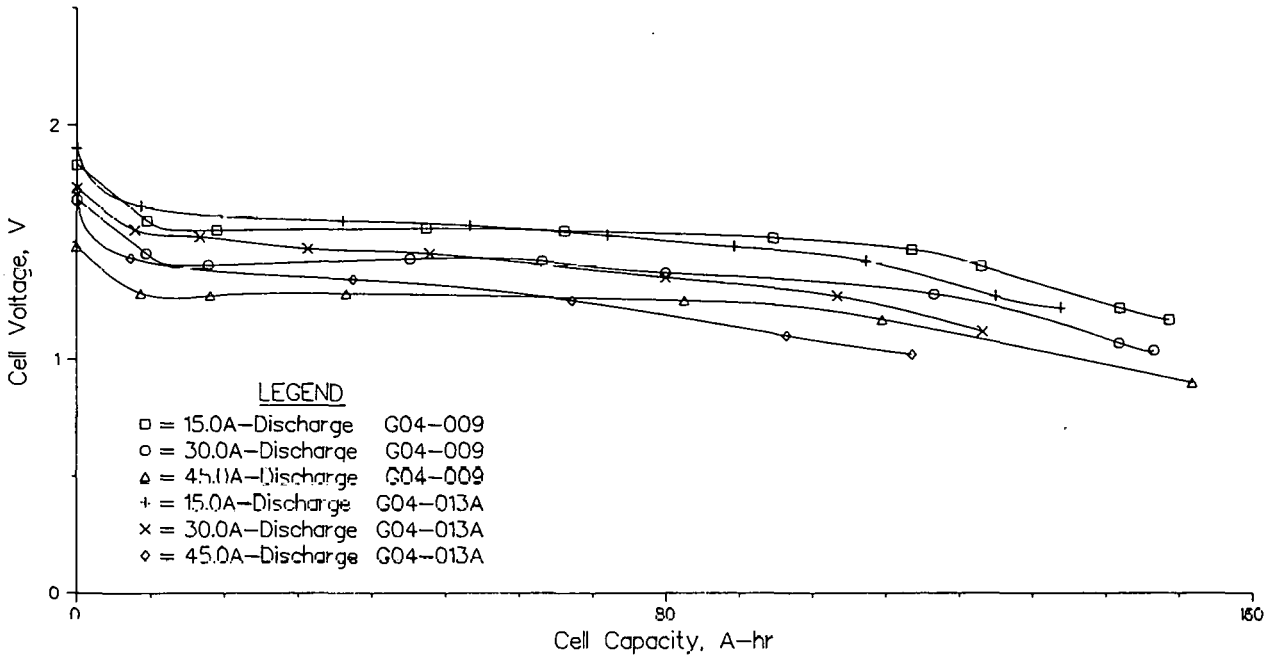

Fig. IV-12. Performance Data for Cells Having Different Negative Electrode Compositions (50 at.% Li in G04-009 and 45 at.% Li in G04-013A)

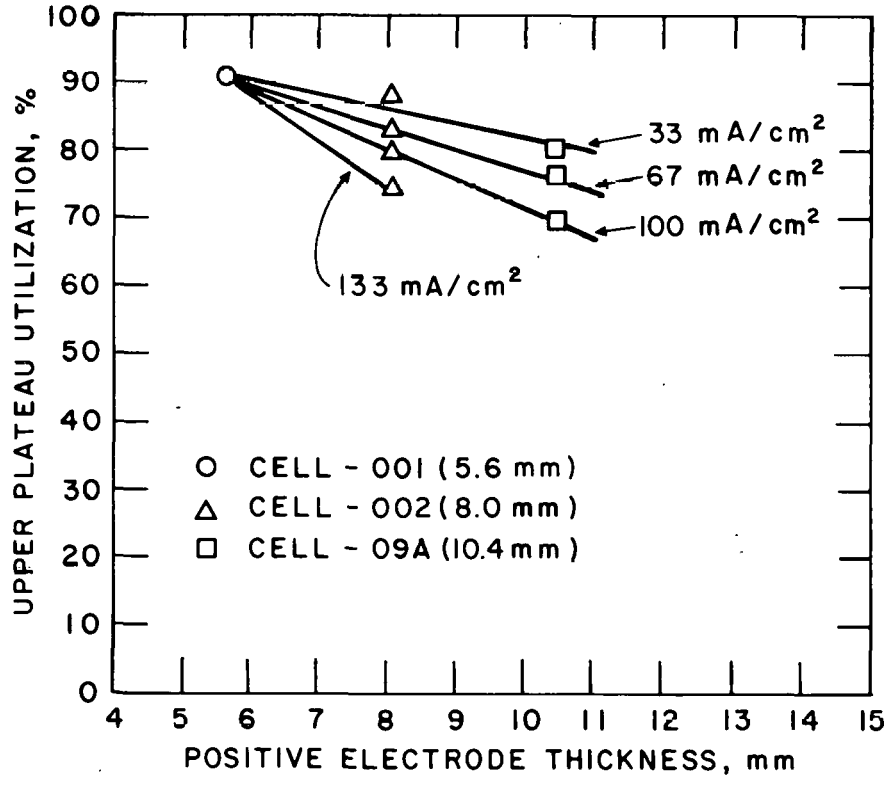

Fig. IV-13. Positive-Electrode Utilization as a Function of Thickness for Three Gould Li-Al/FeS_2 Cells

cells (G04-002 and -09A), the capacity decline is about 1% for every 6 mA/cm^2 increase in current density. For the thin-electrode cell (G04-001), no capacity decline occurred at current densities up to 133 mA/cm^2.

Some general conclusions can be drawn from the results of the above tests. For optimum operation of the FeS_2 electrode in a Li-Al/FeS_2 cell, it is suggested that the cell be designed to have 50 at.% lithium in the negative electrode and to utilize less than 70% of the lithium. The use of more than 30 vol % electrolyte in the FeS_2 electrode does not appear to offer any benefit in cell performance. For FeS_2 electrodes that are more than 5.6-mm thick, the effect of electrode thickness on utilization of the active material should be considered in the cell design.

C. Mark IA Program

(V. M. Kolba, R. F. Malecha)

1. Introduction

A major objective of the Lithium/Metal Sulfide Battery Program is to transfer basic technology from ANL to industrial contractors. These industrial firms have manufactured electrodes, other cell components, and complete cells. To accelerate the commercial availability of lithium-aluminum/iron sulfide batteries, it will be necessary for industry to expand its role and become involved in the total battery system. This includes components such as insulated battery cases, electrical feedthroughs, electrical/electronic hardware, and thermal management systems for the battery.

In support of this objective, ANL has contracted Eagle-Picher Industries, Inc. to develop and fabricate the first large lithium/metal sulfide battery. Work began under this contract in February 1978, and the technical goals for this battery are listed in Table I-2. Under the terms of this contract, Eagle-Picher will be involved in the following activities: cell and battery case development, thermal management methods, cell testing, and final assembly of the battery. The work done at Eagle-Picher is discussed in detail in Section III.A of this report.

2. Contract Support and Management

A Mark IA Team at ANL provides technical direction to the contracted effort. The team is composed of seven members (including a technical monitor) who have expertise in the areas of cell chemistry, electrode and cell fabrication and testing, materials, electric-vehicle/battery interface, and battery design and testing. On a weekly basis, the team reviews the progress being made towards the goals of the contract to identify problem areas. When a problem is identified, recommendations are made on investigations to be conducted by the contractor or by ANL to resolve the problem. The contractor's schedule includes preliminary and final design reviews for the cell, case, and assembled battery. Major recommendations are presented to a Mark IA Review Board for approval prior to implementation. The Chemical Engineering Division (CEN) Contract Coordinator and Technical Monitor interact with the contractor's Project Manager on a daily basis. All formal technical correspondence is forwarded through the Contract Coordinator to the ANL Subcontracts

Administrator. At approximately six-week intervals, meetings are held with the contractor to review progress to date and to discuss mutual areas of concern.

Periodic quality-control audits have been conducted at Eagle-Picher, and ANL has assigned an on-site Quality Engineering Representative for the later segment of the development phase and for all the fabrication phases of the contract.

3. Contract Status

When the Mark IA request for proposals was prepared (November 1977), the performance of the FeS and FeS_2 bicells then under development did not approach the goals listed in Table I-2. The Li-Al/FeS_2 bicells had high specific energy and specific power, but limited lifetime (<200 cycles). The Li-Al/FeS bicells had low specific energy and specific power, but operated for very long periods (up to 1000 cycles). The relatively low specific energy and power of the FeS cell was expected to be significantly improved by a multiplate cell design. Consequently, Eagle-Picher selected the Li-Al/FeS multiplate cell for use in Mark IA. Preliminary tests (see Section III.A.1) have indicated that the multiplate cells will meet the Mark IA goals.

A prismatic, insulated case is required to attain the overall performance, weight, heat-loss, and physical-dimension goals for the Mark IA. The design and development of such a case have been undertaken by Eagle-Picher under subcontracts to two other firms--Budd Co., and Thermo Electron Corp. Eagle-Picher has also subcontracted the weaving and heat treatment of the BN cloth for cell separators. All other procurements and fabrication are being handled directly by Eagle-Picher.

4. Cell Development

Cell matrices have been developed to aid in defining the optimum cell design that will provide the desired performance. To date, about 50 multiplate cells have been fabricated by Eagle-Picher, and a majority of these cells has been or is being tested. Some cells have achieved specific energies greater than 100 W-hr/kg at the 4-hr rate. However, several problems have been revealed by cell testing and post-test analyses: a gradual loss of cell capacity beyond ~60 cycles, high resistance (>1 mΩ), and poor wetting of the separator by the electrolyte. Vigorous actions are being taken to correct these problems.

5. Case Development

Prototype battery cases have been designed and are being fabricated. The requirements of a 500°C operating temperature and layers of foil in an evacuated space surrounding a prismatic unit have led to a corrugated design using Inconel 718 for the inner and outer surfaces of the case. The fabricator has experienced problems in welding dissimilar metals, but these problems have been resolved. Difficulties have also been encountered with pinholes, and repair welding of the pinholes is in progress. The present case design requires much intermittent welding, which leads to a high probability of pinholes. Other potential case designs that minimize this type of welding are being investigated.

D. Post-Test Examinations of Industrial Subcontractors' Cells (F. C. Mrazek, N. C. Otto, and J. E. Battles)*

During this report period, 35 industrial cells were examined. These cells were fabricated by Eagle-Picher Industries, Inc. (EPI) and Gould Inc. (G). The cells were tested for electrical performance either by ANL or by the contractor. The results of the post-test examinations are summarized in Appendix D (post-test results of cells fabricated by ANL are presented in Section VII.D.1). Four of the cells in this table are multiplate cells; the rest are bicells. The positive electrodes were either FeS or FeS_2; and the negative electrodes utilized 48 at.% Li-Al, except for Cells EPI-6A1 and 6A2 which used a Li-Al alloy of 55 at.% Li. A summary of the cell failure modes and the number of cases of each mode is presented in Section VII.D.2.

In FeS_2 cells, metallographic examinations have shown that a band of Li_2S and metallic iron particles is deposited within the separator near the negative electrode and parallel to the electrode face† (see ANL-77-35, p. 48 and ANL-77-75, p. 48). Chemical analyses have shown that the sulfur concentration within the separator averages about 6-8 wt %; however, in Cell EP-I6A-1 the sulfur concentration was 15 wt %. This represents a significant loss of active materials (lithium and sulfur), and must be a factor in the loss of capacity with cycling observed in FeS_2 cells. Also, the morphology indicates that the Li_2S-Fe deposits would hinder ionic transport between the electrodes. The Li_2S-Fe deposits do not appear to cause short circuits, except in Cell EP-I8C-010 where the deposit completely bridged the thin BN-felt separator.

For the four multiplate cells, metallography showed a significant deficiency of electrolyte in the negative electrodes and separators. These examinations also showed that the Li-Al in the center portion of the electrode had undergone agglomeration (densification) rather than forming the typical porous, skeletal microstructure. This agglomeration was particularly severe in Cell EPMP-5-018. Agglomeration of the Li-Al alloy has been observed in some bicells with thick (>6 mm) electrodes. In these cells, the agglomeration occurred in the back portion of the electrode (opposite the working face). The electrodes in the multiplate cells are thinner (<6 mm) and are reacted from both faces. The bicell electrodes were fabricated (cold-pressed in most cases) with low volume fractions of Li-Al (<0.6) and with electrolyte present in the mix. The multiplate electrodes were fabricated with a Li-Al volume fraction of about 0.7 and generally with little or no electrolyte. At this time, these different fabrication techniques are believed to be a major factor in the Li-Al agglomeration.

Data on the corrosion rates for the current-collector materials that were determined from the post-test examinations are presented in Section VII.D.5.

---

*Materials Development Group.

†This does not occur in FeS cells.

REFERENCES

1. U.S. Energy Research and Development Administration (ERDA), Office of Electric and Hybrid Vehicles, *Test and Evaluation Procedures for Electric Vehicles* (1976).

2. M. L. Saboungi, J. J. Marr and M. Blander, *Measurements of the Solubility of Iron Sulfide in the Molten LiCl-KCl Eutectic,* The Electrochemical Society, Extended Abstracts, Vol. 77-2, Abstract No. 37.

3. D. R. Vissers, *et al., Effect of the LiCl-KCl Electrolyte Composition on the Performance Characteristics of the Li-Al/FeS Cells, ibid.,* Vol. 78-2, Abstract No. 34.

4. M. L. Saboungi and A. E. Martin, *Electrochemical and Metallographic Investigations of the Stability of the J($LiK_6Fe_{24}S_{26}Cl$) Phase in Several Molten Salt Mixtures, ibid.,* Abstract No. 339.

V. BATTERY DESIGN
(A. A. Chilenskas)

The approaches taken in the design of the batteries for the electric-vehicle and stationary-energy-storage applications differ significantly. The work done on these two designs at ANL over the past year is discussed below.

A. Electric-Vehicle Battery

Eagle-Picher Industries, Inc. is developing a battery case for the Mark IA; their work is reported in Section III.A.1. The work done at ANL on battery cases for electric-vehicle applications is reported below.

1. Thermal Management Studies
(M. Farahat, B. Zalph*)

An experiment was completed that permitted an experimental verification of the calculated value of the reversible ($T\Delta S$) heating of Li-Al/FeS cells. Two effects lead to the generation of heat in an electrochemical cell. The first is called the reversible heating. The reversible heating is due to the change in entropy of the reactive materials and can be positive (heat liberated) or negative (heat absorbed). The second, irreversible heating ($I\eta$), is always positive. The cell polarization voltage (η) is the product of the current and the effective internal impedance and represents the difference between actual and theoretical cell potential.

An experiment was designed to determine the thermal effects resulting from the charge and discharge of an FeS cell (Cell EP-1A3) by making two independent measurements, electrical and thermal. The electrical measurement is made by integrating the product of the cell current, I, and the voltage drop due to cell polarization, η. The thermal measurement is made by monitoring the transient temperature change on and around the cell. The change in the heat content of the system yields the net heat generation or absorption.

Thus,

$$\dot{Q}_{net} = MC \frac{\Delta T}{\Delta t} + K \left(A_x \frac{\Delta T}{\Delta x} + A_y \frac{\Delta T}{\Delta y} \right)$$

where

A = heat transfer area
C = specific heat
K = thermal conductivity
M = mass
$\dot{Q}$ = rate of heat generation or absorption
T = absolute temperature
Δt = temperature change

The reversible heat generation or absorption ($T\Delta S$) is determined by taking the difference between the net heat generated (Q_{net}) and the irreversible heat generation ($I\eta$). A schematic of the test apparatus is given in Fig. V-1.

---

*Co-op Student from Duke University.

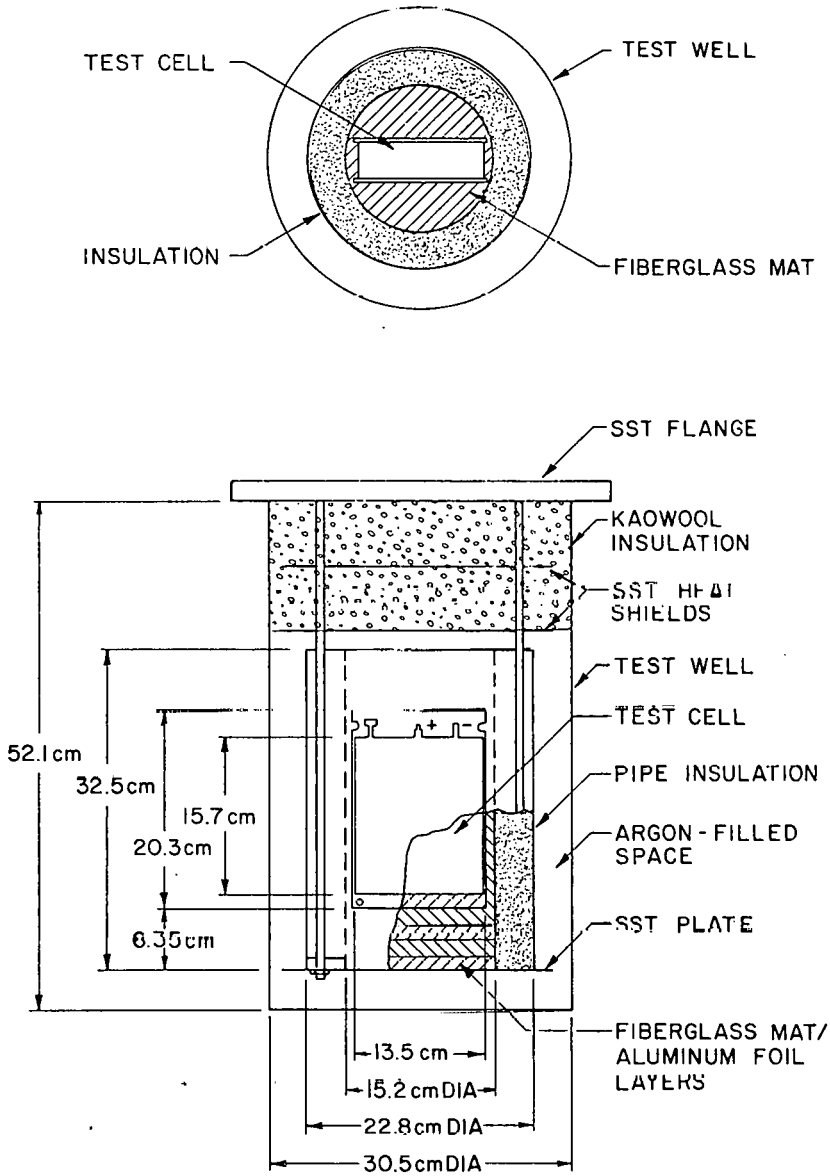

Fig. V-1. Experimental Apparatus for the Measurement of Entropic Heating.

The results of an experiment using a Li-Al/FeS cell (EP-1A3) cycling at a 10 A discharge and charge current (4.5-hr rate) are given in Table V-1. At the time of the thermal measurements, the capacity of this cell was 44.19 A-hr on discharge and 44.57 A-hr on charge. As shown in the table, the entropic heating measured at 10 A was +0.98 W (heating) during discharge and -1.10 W (cooling) during charge. The average value of these two measurements is ±0.104 W/A (1.04 W/10 A), which compares very well with the value of ±0.112 W/A calculated from theoretical considerations.* The information from these tests will be used in the design of an electric-vehicle battery case.

*Based upon 5.16 kcal/mole for $T\Delta S$ (FeS ⇄ Fe).

Table V-1. Heating Calculations for Cell EP-1A3.

Heat, W	Cycle 19[a] (discharge)	Cycle 20[a] (charge)
Average Irreversible Heating[b]	+ 1.37	+ 1.25
Average Heat Flow		
Radial	+ 0.64	+ 0.58
Axial	+ 0.17	+ 0.16
Leads	+ 0.20	+ 0.10
Average Transient Heating		
Cell	+ 0.29	- 0.12
Retainers	+ 0.73	- 0.34
Pipe ins.	+ 0.15	- 0.13
Glass mat	+ 0.17	- 0.10
Total Heating[c]	+ 2.35	+ 0.15
Reversible Heating	+ 0.98	- 1.10

[a]Cycles as numbered by data acquisition system.

[b]Obtained from voltage and current as a function of time.

[c]A thermal measurement.

2. Battery Configuration Studies
(J. A. E. Graae, A. A. Chilenskas)

An analysis[1-2] has been completed at ANL to assess a rectangular* versus a cylindrical configuration for a 50 kW-hr battery. The results of the analysis,† given in Table V-2, suggest that a cylindrical battery configuration has significant advantages over a rectangular one. As can be deduced from the table, the manufacturing cost for the rectangular jacket is about $5/kW-hr more than that of the cylindrical jacket. Analysis of these two designs with respect to battery/vehicle integration, crash worthiness, and vibrational effects are preliminary; however, based upon these latter criteria, the cyclindrical design still appears to be the more favorable.

*This design is based on the jacket shown in Fig. III-5.

†This analysis is valid only if the present prismatic cell design can be changed to a circular shape without significantly affecting cell performance or cost, cell cost was not taken into consideration in this analysis.

Table V-2. Preliminary Assessment of the Battery Configuration for a 50 kW-hr Battery.

	Design Estimates	
	Rectangular	Cylindrical
Battery Case Weight, kg	144	96
Battery Volume, L	312	242
Heat Loss, W	262	133
Jacket Manufacturing Cost, $	554[a]	316[b]
	(11.08)[c]	(6.32)[c]

[a]Priced at $3.85/kg in high-volume production.

[b]Priced at $3.30/kg in high-volume production.

[c]Numbers in parentheses are manufacturing costs in dollars per kilowatt hour.

B. Stationary Energy Storage Batteries
(S. Zivi, A. A. Chilenskas)

A conceptual design of an 100 MW-hr energy-storage plant is under development. This work is being carried out by Argonne National Laboratory (ANL) and by the Rockwell International Energy Systems Group (ESG) under contract to ANL. Detailed reports on this work are in press.[3-4] The design criteria for the plant are given in Table V-3; a drawing of the plant is shown in Fig. V-2. A description of the conceptual design for this plant follows.

Table V-3. Technical Requirements for the 100 MW-hr Energy-Storage Plant.

Plant Characteristic	Requirement[a]
Footprint, kW-hr/m^2	80
Lifetime[b], years	
for cells	10
for plant	20
Voltage, V	1000
Energy Efficienty,[c] %	75

[a]Values given below are minimums.

[b]Calculated for 250 cycles/yr.

[c]DC out/DC in.

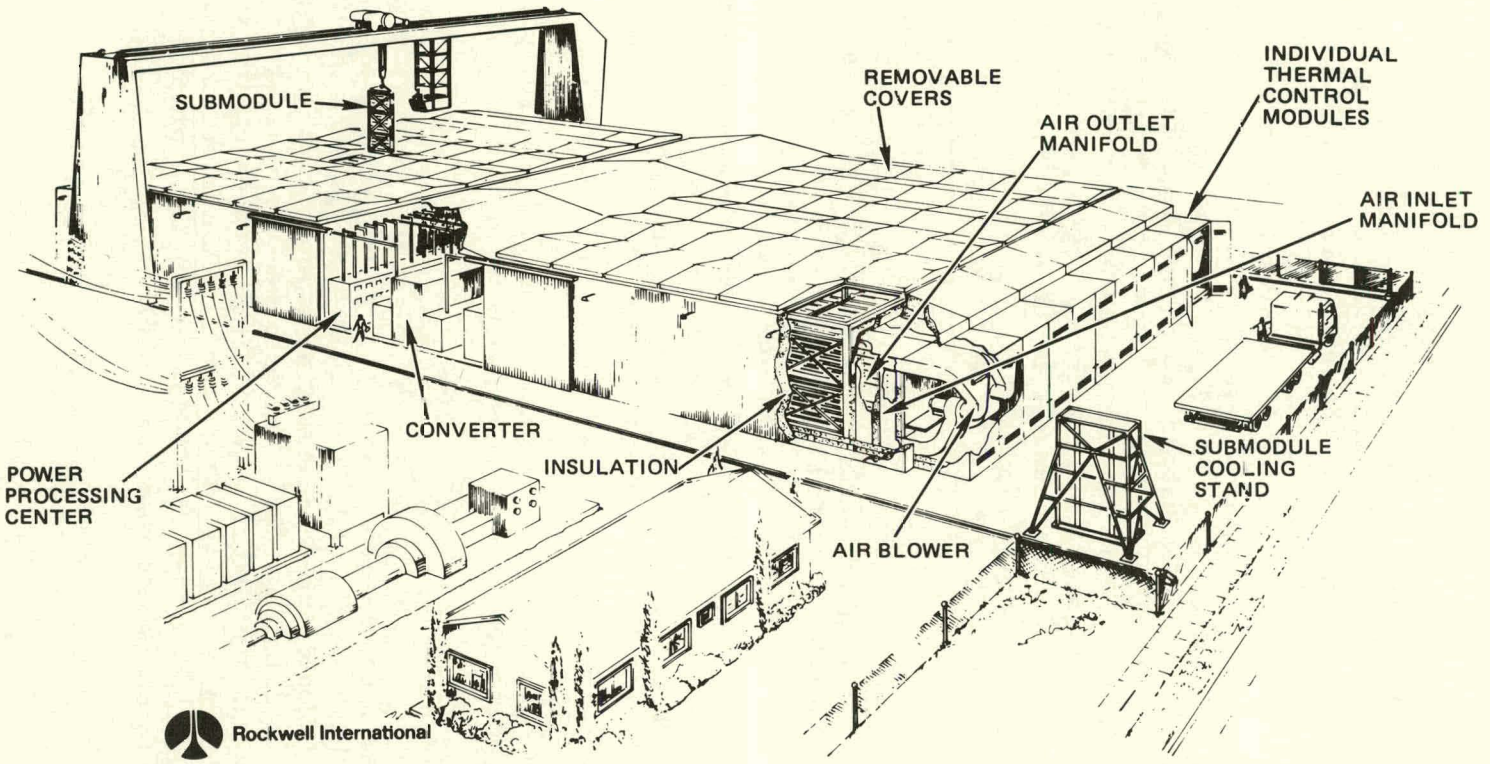

Fig. V-2. The 100 MW-hr Energy-Storage Plant

Lithium/metal sulfide cells with a capacity of 2.5 kW-hr were selected for use in the plant. Four of these cells are connected mechanically and electrically (in parallel) to form a 10 kW-hr ensemble. This cell ensemble is the basic replaceable unit of the plant, and is separately charged during the charge equalization process. Twenty-four ensembles compose one submodule, which has a configuration resembling a bookcase. This submodule consists of 12 shelves with two cell ensembles each, and is installed in or removed from the modules through hatches in the plant roof. A gantry spans the 23-m width of the plant for loading or replacing the submodules. The module is constructed of alloy steel ($2\frac{1}{4}$% Cr, 1% Mo) tubing and bars, and contains six rows of six submodules each (a total of 864 cell ensembles) connected in series. Nominal dimensions for an uninsulated, assembled module are 12 × 2.8 × 6 m. Fiberglass insulation panels, 43-cm thick, will be attached to the battery module (top, bottom, and sides) in order to reduce heat losses.

The 100 MW-hr facility contains two groups of six modules (a "battery bank") arranged on either side of an electrical-power processing center. This central area contains AC-DC converters, circuit breakers, and transformers interfacing with the utility distribution or transmission system. Each module group has a 10 MW converter; interties permit reassignment of the converters to alternate battery banks. Also in the central area are ancillary buildings (sheet metal sheds) which house switchgear, equalizer electronics, and other instrumentation. Centrifugal blowers for the thermal management system are housed in sheet-metal structures on the outside of each bank. Submodules to be installed in an already heated module are brought up to operating temperature in an external furnace on site. Each of the 12-module structures is assembled from 4 prefabricated structures which are trucked to the site. These four structures are the insulated base, two frameworks which are mounted one above the other to form the shell of the module and which contain guide channels for the submodules, and a hatchway supporting section which is set on top of the frameworks and provides room above the module for equalizer-conductor trays.

Several technical issues have dominated the design efforts at ANL and Rockwell International, and they are discussed below.

1. Materials

At present, the materials selection remains uncertain, although tentative choices have been made. The oxidation resistance of electrical conductors at 450°C continues to be a matter of considerable concern. The present choice of material for the electrical conductor is stainless-steel clad copper, which has a price of about $11/kg; less expensive material is needed. The structural material chosen for use in the portions of the plant at 450°C is an alloy steel ($2\frac{1}{4}$% Cr, 1% Mo), which has a price of about $2/kg in a few standard forms (sheet, bar, and tube).

2. Packing Density

The volumetric packing fraction of cells in the battery modules is 0.16 in the present plant design. Despite the low packing fraction, a high energy per unit plant area (the footprint) is achieved by using all of the allowable plant height ($\sim$7 m). The footprint of the present conceptual design is about 100 kW-hr/m^2, including the converters, although the guideline given

in Table V-2 is 80 kW-hr/m^2. A higher volumetric packing fraction than 0.16 is desirable because the costs of conductors and structural components are directly related to the dimensions of the plant.

3. Charge Equalization

Because operation of lithium/metal-sulfide cells can fail due to overcharge, it is necessary to provide a charge-equalization system to compensate for variations in self-discharge rates from cell to cell. The present plant design is encumbered with significant complexities and high costs that are attributed to the charge-equalization requirement. The present equalizer system for the energy-storage plant is based on the equalizer being used for electric-vehicle batteries; no better method of equalization for this type of battery is now known. In the future, a concerted effort will probably have to be devoted to finding a cheaper system for equalizing.

4. Cell Characteristics

Work has been devoted to (1) a verification that the cell characteristics assumed for the 100 MW-hr plant design are consistent with laboratory data on experimental cells and (2) a derivation of the required cell reliability. In regard to the latter, it has been found that the plant must have a very low annual rate of cell failure (approximately 4 per 1000 cells) in order to operate for ten years without a major overhaul. Whether a low cell cost and a high cell quality can be achieved while maintaining a very low failure rate is uncertain.

A compromise was involved in the selection of the size of the cells. Large-capacity cells are desirable for minimizing the number of items to be handled and connected, and probably for minimizing the cost (per kilowatt hour) of the cells. However, small-capacity cells have been chosen for the present design because almost all existing laboratory experience has been obtained with small cells.

5. The Module Container

At the initiation of this design project, the ANL module container design was based on a modified International Standards Organization (ISO) shipping container. The advantage of this type of container was that it could be factory produced by methods similar to those used today in the manufacture of truckable ship cargo containers. This modified shipping container was expected to have a low manufacturing cost and to require minimal labor on site. The Budd Co., a manufacturer of ISO containers, was contracted to study the modifications that would be required for the high-temperature battery application, and the expected cost of such a modified ISO container. However, Rockwell International recently found that the packing density of cell ensembles would have to be significantly lower than had been anticipated at the time that ANL had proposed the use of an ISO container; consequently, the ISO module container design lost its economic attractiveness.

6. Thermal Control

The cell energy efficiency is expected to be approximately 80%. About 20% of the electrical energy charged into the cell is released as heat from the cell, primarily during discharge. This heat is removed by the thermal management system, which also maintains a uniform temperature throughout the battery and provides heat for battery start-up and for occasional lengthy periods of battery idleness. The thermal management system consists of hairpin-shaped heat exchanger tubes which run the length of the module aisles between rows of submodules. The principal mode of heat transfer between the cell surfaces and the tubes is thermal radiation. During start-up, air heated to a high temperature by electrical-resistance heaters is forced through the tubes at high speed by centrifugal blowers; this same method can be used during battery operation to equilibrate temperature spatially. During operation of the battery, the air inside the tubes is recirculated after being mixed with cool outside air at the blower inlet.

7. Estimated Costs

Cost estimates for the plant are being prepared by ANL and by Rockwell International. Preliminary cost estimates by ANL suggest that the cost of the battery plant as presently described (including cells but excluding AC/DC convertors) is well over $50/kW-hr.* During the next fiscal year (1979), ANL and Atomics International will try to find a way to reduce the battery plant cost to less than $50/kW-hr.

*We assumed a cell cost of $30/kW-hr for this estimate.

REFERENCES

1. A. A. Chilenskas, *A Design Configuration for a 50 kW-hr Electric-Vehicle Battery*, unpublished *(August 1977)*.

2. J. A. E. Graae, *Mark II, 50 kW-hr Battery*, unpublished (August 1978).

3. S. Zivi, I. Pollack, H. Kacinskas, and T. Fornek, *A Conceptual Design Study of a 100 MWh Electrical Load Levelling Plant Utilizing Lithium/Metal Sulfide Batteries*, unpublished (October 1978).

4. E. Adler, C. Dunsmore, I. Goldstein, W. Grieve, and W. Wood, *System Design Description, Conceptual 100 MWh Utility Battery Design Based on on Lithium Alloy/Iron Sulfide Cells*, Rockwell International, Energy Systems Group, Report N001SDD100001 (1978).

VI. CELL DEVELOPMENT AND ENGINEERING
(E. C. Gay, H. Shimotake)

The effort in this part of the program is directed toward the development of Li-Al/FeS_x cells capable of meeting the requirements for electric-vehicle and stationary-energy-storage applications. Recent cell development work has concentrated on improving lifetime and specific energy at high discharge current densities (>75 mA/cm^2). An effort was also placed on the development of multiplate cells and powder separators. Whenever advances in cell technology are demonstrated at ANL, these advances are incorporated as quickly as possible into the industrial contractors' cells. Cell performance data for the ANL fabricated cells are presented in Appendix E.

A. Development of FeS Cells

In the past, two types of metal sulfides have been used as the active material in the positive electrode--FeS and FeS_2. The FeS_2 electrode is capable of high specific energy and specific power, but has the disadvantages at present of limited lifetime and the requirement for expensive current-collector materials. Consequently, the FeS electrode has been selected for the Mark IA electric-vehicle battery (see Section III.A.1.). Efforts are currently under way to develop a Li-Al/FeS cell that meets the performance goals for the Mark I battery (see Table I-1).

Cells are assembled in either an uncharged or charged state. In both cases, the electrodes are usually pressed mixtures of active materials and electrolyte. Either method is easily adaptable to a mass-production process. For this reason, both methods of assembly are being investigated.

1. Tests on Cells with R-Series Design
(L. G. Bartholme, C. Hsiang* and J. Shaefer†)

There are strong indications that the formation of J phase ($LiK_6Fe_{24}S_{26}Cl$) in FeS electrodes has an adverse effect on the electrode kinetics (ANL-77-35, p. 57). Previous results (ANL-78-45, p. 35) have suggested that J-phase formation can be modified by adding Cu_2S to the FeS electrode or by increasing the LiCl content of the LiCl-KCl eutectic.‡ During this reporting period, a series of R-series FeS cells were built either with Cu_2S additions to the positive electrode, or with LiCl-rich electrolyte. The basic R-series cell design consists of a central pressed positive electrode and two negative plaques of pressed aluminum wire.

The practical value of Cu_2S additive in the positive electrode of Li-Al/FeS cells has been questioned, because copper migration to the electrode face and into the separator has been observed in cells using this additive (ANL 77-75, p. 44). However, it has not been established under what conditions the copper migration will cause this short circuit. Some Li-Al/FeS-Cu_2S bicells have shown long cycle life (Fig. I-3); recent bicells have shown high utilization of the active material in the positive electrode,

---

*Research Student Associate, Institute of Nuclear Energy Research, Taiwan.

†Industrial Participant from ESB Technology, Inc.

‡The eutectic composition is nominally 58 mol % LiCl-42 mol % KCl.

74% at the 4-hr rate (current density, 72 mA/cm^2). Post-test examinations of these cells showed a layer of copper in the separator, although the copper migration did not cause the cell failure. Recent Li-Al/FeS-Cu_2S cells that use BN felt (3-mm thick) instead of the usual BN cloth as the separator/retainer are still in operation after 200 cycles (100 days) with less than 4% capacity decline.

Previous work (ANL-75-36, pp. 23-24) had shown that the use of an electrolyte containing only lithium cations results in a great increase in positive-electrode utilization. More recent work at ANL (see Ref. 3 from Section IV) has also shown that the use of LiCl-KCl mixtures containing over 67 mol % LiCl results in improved utilization. Since the liquidus temperatures of LiCl-rich electrolyte are high (>425°C), the cell operating temperature must be kept sufficiently high to maintain effective ionic transport in the electrodes. Bicells with 67 mol % LiCl have shown high utilizations, 75% at the 4-hr rate (current density, 72 mA/cm^2). These results show that the use of the LiCl-rich electrolyte is as effective as the Cu_2S addition in improving the cell utilization. Recent Li-Al/FeS bicells having LiCl-rich electrolyte have been built with BN-felt separator/retainers. One of these cells has operated for over 48 days (78 cycles) without capacity decline. Wetting of the BN felt by the electrolyte in these cells was effectively promoted by application of a small amount (10 mg/cm^2) of $LiAlCl_4$ to the surface of the BN felt. This wetting technique, which was developed by the Materials Group (Section VII.C), is essential for the successful use of the BN-felt separator/retainer.

2. Tests on Cells with M-Series Design

(F. J. Martino, M. Fitzgibbons*)

This development effort is directed at examining a number of bicell designs which may result in improved specific energy, specific power, and cycle life of Li-Al/FeS cells. The cells that are mentioned in the following discussion are of the compact "M-Series" design (ANL-78-21, p. 35). In the design and assembly of these cells, care was taken to make each cell as nearly identical to the others as possible. The electrodes were formed by hot-pressing active material into iron honeycomb current collectors. A BN felt separator/retainer that had been pre-wet with electrolyte was used in all cells tested. Preliminary tests indicated that a higher theoretical capacity density (A-hr/cm^3) in the positive electrode reduces the utilization of the active material somewhat, most probably as a result of the reduced electrolyte volume; the presence of more active material does, however, provide the capability for achieving higher cell capacity for a given cell volume. Also, peak power may be increased as a result of higher electrode conductivity through an increased loading density (*i.e.*, more active material loaded per unit area of electrode face.

Recent development work on engineering-size Li-Al/FeS bicells has included the operation of five M-series cells--M-6, -8, -9, -10, and -11. These cells were designed to test the effects of increased loading densities (from 0.7 to 1.6 A-hr/cm^3) on cells with either (1) 15 mol % Cu_2S additive to

*Co-op Student from Northwestern University.

the positive electrode and an eutectic electrolyte, (2) no Cu_2S additive and an eutectic electrolyte, or (3) no additive and 67 mol % LiCl-33 mol % KCl electrolyte (liquidus temperature, 410°C). All of these cells were assembled in the charged state, with the exception of M-6 which was assembled uncharged. Performance data from these cells are presented in Figs. VI-1, -2, and -3.

The two Li-Al/FeS-Cu_2S cells, M-6 and -9, had theoretical capacity densities of 0.70 and 1.60 A-hr/cm^3, respectively. In an attempt to improve electrode utilization, 10 wt % carbon that had been heat-treated at 1000°C was added to the positive electrode of Cell M-6. The achieved utilization of 65% at a current of 20 A (current density, 74 mA/cm^2) was not as high as anticipated; however, the positive electrode utilization at 10 A (current density, 37 mA/cm^2) was nearly 90% (Fig. VI-1). After 64 cycles, operation of Cell M-6 was terminated, because the capacity had declined by ∿20% (to 68 A-hr). However, the coulombic efficiency remained at about 99%. Detailed post-test examination by the Materials Group did not reveal the cause of declining cell capacity.

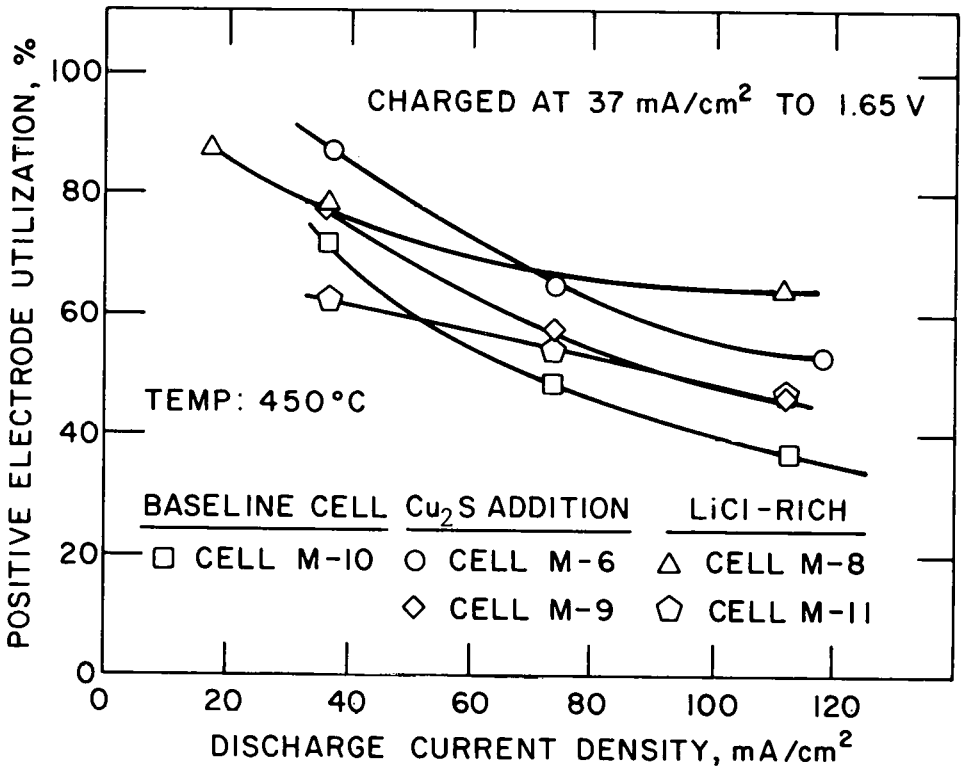

Fig. VI-1. Utilization *vs.* Current Density of Five M-Series Cells.

The other FeS-Cu_2S cell, M-9, contained a "wishbone"-type current collector which was designed to reduce the current-flow distance to the positive terminal and to provide rigidity to an open (no center sheet) honeycomb current collector. In comparison with Cell M-6, this cell had a lower positive-electrode utilization, 53% at a current of 20 A (current density, 74 mA/cm^2).

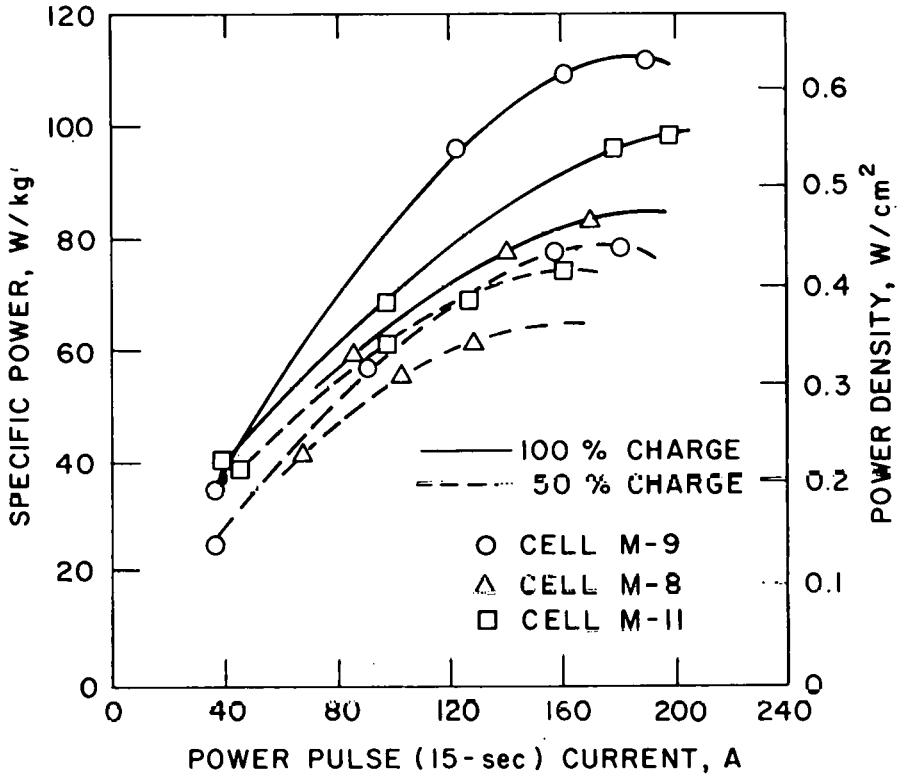

Fig. VI-2. Power Data *vs.* Current for Three M-Series Cells.

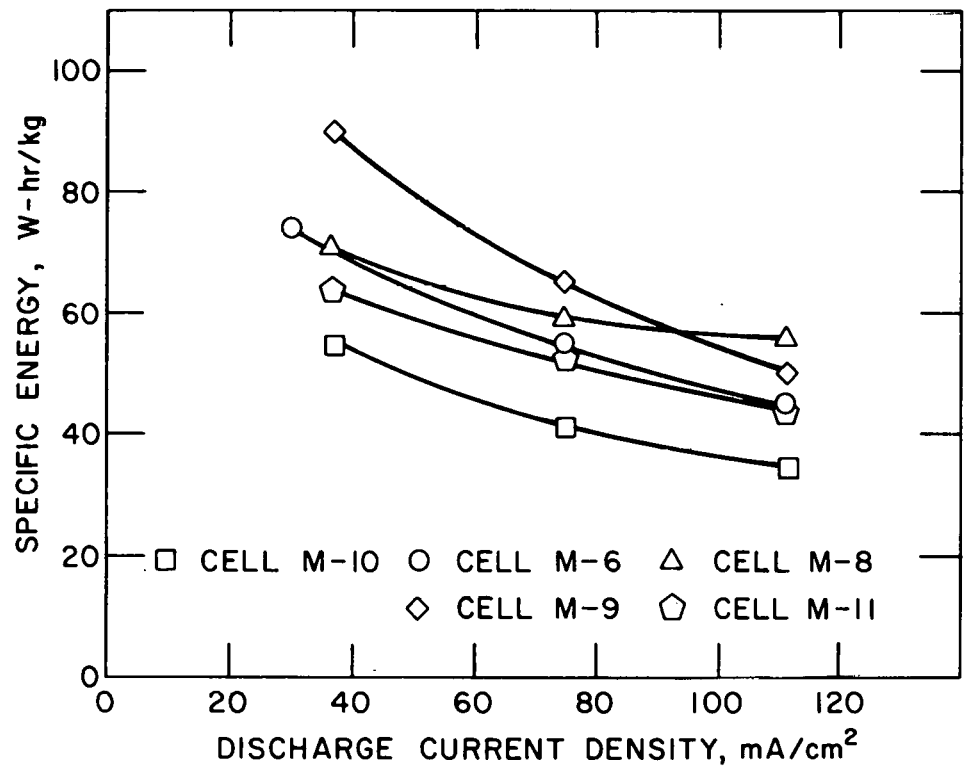

Fig. VI-3. Specific Energy *vs.* Current Density for Five M-Series Cells.

This result was expected on the basis of the lower electrolyte content (40 vol % at full charge) of Cell M-9. However, the thinner positive electrode and higher theoretical capacity used in Cell M-9 makes more active material available for reaction and reduces the cell weight, thereby increasing the specific energy (see Fig. VI-3). Cell M-9, which had a typical resistance of 3.4 mΩ, achieved specific energies of 65 and 50 W-hr/kg at the 4-hr (74 mA/cm^2) and 2-hr (110 mA/cm^2) discharge rates, respectively. As shown in Fig. VI-2, peak-power values (15-sec pulse) were 120 W/kg at full charge and 76 W/kg at 50% state of charge; this is the highest specific power achieved by the M-series cells. After 200 cycles, the cell capacity at the 4-hr discharge rate (current density, 74 mA/cm^2) had declined about 20% from a typical high of ∿78 A-hr; however, the capacity at a discharge current density of 37 mA/cm^2 remained nearly constant.

Cells M-8, -10, and -11 contained no metal additive to the positive electrode. Cell M-10 (115 A-hr capacity) was designed as a baseline cell and used LiCl-KCl eutectic electrolyte; the theoretical capacity density of the positive electrode was 1.40 A-hr/cm^3. Cells M-8 (113 A-hr) and M-11 (132 A-hr) were similar in design to Cell M-10 but had LiCl-rich electrolyte (67 mol % LiCl-KCl; liquidus temperature 425°C). The theoretical capacity densities for the positive electrode were 1.40 A-hr/cm^3 for Cell M-8 and 1.60 A-hr/cm^3 for Cell M-11. As expected, the cells with LiCl-rich electrolyte (M-8 and -11) had a higher positive-electrode utilization than that of the cell with no Cu_2S additive and eutectic electrolyte (M-10). In the cells with LiCl-rich electrolyte, a higher capacity density resulted in a higher specific power (Fig. VI-2) but a lower positive-electrode utilization (Fig. VI-1) and specific energy (Fig. VI-3). One of the anticipated effects of the use of LiCl-rich electrolyte in FeS cells is to increase cycle life through a reduction of J-phase formation (ANL-77-17, p. 45). Cycling at a 4-hr discharge rate, Cell M-8 has operated for more than 180 cycles with virtually no loss in cell capacity and a coulombic efficiency of 98%. The operation of Cell M-11 has yet to indicate clearly whether this stability will occur in a cell having a higher theoretical capacity density; however, after 50 cycles, no capacity loss has been observed.

In summary, it is apparent that without the use of either Cu_2S additive or LiCl-rich electrolyte in these FeS cells, the utilization of the positive electrode is quite poor; this effect is especially obvious at current densities above 75 mA/cm^2. Of the five M-series cells under test, the cell with Cu_2S additive and a loading density of 1.6 A-hr/cm^3 and the cell with LiCl-rich electrolyte and a loading density of 1.4 A-hr/cm^3 appeared to exhibit the best performance characteristics with respect to the Mark I and II goals.

3. Small-Scale FeS Cells

(K. E. Anderson, D. R. Vissers,* T. Ho†)

A small-scale FeS cell (15-cm^2 electrode area) was operated to determine the effect on performance of varying the LiCl concentration in the electrolyte. Four different LiCl-KCl electrolyte compositions, 58, 61, 65,

*Cell Chemistry Group of Chemical Engineering Division at ANL.
†Research Student Associate, Institute of Nuclear Research, Taiwan.

and 67 mol % LiCl (liquidus temperatures of 350, 375, 400 and 425°C, respectively), were investigated. A separate cell containing a KCl-rich electrolyte (*i.e.*, 53 mol % LiCl-47 mol % KCl with a liquidus temperature of 415°C) was also constructed. The results indicate that the utilization of the positive electrode increased from 50 to 80% when the LiCl content of the electrolyte was increased from 58 to 67 mol %. Utilizations obtained at the 61 and 65 mol % LiCl concentrations were 66 and 79%, respectively. The utilization for the cell operated with the KCl-rich electrolyte was approximately 25%. These results confirm the earlier observation that LiCl addition to the eutectic LiCl-KCl electrolyte improves FeS utilization. Lithium chloride concentrations higher than 67 mol % were not investigated because of the high liquidus temperature associated with that electrolyte concentration. Another effect associated with the use of LiCl-rich electrolyte is an improvement in peak power density (W/cm^2). In Fig. VI-4, results from a baseline Li-Al/FeS cell are compared with those from a Li-Al/FeS-5.8 mol % Cu_2S cell with LiCl-KCl eutectic electrolyte and a Li-Al/FeS cell with LiCl-rich (67 mol % LiCl) electrolyte.

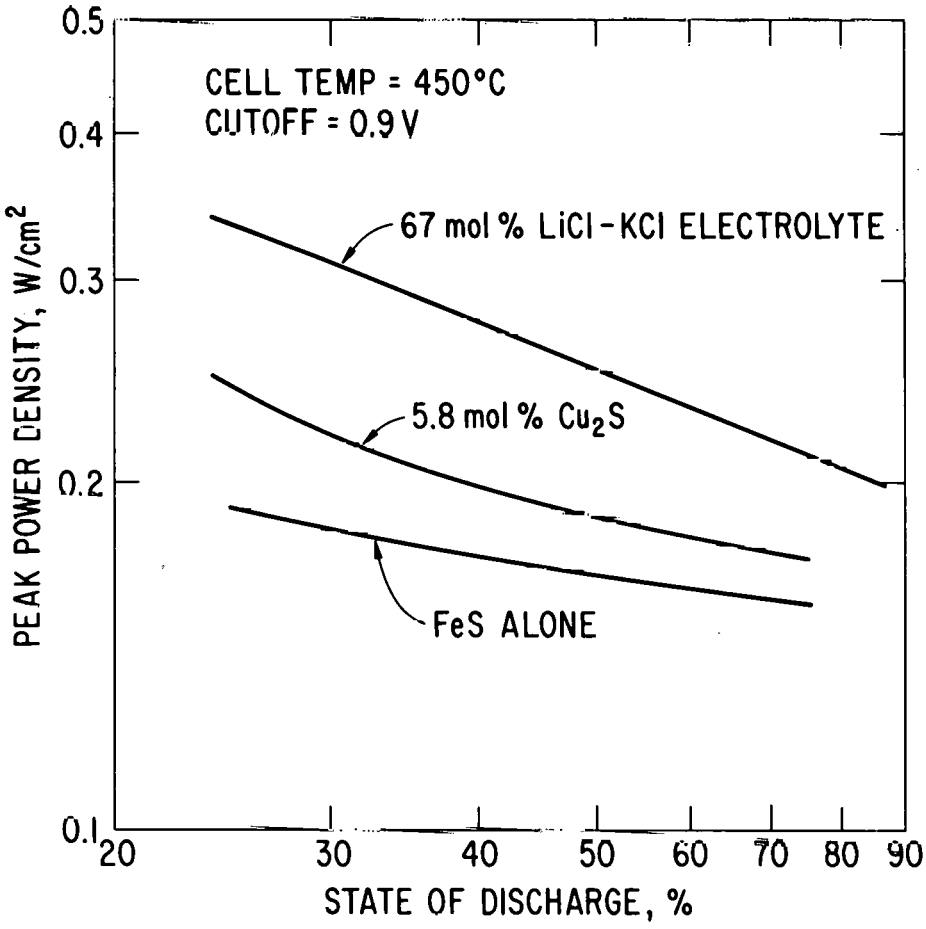

Fig. VI-4. Effects of Cu_2S Addition to the Electrode and LiCl Enrichment of the Electrolyte on the Peak Power Density of Li-Al/FeS Cells.

Investigations of additives to the positive electrode were conducted. Five small-scale cells were constructed with the following additives to the FeS positive electrode: 0, 2.8, 5.8, and 12.1 mol % Cu_2S, and 10.7 mol % CoS. The results indicate that 5.8 mol % Cu_2S positive additive improves the positive-electrode utilization and that the utilization is about the same for cells with either 5.8 or 12.1 mol % Cu_2S positive additive. No beneficial effect could be attributed to the addition of CoS.

4. Multiplate Cell Design
(H. Shimotake)

In order to increase the specific energy of the Li-Al/FeS cell to meet the goals for the Mark I and II batteries (>100 W-hr/kg at the 4-hr rate), a multiplate cell (Fig. VI-5) has been proposed. Because of the large electrode area for a given cell capacity, the multiplate cell is expected to have a higher utilization of active material than that of the bicell.

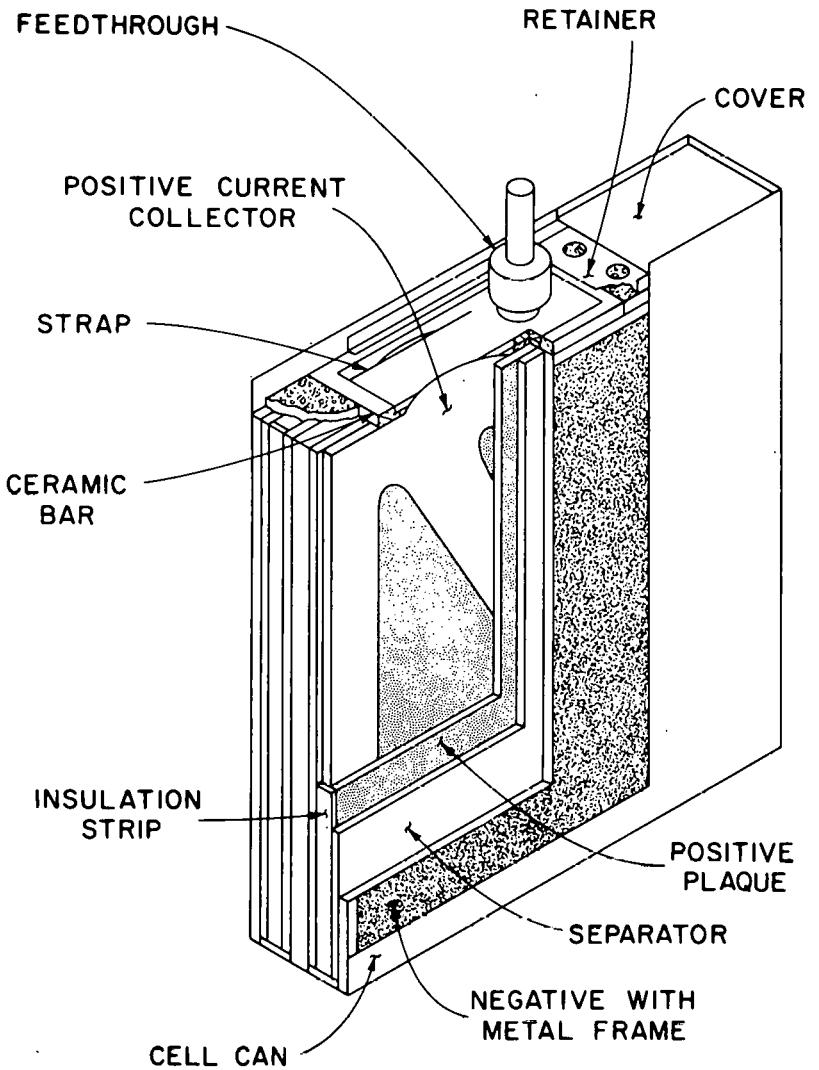

Fig. VI-5. Multiplate Cell Design.

The cell shown in Fig. VI-5 is assembled with two uncharged positive electrodes* and three partially charged negative electrodes (typical electrode dimensions, 16.9 × 17.8 cm). The uncharged FeS positive electrode consists of a hot-pressed plaque of Li_2S and iron powder placed on each side of a flat-sheet iron current collector, and is held together by metal frames. The electrode is completely covered by a BN-felt separator/retainer, which is pre-wet with electrolyte. The negative electrode consists of pressed aluminum wire plaques containing a predetermined amount of Li-Al alloy; an iron frame surrounds this electrode. An iron-screen current collector is used in the negative electrode; the tab of the negative electrode is welded to the cell can (also iron) on assembly. The surface area of the positive electrode is slightly less than that of the negative electrode to allow insulation of the edges of the positive electrode from negative potential. The electrical connection of the positive electrode plates to the feedthrough is made by a strap that is welded to the current collectors of both positive electrodes. This strap, which is made of the same material as the current collector, is insulated from the negative plates by a thin bar of BN. The space above the electrode plates, other than that occupied by the BN, is completely filled with BN power. The electrical feedthrough for this cell is an ANL snap-ring type (ANL-77-75, p. 32).

The total weight of this multiplate cell is about 2.55 kg. Calculations indicated that a multiplate cell of this design will achieve an energy of 334 W-hr and a utilization of 75% (theoretical capacity, 278 A-hr) at a current density of 60 mA/cm^2. These figures correspond to a specific energy of 131 W-hr/kg at the 4-hr rate. The materials cost is expected to be about $23/kW-hr. However, if a MgO powder separator were used in this cell instead of BN felt, the materials cost would be reduced to about $13/kW-hr.

B. Development of MS_2 Cells

The FeS_2 cell is capable of delivering high specific energy and specific power, but has problems of limited lifetime and the requirement for expensive current-collector materials. Currently, efforts are being made to solve these problems. If successfully developed, this electrode will be incorporated in the Mark III cells.

Cell chemistry studies (ANL-77-75, p. 52-53) have indicated that NiS_2 may be an attractive alternative to FeS_2 as the active material in the positive electrode. Consequently, the recommendation was made that the use of NiS_2 as a substitute for the active material in the positive electrode or as an additive in Li-Al/MS_2 cells be investigated in engineering-scale cells. During the reporting period, these positive electrode mixtures were investigated in uncharged and charged cells with pressed electrodes and with carbon-bonded electrodes.

1. Tests of Cells with R-Series Design
(L. F. Bartholme)

The first two engineering-scale NiS_2 cells, R-31 and R-32, were assembled in the uncharged state with hot-pressed electrodes of LiAl and NiS_2. Cobalt disulfide has been used as an additive for FeS_2 electrodes for some

*In this cell design, each positive electrode has two facing negative electrodes.

time (ANL-75-1, p. 29) to improve electronic conduction; in Cell R-31, 9 mol % CoS_2 was mixed with the NiS_2. Tests on small-scale cells have shown that the addition of heat-treated (>1000°C) carbon powder to the FeS_2 electrode improves performance (ANL-77-75, p. 27); in Cell R-32, this heat-treated carbon powder was added to the NiS_2 electrode. Both cells have shown excellent coulombic efficiencies (>99%). However, Cell R-31 exibited high resistance (>12 mΩ) and low utilization (<30%) in the early cycles. This appears to result from the low electronic conductivity of NiS_2. With further cycling, the utilization improved and stabilized at 50% (3.5-hr rate). The cell has operated for 378 days (1025 cycles) with less than 30% capacity decline. Cell R-32 has shown a much lower resistance (<4.5 mΩ) and higher utilization than Cell R-31, but it developed a short circuit after 95 days (178 cycles) and operation was terminated. In view of the results, a Li-Al/NiS_2-CoS_2 cell, R-36, which is similar to Cell R-31 but contains the heat-treated carbon powder in the positive electrode, was built. Its performance was significantly better than that of Cell R-31, and it showed none of the capacity fluctuations that had been observed during the early cycles of Cell R-31. The improvement was attributed to more effective current collection provided by the carbon powder. The cell has exhibited a capacity decline of 24% after 253 days (472 cycles), but it continues to operate with high (>98%) coulombic efficiency.

Since nickel is an expensive material, nickel sulfide plus iron sulfide mixtures have been examined as potential active materials for the positive electrode. A 50 mol % FeS_2-50 mol % NiS_2 mixture was examined in Cell R-33. A slightly higher cell voltage and utilization than those obtained with NiS_2 alone were observed. However, the cell developed a short circuit after 55 days and 90 cycles and its operation was terminated. A mixture containing 78.8 mol % $FeS_{1.65}$-8.2 mol % $CoS_{1.65}$-13.0 mol % $NiS_{1.65}$ was tested in Cell R-35. An identical mixture had been tested previously in Cell R-30, which showed excellent utilization and good performance (ANL-78-20, p. 16). In Cell R-35, a partially graphitized carbon fiber* was added to the positive electrode to improve current collection. This cell demonstrated higher utilization (65% at the 2-hr rate) than the cells using NiS_2 alone. However, the average voltage of the cell was about 0.1 V lower than that of Cell R-30. It is expected that insufficient wetting of the carbon fiber by the electrolyte resulted in a higher internal resistance and consequently a lower cell voltage.

2. Tests of Cells with M-Series Design
(F. J. Martino)

Efforts to improve the performance of metal disulfide cells were continued. Studies by the Cell Chemistry Group had shown that gradual loss of capacity in Li-Al/FeS_2 cells results from irreversibility of the FeS_2 electrode. As a potential solution to this problem, a lower sulfur-to-metal ratio, 1.44, was tested in two compact M-series cells,† M-4 and M-7, which had an

---

*A product of Great Lakes Research Corp., Elizabethton, TN.

†A schematic drawing of the M-series cell design can be found in ANL-78-20, p. 15.

FeS_2-NiS-Mo-Fe mixture in the positive electrodes. The capacity of Cell M-4 was limited to 165 A-hr by the negative electrodes, whereas the negative electrodes of Cell M-7 had ∿17% excess capacity (233 A-hr). As a result of these differences, the positive-electrode thickness of Cell M-4 was 12 mm (theoretical capacity, 264 A-hr) and that of Cell M-7 was 9.6 mm (theoretical capacity, 194 A-hr). The only other difference in design between the two cells was the use of 55 at. % Li in the negative electrodes of Cell M-7 as compared to 48 at. % in Cell M-4. Both cells used pressed electrodes and a Y_2O_3-felt separator/retainer, and were assembled in the charged state.

During the initial cycles, both of these cells had very low resistances (2.6 mΩ). It is uncertain whether the initial low cell resistance can be attributed to the overall positive-electrode mixture or to the 3.5-wt % molybdenum powder added to the positive electrode. Lifetime tests showed stable cell resistance in the range of 3.0-3.5 mΩ (Cell M-4) and 2.5-3.0 mΩ (Cell M-7), depending on the state of charge (lowest resistance at full charge). A post-test examination of Cell M-4 by the Materials Group revealed the formation of Li_2S and semi-conductive Y_2O_2S in the separator, which most likely was responsible for the slightly increased cell resistance during the later cycles. The effect of low cell resistance was seen in the specific power of both cells (Fig. VI-6). The specific power of Cell M-7 was especially

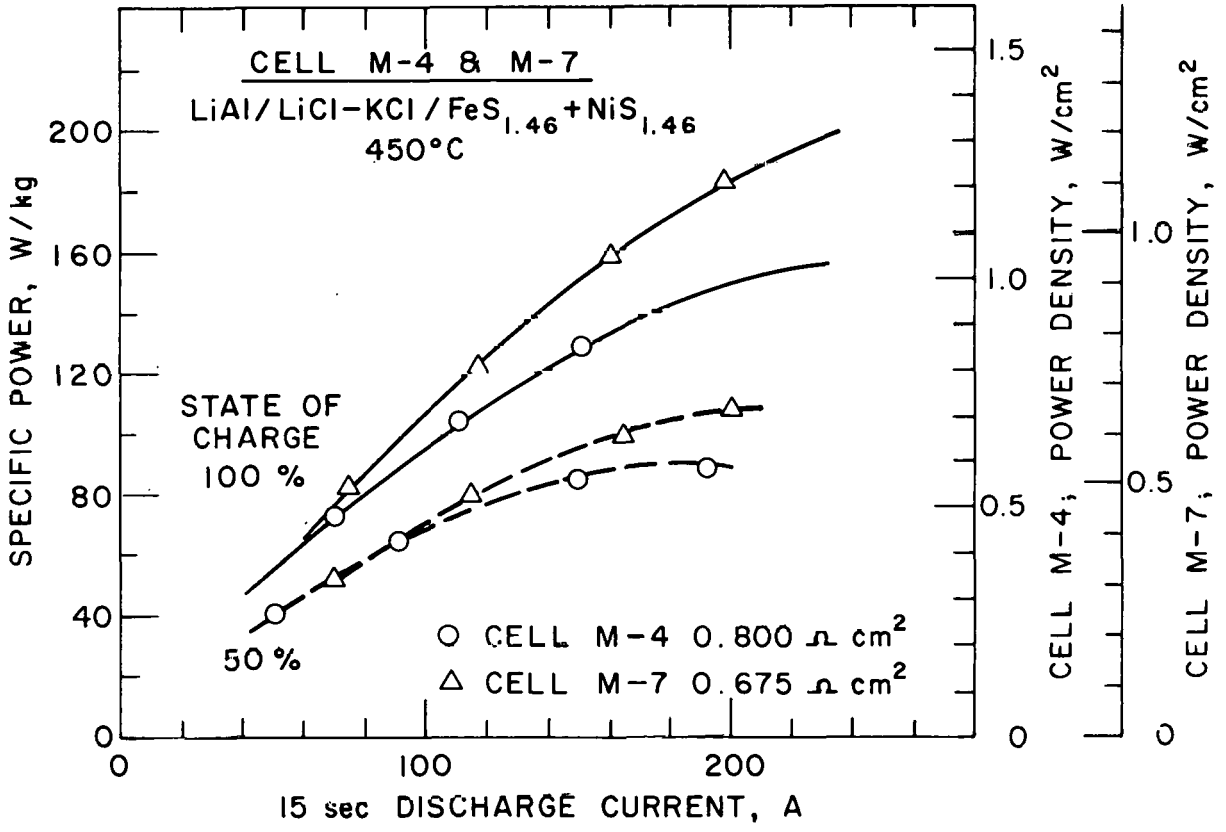

Fig. VI-6. Power Characteristics of Cells M-4 and M-7.

high--200 and 125 W/kg, respectively, at 100 and 50% state of charge; the corresponding values for Cell M-4 were 145 and 90 W/kg. The specific energies of Cell M-4 at the 4-hr and 2-hr discharge rates (current densities of 93 and 185 mA/cm^2) were 87 and 70 W-hr/kg, respectively. The specific energies of Cell M-7 with its more compact design were 97 and 78 W-hr/kg at the same discharge rates.

The operation of Cell M-4 continued for 300 cycles and 172 days. While the cell was cycled at the 4-hr discharge rate, its capacity declined by only 11% (from 107 to 95 A-hr) after 255 cycles. The stability of this cell's overall performance was very encouraging. Because of the limiting negative electrode, the positive-electrode utilization was typically limited to ∿38%. The reserve of positive-electrode active material may have been partly responsible for its extended operation. Cell M-7 demonstrated similar performance stability for ∿135 cycles, and achieved ∿42% positive-electrode utilization (85 A-hr); operation of the cell was terminated, however, because of a sharp decrease in its coulombic efficiency. The performance of Cells M-4 and M-7, with their low sulfur-to-metal mixture in the positive electrode, is encouraging with respect to the performance goals of Mark III.

The results of these studies (both R-series and M-series) suggest that the use of sulfur-to-metal ratios that are somewhat less than 2.0 in Li-Al/MS_x-type cells tends to improve the stability of the cell capacity for at lease a few hundred cycles.

C. Carbon-Bonded Electrode Cell Development

(T. D. Kaun, V. A. McCann*)

Carbon-bonded positive electrodes are being developed as an alternative to those made by pressing techniques. In the carbon-bonded electrode, the particulate active material is supported in a 5 vol % matrix of pyrolyzed carbon. This structure is formed by the pyrolysis (450-550°C) of a paste-like mixture of active material (*e.g.*, FeS or FeS_2), a volatile pore-forming agent (ammonium carbonate), a binder (furan resin†), and a carbonaceous filler.

In the development of the carbon-bonded electrode, an effort has been made to maximize the deliverable energy per unit volume of positive electrode ($W-hr/cm^3$) by optimizing the type, amount (vol %), and degree of dispersion of the carbonaceous filler material. The results of parametric tests using Li-Al/FeS cells with disk electrodes (20-cm^2 area) indicated that 8-10 vol % carbon (5 vol % from the pyrolyzed resin) with dense carbon powder or fibers‡ as the filler results in greater than 70% utilization of the FeS electrode at a current density of 100 mA/cm^2. A cell resistance of 40-60 mΩ was obtained with 8 vol % carbon in the FeS electrode; when 16 vol % carbon was used, the resistance was about 20% less. An electrode containing carbon fibers as a dispersed current collector gave a cell resistance that was about 10% less than that obtained with the dense carbon powder.

---

*Co-op Student from Howard University.

†A product of Quaker Oats Chemical Co., Morton Grove, IL.

‡A product of Union Carbide Corp.

In the investigation of potential manufacturing methods for carbon-bonded electrodes, the use of a heat-activated catalyst (1 wt % maleic anhydride) to polymerize the furan resin reduced the curing time to about 15 min at 200°C. The catalyst also resulted in faster curing at higher temperatures. A successful attempt to extrude the paste with a household cookie maker indicated that extrusion is a potential fabrication method.

Tests have been conducted on engineering-scale cells having carbon-bonded positive electrodes and a design similar to that of the M-series cells (ANL 77-68, p. 29), which had a felt (BN or Y_2O_3) separator/retainer. The M-series cell design was simplified by eliminating the positive-electrode frame. A wrapping of 200-mesh stainless-steel screen was the only particle retainer used in the positive electrode. Cell KK-11, a Li-Al/FeS_2 cell with a carbon-bonded FeS_2 electrode, was operated for 223 cycles and 120 days, when the test was terminated voluntarily. The cell showed little dependence of the capacity on discharge rate (at current densities up to 150 mA/cm^2), which indicates little electrode polarization. The specific power of Cell KK-11 was 180 and 100 W/kg, respectively, at 100 and 50% state of charge. The cell resistance was 3.5 mΩ. When the operation of Cell KK-11 was terminated, it had lost less than 11% of its 70 A-hr peak capacity (theoretical capacity, 75 A-hr) at a current density of 50 mA/cm^2. A post-test examination of the sectioned cell by the Materials Group showed about the same amount of Li_2S in the separator that had been observed in an earlier Li-Al/FeS_2-CoS_2 cell, M-3. Since these cells had been operated for different periods of time (M-3, 55 days; KK-11, 120 days), it is possible that the formation of Li_2S in the separator does not proceed beyond a particular level.

A test of a carbon-bonded Li-Al/NiS_2-CoS_2 cell, KK-13, gave indications that the carbon current collector has a stabilizing effect on cells with a NiS_2 positive electrode. Kinetic effects appeared to limit the utilization of the cell capacity (theoretical capacity, 160 A-hr). The utilization is shown as a function of current density in Fig. VI-7. The NiS_2 electrode in these cells was appeared to charge only to a $NiS_{1.5}$ phase.

Two carbon-bonded Li-Al/FeS cells with BN-felt separators were fabricated and tested. In one cell, KK-14, Cu_2S was added to the FeS electrode; the other cell, KK-15, had LiCl-rich (67 mol % LiCl) electrolyte. Cell KK-14 has provided the longest test to date of a BN-felt separator--300 cycles and 162 days. Its specific energy was 67 W-hr/kg at the 4-hr rate, which corresponds to a utilization of 69% at a current density of 75 mA/cm^2 (see Fig. VI-7). The specific power was 87 and 54 W/kg, respectively, at 100 and 50% states of charge.

Use of the LiCl-rich electrolyte in Cell KK-15 resulted in higher performance. This cell had essentially the same design characteristics as Cell M-8, including a high loading of the positive electrode (1.4 A-hr/cm^3). In the assembly of this cell, $LiAlCl_4$ was used to enhance wetting of the BN-felt separator by the electrolyte. At the 4-hr rate the specific energy of Cell KK-15 was 70 W-hr/kg, or 77% utilization of the 113 A-hr theoretical capacity at a current density of 75 mA/cm^2 (Fig. VI-7). Thus the utilization of this cell is higher than that of KK-14. A low cell resistance (~3.0 mΩ at 50% discharge) resulted in high specific power--104 and 80 W/kg, respectively, at 97 and 50% state of charge. The power for Cell KK-15 is shown as a function of current in Fig. VI-8.

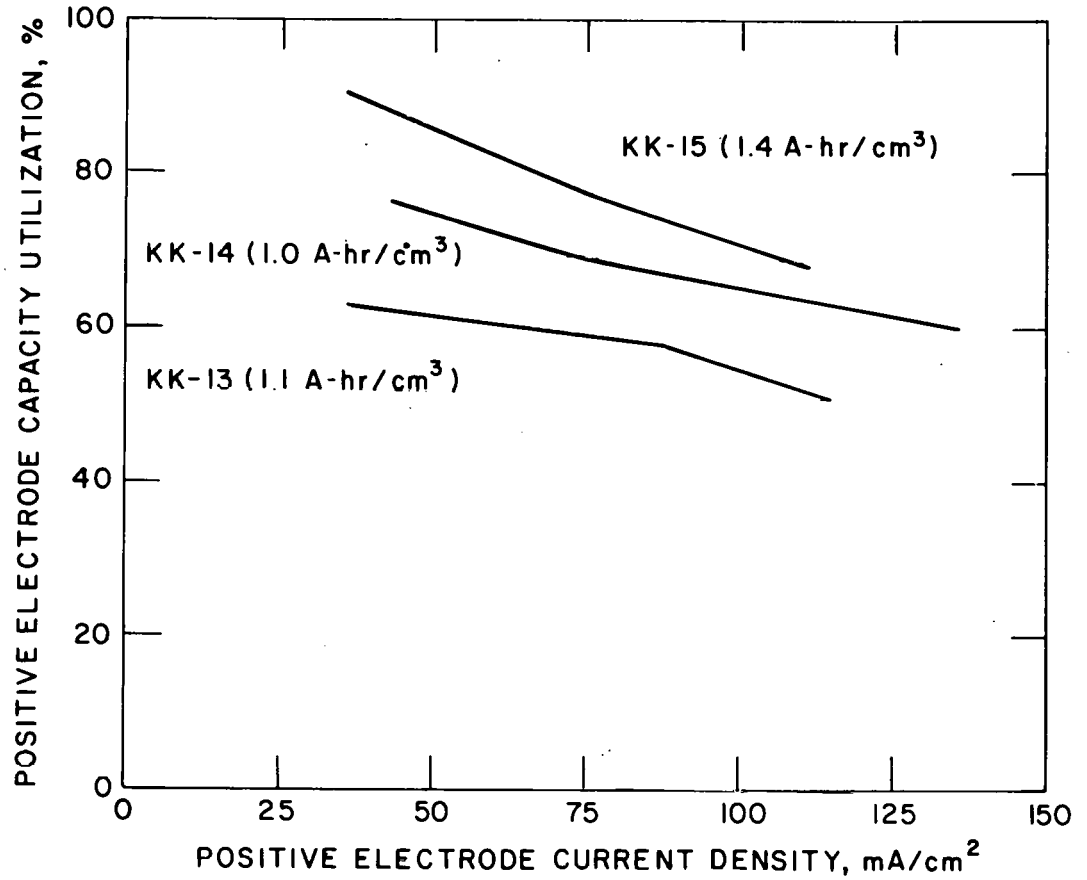

Fig. VI-7. Positive-Electrode Capacity Utilization of Carbon-Bonded Electrodes.

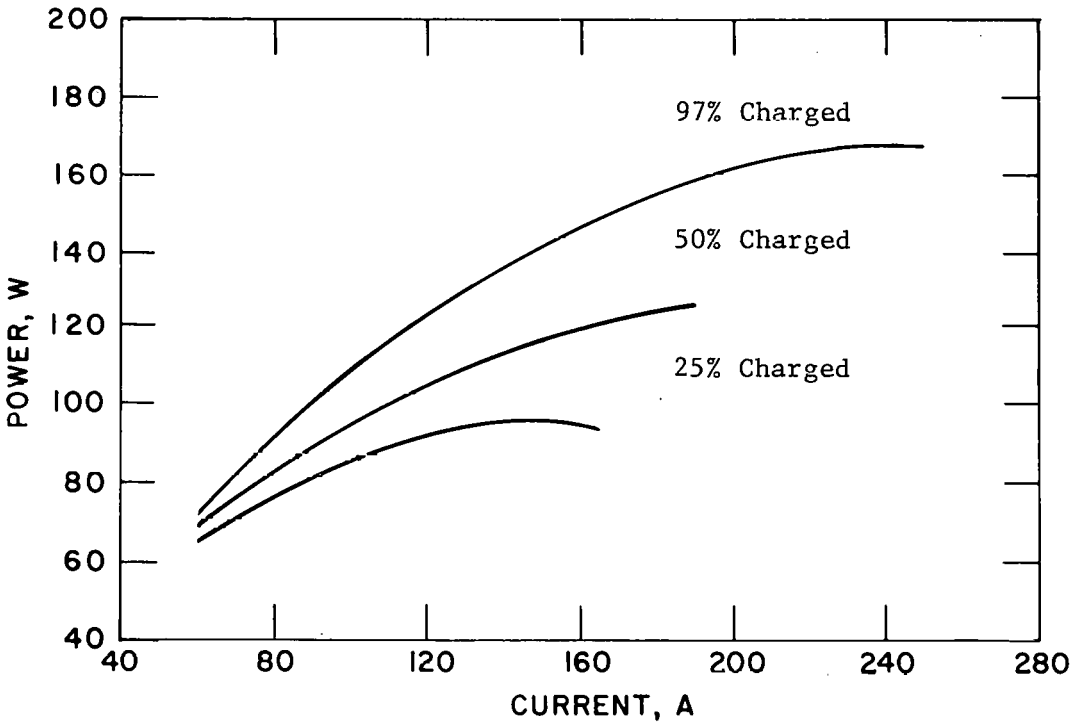

Fig. VI-8. Power Curves of Cell KK-15.

These studies have shown that carbon-bonded positive electrodes are a viable alternative to cold- or hot-pressing techniques for the fabrication of electrodes and that they have good electrical performance characteristics. A choice between carbon-bonding and pressing probably will depend primarily on relative costs and adaptability to mass production.

D. Development of Powder Separators

(T. W. Olszanski, G. B. Tuson*)

Earlier work (ANL-77-75, p. 35; ANL-78-21, p. 41) had indicated that nonconductive ceramic powders are a possible low-cost alternative to the BN fabric and felt that are currently being used as electrode separators in lithium/metal sulfide cells. The purpose of these investigations was to evaluate the use of MgO-powder separators in engineering-scale Li-Al/FeS cells. Two techniques, vibratory compaction and hot pressing, were used to form the powder separators. In both cases, the MgO powder was first heated to 500°C under vacuum for 4 hr.

The vibratory-compaction procedure consists of vibrating the MgO into the space between the electrodes, which are separated by temporary spacers. With a vibratorily compacted separator, it is necessary to use screens and frames on both the positive and negative electrodes. The hot-pressed separator is formed by pre-mixing the insulating powder with electrolyte and hot-pressing the mixture onto a previously fabricated positive electrode. In this case, only the negative electrodes require a screen and frame. The pre-mixing step consists of mixing 70 vol % MgO powder and 30 vol % LiCl-KCl for 30 min in a blender, and then heating the mixture at 450° C under vacuum for 2 hr to ensure that all the MgO particles are coated with electrolyte. The material is then ground and passed through a 60-mesh sieve.

A list of eight powder-separator cells and their characteristics is given in Table VI-1. All of the cells were assembled in a 50% charged state to minimize swelling effects; the capacities of all the cells were limited by the positive electrode. The data in Table VI-1 indicate that the method of fabrication (vibratory compaction or hot-pressing) had little, if any, effect on the performance characteristics of the cells. When the volume fraction of MgO was lowered to 30 vol %, the cell resistances were low (3-6 mΩ), but the coulombic efficiency was decreased.

In general, the powder-separator cells have a high coulombic efficiency (>99%) and stable capacity after break-in cycling (Fig. VI-9). The specific energies are essentially the same as those obtained with cells of a similar design that have BN-felt or fabric separators. The cell resistances and corresponding power characteristics were also similar to those of cells having BN-type separators. The specific power of Cell PW-14 is shown as a function of current and state of charge in Fig. VI-10.

---

*Co-op Student from North Carolina State University.

Table VI-1. Results of Tests on Powder-Separator Cells

Cell No.	Separator Fabrication Method	MgO Content of Separator, vol %	Operating Time		Theor. Cell Capacity, A-hr	Specific Energy, W-hr/kg	Discharge Rate, hr	Coulombic Eff, %	Cell Resistance, mΩ
			Cycles	Days					
PW-8	Vibratory	50[a]	687	280	115	27	4.5	99+	8-10
PW-9	Hot-Pressed	70[a]	412[b]	269[b]	144	33	4.0	99+	8-10
PW-10	Vibratory	50[a]	470	170	131	37	4.0	98+	5.5-8
PW-11	Vibratory	30[c]	24	30	150	59	10.0	90	2.9-5
PW-12	Hot-Pressed	30[c]	57[b]	47[b]	129	50	6.5	96	4.6-6
PW-13	Vibratory	50[a]	60[b]	43[b]	145	56	10.7	99+	5-7
PW-14	Vibratory	50[a]	22	21	152	68	13.8	99+	5-7.8
PW-16	Vibratory	50[a]	30[b]	21[b]	131	53	4.0	99+	4.5-5.7

[a]MgO Source: Cerac/Pure, Inc., Menomonee, WI; -60, +120 mesh, fused, 99% purity.

[b]Cell still in operation.

[c]MgO Source: Martin Marietta Chemicals, Inc., Hunt Valley, MD; Type 469; -325 mesh; 97.5% purity.

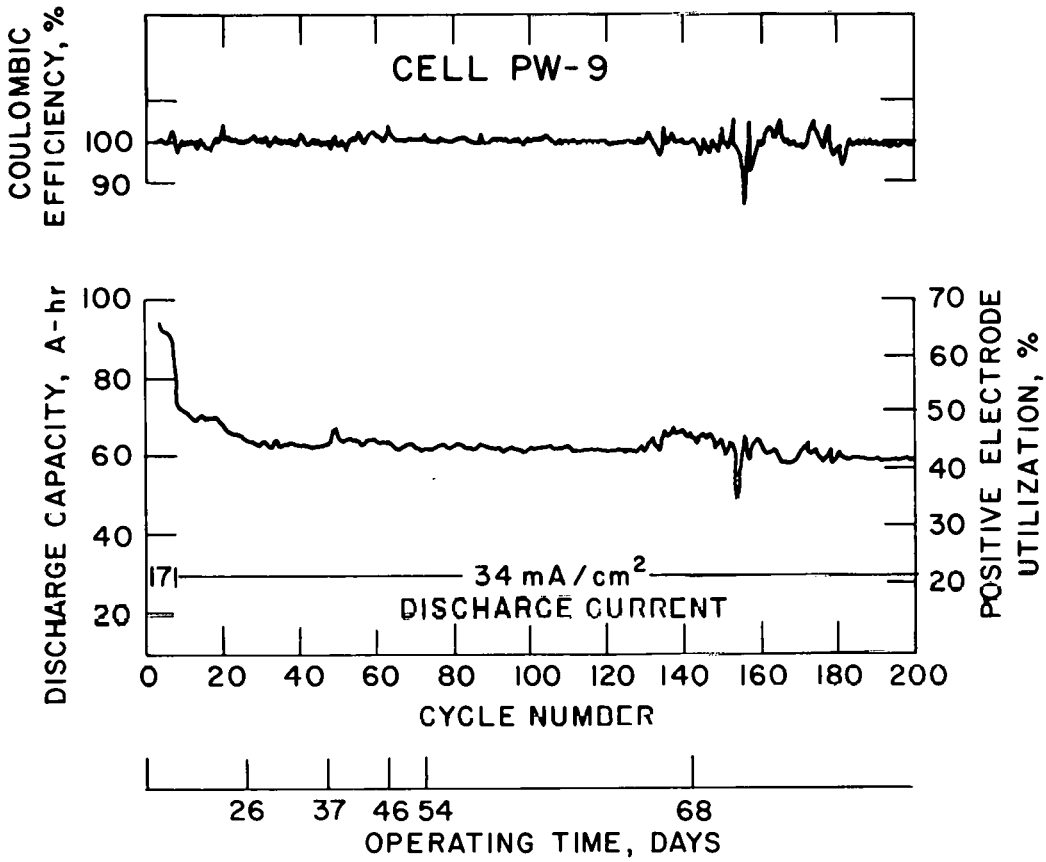

Fig. VI-9. Performance Data on Cell PW-9

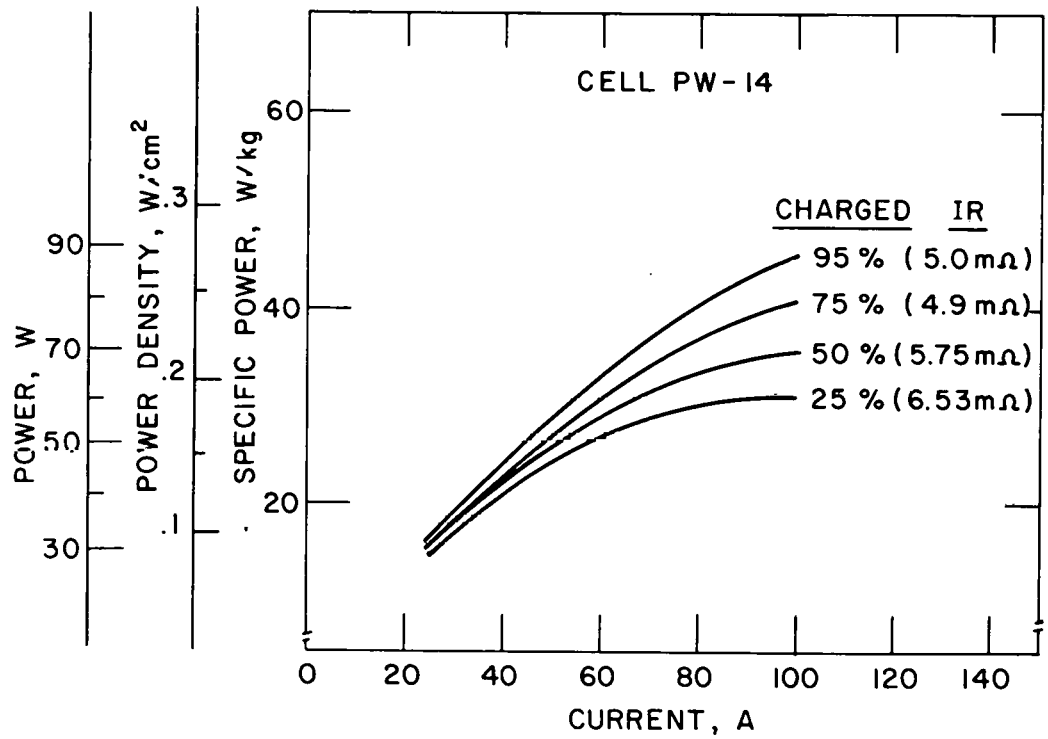

Fig. VI-10. Power Characteristics of a Cell with a Powder Separator.

The results of these studies indicate that powder separators may be an alternative to BN felt or fabric. They offer several potential advantages--ease of fabricating various shapes, the possibility of using a variety of different ceramic powders, and low cost. It is also possible that a thinner powder separator can be developed with a resulting decrease in the weight of the cell and improved power characteristics. At the present time, however, further work is needed to demonstrate the long-term stability of powder separators, particularly under vibration, and to develop multiplate cell designs that can accommodate powder separators.

VII. MATERIALS DEVELOPMENT
(J. E. Battles)

Efforts in the materials program are directed toward the development of various cell components (electrode separators, current collectors, and cell hardware), testing and evaluation of cell materials (corrosion and wettability testing), and post-test examinations of cells. The post-test examinations are conducted to evaluate the corrosion of construction materials, changes in electrode morphologies, and the causes of cell failures.

A. Corrosion Studies of Cell Materials
(J. A. Smaga, G. Bandyopadhyay*, J. T. Dusek*, T. M. Galvin*)

The corrosiveness of the cell active materials (metal sulfides, lithium, and lithium-aluminum) and the molten electrolyte places severe restrictions on the materials that can be used for current collectors, separators, and feedthrough insulators. For this reason, extensive corrosion studies are being conducted to identify materials that are compatible with the cell environment.

1. Metal-Sulfide Corrosion Studies

Current collectors in the positive electrode are exposed to a corrosive environment consisting of one or more metal sulfides and molten electrolyte. The complete or partial substitution of either FeS or FeS_2 with another metal sulfide has been used in some engineering cells. A series of static corrosion tests was conducted to determine the relative effects of these additives on the corrosion resistance of metallic components in the positive electrode. The four test environments consisted of equal-volume mixtures of LiCl-KCl eutectic and one of the following four metal sulfides: either NiS, NiS_2, $CuFeS_2$, or TiS_2.† The corrosion rates of the following materials were determined: molybdenum (NiS_2 and TiS_2 environments only), Hastelloy B, Inconel 625, Type 304 stainless steel, nickel, and AISI 1008 steel (NiS and $CuFeS_2$ environments only). The test samples were sealed in quartz tubes and heated at 450°C for 500 or 1000 hr. The results are summarized in Table VII-1.

The iron-base alloys, AISI 1008 and Type 304 stainless steel, were rapidly corroded in all environments tested. In the $CuFeS_2$ and NiS environments, stainless steel showed excessive intergranular attack, and the low-carbon steel was completely corroded. Similarly, the stainless steel was completely corroded by the TiS_2 and NiS_2 environments. For the Type 304 stainless steel, the reaction products were iron sulfide and mixed iron-chromium sulfides.

The nickel samples showed uniform surface attack in the NiS and electrolyte mixture, and general and intergranular corrosion in the $CuFeS_2$ and electrolyte mixture. In NiS_2 and electrolyte, nickel was completely reacted and massive sulfide scales formed. These scales were monolithic in

---

*Materials Science Division, ANL.

†The results of similar tests using FeS, FeS_2, CoS_2, and Cu_2S were previously reported in ANL-77-68, p. 40.

Table VII-1. Corrosion Rates Determined in Metal Sulfide Plus LiCl-KCl Environments at 450°C

Material	Sulfide Constituent	Average Corrosion Rate, μm/yr[a]	Remarks and Reaction Products[b]
AISI 1008	$CuFeS_2$	>5000	Complete reaction in 500 hr.
	NiS	>5000	Complete reaction in 500 hr.
Type 304 SS	$CuFeS_2$	4500	Severe intergranular attack.
	NiS	2200	Intergranular attack.
	TiS_2	>6300	Complete reaction in 500 hr.
	NiS_2	>6300	Complete reaction in 500 hr.
Nickel	$CuFeS_2$	1600	Localized intergranular attack.
	NiS	2400	Uniform surface attack.
	TiS_2	3200	Open, detailed scale structure; Ni_3S_2.
	NiS_2	>6000	Compact, monolithic scale; NiS, NiS_2.
Inconel 625	$CuFeS_2$	430	Surface depletion zone.
	NiS	490	General surface attack.
	TiS_2	1700	Intergranular attack.
	NiS_2	1900	Complex scale structure; NiS, NiS_2.
Hastelloy B	$CuFeS_2$	98	Minor surface depletion zone.
	NiS	120	Moderate surface attack.
	TiS_2	650	General surface attack; $NiS_{1.03}$.
	NiS_2	530	Surface depletion zone.
Molybdenum	TiS_2	+0.2	No apparent attack.
	NiS_2	+5.5	Probably MoS_2 layer.

[a]Each corrosion rate listed is the average value for 500 and 1000 hr tests. Values preceded by "+" represent the rate of formation for an adherent reaction layer; those preceded by ">" represent the minimum corrosion rate based on initial sample thickness.

[b]X-ray diffraction analyses to determine reaction products were conducted by B. S. Tani, Analytical Chemistry Laboratory, ANL.

structure, except for some internal porosity, and were composed of NiS and an external layer of NiS_2. In the TiS_2 and electrolyte mixture, the nickel sample showed scale formation and some intergranular penetration. The sulfide scales appeared to be very open and highly detailed in structure. The major phase was Ni_3S_2 rather than NiS, and secondary phases included titanium as well as nickel. These structural and compositional features were atypical of the scales formed in other metal disulfide test environments.

The nickel-base alloys, Hastelloy B and Inconel 625, developed surface depletion zones in both the $CuFeS_2$ and NiS_2 environments. These

zones, which were 15- to 25-μm deep for Hastelloy B and 50- to 70-μm deep for Inconel 625, occurred as part of the general corrosion attack, and were attributed to the preferential diffusion of nickel and iron from the alloy surface. The Inconel 625 alloy tested in the NiS_2 environment developed sulfide scales consisting of three zones. The innermost zone was an open structure of interconnected particles rich in both nickel and chromium. The intermediate layer had a similar scale structure, the major metallic elements present being nickel and aluminum. The outer layer was monolithic in appearance, and was composed of NiS and NiS_2 similar to the sulfide scale formed on nickel in the NiS_2 environment. In the TiS_2 environment, the Inconel 625 alloy showed intergranular corrosive attack, and some reaction products were dispersed within the solidified test environment. A nickel-deficient NiS was formed on the surface of Hastelloy B in the TiS_2 environment.

Molybdenum was the only material that showed excellent corrosion resistance in all of the metal disulfide environments, and it formed a thin, adherent layer of MoS_2. Similar results were previously reported (ANL-77-68, p. 40) for tests conducted in CoS_2 and FeS_2 environments.

As can be seen in Table VII-1, the sulfide environments for any given current-collector material are listed in order of increasing corrosiveness, with one exception (the corrosion rate of Type 304 SS is less in $CuFeS_2$ than in NiS). Also, the metallic materials are listed in order of increasing resistance to corrosion. By combining the results in this table with the results of previous studies (ANL-77-68, p. 40), we deduced that the corrosiveness of the metal sulfide environments increases in the following order: FeS, Cu_2S, $CuFeS_2$, NiS, FeS_2, TiS_2, NiS_2, CoS_2. The corrosion rates for all of the current-collector materials were two or three orders of magnitude higher in the NiS and $CuFeS_2$ environments than in the FeS environment. The corrosion rates for all of the current-collector materials were also higher in the NiS_2 and TiS_2 environments than in FeS_2, although the differences in corrosion rates were never more than a factor of two. These results indicate that an alloy material probably should not be used in FeS_2 cells.

2. Oxidation Potentials of Alloys

The oxidation potential for a metal in an electrolyte represents a transition of the anodic dissolution kinetics from slow to rapid. The oxidation potentials have been determined for selected nickel-base alloys in LiCl-KCl eutectic (supplied by Lithcoa*) at 425°C. The measurements were conducted using 100 g of electrolyte and a test (alloy) electrode with a surface area of 10 cm^2. A single lithium electrode served as both the reference and counter electrode, and the scan rate was 20 mV/sec. The oxidation potential was determined from the intersection of two lines which were drawn tangent to the linear portions of the voltammetry curve below the oxidation potential and above the oxidation potential. The second line was drawn with a slope of 0.05 mA/mV per unit area (cm^2).

The measured oxidation potentials are listed in Table VII-2. Each alloy was tested at least twice, and the reproducibility was $\pm$ 0.01 V of the average value. These values fall within the oxidation potential range between

*Lithium Corporation of America.

Table VII-2. Oxidation Potentials of Nickel-Base Alloys in LiCl-KCl[a] at 425°C

Alloy	Nominal Composition, wt %	Oxidation Potential (*vs.* Li), V
Hastelloy B	Ni-28Mo-5Fe-1Cr	2.60
Hastelloy C	Ni-16Mo-16Cr-5Fe	2.60
Inconel 617	Ni-22Cr-12Co-9Mo-1Al	2.56
Inconel 625	Ni-22Cr-9Mo-5Nb-3Fe	2.53
Inconel 718	Ni-19Cr-19Fe-5Nb-3Mo-1Ti	2.52
Incoloy 825	Ni-30Fe-22Cr-3Mo-1Ti	2.51
Inconel 706	Ni-37Fe-16Cr-3Nb-2Ti	2.49

[a]Filtered Lithcoa eutectic salt was used in these tests.

nickel (2.48 V) and molybdenum (2.70 V) and above the normal charge cut-off voltage (2.4 V) employed for FeS_2 cells. The alloys with high molybdenum concentrations (Hastelloy B and C) showed the highest oxidation potentials, whereas those alloys with high iron content (Incoloy 825 and Inconel 706) had the lowest potentials. In static corrosion tests in FeS_2 environments at 400 and 450°C, these alloys showed the same relative ranking, Hastelloy B being the most corrosion resistant and Inconel 706 the least resistant. With the exception of Hastelloy B, all of these alloys showed the same characteristic curve. Hastelloy B exhibited a secondary reaction which reached a maximum current density of 3 mA/cm^2 at 2.48 V, which corresponds to the oxidation potential of nickel.

3. Compatibility of BeO Insulators

Preliminary corrosion studies in Li-Al and LiCl-KCl mixtures had indicated that high-purity BeO was a suitable replacement for Y_2O_3 as the lower insulator in the feedthrough. Additional studies were conducted to determine the compatibility of BeO insulators from the 3M Company (ALSIMAG 794). The tests were conducted at 450°C for over two months in an equal-volume mixture of β-LiAl and LiCl-KCl eutectic. Both test insulators remained nonconductive, were free of any surface cracks, and showed no discoloration. The average corrosion rate for this feedthrough component was an extremely low 0.29 μm/yr. The excellent compatibility of the BeO insulators, combined with the higher mechanical strength and lower cost of BeO in comparison with Y_2O_3, make them a superior replacement for similar Y_2O_3 components.

4. In-Cell Corrosion Studies

Static corrosion tests have been used to identify candidate materials which may be suitable for application as positive-electrode current collectors. Subsequently, in-cell corrosion tests were conducted to evaluate the candidate materials identified by the static-corrosion tests. Small-

scale, prismatic cells (7.6 x 12.7 cm) are used in this study.* Identical cells are operated for time intervals of 1, 3, and 5 months to determine the time dependence of the corrosion attack. Each cell is fabricated with a theoretical capacity of about 50 A-hr and a negative-to-positive capacity ratio of 1.2. The electrodes are either hot-pressed or cold-pressed in the semicharged state. The BN fabric separators are treated with $LiAlCl_4$ to enhance wetting by the electrolyte.†

The results of the tests that have been completed thus far are summarized in Table VII-3. These cells were operated at a temperature of 450°C and a current density of 50 mA/cm^2 on both charge and discharge, except for Cell 3C-1 which was discharged at 75 mA/cm^2. Measurements indicated that the internal cell resistance was ∿35% higher in cells with Hastelloy B current collectors than in cells with nickel collectors. Using metallography and thickness measurements, we conducted post-test cell examinations to determine the extent and nature of the corrosion attack.

Table VII-3. Corrosion Rates Determined for the Structural Components of the Positive Electrodes in the 3C-Series Cells

			Corrosion Rates, μm/yr			
	Lifetime[a]		Current Collector		Electrode Frame	
Cell No.	Days	Cycles	Average	Mean	Average	Mean
3C-1[b]	76	184	110	110	110	120
3C-2[b]	31	43	170	200	240	340
3C-4[b]	35	50	240	210	280	310
3C-5[b]	>92	>121	-	-	-	-
3C-8[b]	>31	>48	-	-	-	-
3C-3[c]	31	38	610	97	950	170
3C-6[c]	31	97	640	87	1000	170
3C-7[c]	>63	>83	-	-	-	-

[a] All of these cells maintained coulombic efficiencies of 99% or better, with the exception of Cell 3C-1 which slowly declined to 80% after the 140th cycle.

[b] Li-Al/FeS cells with nickel current collectors.

[c] Li-Al/FeS_2 cells with Hastelloy B current collectors.

*See ANL-77-75, p. 35 for the general design of the cell.

†See ANL-78-21, p. 48.

For nickel current collectors, examination showed localized areas of extensive intergranular attack, while the remaining surface showed only minor, general corrosion. The intergranular attack showed a strong tendency to spread by lateral penetration. The mean corrosion rates determined for the nickel structural components are listed in Table VII-3. The very large standard deviations associated with these values reflected the wide variation in the degree of corrosion due to the localized form of intergranular attack. For a given cell the mean corrosion rates for the collector and frame were roughly equivalent. The highest rate was observed for Cell 3C-4, which was cycled for the equivalent of one month, with four hour periods on open-circuit voltage after alternate charge cycles. The average corrosion rate for both the collector and frame was 25% higher than that of a similar cell, Cell 3C-2, which also operated for one month but was not placed on open-circuit voltage. The data indicates that maintenance of a FeS cell in the fully charged condition* for long periods of time will adversely affect the lifetime of structural components in the positive electrode. The strong time dependence of the corrosion attack in these cells (*i.e.*, as operating time increases, the corrosion rate decreases) is illustrated by Cells 3C-1 and 3C-2. The lower utilization of Cell 3C-1 may have been a contributing factor to the lower corrosion rate.

The high corrosion rates observed for nickel in FeS cells were unexpected on the basis of static corrosion tests in the FeS environment (ANL-77-17, p. 38). In the static tests, nickel showed a small net weight gain due to the deposition of iron and its interdiffusion with the nickel substrate. The observed in-cell corrosion attack upon nickel was more closely related, both in degree and nature, to the random, localized attack previously observed for the nickel in the $CuFeS_2$ environment. The high in-cell corrosion rates may have been influenced by two factors: the use of semicharged electrodes and the use of a 1.7-V charge cutoff voltage. In microscopically examined cell sections, a significant fraction of the iron particles added to the semicharged mix were observed to be only partially reacted, even after nearly three months of cell operation. The slow reaction of the iron particles could be considered to be a shift in the effective sulfur-to-metal ratio to values greater than one, which would be a more corrosive environment for the nickel components. The use of a 1.7 V rather than the usual 1.6 V cutoff voltage may also be a contributing factor to the type of intergranular attack observed. In the construction and operation of later cells in this series, we have taken these two factors into consideration. If neither of these two changes eliminate the problem of localized intergranular attack, nickel must be classified as unsuitable for long-term application in FeS electrodes.

Two FeS_2 cells with Hastelloy B components in the positive electrode, 3C-3 and 3C-6 (see Table VII-3), were tested for a period of one month and then examined. Cell 3C-6 was operated as an upper-plateau cell, with a cutoff voltage of 1.3 V rather than the usual 1.0 V. For both cells, the exposed surfaces of the collector and inner frame exhibited a uniform surface attack, with less corrosion occurring near the conductor rod. The corrosion was the lowest for the upper section nearest the conducting rod

*This situation may result from charge equalization or prolonged inactivity in the charged state.

and the highest for the bottom section. The electrode frames showed the same effect. The electrode frames received no post-fabrication heat treatment and were susceptible to cracking under the combined influences of the corrosive environment, the residual stress from forming the 90° bends in the frame, and the cyclical stresses generated by electrode expansion and contraction during cell operation. For both cells, the frames had split at the 90° bend. The 200-mesh Hastelloy B screens showed severe attack in both of these cells and were completely reacted in less than one month of operation.

The corrosion rate for the Hastelloy B components are also given in Table VII-3. The calculated mean corrosion rates for the frames were more than 50% higher than the respective rates for the current collectors. The corrosion rates for the upper-plateau cell (3C-6) were only slightly greater than the rates for the two-plateau cell. In view of very high corrosion rate (>600 μm/yr) determined for cells 3C-3 and -6, Hastelloy B appears to be unsuitable for application in FeS_2 cells.

The three other cells listed in Table VII-3 are still in operation; therefore, no corrosion data are available for these cells. Cell 3C-5 is an FeS cell with a nickel collector which has completed three months of a planned five-month test period. Cell 3C-7 is an FeS_2 cell with Hastelloy B components and has completed more than two months of operation. Cell 3C-8 is being operated to evaluate nickel in an FeS-Cu_2S (20 wt %) positive electrode mix. The cell was started in the fully charged condition and has a 1.65-V charge cutoff voltage.

5. Ceramic Coatings for the Current Collector of the Positive Electrode

Electrically conductive ceramic coatings on inexpensive metallic substrates are being investigated as substitutes for the high-cost molybdenum current collectors now being used in the positive electrodes of FeS_2 cells. The requirements of a coating-substrate system include: sufficient electronic conductivity to provide adequate current-collection efficiency, corrosion resistance in the FeS_2 and molten LiCl-KCl environment at 450°C, and resistance to spalling under mechanical and thermal stresses, and less expensive than molybdenum.

Selected properties of some transition-metal borides, carbides, and nitrides have been reviewed to determine their potential as coating materials. Electrical resistivities of these materials generally range from 10 to 200 μΩ-cm at room temperature, with the borides generally having lower resistivities than the corresponding metal nitride and carbide compounds.

The chemical stabilities of the borides, carbides, and nitrides of niobium, tantalum, titanium, and zirconium with respect to formation of the metal sulfides at 427°C have been evaluated by calculation of the free-energy changes associated with the sulfidation reaction. These data indicated that TiB_2 would be stable in the FeS_2 positive electrode at 427°C with a boron activity of at least 0.3 and that TiN would be stable with a nitrogen activity equivalent to a N_2 partial pressure $\geq 6 \times 10^{-6}$ atm. In an earlier effort (ANL-75-1, p. 57), iron boride, TiC, and niobium carbides were reported to be stable in an FeS_2 environment.

Based on these calculations, a number of AISI 1008 steel specimens were coated (10-20 μm thick) with iron boride (FeB/Fe_2B), TiB_2, TiN, and TiCN by outside vendors. The iron boride coating was prepared by a gaseous diffusion process using a pack cementation method.* Coatings of TiN, TiCN, and TiB_2 were deposited by the chemical vapor deposition (CVD) technique.†

Preliminary microstructural examination (Fig. VII-1) indicated that the CVD coatings (TiN, TiCN, and TiB_2) were free of microcracks and appeared to be 100% dense. The interface between the TiN and TiCN coatings and the substrate appears to be reasonably adherent (Figs. VII-1a and 1b). However, the interface between the TiB_2 coating and the substrate showed considerable damage (Fig. VII-1c). The iron boride coating (Fig. VII-1d) appeared rather inhomogeneous. Also, a significant microcrack appeared in the region coated with iron boride.

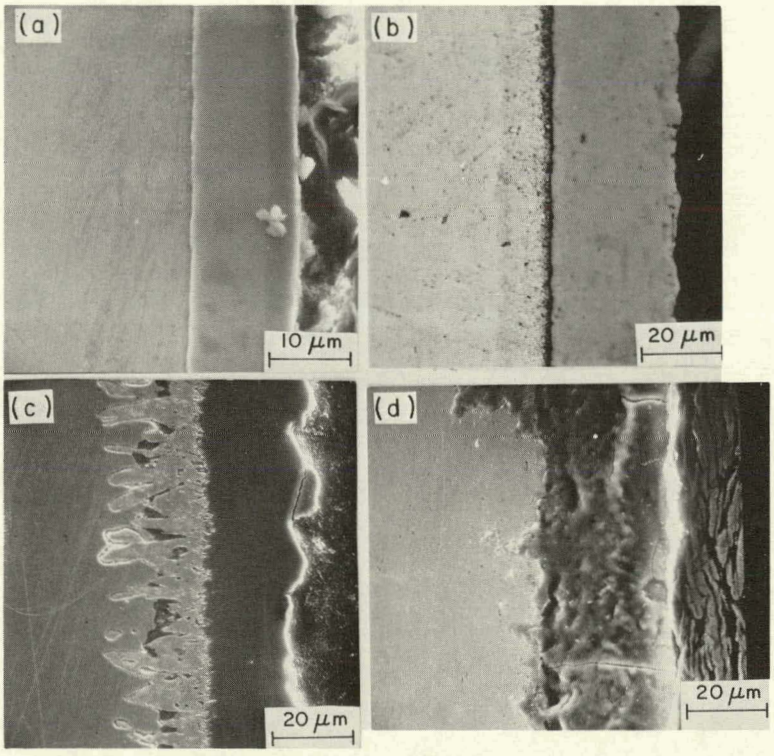

Fig. VII-1. Scanning Electron Micrograph of Samples Coated with (a) TiN, (b) TiCN, (c) TiB_2, and (d) Iron Boride. (Neg. No. MDS-65577)

Preliminary static corrosion tests have been performed on substrates coated with iron boride, TiB_2, and TiN in an FeS_2 and LiCl-KCl mixture at 500°C. The test results are summarized in Table VII-4. The samples with iron boride coatings were completely reacted in <24 hr. Since the quality of the

*"Boroloy Process", Lindberg Heat Transfer Company, Melrose Park, IL 60160.

†Materials Technology Corp., Dallas, TX.

iron boride coatings were poor (Fig. VII-d), no definite conclusion about the stability of this coating can be reached. Alternative techniques for preparing iron boride coatings will be considered for further examination.

The TiB_2 coatings also showed (see Table VII-4) poor stability in the FeS_2 and LiCl-KCl mixture. Corrosion tests were conducted to determine the effect of providing an *in situ* boron activity (which is necessary for the thermodynamic stability of TiB_2 in FeS_2). In these tests, small amounts of elemental boron or iron boride were added to the corrosion bath. Only the samples from the corrosion bath with iron boride were recoverable. A large section of this TiB_2 sample remained reasonably intact. The increased stability of TiB_2 with the addition of iron boride in the corrosion bath is probably the consequence of a reduction of sulfur activity.

Table VII-4. Summary of Corrosion Results at 500°C on Coated Specimens (maximum duration of test, 162 hr)

Coating Compositon	Corrosion Bath Composition[a]	Comment
Iron Boride (FeB/Fe_2B)	FeS_2 + LiCl-KCl	Reacted completely in <24 hr.
TiB_2	FeS_2 + LiCl-KCl	Reacted completely in <143 hr.
TiB_2	FeS_2 + LiCl-KCl + B (2.6 wt %)	Reacted completely in <143 hr.
TiB_2	FeS_2 + LiCl-KCl + FeB/Fe_2B (15.9 wt %)	About 60% reacted in <143 hr. The coating on the remainder of the sample was relatively intact.
TiN	FeS_2 + LiCl-KCl	Discolored. Minor reaction on the edges.
TiN	FeS_2 + LiCl-KCl + TiN (7.1 wt %)	Discoloration in <10% of the sample. Very little reaction at the edges.
TiN	FeS_2 + LiCl-KCl + Fe_2N/Fe_4N (7.1 wt %)	Discolored. Minor attack at the edges.

[a] FeS_2 and LiCl-KCl in an equal-volume mixture.

The TiN coatings showed good stability in FeS_2 and LiCl-KCl (with and without additives to the bath such as TiN or iron nitrides that provided some positive nitrogen activity) at 500°C after 150 hr. Some attack on the edges and corners was evident in these TiN specimens. Such attack is clearly caused by the poor quality of the coating on the sharp corners and edges, and indicates the need to devise special procedures for coating these areas of the current collectors. Figure VII-2 shows preferential corrosion of the substrate through an exposed area of TiB_2- and TiN-coated samples.

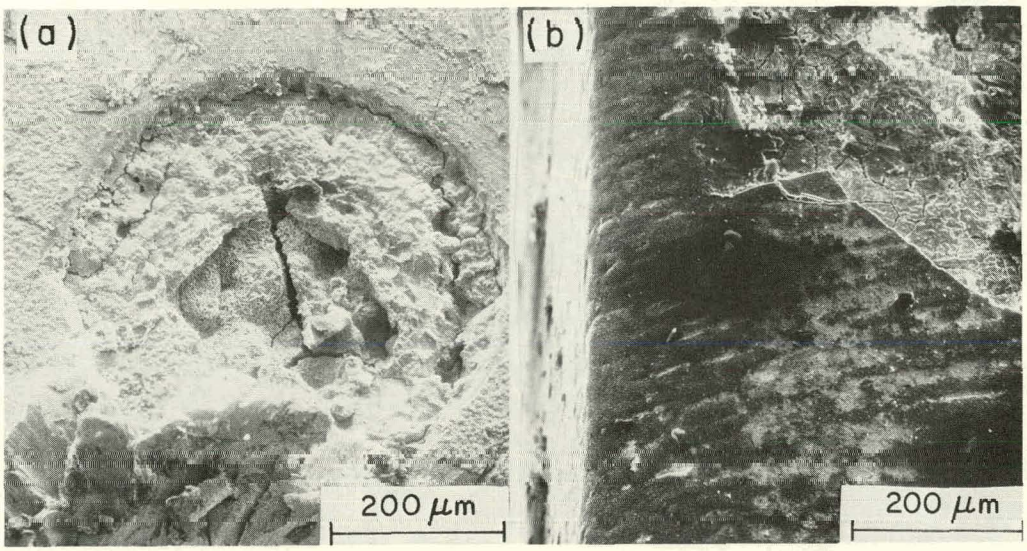

Fig. VII-2. Scanning Electron Micrograph of (a) TiB_2 Coated Sample after ∿143 hr in the FeS_2/LiCl-KCl + Iron Boride Environment at 500°C and (b) TiN Coated Sample after ∿120 hr in the FeS_2/LiCl-KCl Environment at 500°C. (Neg. No. MSD-65578)

The above results have shown that the coating quality is extremely important in determining the success of the candidate coating materials. Therefore, alternative coating techniques are being evaluated. Also, efforts are continuing to identify other possible coating materials that can be used for the positive current collectors.

B. Development of Electrode Separators

(R. B. Swaroop, G. Bandyopadhyay,* J. T. Dusek,* and T. M. Galvin*)

The primary functions of the electrode separator are to provide electrical isolation of the electrodes from each other, to contain sufficient electrolyte for the ready transport of lithium ions between the electrodes, and to prevent escape of active material from the electrodes. A practical cell requires a porous separator that is chemically stable in the cell environment, permits close electrode spacing, is mechanically strong enough to sustain small dimensional changes that occur in the electrodes during operation, is easily wet by molten LiCl-KCl electrolyte, and has low-cost potential. Because the BN cloth separators currently used are too expensive, efforts have been directed toward the development of the following separator materials: porous felt, loose powder, and porous, rigid ceramic. Felt separators are more porous, use less material, and are less expensive than BN cloth separators. The development of powder and porous, rigid ceramic separators (such as AlN, MgO, β-Si_3N_4, and Y_2O_3) is being pursued because separators of this type are amenable to low-cost mass production and permit the use of materials that are not available in fibrous form.

---

*Materials Science Division, ANL.

1. Separators of BN Felt

a. Characterization of BN Felt

Nearly two years ago Carborundum Co. was contracted to develop BN felt for use as electrode separators (see Section III.D.1); in this time, the quality of the Carborundum BN felt has improved considerably. During this report period, four lots (total of 20 m^2) of BN felt were received from Carborundum Co. The thickness of the as-received felt was 0.7, 1.5, 2.0 and 3.0 mm. The as-received felts were stabilized at 1750°C in flowing nitrogen for 24 hr; this stabilization is required in order to convert residual B_2O_3 to BN. The as-received and stabilized felts were characterized for basis weight, porosity, and burst strength. The felts currently being fabricated have a basis weight of 10-13 mg/cm^2 per 1 mm of thickness, 90 to 93% porosity, and a burst strength between 5 and 6.5 kPa/mm. These felts have adequate strength and flexibility to handle in cell construction. The uniformity of fiber distribution is excellent.

b. In-Cell Testing of Separators

During this period, electrode separators of BN felt, MgO powder, and porous, sintered Y_2O_3 were evaluated in small-scale (7.6 x 12.7 cm), prismatic Li-Al/FeS test cells.* This cell configuration was selected because it closely approximates that of engineering-scale cells and meets the mechanical requirements for the successful application of felt, powder, and porous, sintered ceramic separators. This test was designed to allow a comparison to be made between cells using felt and cells using powder separators under similar conditions.

Four separator-test cells using BN felt stabilized at 1750°C in nitrogen were assembled and operated. The thickness of the BN felt was either 1.25, 1.6, 2.8, or 3.2 mm. Performance data on these cells are given in Table VII-5. The best active-material utilization and specific energy were observed in Cell SC-25, which had the thinnest felt separator (1.25 mm). Of the four cells, Cell SC-19 operated for the longest period (205 cycles and 3050 hr). Towards the end of the lifetime of Cell SC-19, a series of freeze-thaw cycles was initiated and these tests resulted in cell failure (ANL-77-75, p. 34).

Figure VII-3 shows the effect of separator thickness on the percent utilization of the active material for these four cells. Utilization for each test cell decreased as the current density increased and the utilization decreased as the thickness of the BN-felt separator was increased. As expected, the thicker separators have a higher resistance to ionic transport, and hence have lower utilization of the positive-electrode material. Similarly, the data in Table VII-5 show a trend toward lower internal cell resistances as the thickness of the separator was decreased. The specific energy at a given current density also varied in a similar manner to that of percent utilization.

---

*See ANL-77-75, p. 34 for the general design of the separator-test cell.

Table VII-5. Performance Data on Separator Test Cells

Cell No.	Separator		Theor. Capacity, A-hr	Util.,[a] %	Specific Energy, W-hr/kg	Lifetime	
	Type	Thick., mm				Cycles	Hours
SC-19	BN Felt	2.8	50	62	55	205	3050
SC-25	BN Felt	1.25	51	72	66	98	1700
SC-27	BN Felt	1.6	48.5	66	59	72	1159
SC-30[b]	BN Felt	3.2	48	60	54	80	1200
SC-21	MgO Powder	1.8	51	61	55	131	1914
SC-28	MgO Powder	0.9	48.5	70	63	50	982

[a]At a current density of 40 mA/cm^2 (10-hr discharge rate).

[b]Cell still in operation.

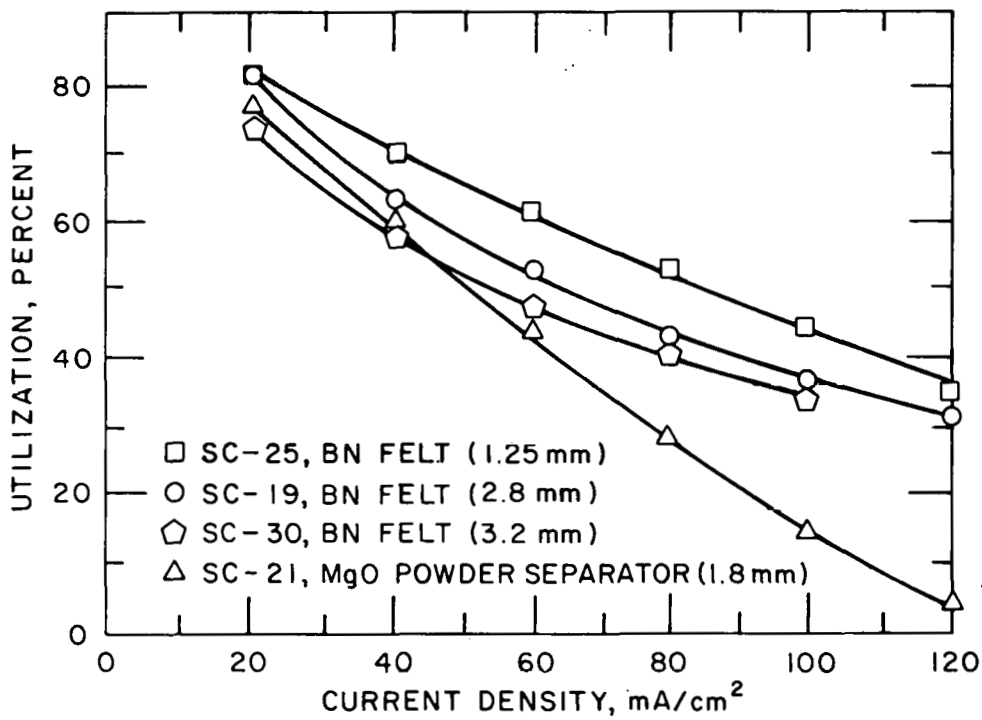

Fig. VII-3. Performance of Four Separator-Test Cells.

In Cells SC-27 and SC-30, $LiAlCl_4$ was used as a wetting promoter for the BN-felt separator (ANL-78-21, p. 48). The separators were dusted with 5 and 14 mg/cm^2 of powdered $LiAlCl_4$. Cell SC-27 had one initial degassing operation and SC-30 had none. Cell SC-30 is still operational after 1200 hr (80 cycles). Operation of Cell SC-27 was terminated after 1159 hr because a short circuit developed between the negative and positive electrodes as a result of swelling of the negative electrode. A post-test examination indicated (1) no precipitation of aluminum particles in the separator, and (2) no chemical reaction of the BN felt with the active materials.

2. Separators of MgO Powder

The development of powder separators, such as AlN, MgO, β-Si_3N_4, and Y_2O_3, is being pursued because separators of this type can be easily fabricated and are amenable to low-cost mass production. These materials are commercially available and are generally 98+% in purity and low in silica content (<0.3%)

For the MgO powder separators, a commercial grade* of MgO powder was used which had a sieve size of -60 +120 mesh and an irregular particle shape. The cell design and testing procedure were essentially the same as those used with felt separators. The MgO powder was vibratorily loaded into the cell and has a porosity of 40-50% and a thickness of either 0.9 or 1.8 mm.

Performance data for Cells SC-21 and SC-28, which used MgO powder separators, are listed in Table VII-5, and the percent utilization at various discharge current densities is shown in Fig. VII-3. The results show that at low current densities (<60 mA/cm^2) the utilization of cells with powder separators was comparable to that obtained for cells with felt separators. However, the percent utilization decreased rapidly as the discharge current density was increased beyond 60 mA/cm^2. This effect is apparently caused by the low porosity of powder separators ($\sim$50% *vs.* 90%) which restricts ionic transport at the higher current densities.

3. Porous, Rigid Ceramic Separators

The objectives of this task are to develop procedures for fabricating porous, rigid ceramic separators and to determine their technical feasibility. The ceramic materials currently under investigation are Y_2O_3 and MgO.

The fabrication of ceramic separator plates requires special processing techniques because the plates must be thin ($\sim$1-2 mm thick), highly porous ($\sim$50-70% porosity) with pores sufficiently small to retain the electrode particles, and strong enough to handle during cell assembly.

Since the plates have to be highly porous and very thin, special care was needed in the processing steps to avoid damage to the plates before firing and to avoid warping during firing. The magnitude of these problems increases with increasing porosity and/or decreasing plate thickness, both of which are desirable for reduction of internal cell resistance. Because of the above requirements for the separators and the associated fabrication problems, a number of different processing techniques were investigated.

---

*Martin Marietta Inc., Hunt Valley, MD, and Cerac/Pure, Inc., Milwaukee, WI.

Although most of these studies were directed toward the fabrication of porous Y_2O_3 separator plates, preliminary studies on porous MgO ceramics were also conducted. A summary of the various processing techniques and the resulting properties is presented in Table VII-6.

The foaming technique has produced Y_2O_3 bodies with porosities up to 90% and an average pore size of 1 to >25 μm (ANL-77-17, pp. 35-37). However, these samples are usually fragile, and often a significant fraction of the pores is rather large (>150 μm). The Y_2O_3-nitric acid plaster composition (ANL-78-21, pp. 43-46), which was allowed to set up at room temperature before sintering, produced porosities up to 70%. Microstructural examination revealed a rather uniform, small-size (<1-5 μm) pore in these samples. However, the firing shrinkage, 20-25% linear, and the resulting warpage in the body are serious problems in this technique.

Acceptable Y_2O_3 plates, although having some warpage, could be formed by the following two techniques: (1) as-received Y_2O_3 powder was cold pressed with a binder, and (2) crushed Y_2O_3-nitric acid plaster was cold pressed and subsequently sintered. Thus far, the best processing technique developed for the fabrication of Y_2O_3 separator plates involves calcination of the starting powder prior to the cold-pressing and sintering operation. In addition to the calcination step, proper positioning of the plates in the furnace, a small load on the plates, and a very precise firing schedule were necessary during the sintering process to obtain the best results. As can be seen in Table VII-6, calcination of the starting powder at 1200°C led to flat plates, with porosities up to ∿57% and thicknesses >2 mm, and calcination of the starting powder at a temperature of 1500-1550°C, which is higher than the sintering temperature (1450°C), produced flat plates with porosities up to ∿60% and thicknesses of ∿1.5 mm. These separator plates have been used to assemble the first cells using rigid, ceramic separators.

Fabrication of MgO separator plates, similar to those of Y_2O_3, has been initiated because MgO is much less expensive than Y_2O_3. As can be seen in Table VII-6, the addition of binder has a strong effect on the sintered densities of MgO. The processing method which proved successful for the fabrication of Y_2O_3 separator plates is being used for the fabrication of MgO separators.

Two test cells (MS-1 and -2) using porous, rigid Y_2O_3 separators* were assembled in the semicharged state. Calcined Y_2O_3 powder was used to fill the electrode edges to prevent short-circuiting in those areas. Wetting of the separator by LiCl-KCl electrolyte required ∿1-2 hr in vacuum. The theoretical capacity of the cells, the processing conditions for the separators used in these cells, and the thickness and the density of the separators are shown in Table VII-7. Cell MS-1 had thicker and higher density separators than those used in Cell MS-2. In addition, the theoretical capacity of Cell MS-1 was lower than that of MS-2 (35.7 *vs.* 50.0 A-hr). Cell MS-1 was operated successfully for 83 days (283 cycles) before voluntary termination for post-test examination, and Cell MS-2 has operated for more than 20 days (25 cycles) at current densities up to 60 mA/cm^2. The utilization of the active material as a function of discharge current density of Cells MS-1 and -2 is shown in Fig. VII-4. For comparison, this figure includes the data for SC-21 (MgO powder separators) and SC-25 (BN felt, ∿1.25 mm thick).

*The cell design was the same as used with felt separators.

Table VII-6. Processing Variables and Some Characteristics of Fired Y_2C_3 and MgO Bodies

Starting Composition	Firing Conditions	Properties of Fired Samples[a]				Comments
		Porosity, %	Shrinkage, % Linear	Cumulative Pore Volume,[b] cc/g	Average Pore Diameter,[b] μm	
Y_2O_3[c] foam.	Dried & sintered at 1500-1800°C for 0-2 hr	60-90	-	0.60-0.64	1 to >25	Usually fragile with a large pore distribution.
Y_2O_3-nitric acid plaster. Set at room temperature.	1500-1800°C for 0-15 hr	55-70	20-25	-	-	Easy handling. Extensive warpage.
Crushed Y_2O_3-nitric acid plaster. Cold pressed.	1400-1500°C for 0-8 hr	46-62	21-26	0.14-0.19	0.1-1.1	Easy handling. Some warpage. Large shrinkage.
Calcined (~1200°C) Y_2O_3 plaster. Cold pressed.	1400-1500°C for 0-8 hr	36-56	2-12	0.23	0.15	Easy handling. Good flat plates at plate thickness >2 mm.
Y_2O_3 mixed with organic binder[d] and cold pressed.	1400-1500°C for 0-12 hr	40-67	4-9	0.09-0.18	0.4-0.7	Easy handling. Some warpage.
Calcined (1550°C) Y_2O_3 with or without as-received Y_2O_3. Cold pressed without binder.	1450-1460°C for 6 hr	53-61	<2%	-	-	Good strength. Excellent flat plates with plate thickness <2 mm.
Cold-pressed MgO.[e]	1400-1500°C no hold	52-57	8-12	-	-	Poor quality bodies with cracking.
MgO with binder. Cold pressed.	1450-1500°C for 0-8 hr	15-18	29-30	-	-	High strength. Warped.

[a] Often disc-shaped samples (considerably easier to fabricate compared to the fabrication of plates) were used to determine the effect of processing conditions on the density and pore distribution in fired bodies. Subsequently, plates were sintered using the optimized processing parameters.

[b] Determined by the mercury penetration method.

[c] Molycorp, 99.99% Y_2O_3.

[d] Stearic acid: acryloid ratio of 1:3.

[e] Mallinckrodt, reagent grade MgO.

Table VII-7. Processing Conditions and Description of the Rigid Separators Used for In-Cell Testing

Cell No.	Theor. Capacity, A-hr	Separator Plate No.	Composition	Calcination		Sintering		Porosity, %	Thick., mm
				Temp., °C	Time, hr	Temp., °C	Time, hr		
MS-1	35.7	115	Crushed Y_2O_3-nitric acid plaster (-30 +100 mesh) and 12% binder. Ball milled.	1250	8.5	1500	No hold	50.6	2.47
		125	Crushed Y_2O_3-nitric acid plaster (-30 mesh). No binder.	1250	8.5	1440	No hold	51.3	2.13
MS-2	50.0	179	Y_2O_3 foam with albumin. Calcined, crushed, and mixed with 10% as-received Y_2O_3. Cold pressed.	1550	13	1450	6	60.8	1.50
		180	Y_2O_3 foam with albumin. Calcined, crushed, and mixed with 10% as-received Y_2O_3. Cold pressed.	1550	13	1450	6	60.1	1.47

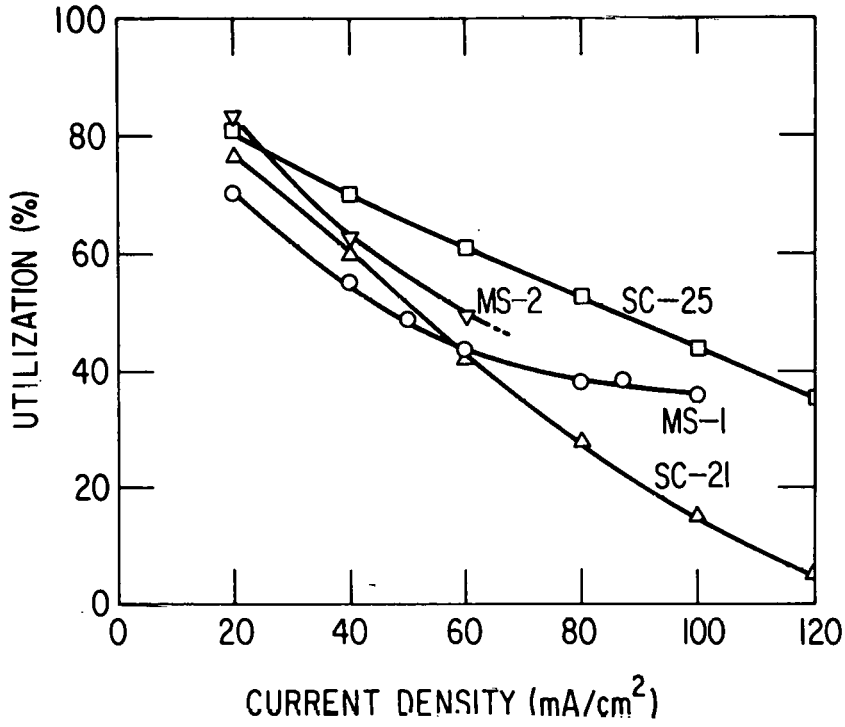

Fig. VII-4. Performance of Cells with Rigid Y_2O_3 (MS-1 and -2), BN Felt (SC-25), and MgO Powder (SC-21) Separators.

The coulombic efficiency of Cell MS-1 remained at 100%. At 20 mA/cm^2, the utilization of Cells MS-1 was 70%, which is lower than the corresponding utilization of SC-25 and -21. However, at high current densities (>80 mA/cm^2), Cell MS-1 showed good utilization compared to that of the other cells. Also, the utilization of MS-1 did not change significantly (within 2%) when the current density was raised to 100 mA/cm^2 and then brought back to 60 mA/cm^2.

The utilization of Cell MS-2 was better than that of MS-1 at all measured current densities, apparently because of the thinner and lower density separators (See Table VII-7). The coulombic efficiency of Cell MS-2 has remained at 100% for all current densities.

In conclusion, cells with rigid Y_2O_3 separators have shown good performance in comparison with cells using BN felt and MgO powder separators. Post-test examinations will be performed soon on MS-1 and -2, and should provide further insight about the performance of these rigid separators. In-cell testing will also be carried out using rigid MgO separators. Although the test cells with rigid separators showed very good performance characteristics, tests of these separators in engineering-scale cells should be conducted. The fabrication of larger-size separators may require some modification in the processing steps.

4. Thermomechanical Behavior of Electrode-Separator Systems

Post-test examination of cells indicated that a mode of cell failure is short-circuiting caused by the extrusion of active materials at the edges or corners of electrodes (ANL-77-35, p. 44). In order to understand the thermomechanical extrusion behavior, we studied the flowability (extrusion) behavior in powder separators and electrode-separator systems in the absence of discharge-charge cycles.* The following specimens were either hot-pressed or cold-pressed; MgO powder saturated with 30 vol % LiCl-KCl eutectic, FeS powder saturated with 50 vol % LiCl-KCl eutectic, MgO-FeS saturated with 30 vol % LiCl-KCl eutectic, and LiAl powder saturated with 36 vol % LiCl-KCl eutectic. The results of this investigation are summarized in Table VII-8. The major conclusions from this study are: (1) a MgO powder separator of 70 vol % solid will hold its shape after some initial degree of compaction, (2) cold-pressed or hot-pressed FeS electrodes will easily flow or extrude (see Fig. VII. 5) at stresses as low as 200 kPa, (3) the extrusion of the FeS and LiCl-KCl eutectic is possible above the stress level of 200 kPa at 350 and 450°C, and (4) cold-pressed negative electrodes will easily flow or extrude at 450°C under stresses as low as 56 kPa.

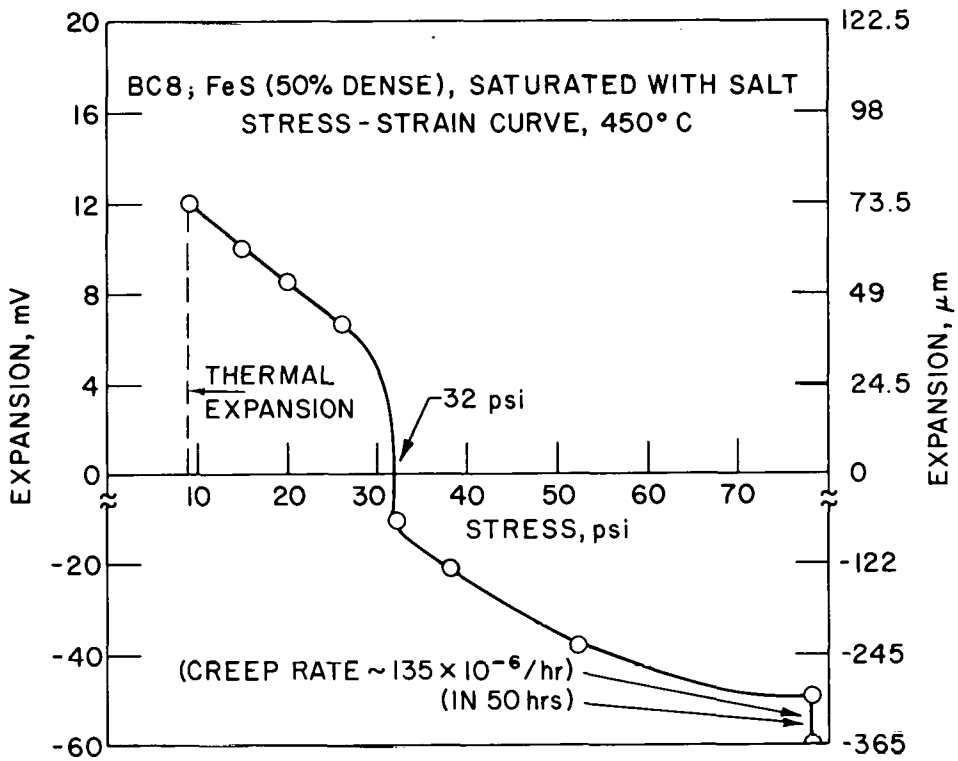

Fig. VII-5. Creep Behavior of FeS + LiCl-KCl Sample (Constrained) at 450°C.

*See ANL-77-75, p. 37 for a schematic of the test apparatus.

Table VII-8. Thermomechanical Data on Powder Separator and FeS Electrode Material

Specimen Composition[a]	Thickness, mm	Thermal Expansion Coefficient,[b] (per °C) x 10^{-6}	Creep Rate,[c] m/m per hr	Total Creep,[d] %	Remarks
MgO (71% dense)[e]	10.7	9	7×10^{-6} (at 700 kPa)	0.13	Creep in 140 hr.
MgO (70% dense)[e]	10.6	13.5	5.6×10^{-6} (at 700 kPa)	0.06	Creep in 70 hr.
MgO-FeS (71% dense)[f]	12.0	17.4	-	68	Instantaneous flow at 350°C. MgO and FeS both crept extensively.
MgO-FeS (70% dense)[e]	12.0	12.3	103×10^{-6} (at 700 kPa)	3	Only FeS crept (in 240 hr).
FeS (50% dense)[e]	11.8	18.6	-	-	Instantaneous flow beyond 224 kPa
FeS (50% dense)[e]	12.7	15.0	135×10^{-6} (at 546 kPa)	3.6	-
LiAl (64% dense)[f]	9.0	20	-	-	Instantaneous flow beyond 224 kPa.
LiAl (64% dense)[f]	8.8	22	8.8×10^{-3} (at 55 kPa)	26	Instantaneous flow beyond 224 kPa

[a] Saturated with LiCl-KCl eutectic. The particle size for all materials was between -50 and +200 mesh.

[b] Measured between room temperature and 350°C under stresses of 55-65 kPa.

[c] Measured at 450°C. Static-compressive stress values given in parentheses.

[d] Percent of original thickness.

[e] Hot pressed.

[f] Cold pressed.

C. Cell Wetting and Degassing Studies
(J. G. Eberhart*)

During this period, studies were continued in an effort to identify the factors that influence the wettability of cell materials by the electrolyte and to develop means of improving the wetting behavior where needed. The internal resistance of a lithium-aluminum/iron sulfide cell is determined in part by the extent to which the molten LiCl-KCl electrolyte fills the pore systems of the cell electrodes, particle retainers, and separators. Pore filling is, in turn, a function of the wettability of these cell materials by the electrolyte and the geometry of their pore structures.

Measurements of the advancing and receding contact angles (θ_A and θ_R respectively) for molten LiCl-KCl on various cell materials have been continued. The results of these measurements are summarized in Fig. VII-6, which shows the range of contact angles for the electrolyte on a variety of cell materials at 400°C. All measurements were conducted in a helium-atmosphere glove box. The Li-Al alloy of the negative electrode was the only material that was instantaneously wetted by the molten electrolyte ($\theta_A = \theta_R = 0$). Easy-to-wet behavior ($\theta_R < \theta_A < 90°$) was exhibited by Type 304 stainless steel and Y_2O_3. Difficult-to-wet behavior ($\theta_R < 90° < \theta_A$) was observed on the

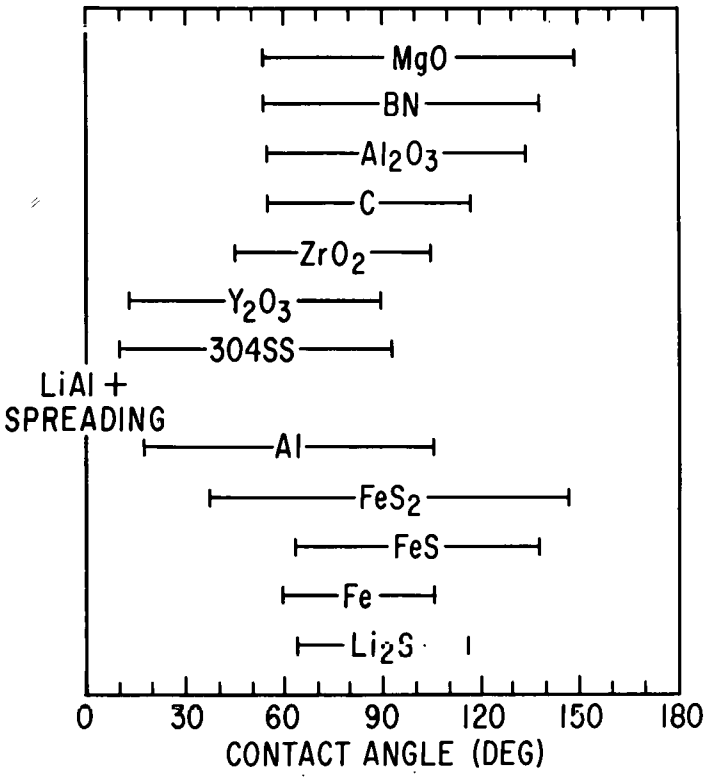

Fig. VII-6. Contact Angle Ranges for Molten Salt (400°C) on Various Solid Surfaces.

*Now associated with the Aurora College, Aurora, IL.

positive-electrode materials (FeS_2, FeS, Li_2S, and Fe) and on the candidate separator and particle retainer materials (BN, MgO, and ZrO_2). Electrolyte will spontaneously fill the pore structure of easy-to-wet materials, but must be pushed into the pores of difficult-to-wet materials.

A knowledge of receding contact angles for cell materials permits the estimation of the height to which a porous electrode material can maintain electrolyte infiltration in a vertical cell under the influence of gravity. The receding capillary height, h_R, can be calculated from the equation

$$h_R = 2\gamma \cos \theta_R/\rho g r \quad (1)$$

where γ and ρ are the surface tension and density of the molten electrolyte, respectively; g is the gravitational acceleration; and r is the pore radius in the porous material. A conservative model was used to calculate the receding capillary height for the porous cell material; this model[2] assumes a cubic packing of uniform, spherical particles having a diameter D. The pore radius is given by

$$D = 2r/(\sqrt{2} - 1) = 4.83\ r \quad (2)$$

Using Eqs. (1) and (2) and the known values of γ, ρ and g, h_R can be estimated from θ_R. The largest θ_R observed for a cell material is 64° (for Li_2S). For the cell material with the poorest wetting characteristics (Li_2S), particle sizes of 1000, 100, and 10 μm yield h_R values of 3.5, 35, and 350 cm, respectively. A receding capillary height of 35 cm is adequate for any foreseeable engineering cell. Thus, a particle size of 100 μm or less is recommended for powder-formed cell components on the basis of simple capillarity considerations.

Cells containing difficult-to-wet materials (such as BN separators, stainless steel particle retainers, or carbon fabric) must be evacuated and repressurized with helium in order to force electrolyte into their pore structure. Wetting tests have shown that, following a light dusting of the surface with a fine $LiAlCl_4$ powder, these cell materials are spontaneously wetted and penetrated by the electrolyte. The method of application of $LiAlCl_4$ to a cell component is quite important. No improvement was observed in the wetting behavior when $LiAlCl_4$ was added directly to the LiCl-KCl electrolyte and then the $LiAlCl_4$ and electrolyte mixture applied to the material. However, if the $LiAlCl_4$ is applied to a cell component (such as a separator) and allowed to melt and spread over the surface, then the component surface is readily wet during later contact with electrolyte. Thus, the $LiAlCl_4$ probably acts as a "flux" which cleans a solid surface, and is not a wetting agent or surfactant which must be dissolved in the electrolyte.

Measurements of molten-electrolyte penetrability were made on BN felts with various levels of $LiAlCl_4$ dusted into the felt pores. As little as 7.5 mg of $LiAlCl_4$ per square centimeter of BN felt was effective in promoting electrolyte penetration. Higher concentrations of $LiAlCl_4$ are possible through melting of the wetting promoter into the pore structure at the time of application to the separator; however, there seems to be no advantage to using these higher loadings.

A variety of wettability tests were performed to determine the behavior of molten electrolyte on MgO. A contact-angle measurement was made of a sessile drop on a compacted bed of MgO powder, and the sessile drop indicated nonwetting behavior. In addition, MgO felt was subjected to electrolyte penetration testing. As anticipated from the contact-angle determination, the felt exhibited difficult-to-penetrate behavior. Next, a similar powder bed with 6 vol % $LiAlCl_4$ was heated to 400°C and then contacted with electrolyte. The MgO powder was instantaneously wet by the electrolyte, which demonstrates that $LiAlCl_4$ is also an effective wetting promoter for MgO.

Finally, since LiCl-rich electrolyte is currently being used in many engineering cells, a wettability determination was made for 54 wt % LiCl-46 wt % KCl. At 400°C, this molten salt has θ_A and θ_R of 153° and 81°, respectively, on a hot-pressed BN surface. For eutectic electrolyte on the same surface, θ_A and θ_R are 138° and 53°, respectively. Thus, although BN is difficult to wet by both salts, LiCl-rich electrolyte has poorer wetting characteristics than eutectic electrolyte.

D. Post-Test Cell Examination

(F. C. Mrazek, N. C. Otto, and J. E. Battles)

Post-test examinations are conducted on small laboratory cells* and on engineering-scale cells.† The objectives of these examinations are to determine (1) cell morphology (such as electrode microstructure, active material distribution and utilization, reaction uniformity, components' performance, impurities, and cross-contamination of electrodes), (2) in-cell corrosion reactions and kinetics, and (3) causes of cell failure. These results are evaluated, and appropriate recommendations for improving cell performance and lifetime are made.

The results of the post-test examinations of industrial-contractor cells are reported in Appendix D (see Section IV.D). The results of post-test examinations of cells fabricated at ANL are reported below.

1. Post-Test Examination of ANL Cells

During this report period, 17 vertical, prismatic engineering bicells were examined, all of which were fabricated and tested at ANL. The results of the post-test examination of ANL cells are summarized in Appendix F. An additional twenty small-scale cells and single electrodes were sectioned and examined microscopically. Characteristics such as composition, concentration gradients, and general morphology were obtained, and the results presented to the cell builder for evaluation.

All of the cells listed in Appendix F utilized Li-Al in the negative electrodes, except Cells CA-12 and -14 which had Ca-Mg-Si negative electrodes. Cells TiSp-1 and -2 had TiS_2 positive electrodes; a number of cells had nickel sulfide in the positive electrode (CA-12, -14, R-32, -33, and A-5), and the rest of the cells had iron sulfide in the positive electrode.

---

*Fabricated and tested at ANL.

†Fabricated either at ANL or an industrial firm and tested at ANL.

As previously reported (see ANL-77-35, p. 48 and ANL-77-75, p. 43), post-test examinations have shown that a band of Li_2S and metallic iron particles is depositied within the separator of all FeS_2 cells, except for FeS_2 cells which have positive current collectors of Hastelloy B rather than the usual molybdenum. Metallographic examination showed that the Hastelloy had reacted extensively with the FeS_2 and that only a very minor amount of Li_2S was deposited in the separator. On the basis of this result, several cells were constructed with sulfur-to-metal ratios of less than 2.0 (R-30, R-35, M-4 and A-6). In each of these cells, the amount of Li_2S-Fe deposited within the separator was significantly reduced relative to typical FeS_2 cells. In cells utilizing positive electrodes of nickel sulfide (NiS_2), examination showed the typical Li_2S deposits within the separator previously observed in FeS_2 cells, but without the metallic particles (Ni). This phenomenon was not observed in TiS_2 cells.

2. Causes of Cell Failure

During FY 1978, a total of 52 engineering cells (fabricated by both ANL and industrial contractors) has undergone post-test examinations. This includes four Eagle-Picher multiplate cells being developed for the Mark IA battery. A summary of the cell failure mechanisms and the number of each case is presented in Table VII-10 for FY 1978. In addition, this table includes all vertical prismatic cells that have undergone post-test examination to date. Cell failure has been caused by electrical short circuits, except in cases of loss of capacity, broken conductors, or declining coulombic efficiency. A decline in coulombic efficiency is generally indicative of the early stages of a developing short circuit. Five cells completed the scheduled test period, and have been included in Table VII-10 only for the completeness of the post-test examinations.

For the past year, the major causes of short circuits have been the honeycomb current collector cutting the separator and cell assembly problems. The cells with cut separators were fabricated before the recommendation to add protective screens had been made. Short circuits caused by cell assembly problems, a particular source of difficulty this past year, included misaligned (or broken) electrodes, absence of separators because of misplacement, and both electrodes contacted with ZrO_2 cloth. In the latter case, the ZrO_2 cloth reacts with lithium and becomes conductive. Extrusion of active material, which was the major cause of short circuits before FY 1978, appears to have been solved by the newer cell designs. The short circuits have been mechanical in origin and can be avoided by modification of the cell designs and assembly procedures. The mechanism involved in the loss of capacity is being studied, but has not been identified as yet.

3. Lithium Gradient in Negative Electrodes

As previously reported (ANL-77-35, p. 44), metallographic and chemical analyses indicate that a significant lithium concentration gradient occurs in charged Li-Al electrodes. This observation was confirmed by ion microprobe analysis.* A plot of the probe results is shown in Fig. VII-7 for three cells: Cells LT-2 (totally charged and discharged), EP-I-6A1 (fully charged), and G04-008A (about 50% charged). The thickness of the electrodes is indicated by the end-point of the curves. In Cell LT-2, the lithium was

*D. V. Steidl, Chemical Engineering Division at ANL.

Table VII-10. Summary of Cell Failure Modes

Classification	Number of Cases		
	FY 78	Pre-FY 78	Total[a]
Extrusion of active materials (inadequate confinement)	5	17	22
Metallic copper deposits in separator[b]	3	9	12
Separator cut by honeycomb current collector	11	9	20
Equipment malfunction[c]	2	8	10
Short circuit in electrical feedthrough	4	3	7
Cell assembly difficulties (see text)	10	2	12
Broken positive electrode conductor	0	2	2
Declining coulombic efficiency	1	8	9
Unidentified short circuits	3	2	5
Loss of capacity-poor utilization	3	0	3
Metallic and/or sulfide deposits across separator	4	3	7
End of test	6	2	8
Total	52	65	117

[a]This includes all vertical, prismatic cells that have undergone post-test examinations to date.

[b]FeS cells with Cu_2S additive.

[c]Overcharge, temperature excursion, or accidental polarity reversal.

cycled between two aluminum electrodes so that at full charge one electrode would be LiAl while the other would be aluminum. The curves should be considered as an indication of the trend in the lithium concentration gradient rather than as quantitative results because of the large scatter in the data. Efforts are under way to improve the accuracy of the data. The electrodes from cells EP-I-6A1 and LT-2 in the fully charged state show a very steep lithium gradient. The 50% charged electrode from Cell G04-008A shows a lesser gradient. The data on this electrode showed a larger scatter than the data from the other two electrodes, which was attributed to a greater degree of lithium nonuniformity within a given Li-Al particle. This nonuniformity is probably the result of the cell's short operating time and its having been assembled in an uncharged state.

4. Formation of Y_2O_2S in Y_2O_3 Separators

Post-test examinations of Y_2O_3 separators (both felt and powder) from FeS_2 cells have shown evidence of sulfur reaction with the Y_2O_3. The reaction product was identified as Y_2O_2S by X-ray diffraction* and scanning

*B. S. Tani, Analytical Chemistry Laboratory at ANL.

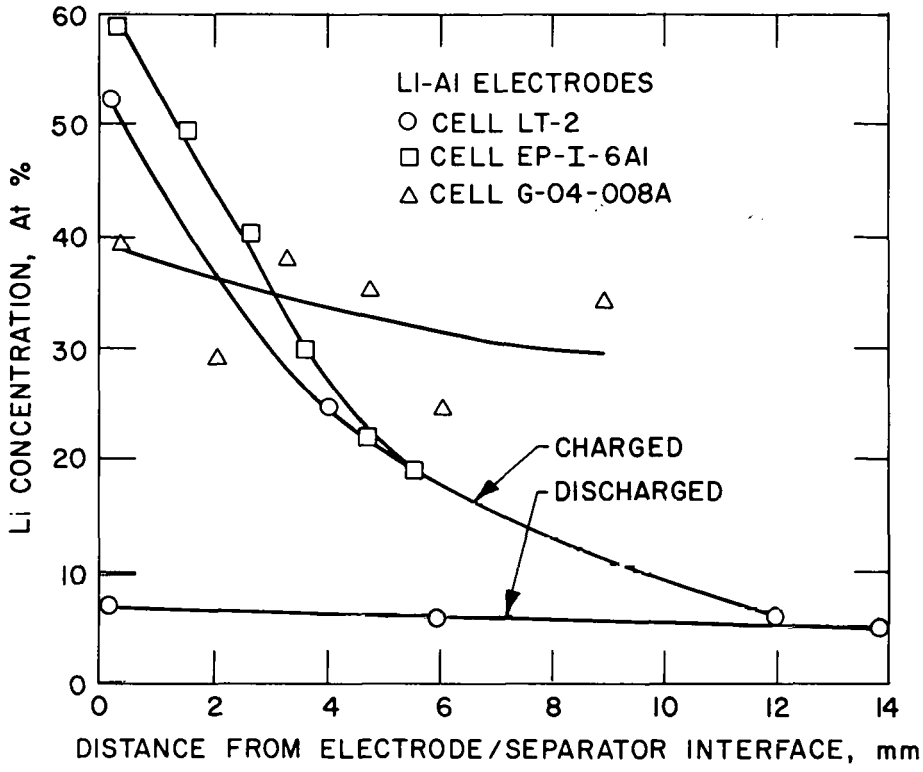

Fig. VII-7. Lithium Concentration Profiles in the Negative Electrodes of Three Cells

electron microscopy. This yttrium oxysulfide has also been identified in an FeS cell that was operated for 83 days. Examinations of three other FeS cells with Y_2O_3 separators that had operated for shorter periods of time showed no evidence of Y_2O_2S. In FeS_2 cells with Y_2O_3 separators, Y_2O_2S was identified in two cells that had operated for less than 42 days. The formation of Y_2O_2S leads to reduced cell performance through loss of sulfur in the positive electrode and through reduced porosity of the separator. These results indicate that Y_2O_3 may be unsatisfactory as a separator material.

5. In-Cell Corrosion Results

Data on the in-cell corrosion rates of current collector materials have been obtained from metallographic examinations of both positive and negative electrodes. The corrosion penetration as a function of time has been plotted for low-carbon steel in the Li-Al electrode (Fig. VII-8), molybdenum in the FeS_2 electrode (Fig. VII-9), and low-carbon steel in the FeS electrode (Fig. VII-10). In Figs. VII-8 and -9, the solid line is based on data from post-test examinations; the dotted line is a projection of these data. The normal cell operating temperature was 435 to 450°C. For a given material thickness, the plots can be used to predict the expected lifetimes in engineering-scale cells.

In the negative electrode, the current-collector material is normally AISI-1008 low-carbon steel (cold rolled, fully annealed), which reacts

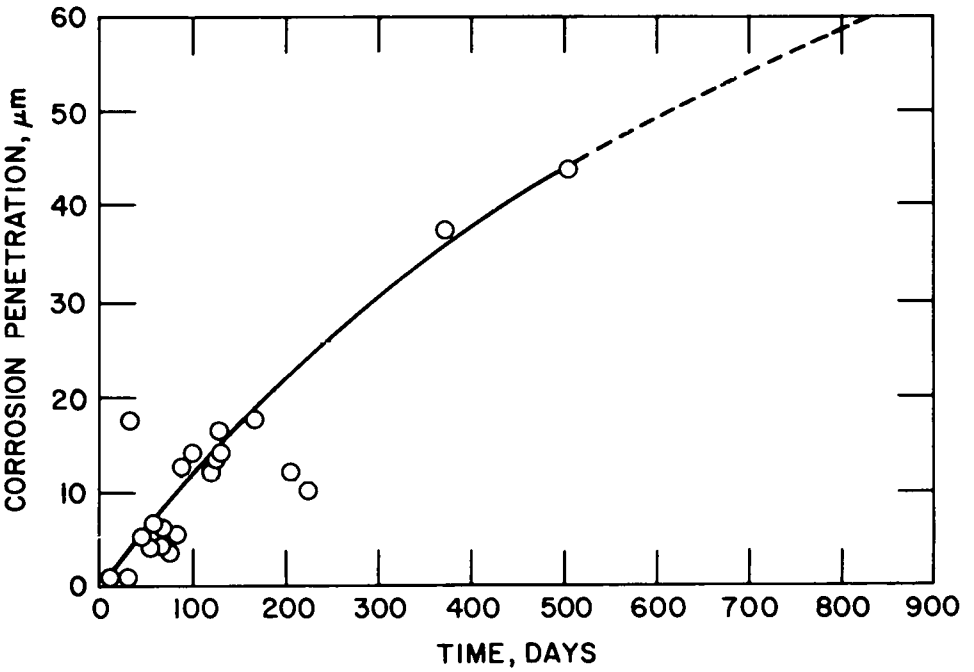

Fig. VII-8. Corrosion of Low-Carbon-Steel Current Collector by the Negative Electrode (Fe + 2Al → $FeAl_2$)

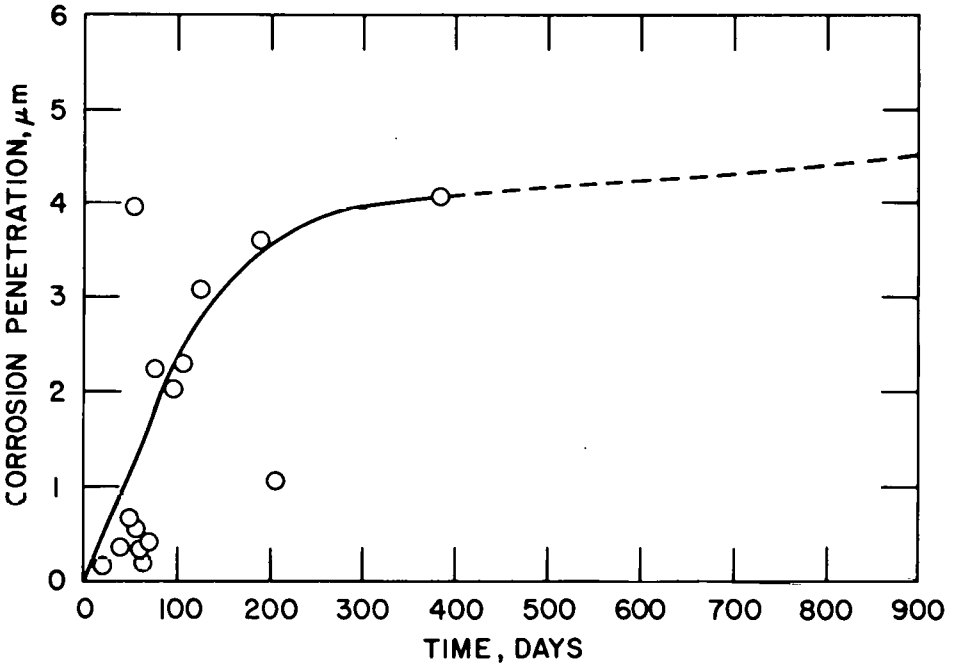

Fig. VII-9. Corrosion of Molybdenum Current Collector in the Positive Electrode (Mo + 2S → MoS_2)

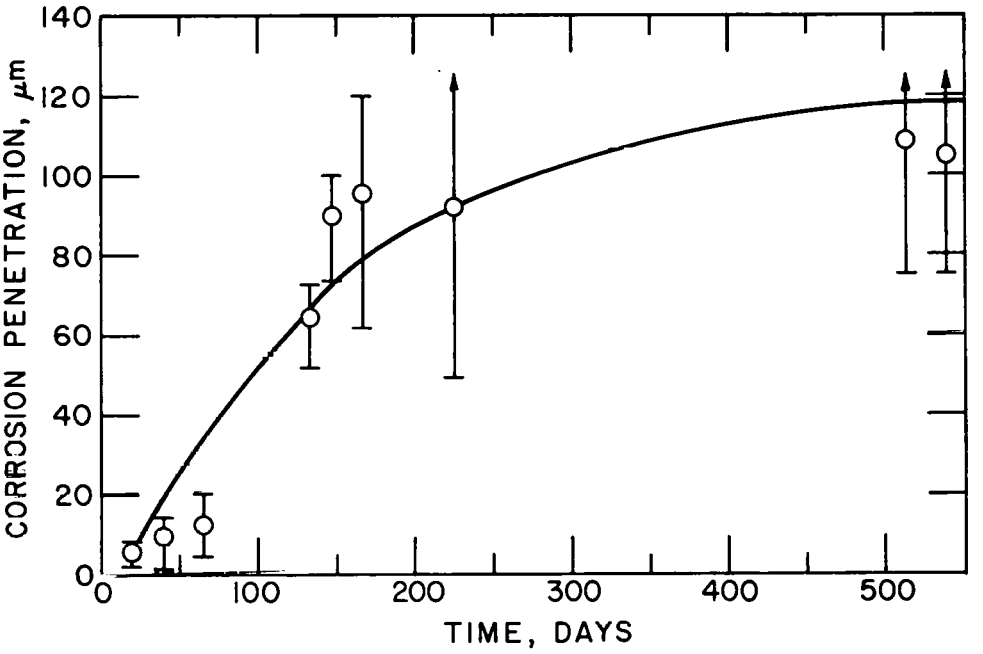

Fig. VII-10. In-Cell Corrosion of Low-Carbon Steel Current Collectors in the Positive Electrode of Li-Al/FeS-Cu_2S Cells

with aluminum (lithium depleted Li-Al). Using X-ray diffraction and electron microprobe analysis, we identified the brittle reaction product as the intermetallic compound $FeAl_2$.* Static corrosion studies have shown that the reaction is suppressed by the presence of LiAl and by the presence of impurities in the electrolyte (ANL-77-75, p. 40), and that the reaction is accelerated at higher temperatures (ANL-76-9, pp. 44-46). A plot of corrosion penetration *vs.* the square root of time yielded a straight line, thus indicating that the Fe-Al reaction is diffusion controlled. As can be seen in Fig. VII-8, the corrosion penetration of a steel current collector by the Fe-Al reaction is projected to be ~60 μm at 800 days (2.5 years). A current collector with a thickness of 125 μm would be totally reacted in this time. Obviously, the useful life of the current collector would be considerably less.

Metallographic and X-ray diffraction examinations have shown that a thin, partially adherent layer of MoS_2 forms on the surface of the molybdenum current collectors used in the positive electrodes of FeS_2 cells. As shown in Fig. VII-9, the rate is exceedingly slow for this reaction. After 900 days of operation, the depth of MoS_2 penetration is projected to be less than 5 μm.

*The resistivity of this compound[3] is 1.9×10^{-4} Ω.

In the FeS positive electrode, the current-collector material is AISI-1008 low-carbon steel,* which is corroded by reactions with the metal sulfides (FeS and Cu_2S). The corrosion process appears to be a combination of uniform sulfidation followed by dissolution and intergranular attack. Generally, the corrosion is greater near the electrode face and in areas of high copper concentrations (from the Cu_2S additive), which accounts for the scatter observed in the data shown in Fig. VII-10. The data indicate that a 125-μm-thick current collector would be completely corroded in about 225 days of operation at 450°C.

6. Chemical Analyses

The positive electrode of a pellet-type cell (ANL-77-75, p. 28), Cell PMC-2-01, was analyzed to determine the extent (if any) of slumping or segregation in the active material. This engineering-scale cell, which was operated at 430°C for 50 days, had 16.6 wt % molybdenum powder added to the FeS_2 positive electrode. The results of the chemical analysis are summarized in Table VII-11. The five samples were obtained at equally spaced intervals through a vertical section of the electrode. Although the density of the molybdenum powder additive is more than twice that of FeS_2, the results showed no evidence of significant segregation or settling. Further, measurements of the ratio of active material (Fe, Mo, S) to electrolyte indicate good uniformity for the active material distribution and loading density. This result is in agreement with the metallographic examination.

Table VII-11. Chemical Analyses[a] on the Positive Electrode of Cell PMC-2-01

Sample Location	Composition,[a] wt %			
	S	Fe	Mo	LiCl-KCl
Top	24.56	21.62	8.95	Balance
	23.64	23.13	9.38	Balance
Middle	23.99	23.42	9.42	Balance
	24.82	22.74	9.21	Balance
Bottom	20.94	20.61	8.33	Balance

[a]Determined by A. Essling and R. Crooks, Analytical Chemistry Laboratory, ANL.

The negative electrodes from cells utilizing positive electrodes with carbon additives (or carbon bonded) have been analyzed to determine the extent of carbon migration. The results are summarized in Table VII-12 and indicate that some carbon is transported from the positive to the negative electrode. Analysis of the LiCl-KCl electrolyte showed only 40 and 30 ppm of carbon for as-received and filtered Lithcoa electrolyte, respectively. Cells KK-4 and KK-5 used carbon-bonded positive electrodes which may account

*Nickel current collectors are being used in some of the multiplate test cells for the Mark I battery.

Table VII-12. Carbon Analyses of Negative Electrodes

Cell[a]	Operation Time, days	Carbon Content,[b] wt %
R-30	48	0.089
R-32	94	0.051
R-33	65	0.078
KK-4	204	0.21
KK-5	340	0.23
PC-2-01	31	0.07
M-6	44	0.16

[a] The positive electrode of these cells contained a carbon additive. Cells KK-4 and KK-5 used carbon-bonded positive electrodes. The carbon content is 0.06 wt % for a cell without carbon additive.

[b] Determined by I. Fox, Analytical Chemistry Laboratory, ANL.

for the higher carbon in the negative electrodes. However, it is possible that the electrolyte used in these cells had a higher concentration of carbon. Attempts to locate an archive sample for analysis have been unsuccessful. The amount of carbon transported to the negative electrode should be dependent on the amount (and form) added to the positive electrode and on the cell operating time. At this time, the effects of carbon migration on cell performance are unknown and need further study.

REFERENCES

1. J. A. Plambeck, J. Chem. Eng. Data, *12* (1), 77 (1967).

2. J. von Brakel, Powder Tech., *11*, 205 (1975).

3. M. Slawecki, ANL, private communication, 1977.

VIII. CELL CHEMISTRY
(M. F. Roche)

The objectives of the cell chemistry studies are (1) to provide solutions for specific chemical and electrochemical problems that arise in the development of cells and batteries, (2) to develop improved compositions for electrodes and electrolytes, and (3) to acquire a basic understanding of the chemistry and electrochemistry of the cells.

A. Properties of Metal Disulfide Electrodes

The following discussion concerns the properties of the metal disulfide electrode, which were investigated through use of an Li-Fe-S phase diagram, cyclic voltammetry, and small-scale cell tests.

1. The Li-Fe-S Phase Diagram
(A. E. Martin)

The region of the Li-Fe-S phase diagram that is of interest in the operation of lithium/metal sulfide cells is the Li_2S-FeS_2-Fe triangle. This region of the phase diagram has been studied in a variety of in-cell and out-of-cell tests at cell operating temperatures (see, for example, ANL-77-75, pp. 49-50). The results of these studies are presented in Fig. VIII-1.

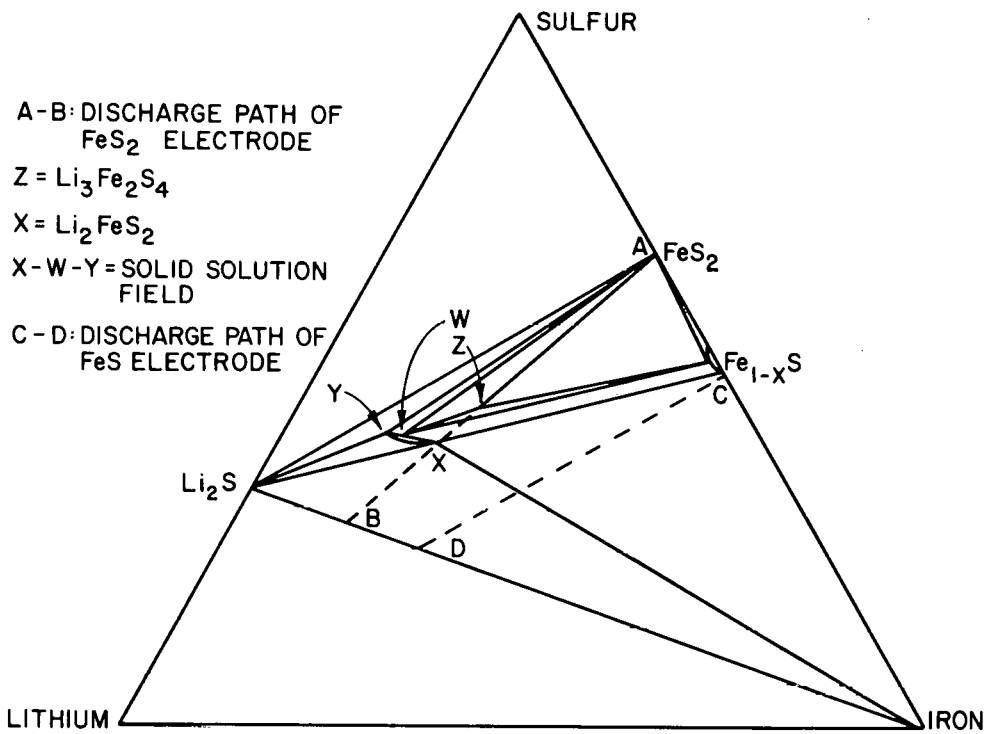

Fig. VIII-1. Isothermal Section of Li-Fe-S Phase Diagram at 450°C Showing the Charge-Discharge Path of FeS_2 Electrodes and FeS Electrodes

The path representing the change in average composition of an FeS_2 electrode as it is charged and discharged at 450°C is indicated by the line A-B. The fully charged electrode contains FeS_2 (point A) and the fully discharged electrode contains Li_2S and iron (point B). Between these extremes, two well-defined compounds are found on the line A-B, namely, Z phase ($Li_3Fe_2S_4$) and X phase (Li_2FeS_2). In addition, more complex phases occur in the region between Z and X phase (*e.g.*, mixtures of the compounds $Fe_{1-x}S$, W, and Z).

The in-cell behavior of FeS_2 electrodes can be described with the aid of Fig. VIII-1. During discharge, FeS_2 is converted to Z phase. Next, Z phase is converted to a mixture of the compounds $Fe_{1-x}S$ and W. The latter compound lies on the boundary of a solid-solution field labeled X-Y. The extent of this solid solution field and the approximate location of the W compound on the field boundary are indicated in the figure. Further discharge of the compounds $Fe_{1-x}S$ and W leads to formation of the single-phase compound, X phase. Finally, X phase is discharged to a mixture of Li_2S and iron. The phases during charge are more complex than those during discharge, and are still under investigation.

In the positive electrode, solid phases other than those shown on the Li-Fe-S ternary diagram can exist because of the presence of LiCl-KCl electrolyte. One such phase is J phase ($LiK_6Fe_{24}S_{26}Cl$), which is a minor phase in FeS_2 electrodes and a major phase in FeS electrodes. Another is $KFeS_2$, which forms in FeS_2 electrodes in the presence of KCl-rich electrolyte. The properties of these potassium-containing phases are discussed below.

2. Cyclic Voltammetry of Metal Disulfides
(S. K. Preto)

Cyclic voltammetry studies of FeS_2, CoS_2, and NiS_2 electrodes at ~400°C in LiCl-KCl electrolyte (eutectic composition) were presented in earlier reports (ANL-77-68, p. 46; ANL-77-75, p. 51; ANL-78-21, p. 54). These electrodes were cycled over a broad voltage range (1.0-2.0 V *vs.* LiAl), with a very slow voltage-scan rate (0.015-0.020 mV/sec). The broad voltage range encompassed all the electrode reactions from full discharge (Li_2S + the transition metal) to full charge (the transition-metal disulfide). The slow scan rate insured high resolution of the current peaks associated with each of the electrode reactions. Electrode reactions that give rise to voltage plateaus in constant-current cycling produce current peaks in a cyclic voltammogram of this type.

a. Cyclic Voltammetry of FeS_2 Electrodes

Fig. VIII-2 is a voltammogram of the FeS_2 electrode. If the electrode reaction is electrochemically reversible, then the left side of the charge peak (above the axis) and the right side of the corresponding discharge peak (below the axis) will intercept the voltage axis at the reaction emf. Differences in these intercept voltages indicate poor reversibility due to overpotentials or to differences in the charge and discharge reaction mechanisms. Reaction assignments were based on the phase diagram shown in Fig. VIII-1, together with corroborative metallographic and X-ray results.

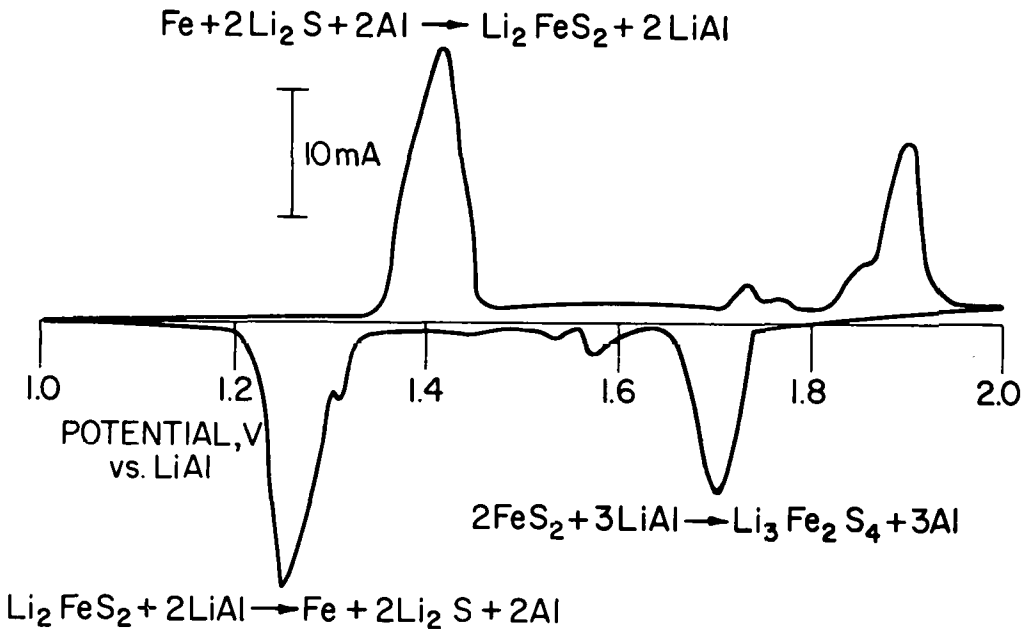

Figure VIII-2. Cyclic Voltammogram of FeS_2 Electrode in LiCl-KCl Electrolyte of Eutectic Composition

As can be seen in Figure VIII-2, the high-voltage (1.5 to 2.0 V) discharge peak began at ∿1.74 V, but most of the associated charge reaction was located in a charge peak beginning at ∿1.86 V. Thus the electrode exhibited 0.12-V irreversibility for its major high-voltage reaction. Because the species involved in this charge reaction are not known, the high-voltage charge reaction has not been labelled in Fig. VIII-2. However, a combination of voltammetry and metallographic studies (ANL-77-68, pp. 46-49) has suggested that the reaction involves formation of soluble sulfur species (of high sulfur activity) that react with $Fe_{1-x}S$ to form FeS_2.

After the poor reversibility of the high-voltage reaction of FeS_2 was discovered, a LiAl/LiCl-KCl/FeS_2 cell was operated only on its high-voltage plateau, thereby utilizing about one-third of the theoretical FeS_2 capacity.* The cell voltage curves exhibited reversible behavior. This surprising result showed that the 1.74-V reaction of FeS_2,

$$2FeS_2 + 3LiAl \rightarrow Li_3Fe_2S_4 + 3Al \qquad (1)$$

becomes reversible under certain conditions. A more thorough investigation of the properties of the FeS_2 electrode was then conducted to test for reversibility under cyclic voltammetry conditions. The effects of discharge cutoff voltage and electrolyte composition were investigated. The discharge-cutoff voltage was varied to alter the utilization of the FeS_2-electrode capacity. The electrolyte composition was varied to determine if changes in the electrode behavior would result. (The electrolyte in the above cell test may have had an off-eutectic composition.)

*This experiment done by K. E. Anderson, C. Hickson, and D. R. Vissers, Cell Chemistry Group.

For these experiments, an FeS_2 working electrode (116 mg of FeS_2 in carbon foam within a molybdenum housing) was cycled at 400°C *vs.* LiAl reference and counter electrodes. The voltage scan rate was 0.02 mV/sec. Electrolyte variations were accomplished by adding either LiCl or KCl to 58 mol % LiCl-42 mol % KCl eutectic* in order to shift the composition to either 61 mol % LiCl-39 mol % KCl or 55 mol % LiCl-45 mol % KCl. During the tests, the electrolyte was occasionally shifted back to eutectic composition, and scans were made to check for recovery of the electrode to its "normal" irreversible behavior (Fig. VIII-2). The voltage range was changed in each voltammogram by varying the discharge cutoff voltage,† as shown in Fig. VIII-3.‡

For the FeS_2 voltammogram in LiCl-rich electrolyte, the discharge cutoff voltages were 1.65, 1.61, 1.56, and 1.43 V. Although not shown in Fig. VIII-3, sweeps were also taken of FeS_2 in this electrolyte to a 1.35-V cutoff and a 1.0-V cutoff. One example of a scan in eutectic electrolyte is shown in Fig. VIII-3 (top). The scan in this electrolyte differed only slightly from that in LiCl-rich electrolyte. Therefore, the discussions that follow of scans in LiCl-rich electrolyte also apply to scans in eutectic electrolyte.

For the LiCl-rich electrolyte, the curves in Fig. VIII-3 show that the change in reversibility of the high-voltage reaction of FeS_2 with electrode utilization is associated with a change in the charge reaction. That is, the charge peak shifts to higher voltages as the discharge-cutoff voltage is lowered, but the discharge peak remains fixed. The voltage separation of the charge and discharge reactions is less than 0.02 V with a 1.65-V cutoff; this separation increases to ∿0.09 V for discharge cutoffs of 1.43 V or below.

The good reversibility obtained with the higher discharge-cutoff voltages (and consequently lower electrode utilizations) in Fig. VIII-3 is in agreement with the cell test described above. Under these reversible conditions, the cell reaction has an emf of 1.74 V. The increasingly poorer reversibility with lower discharge cutoff voltages (and higher electrode utilizations) in Fig. VIII-3 was attributed to a kinetic hindrance in the formation of $Li_3Fe_2S_4$ from its discharge products, $Fe_{1-x}S$ and W phase. However, recent LiAl/FeS_2 cell tests, described below, have indicated that this postulated mechanism may be incorrect.

The dotted curves in Fig. VIII-3 show the behavior of FeS_2 in KCl-rich electrolyte. Two tentative conclusions can be drawn from these curves. First, the discharge reaction is essentially the same in LiCl-rich and KCl-rich electrolyte because the position of the discharge peak is identical in both electrolytes. Second, the charge reactions are different in

---

*Supplied by Anderson Physics Laboratory, Inc., Urbana, IL 61801.

†In all cases, a significant number of scans were obtained after changing conditions to insure that the electrodes and electrolyte had reached a steady state.

‡No great significance should be attached to differences in peak areas. The electrode was operated for 500 hr; during this time the capacity declined by 40%. The peaks differ in area because the sweeps were obtained at different times.

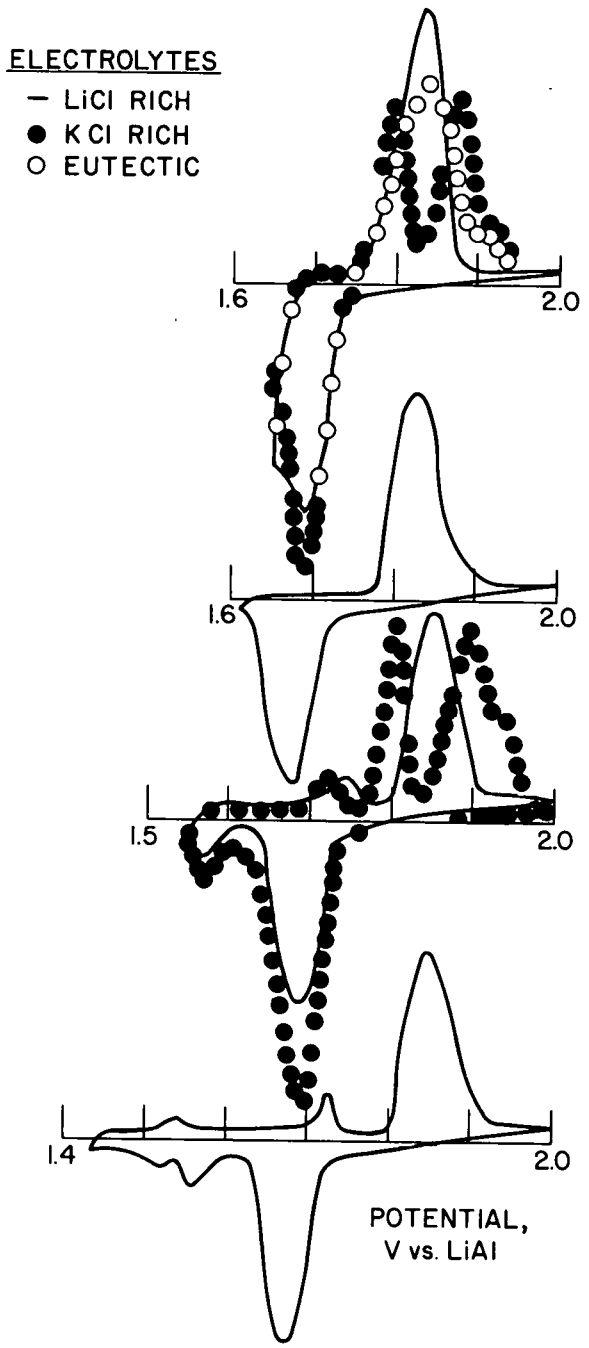

Fig. VIII-3. Cyclic Voltammograms of FeS_2 Electrode in LiCl-KCL Electrolyte of Varying Compositions (Discharge cutoff voltages from top to bottom: 1.65, 1.61, 1.56, 1.43 V)

the two electrolytes. In the case of the KCl-rich electrolyte, the high-voltage charge reactions do not appear to change significantly with shifts in discharge cutoff voltage; the high-voltage charge reactions consist of a narrow peak that begins at about 1.74 V and a poorly resolved doublet that begins at about 1.84 V. The area of the doublet is about twice that of the narrow peak, and the sum of these areas is equal to the area of the discharge peak. (The same features are seen with a discharge cutoff voltage as low as 1.0 V.) Because this type of behavior was only observed in KCl-rich electrolyte, a potassium-containing sulfide phase was suspected.

For an FeS_2 cell using KCl-rich electrolyte the proposed reactions consistent with the above observations are as follows:

$$\text{Discharge}^{*}: \quad 2FeS_2 + 3LiAl \xrightarrow{3e^-} Li_3Fe_2S_4 + 3Al, \sim 1.74\ V \tag{2}$$

$$\text{Charge}^{\dagger}: \quad \text{a)} \quad Li_3Fe_2S_4 + 2KCl + Al \xrightarrow{1e^-} 2KFeS_2 + 2LiCl + LiAl, \sim 1.74\ V$$

$$\text{b)} \quad 2KFeS_2 + 2LiCl + 2Al \xrightarrow{2e^-} 2FeS_2 + 2KCl + 2LiAl, \sim 1.84\ V$$

$$\text{a+b)} \quad Li_3Fe_2S_4 + 3Al \xrightarrow{3e^-} 2FeS_2 + 3LiAl \tag{3}$$

Recent cell tests, metallographic studies, and X-ray analyses (reported below) have now shown that $KFeS_2$ is a major phase in FeS_2 electrodes in KCl-rich electrolyte. This supports the proposed reaction mechanism.

The FeS_2 electrode reactions were also examined using LiF-LiCl-LiBr electrolyte at 460°C in order to eliminate potassium-ion effects. The high-voltage discharge reaction in this voltammogram was shifted to a higher voltage ($\sim$1.77 V) because the high temperature required with this electrolyte generated a higher sulfur activity in the positive electrode. However, the high-voltage charge peaks were identical to those in LiCl-rich electrolyte. This result showed that the irreversibility problem of FeS_2 in eutectic or LiCl-rich electrolyte is not caused by potassium-containing phases.

In conclusion, the reactions in FeS_2 electrodes depend strongly on the depth of electrode discharge and the LiCl-to-KCl ratio of the electrolyte. Conditions that lead to formation of a potassium-containing phase in the FeS_2 electrode were defined, and it was determined that this phase does not cause the irreversibility problem of FeS_2 electrodes. The cause of this irreversibility has not yet been determined.

b. Emfs of CoS_2, NiS_2, and FeS_2 Electrodes

Cyclic voltammograms of CoS_2 and NiS_2 electrodes showed that these two metal sulfides have better reversibility than FeS_2 (ANL-77-75, pp. 51-54). The reactions for the CoS_2 electrode exhibited about 0.06-V

---

*The absence of a potassium-containing intermediate in this discharge step suggests that the reverse of charge reaction (b) is electrochemically hindered.

†The actual reaction for (b) may be more complex than shown; the "charge peak" for this postulated reaction is a poorly resolved doublet.

irreversibility,* and the reactions for the NiS_2 electrode exhibited less than 0.02-V irreversibility. Subsequent engineering-scale tests (Section VI.B) have shown that the NiS_2 electrode also has a longer cycle life than the FeS_2 electrode. Contributing factors to this longer cycle life include the good reversibility of the NiS_2 electrode reactions and the superior resistance of the nickel sulfides to overcharge.[1]

Emfs of cell reactions were obtained from the FeS_2, CoS_2, and NiS_2 voltammograms by averaging the charge- and discharge-intercept voltages, except for the case of the poorly reversible high-voltage reaction of FeS_2. In the FeS_2 case, the emf was determined to be 1.74 V (condition of high discharge-cutoff voltages). In Table VIII-1 the experimental emfs are compared with emfs calculated from thermodynamic data.[1,2] For the calculations, sulfur activities of the transition-metal sulfides were taken mainly from data provided by Craig *et al.*[2] In these calculations, chemical and physical interactions between Li_2S and the transition-metal sulfides were ignored. From the good agreement between the experimental and calculated emfs, it can be seen that this approximation does not lead to serious errors (*i.e.*, the energies of interaction between Li_2S and the transition-metal sulfides are small). Thus, to a close approximation, the emfs of the cells employing Fe, Co, and Ni sulfides can be calculated from existing thermodynamic data.

*In an earlier report (ANL-77-75, pp. 51-54) the irreversibilities of the CoS_2-electrode reactions were given as 0.08, 0.06, and 0.04 V for the $CoS_2 \rightarrow Co_3S_4$, $Co_3S_4 \rightarrow Co_9S_8$, and $Co_9S_8 \rightarrow Co$ reactions, respectively. However, more recent measurements have shown the irreversibility is ~0.06 V for all three reactions.

Table VIII-1. Experimental and Calculated Emfs

	Emf (Volts *vs.* LiAl at 400°C)	
	Exp.	Calc.[c]
$FeS_2 \rightarrow Fe_{1-x}S$[a]	1.74	1.71
$FeS \rightarrow Fe$[b]	1.34	1.36
$CoS_2 \rightarrow Co_3S_4$	1.74	1.72
$Co_3S_4 \rightarrow Co_9S_8$	1.63	1.65
$Co_9S_8 \rightarrow Co$	1.35	1.38
$NiS_2 \rightarrow Ni_{1-x}S$	1.75	1.75
$NiS \rightarrow Ni_9S_6$	1.60	1.60
$Ni_7S_6 \rightarrow Ni_3S_2$	1.56	1.57
$Ni_3S_2 \rightarrow Ni$	1.37	1.38

[a]In-cell reaction: $FeS_2 \rightarrow Li_3Fe_2S_4$.

[b]In-cell reaction: $Li_2FeS_2 \rightarrow Fe$.

[c]Calculated from data in Refs. 1 and 2.

3. Lithium/Metal Disulfide Cell Tests

(Z. Tomczuk, A. E. Martin)

To investigate the properties of metal-disulfide electrodes, we conducted the following cell tests:

(a) A coulometric titration of FeS_2 was done to compare the in-cell behavior of FeS_2 with the behavior predicted from phase-diagram studies.

(b) Phases were determined in an $FeS_{2.0}$ and an $FeS_{1.70}$ cell that had been trickle-charged to selected cutoff voltages. The results were used to interpret cyclic voltammetry data.

(c) An FeS_2 electrode was operated in KCl-rich electrolyte, and the composition of the potassium-containing iron sulfide phase was determined.

a. Coulometric Titration of FeS_2

In a coulometric titration, the product of current and time (in ampere-seconds, or coulombs) is determined for each cell reaction. In the case of the FeS_2-electrode reactions, this method provided a means of comparing the in-cell behavior of the FeS_2 electrode with the behavior predicted from the phase diagram (Fig. VIII-1).

The coulometric titrations consisted of charge-discharge cycling of an LiAl (4 A-hr)/LiCl-KCl(eutectic)/FeS_2 (1 A-hr) cell at a low current density ($\sim$12 mA/cm^2). This low current density resulted in nearly complete utilization of the FeS_2-electrode capacity. In Table VIII-2, the portion of the capacity associated with each electrode reaction is compared with the results of the phase-diagram study.

Table VIII-2. Reactions Obtained from Coulometric Titrations and Phase Diagram of FeS_2 Electrode

Reaction[a]	Emf,[b] V *vs.* LiAl	Percent of Theoretical Capacity	
		Coulometric Titrations[c]	Phase Diagram[a]
$FeS_2 \rightarrow Li_3Fe_2S_4$	1.74	37.2	37.50
$Li_3Fe_2S_4 \rightarrow$ W phase + $Fe_{1-x}S$	$\sim$1.60	4.5	4.25
W phase + $Fe_{1-x}S \rightarrow Li_2FeS_2$	1.60 to 1.34 V	7.7	8.25
$Li_2FeS_2 \rightarrow Fe + Li_2S$	1.34	50.6	50.00

[a]Determined from phase diagram in Fig. VIII-1.

[b]Determined from voltammogram (Fig. VIII-2). Note that the third reaction occurs in a region of variable phase compositions, and, consequently, it has a broad voltage range.

[c]Average of two discharge cycles.

The coulometry data are in good agreement with the phase diagram study. In particular, the composition of the first discharge product of FeS_2 ($Li_3Fe_2S_4$) was confirmed in this study.

b. Phases in Iron Disulfide Electrodes During Charge

The cyclic-voltammetry tests of FeS_2 were concerned with the poor reversibility of this electrode's high-voltage reaction, which occurs at 1.74 V on discharge. However, the electrode phases were not determined in the cyclic voltammetry work. Thus two cell tests were conducted to identify the phases present in the electrode at selected charge-cutoff voltages. The cells employed (4 A-hr) LiAl negative electrodes, eutectic electrolyte, and (1 A-hr) iron sulfide electrodes.

In one of the cells, FeS_2 was employed as the positive electrode. This cell was operated for 5 cycles at 60 mA/cm^2 and at cutoff voltages of 2.0 V (charged) and 1.0 V (discharge). Cell operation was stopped after a charge to 1.71 V followed by trickle charging (less than 1 mA/cm^2) at 1.71 V for 18 hr. This trickle-charging procedure was adopted to insure uniformity of the positive electrode. Analyses by metallographic and X-ray* techniques showed that the positive-electrode charge product was pure $Li_3Fe_2S_4$.

In the second cell test, the ratio of sulfur to iron was 1.70 (an iron-FeS_2 mixture was employed). This cell was operated and stopped in the same manner as the first cell. However, the trickle-charge voltage was 1.80 V instead of 1.71 V. The major phases in this electrode were $Li_3Fe_2S_4$ and $Fe_{1-x}S$, which was imbedded in the $Li_3Fe_2S_4$. The $Fe_{1-x}S$ phase was caused by the presence of excess iron.

The major result of the above tests is that $Li_3Fe_2S_4$ is present at 1.71 V and at 1.80 V, but that FeS_2 is absent at these voltages. Cyclic voltammetry was used to measure the emf of the $Li_3Fe_2S_4$-to-FeS_2 conversion under conditions of low electrode utilization (*i.e.*, where the conversion is reversible); this emf is 1.74 V. The presence of $Li_3Fe_2S_4$ in these cells and the complete absence of FeS_2 shows that, under high utilization conditions, the conversion of $Li_3Fe_2S_4$ to FeS_2 is hindered.

c. Formation of $KFeS_2$ in KCl-Rich Electrolyte

The cyclic voltammetry studies discussed earlier indicated that a potassium-iron-sulfur phase was formed during the reactions leading from $Li_3Fe_2S_4$ to FeS_2 in KCl-rich electrolyte, and it was proposed that the phase was $KFeS_2$. To check this hypothesis, a LiAl (2 A-hr)/LiCl-KCl/FeS_2 (4 A-hr) cell using an electrolyte saturated at 410°C with KCl was operated at 430°C. Following break-in cycling (14 cycles), the cell operation was stopped halfway through the charge of its higher voltage plateau (at a voltage of 1.91 V).

X-ray analysis* showed that FeS_2 and $KFeS_2$ were present as major phases in the positive electrode. Metallographic analysis showed that $Fe_{1-x}S$ and $Li_3Fe_2S_4$ were also present, but as minor phases. Since $KFeS_2$ had

*Conducted by B. S. Tani, Analytical Chemistry Laboratory, ANL.

not been identified in earlier metallographic tests, it could not at first be identified by metallographic techniques. It was apparent, however, that the dominant phase (a pink phase) was not $Li_3Fe_2S_4$, $Fe_{1-x}S$, or FeS_2. To identify this dominant phase by metallography, we prepared it under controlled conditions.

Mixtures of Li_2S and FeS_2 in three different electrolyte compositions were reacted at 525°C under conditions that produce extensive amounts of $Li_3Fe_2S_4$ in eutectic salt. The first mixture contained LiCl-KCl eutectic salt, the second contained LiCl saturated with KCl, and the third contained KCl saturated with LiCl. Metallographic examination of the reaction products showed that the first and third products contained $Li_3Fe_2S_4$, and that the second mixture contained the new phase in addition to $Li_3Fe_2S_4$. The new phase was very similar in morphology to $Li_3Fe_2S_4$, but differed from it in color (pink instead of colorless) and in anisotropy (less anisotropic). The products of the three reactions were leached with water to dissolve the LiCl, KCl and $Li_3Fe_2S_4$. The residues were then examined by X-ray diffraction and by metallography. The X-ray diffraction examination showed that $KFeS_2$ was present in the residue from the second reaction product, but not in the residues of the first or third. The metallographic examination showed that the pink phase was present in the second residue but not in the other residues. Thus the pink phase was established as $KFeS_2$, and it was identified as the dominant phase in the above cell test. With the metallographic properties of this phase more firmly established, it could then be identified as a trace constituent (in admixture with the colorless phase $Li_3Fe_2S_4$) in many of the earlier FeS_2 electrodes that had been operated in electrolyte of eutectic composition. The role of $KFeS_2$ in the charge reactions of FeS_2 electrodes will be explored in future experiments.

4. The Form of Cobalt in FeS_2-CoS_2 Electrodes
(A. E. Martin)

Although CoS_2 has been employed as an additive for FeS_2 electrodes for some time, the identity of the cobalt-containing phases has not been established. The Co-S phase diagram of M. Hansen and K. Anderko[3] shows that Co, Co_9S_8, $Co_{1-x}S$, Co_3S_4 and CoS_2 can exist at cell operating temperatures. In addition, Co, $Co_{1-x}S$, and CoS_2 are known to be capable of forming solid solutions with their iron analogs. Experiments were conducted to search for other interactions.

No metallographic evidence for the formation of Li-Co-S phases was detected when Li_2S, Co_9S_8 and $Co_{1-x}S$ were melted together. Melting of Li_2S, FeS and Co_9S_8 (5:4:1 mole ratio) produced Li_2FeS_2, Li_2S and Co_9S_8. Various mixtures of Li_2S with Co_9S_8, $Co_{1-x}S$, Co_3S_4 and CoS_2 in electrolyte at cell operating temperatures yielded no evidence of Li-Co-S phases, and no reactions were observed in a mixture of Li_2FeS_2, Co_9S_8, $Co_{1-x}S$ and electrolyte at cell operating temperatures. The above tests indicate that no cobalt analogs of Li_2FeS_2, $Li_3Fe_2S_4$, or J phase ($LiK_6Fe_{24}S_{26}Cl$) exist. Cobalt does not appear to be included in these iron compounds to any significant extent. Thus iron and cobalt sulfides in FeS_2 cells appear to follow independent discharge-charge paths; cobalt is only present as binary cobalt-sulfur compounds.

The original purpose of adding cobalt sulfide (ANL-75-1, p. 29) was to improve the electronic conduction of FeS_2 through the formation of solid solutions of iron-cobalt disulfides, which are metallic conductors. The above experiments suggest that solid solution formation of this type is not likely to occur in an FeS_2 cell to a significant extent. Therefore, a reassessment of the effects of this additive on cell performance should be undertaken.

B. Properties of Metal Monosulfide Electrodes

In this effort, cell tests were conducted to define the limits of J phase ($LiK_6Fe_{24}S_{26}Cl$) formation, which has been shown to have an adverse effect on electrode kinetics (ANL-77-35, p. 57). In addition, out-of-cell tests were done to define the chemical conditions that lead to the formation of J phase. In exploratory studies, the use of either NiS or FeSe in FeS electrodes was examined.

1. The FeS Electrode

a. The Formation of J Phase in FeS Electrodes

(Z. Tomczuk, S. K. Preto, A. E. Martin)

Slow scan cyclic voltammetry of FeS *vs.* LiAl in LiCl-KCl eutectic at 430°C showed that the charge curve for this electrode consisted of two peaks of nearly equal size (ANL-77-35, p. 57). In this study, the charge reactions were believed to be:

$$Fe + 2Li_2S + 2Al \rightarrow Li_2FeS_2 + 2LiAl \qquad 1.350\ V \qquad (1)$$

$$Fe + Li_2FeS_2 + 2Al \rightarrow 2FeS + 2LiAl \qquad 1.375\ V \qquad (2)$$

The J phase ($LiK_6Fe_{24}S_{26}Cl$) was thought to occur as an intermediate phase during the second reaction and to convert to FeS by the end of the second reaction peak (1.42 V). However, cell data presented earlier (ANL-75-1, p. 103) indicated that the J-phase transition to FeS at 430°C did not occur below 1.60 V.

In order to determine whether or not a high potential is required for conversion of J phase to FeS, two additional LiAl (1 A-hr)/LiCl-KCl/FeS (2 A-hr) cells were operated at 400-410°C. These cells were cycled at a current density of 12 mA/cm^2 between 1.0 and 1.6 V. Operation of the first cell was terminated during a 12 mA/cm^2 charge at 1.50 V, and the positive electrode was rapidly removed. The second cell was charged at 12 mA/cm^2 to 1.50 V, and was then trickle-charged for four days at a constant voltage of 1.50 V and a current density of about 0.4 mA/cm^2 (probably the self-discharge rate at 1.50 V). At the end of this period, the electrolyte was solidified while the cell voltage was maintained at 1.50 V.

Metallographic examination showed that J phase was dominant in both of the electrodes. In fact, the second cell yielded the most crystalline J phase observed to date in laboratory cells. X-ray results* confirmed the metallographic examination. An FeS working electrode in a voltammetry cell was also trickle-charged potentiostatically at 1.50 V and 400°C for 4 days.

*Conducted by B. S. Tani, Analytical Chemistry Laboratory, ANL.

Metallographic examination again showed that J phase was present. These tests indicate that J phase requires a high potential for conversion to FeS, and J phase is the reaction product of the second charge peak in the FeS voltammogram.

b. Chemical Conditions for the Formation of J Phase
(A. E. Martin)

In the absence of J phase, the phases of an FeS electrode* consist of (1) mixtures of Li_2S, Li_2FeS_2, and Fe during the first half of charge (or conversely the second half of discharge) and (2) mixtures of FeS, Li_2FeS_2, and Fe during the second half of charge (or conversely the first half of discharge). The two mixtures probably react with electrolyte to form J phase according to the following reactions:

$$\text{(first mixture)} \quad 6KCl + Fe + 23Li_2FeS_2 \rightarrow J + 5LiCl + 20Li_2S \qquad (1)$$

$$\text{(second mixture)} \quad 6KCl + Fe + 20FeS + 3Li_2FeS_2 \rightarrow J + 5LiCl \qquad (2)$$

Preliminary tests indicated that these two reactions strongly depend on temperature and electrolyte composition (ANL-77-17, p. 42 and Ref. 4). Thus we decided to determine the maximum temperature at which J phase forms in mixtures 1 or 2 and electrolyte of various compositions. In the experiment a mixture of Li_2S (or FeS), Li_2FeS_2, and Fe was heated for 16 hr at a constant temperature in one of the following electrolytes: 58 mol % LiCl-42 mol % KCl (eutectic), 49 mol % LiCl-36 mol % KCl-15 mol % NaCl, the LiCl-KCl eutectic saturated with LiCl, and the LiCl-KCl-NaCl electrolyte saturated with LiCl. After heating, the reaction products were metallographically examined to determine whether J phase had formed. If J phase had formed, then the temperature was slightly increased; if J phase had not formed, then the temperature was slightly decreased. Eventually, these tests defined a temperature, T, at which J phase formed and a slightly higher temperature at which J phase did not form ($T + \Delta T$). The maximum temperature of J phase formation, T_{max}, was thus defined as $(T + \Delta T/2) \pm \Delta T/2$.

The results, given in Table VIII-3, show that the addition of LiCl significantly decreased T_{max}. With mixture 2, for example, T_{max} was 623°C with LiCl-KCl eutectic, but only 481°C with the eutectic electrolyte saturated with LiCl. Thus, use of a LiCl-rich electrolyte in FeS cells should result in substantial improvements in performance. Additions of NaCl to LiCl-KCl eutectic caused only slight decreases (20°C) in T_{max} for mixture 1 and no decrease in T_{max} for mixture 2.

Reactions (1) and (2) are both important in FeS electrodes, but only reaction (1) can lead to J phase in stoichiometric FeS_2 electrodes (see Fig. VIII-1). The temperatures for suppressing J phase formation via reaction (1) are quite low, as can be seen by examining the first column of Table VIII-3. This is the reason that J phase is less of a problem in FeS_2 electrodes than in FeS electrodes.

Additional tests were conducted to check the reversibility of reactions (1) and (2) in eutectic electrolyte. First, J phase was formed by

*A phase diagram of the Li-Fe-S system is given in Fig. VIII-1.

Table VIII-3. Maximum Temperature for Formation of J Phase in FeS Electrodes

Electrolyte	T_{max}, °C	
	Mixture (1)[a]	Mixture (2)[b]
58 mol % LiCl-42 mol % KCl (eutectic)	455 ± 4	623 ± 7
49 mol % LiCl-36 mol % KCl-15 mol % NaCl	435 ± 5	623 ± 7
LiCl-KCl eutectic saturated with LiCl	419 ± 2	481 ± 5
LiCl-KCl-NaCl (above mixture) saturated with LiCl	413 ± 5	477 ± 9

[a]Mixture of Li_2S, Li_2FeS_2, and Fe with electrolyte.

[b]Mixture of FeS, Li_2FeS_2, and Fe with electrolyte.

heating mixture 1 and eutectic electrolyte at 445°C and mixture 2 and eutectic electrolyte at 600°C. Portions of these samples were then reheated for 41 to 88 hr and a similar procedure to that described above was done to determine the temperature at which J phase decomposes. These tests showed that J phase decomposed at 465 ± 7°C in the reheated mixture 1 and at 624 ± 4°C in the reheated mixture 2. The good agreement between these temperatures and those in the first row of Table VIII-3 demonstrated the reversibility of reactions (1) and (2).

c. Effects of Electrolyte Composition and Cell Temperature on FeS Cell Performance
(Ching-Kai Ho,* K. E. Anderson,† D. R. Vissers)

After the above out-of-cell tests were completed, we decided to study the effects of electrolyte composition and cell temperature on the positive electrode utilization of small-scale LiAl/FeS cells. The tests were conducted on LiAl (10 A-hr)/FeS (6.5 A-hr) cells that had LiCl-KCl electrolytes having LiCl concentrations of either 53, 58 (eutectic), 63, or 67 mol % LiCl. All of these cells were operated at 450 and 500°C and at current densities of 50 and 100 mA/cm^2 (electrode area, 15.6 cm^2).

The test results, given in Table VIII-4, show that the positive-electrode utilization increases with increasing LiCl concentration and/or cell temperature. Satisfactory electrode utilization is achieved in cells using a lithium chloride concentration of 67 mol % and a cell temperature of 450°C.

2. The FeS-NiS Electrode
(Z. Tomczuk, S. K. Preto, A. E. Martin)

Because of the recent interest in the nickel disulfide electrode, either alone or in admixture with FeS_2 (see Section VIII.A.2), the properties

*Resident Associate from Institute of Nuclear Energy Research, Taiwan, Republic of China.

†Cell Development and Engineering Group.

Table VIII-4. Utilization of Positive Electrode in LiAl/LiCl-KCl/FeS Cells

LiCl Concentration, mol %	Temp., °C	Current Density, mA/cm²		FeS Electrode Utilization, %
		Charge	Discharge	
53	450	50	50	25
	500	50	50	44
	450	100	100	14
	500	100	100	40
58[a]	450	50	50	52
	500	50	50	70
	450	100	100	44
	500	100	100	55
63	450	50	50	74
	500	50	50	77
	450	100	100	68
	500	100	100	71
67	450	50	50	91
	500	50	50	90
	450	100	100	85
	500	100	100	86

[a]Eutectic composition.

of a monosulfide mixture were also of potential interest. Therefore, a few experiments of an exploratory nature were conducted with FeS-NiS electrodes.

Two LiAl (2 A-hr)/LiCl-KCl/$Fe_{0.5}Ni_{0.5}S$(1 A-hr) cells were operated to determine the effect of NiS additions on FeS cell performance (NiS and FeS were fused together prior to use in the cells). Operation of one of these cells was stopped during its first discharge. Metallographic examination and X-ray diffraction* showed that a phase similar to J phase ($LiK_6Fe_{24}S_{26}Cl$), probably with nickel substituted for a portion of the iron, had formed. This material can thus be represented as $LiK_6Fe_{24-y}Ni_yS_{26}Cl$.

The second cell was operated for 46 cycles at 460°C. The electrode utilization was only 60%, but it was constant for discharge times ranging from 3 to 9 hr. Operation of this cell was stopped at full charge (1.74 V); examinations again indicated that the above nickel-substituted J phase was present.

In a voltammetry experiment, an equimolar FeS-NiS electrode (75 mA-hr capacity) yielded two, well-resolved charge and discharge peaks (beginning at 1.34 V and 1.40 V) that were nearly equal in capacity. The

*Conducted by B. S. Tani, Analytical Chemistry Laboratory, ANL.

reactions appeared to be more reversible than those found with FeS alone (ANL-77-35, p. 57), but the utilization of the electrode was again only 60%.

To determine how the thermal stability of $LiK_6Fe_{24-y}Ni_yS_{26}Cl$ compares with that of $LiK_6Fe_{24}S_{26}Cl$, we conducted out-of-cell experiments. Three Fe-Ni-S compositions were prepared by melting FeS and NiS mixtures at 1100°C (the resulting alloys were ground to fine powders). These compositions were $Fe_{0.9}Ni_{0.1}S$, $Fe_{0.8}Ni_{0.2}S$, and $Fe_{0.7}Ni_{0.3}S$. The Fe-Ni-S powders were then mixed with 50 mol % Fe-Ni powder, Li_2FeS_2 powder, and LiCl-KCl eutectic salt, and were heated for 16 hr at 582°C. This same procedure was repeated at 625 and 713°C. Metallographic examination showed that a nickel-substituted J phase formed in all cases except when the $Fe_{0.9}Ni_{0.1}S$ was utilized in the 713°C test. These tests showed that appreciable quantities of nickel (*e.g.*, 20 mol % in the mixed sulfide) lead to a nickel-substituted J phase that has higher thermal stability than the nickel-free J phase, which does not form above 623°C (see Table VIII-3).

From these experiments it was concluded that, in the development of an Fe-Ni-S electrode, a relatively poor utilization and a form of J phase may be difficult to avoid.

3. Iron Selenide Electrodes
(Z. Tomczuk)

In an exploratory study, cell tests of Fe-Se-S electrodes were conducted to determine whether or not the phases in iron-selenium electrodes are analogs of those in iron-sulfur electrodes.

A LiAl (2 A-hr)/LiCl-KCl/FeSe (1 A-hr) cell was operated at 433°C for 18 cycles; the best utilization was about 60%. The cell voltage was about 50 mV higher than that of a Li-Al/FeS cell, but the behavior of the FeSe cell was identical to that of FeS cells in other respects. Near the end of a charge, a short, high-voltage plateau occurred at about 1.8 V in the FeSe cell; in FeS cells this plateau is attributed to conversion of J phase ($LiK_6Fe_{24}S_{26}Cl$) to FeS. Operation of the cell was terminated after a 4-hr trickle charge to a cutoff voltage of 1.45 V. The phase found by X-ray examination* was similar to J phase. The selenium compound had a cubic lattice parameter of 10.86 Å, whereas that of the sulfur compound was 10.36 Å The selenium compound, like J phase, was insoluble in water.

In addition, a LiAl (2 A-hr)/LiCl-KCl/$FeS_{0.5}Se_{0.5}$(1 A-hr) was tested. The cell was operated for 24 cycles at temperatures up to 443°C; the best utilization was 70%. Cell operation was stopped at 1.67 V during charge, and the positive electrode material was submitted for X-ray examination.* As before, a material structurally similar to J phase was found. Its lattice parameter, 10.5 Å, was halfway between that observed with sulfur and with selenium. Thus, selenium substitutes for sulfur in J phase.

---

*Conducted by B. S. Tani, Analytical Chemistry Laboratory, ANL.

C. Properties of Negative Electrodes

(D. R. Vissers, K. E. Anderson*)

Studies are being conducted on additives to the Li-Al negative electrode that may result in sustained high capacities during extended cycling. The decreasing capacity presently observed in Li-Al electrodes may be due, in part, to morphological changes of the active material over a period of time. The present studies are focused on the use of various metallic additives to the binary Li-Al alloy as a means of controlling or modifying these morphological changes. The additives under investigation include indium, lead, tin, copper, zinc, magnesium, antimony, and silver.

A liquid-lithium electrode was chosen as the counter electrode for these studies because it becomes only slightly polarized during cycling, even at relatively high current densities (0.10 A/cm^2). Thus, the Li-Al alloy electrode completely limited the cell capacity, and the lithium electrode served both as a counter and reference electrode. The lithium was contained in a Type 347 stainless steel Feltmetal support sized to give an area of ∿20 cm^2.

The Li-Al-M (M = metal additive) electrodes were prepared by melting mixtures of the desired composition at about 800-900°C in tantalum crucibles. The alloy was ground to a powder and loaded into a porous iron disk, which was enclosed in a 325-mesh stainless steel screen basket to contain the particulate material. The electrodes were approximately 0.8-cm thick and had surface areas of ∿15.6 cm^2. The cells were assembled with the electrodes mounted horizontally in a housing of Type 304 stainless steel. The interelectrode spacing was ∿0.6 cm; a BeO spacer served as the electrode separator. The electrolyte was LiCl-KCl eutectic.

In general, the following cutoff potentials were used during cell cycling: 0.15 V during Li-Al electrode charge and 0.70 V during Li-Al electrode discharge (all cutoff potentials cited are IR-free voltage *vs.* lithium). The capacity density of the electrode at constant current was used as a measure of electrochemical performance. Capacity-density measurements were carried out at current densities of 0.05 to 0.10 A/cm^2 during charge and 0.05 to 0.30 A/cm^2 during discharge. The effect of the additive on the capacity retention of the electrode was assessed by measuring the rate of capacity-density decline at 0.05 A/cm^2 during cycling.

The data from these studies are summarized in Table VIII-5. Indium appears to be the only additive which markedly improves the capacity retention characteristic of the electrode. It also (at the 1 wt % level) improves the electrode utilization at the higher charge current density. Zinc had a similar beneficial effect on utilization, but had little effect on capacity retention.

---

*Cell Development and Engineering Group.

Table VIII-5. Utilization and Capacity Retention of LiAl Electrodes with Additives

Additive	Charge Current Density, mA/cm^2	Utilization[a] at Discharge Current Density				Capacity Decline,[b] %/Cycle
		50 mA/cm^2	100 mA/cm^2	200 mA/cm^2	300 mA/cm^2	
None	50	92.3	89.2	84.6	81.9	0.06
	100	80.2	76.6	76.6	65.6	
3.9 wt % In	50	92.7	90.5	88.6	83.2	<0.01
	100	70.0	70.0	70.0	65.4	
1 wt % In	50	92.2	90.4	83.8	71.7	<0.01
	100	90.4	80.1	82.7	74.1	
5 wt % Sn	50	94.1	92.4	90.6	83.7	0.14
	100	81.9	81.9	81.9	78.4	
10 wt % Pb	50	92.2	90.2	86.2	84.2	0.30
	100	82.2	74.1	74.1	72.1	
5 wt % Cu	50	98.6	96.6	83.7	80.9	0.06
	100	66.7	65.9	65.3	63.5	
5 wt % Ag	50	94.3	93.4	91.3	88.3	0.06
	100	67.5	68.5	67.8	67.5	
5 wt % Sb	50	91.3	89.7	86.5	83.2	0.07
	100	73.4	78.3	78.3	76.7	
5 wt % Zn	50	96.5	95.0	90.6	70.2	0.06
	100	83.3	84.8	83.3	83.3	
15 wt % Mg	50	85.7	84.0	81.3	81.0	0.04
	100	61.0	58.7	58.0	57.0	

[a]Percent of theoretical lithium capacity. Data obtained during first 50 cycles.

[b]Measured at 50 mA/cm^2 charge and discharge current densities after 200 cycles unless operation of the cell was terminated earlier.

REFERENCES

1. R. K. Steunenberg and M. F. Roche, *Electrochemistry of Lithium/Metal Sulfide and Calcium/Metal Sulfide Cells Using Molten Salt Electrolytes*, in Proc. Symp. on Electrode Materials for Energy Conversion and Storage, Vol. 77-6, The Electrochemical Society, Inc., Princeton, NJ (1977).

2. J. R. Craig and S. D. Scott, *Sulfide Mineralogy*, Vol. 1, Ch. 4 and 5, P. H. Ribbe, ed., Southern Printing Co., Blacksburg, VA (1974).

3. M. Hansen and K. Anderko, *Constitution of Binary Alloys*, McGraw-Hill, New York (1969).

4. M.-L. Saboungi, J. J. Marr, M. Blander, J. Electrochem. Soc. *125*, 1567 (1978).

IX. ADVANCED BATTERY RESEARCH
(M. F. Roche)

The objective of this work is to develop secondary cells that use inexpensive, abundant materials. The experimental work ranges from cyclic voltammetry studies and preliminary cell tests through the construction and operation of engineering-scale cells for the most promising systems. During the past year, studies were conducted of cells having either calcium alloy or magnesium alloy negative electrodes and molten-salt electrolytes. Recently, owing to the higher performance of the cells with calcium negative electrodes, we decided to abandon research on cells with magnesium negative electrodes. The efforts in the next year will be focused on developing a calcium/metal sulfide cell that has a performance equivalent to the Mark III goals presented in Table I-1 and a materials cost of $10-15/kW-hr in mass production.

A. Calcium/Metal Sulfide Cells

1. Engineering-Scale Cell Tests
(L. E. Ross, P. F. Eshman*, M. F. Roche)

Since the beginning of 1976, fourteen engineering-scale calcium/metal sulfide cells have been fabricated and operated. These cells, which were fabricated with various calcium alloys, molten salts, and metal sulfides, had theoretical capacities of up to 100 A-hr. The performance data obtained from the operation of these cells helped to guide the fundamental research that was carried on in parallel with the engineering studies. These cell tests and the recent research have indicated that calcium/metal sulfide cells can ultimately achieve high performance.

During this year, a sealed, prismatic (13.5 x 13.5 x 2.5 cm) calcium/metal sulfide cell (theoretical capacity, 70 A-hr) was fabricated in the uncharged state. The two negative electrodes (0.4-cm thick) contained Mg_2Si powder. When the cell is charged, the Mg_2Si powder becomes a mixture of Ca-Mg-Si phases having an overall stoichiometry of approximately $Ca_{1.5}Mg_2Si$. These electrodes employed iron Retimet† as the current collector and 325-mesh stainless steel screens as the particle retainer. The uncharged positive electrode (0.8-cm thick) contained calcium sulfide and Ni_3S_2 (added as a mixture of Ni and NiS), which becomes NiS_2 when the cell is charged. This electrode contained a current collector of carbon fibers‡ and molybdenum sheet, a particle retainer of zirconia cloth, and a separator of BN fabric.

The electrolyte used in this cell was 54 mol % LiCl-39 mol % KCl and 7 mol % $CaCl_2$ (mp, 350°C) and the cell operating temperature was 450°C. However, it has been learned in recent experiments that positive-electrode reactions are inhibited in this electrolyte, and a new electrolyte, which will be discussed later, has been found that avoids this problem. This new electrolyte will be employed in future engineering-scale tests.

---

*Industrial Cell and Battery Testing Group.

†A product of Dunlop, Ltd., Coventry, England.

‡Fortafil 5 (Great Lakes Carbon Corp., Elizabethton, N. J.) was 7.2 vol % of the electrode solids.

The cell performance for 120 cycles of operation is given in Fig. IX-1. The specific energy was initially about 42 W-hr/kg at the 6-hr rate (50% utilization). Near cycle 65, the cell was cooled to room temperature, and additional $CaCl_2$ was added to raise the $CaCl_2$ concentration to 9.1 mol %. The intent was to determine the effect of a higher $CaCl_2$ concentration on specific energy, but this procedure led to an accelerated decline in coulombic efficiency. Beyond cycle 90, the charge-cutoff voltage was decreased from 2.4 to 2.3 V (the discharge-cutoff voltage was 1.0 V), thereby resulting in a decrease of specific energy from ∿35 to ∿31 W-hr/kg at the 6-hr rate.

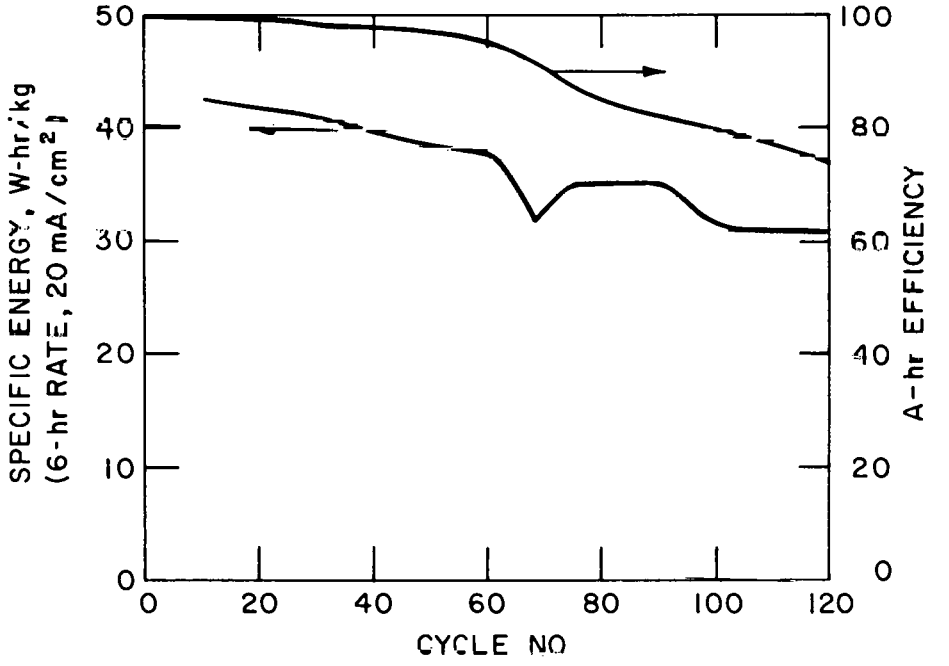

Fig. IX-1. Performance of $Ca(Mg_2Si)/NiS_2$ Cell

The cell operation was stopped at cycle 120 because the coulombic efficiency had dropped to an unacceptable level. The source of the short circuit could not be determined in post-test examinations.* The post-test examinations did reveal, however, that reaction distributions were different in the negative and the positive electrodes. The back portions of the negative electrodes (*i.e.*, regions furthest from the positive electrode) contained larger, poorly reacted Mg_2Si particles while the front portions contained a much finer, well-reacted material (∿2-μm diameter). In addition to NiS_2, the positive electrode contained islands of NiS plus CaS, and did not exhibit distinct front-to-back reaction zones.

Neither the specific energy nor the cycle life of the cell approached the present goals of the program (160 W-hr/kg and 1000 cycles). However, considering the preliminary nature of the test, the cell operated

*Metallographic examination conducted by F. C. Mrazek, Materials Development Group.

well. It is anticipated that the program goals will be achieved through increased active material loadings (only 20 wt % was used in the above cell), improved electrode and electrolyte compositions, and improved cell design.

2. Electrolyte Development
(L. E. Ross, C. C. Sy, S. K. Preto)

Although the electrolyte used in the above cell, LiCl-KCl-$CaCl_2$, has a relatively low melting point (~350°C), it is expensive because of its high concentration of LiCl. Therefore, alternative electrolytes are under investigation. Salts that are relatively inexpensive and compatible with the cell electrodes are the chlorides, fluorides, and bromides of sodium, potassium, calcium and barium. However, mixtures of these salts have a relatively high melting point. To obtain a low melting point, it is necessary to include some lithium salts. The goal of this research is to obtain an acceptable electrolyte containing no more than 10-15 mol % lithium and having a melting point under 400°C. At present, mixtures containing chlorides and fluorides are being studied. (The addition of bromides is not expected to drop melting points more than 5-10°C, and bromides may cause overcharge problems in the positive electrodes.)

The melting points of the molten salts were found by measuring their solidification temperature as they cooled. Previously reported melting points[1] and those determined in this study are listed in Table IX-1 in order of decreasing melting point. The salt in Table IX-1 that appears to be most promising is the second mixture from the bottom (mp, 390°C), which contains about half as much lithium as the previously used 54 mol % LiCl-39 mol % KCl and 7 mol % $CaCl_2$. The 8.5 mol % LiCl-30.0 mol % NaCl-47.0 mol % $CaCl_2$-14.5 mol % $BaCl_2$ and the 3.5 mol % LiF-35.0 mol % NaCl-47.0 mol % $CaCl_2$-14.5 mol % $BaCl_2$ salts are also of interest because of their very low lithium-ion contents. More mixtures in the neighborhood of these compositions will be prepared to seek a mixture that melts at under 400°C and has a low lithium-ion content.

Table IX-1. Melting Points of Electrolytes

Electrolyte Compositions, mol %						Melting Point, °C	
LiF	LiCl	NaCl	KCl	$CaCl_2$	$BaCl_2$	Reported[1]	This Study
-	-	31.4	3.3	47.8	17.5	428	451
-	-	33.0	8.0	45.0	14.0	421	442
-	-	38.5	-	47.0	14.5	450	440
-	3.3	31.4	-	47.8	17.5	-	434
3.3	-	31.4	-	47.8	17.5	-	434
-	8.5	30.0	-	47.0	14.5	-	423
3.5	-	35.0	-	47.0	14.5	-	421
-	29.0	20.0	-	35.0	16.0	378	390
-	33.3	12.5	-	37.6	16.6	385	383

3. Cyclic Voltammetry of FeS_2 and NiS_2 in Calcium-Cell Electrolytes (S. K. Preto)

The electrochemistry of FeS_2 and NiS_2 electrodes in various calcium-cell elcctrolytes is being investigated by slow-scan cyclic voltammetry. The objective of the study is to identify electrode and electrolyte compositions that have acceptable performance characteristics. A similar study of the FeS_2 and NiS_2 electrodes in the lithium-cell electrolyte (LiCl-KCl) is described in Sect. VIII.A.2. That study provided the baseline information for this series of experiments.

In this study, the voltammetry cell contained a FeS_2 or NiS_2 working electrode (∿100 mg of the metal disulfide in carbon foam within a 5-cm^2 molybdenum housing). The counter electrode and reference electrode contained $CaAl_4$ plus Al mixtures. Two different electrolytes were used: 54 mol % LiCl-39 mol % KCl-7 mol % $CaCl_2$ and 29 mol % LiCl-20 mol % NaCl 35 mol % $CaCl_2$-16 mol % $BaCl_2$. The working electrodes were cycled repeatedly over 1.0-2.0 V *vs.* $CaAl_2$; a low scan rate (0.02 mV/s) insured good resolution of the current peaks.

The voltammograms of the FeS_2 and NiS_2 electrodes using the above electrolytes are shown in Figs. IX-2 and -3, respectively. (Charge reaction peaks are above the voltage axis, and discharge peaks are below this axis.) In general, the current peaks were larger and better resolved in the LiCl-NaCl-$CaCl_2$-$BaCl_2$ electrolyte. In both electrolytes, the ∿1.8-V reactions of FeS_2 and NiS_2 exhibit poor electrochemical reversibility. The voltage-

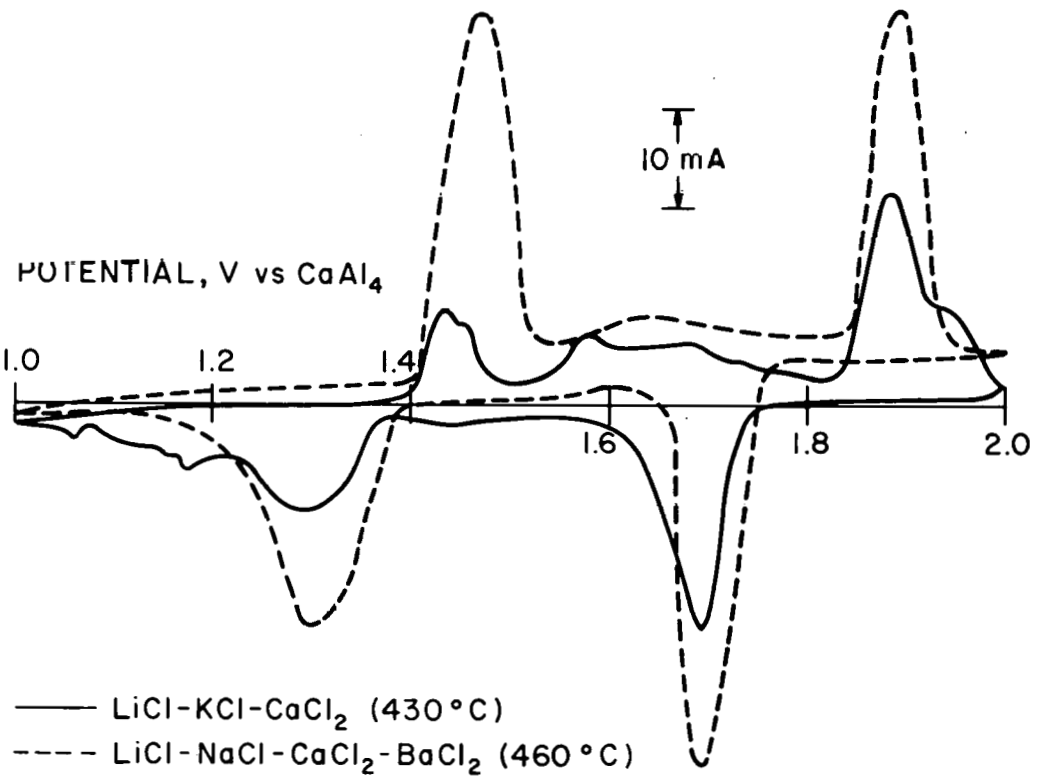

Fig. IX-2. Cyclic Voltammograms for FeS_2 Electrodes

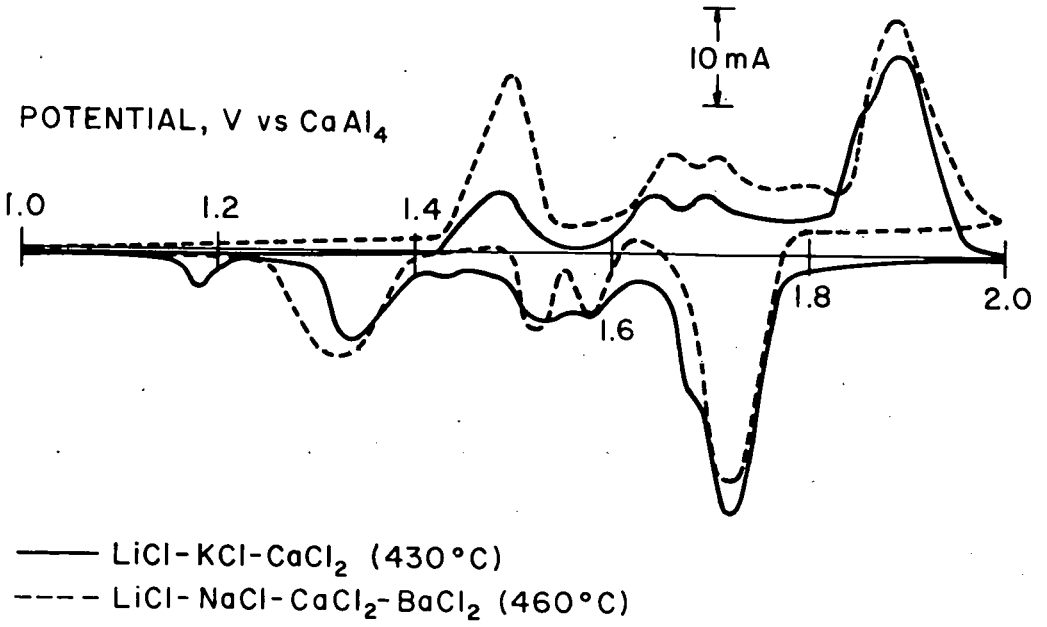

Fig. IX-3. Cyclic Voltammograms for NiS_2 Electrodes

intercept difference (see Section VIII.A.2) is ∿0.09 V for FeS_2 and ∿0.06 V for NiS_2. However, these voltage differences may be the result of minor (relatively harmless) overpotentials for the calcium-ion reactions rather than a problem of a more serious nature [*e.g.*, the marked differences on charge and discharge that exist for FeS_2 electrodes in LiCl-KCl electrolyte (Figs. VIII-2 and -3)]. If this is the case, then performance and lifetime of a calcium/FeS_2 or NiS_2 cell should not be seriously affected by the reversibility problem. The cause of the poor reversibility and (if necessary) methods of eliminating it will be sought in future experiments.

As discussed in Section VIII.A.2, reaction emfs can be estimated from voltammograms by averaging the voltage-axis intercepts of charge and discharge peaks. The values obtained in this manner for the FeS_2 and NiS_2 electrodes using the $LiCl-NaCl-CaCl_2-BaCl_2$ electrolyte are listed in Table IX-2. These emfs differ slightly from those given in Table VIII-1 for the

Table IX-2. Reaction Emfs for FeS_2 and NiS_2 Electrodes

Reaction	Emf, V (*vs.* $CaAl_4$ at 460°C)
$FeS_2 \rightarrow Fe_{1-x}S$	1.78
$FeS \rightarrow Fe$	1.39
$NiS_2 \rightarrow Ni_{1-x}S$	1.81
$NiS \rightarrow Ni_7S_6$	1.65
$Ni_7S_6 \rightarrow Ni_3S_2$	1.59
$Ni_3S_2 \rightarrow Ni$	1.42

reactions of the same electrodes with lithium ions. This is because of the differences in reference electrodes ($CaAl_4$ instead of LiAl) and the differences in the sulfide phase that forms along with the transition-metal sulfides (CaS instead of Li_2S). A comparison of the emfs in Table IX-2 with values calculated from independent thermodynamic data is of interest, but this comparison cannot be made at present because the free energy of formation of $CaAl_4$ is unknown. This free energy will be measured in future experiments.

4. Negative Electrode Development
(L. E. Ross)

The Ca-Mg-Si ternary compound currently used in calcium/metal sulfide cells is formed by charging Mg_2Si in the presence of a molten-salt electrolyte that contains calcium ions. The phases that form under these conditions are unknown, but they have an overall stoichiometry of approximately $Ca_{1.5}Mg_2Si$, or a capacity of about 1 A-hr of calcium per gram of Mg_2Si. Previous studies showed this electrode approached the performance of the LiAl electrode (ANL-77-35, p. 53). However, the $Ca(Mg_2Si)$ electrode has two properties that might cause short circuits during long-term cycling.

(1) If the cell is discharged to low potentials, the magnesium in Mg_2Si may form magnesium ions and subsequently may deposit as magnesium metal in the cell separator.

(2) During cycling, Mg_2Si forms 2-μm-dia particles which may escape from the negative electrode.

Therefore, we initiated a search for alternative alloys for use in the negative electrode. During this year, Ca-Si, Ca-Al-Zn, and Ca-Pb electrodes were investigated.

The Ca-Si electrode was employed in earlier studies (ANL-76-8, p. B-138), and corrosion of current collectors by the discharge product, silicon, was noted. However, this electrode continues to be of interest because of its high theoretical capacity (3.82 A-hr/g Si). In the present study, the Ca-Si electrode (5-cm^2 area and 0.5-cm thick) was cycled between the compositions Ca_2Si (charged) and $CaSi_2$ (discharged). Under these conditions, silicon is not produced in the discharged electrode; this is expected to reduce its corrosiveness toward the iron current collectors. The theoretical capacity of the electrode tested under these cycling conditions was 3.75 A-hr or 0.75 A-hr/cm^2. The electrode contained no distributed current collector; the $CaSi_2$ was simply packed into a screen-covered iron housing.

The electrode was cycled at 445°C between cutoff voltages of -0.41 V (charge) and +0.25 V (discharge) versus a large (area, 15 cm^2; theoretical capacity, 10 A-hr) $CaAl_4$ counter electrode. The electrolyte was 29 mol % LiCl-20 mol % NaCl-35 mol % $CaCl_2$-16 mol % $BaCl_2$. With a charge current density of 20 mA/cm^2, the achieved capacity density was 0.37 A-hr/cm^2 at 60 and 80 mA/cm^2 discharges and 0.31 A-hr/cm^2 at 100 mA/cm^2 discharges. These measurements show the Ca-Si electrode has acceptable performance characteristics for electric-vehicle cells.

Tests of Li-Al-Zn electrodes showed that their performance was superior to that of Li-Al electrodes (Sec. VIII.C.1). Consequently, cell

tests were conducted to compare the performance of Ca-Al and Ca-Al-Zn electrodes. First, a Ca-Al electrode (area, 5 cm^2; theoretical capacity, 2 A-hr) was cycled at 430°C *vs.* a Ca-Al electrode (area, 15 cm^2; theoretical capacity, 6 A-hr). The electrolyte was LiCl-KCl (eutectic) plus 7-9 mol % $CaCl_2$. A similar test was then conducted with a Ca-Al-Zn electrode; the weight ratio of Al to Zn was 9 to 1. With cutoff voltages of ±0.4 V and a current density of 20 mA/cm^2, the utilization of both 2 A-hr electrodes was only 30%. Thus, zinc had no effect on the utilization of the Al electrode.

A Ca-Pb electrode, which has a theoretical capacity of 0.648 A-hr per gram of $CaPb_3$ (assuming the electrode is cycled between the compositions Ca_3Pb and $CaPb_3$), was tested in the same manner as the Ca-Al-Zn electrode. The utilization of this electrode was 60% at a current density of 36 mA/cm^2. This electrode does not appear to be satisfactory for use in high-energy-density cells because of its relatively low theoretical capacity. However, its good utilization and high density indicate that it may be useful for stationary-energy-storage applications.

Of the negative electrodes tested to date, the Ca_2Si electrode and the $Ca_{1.5}(Mg_2Si)$ electrode have exhibited acceptable performance for electric-vehicle applications. Both of these electrodes will be employed in future engineering-scale tests in order to compare their cycle life.

B. Magnesium Alloy/Metal Sulfide (Or Oxide) Cells
(C. C. Sy and Z. Tomczuk)

The investigation of cells having magnesium negative electrodes was prompted by the promising properties of magnesium, *i.e.*, low equivalent weight, high melting point, high abundance, and low cost. The formation of dendrites on the magnesium electrode of these cells has been a persistent problem (ANL-77-75, p. 60) with this type of cell. This problem was not addressed in the current study, which was concerned with the properties of positive electrodes for magnesium cells. The magnesium alloys employed as negative electrodes, in spite of dendrite problems, were Mg_2Al_3 and Mg_2Cu. The capacity of the negative electrodes varied from 5 to 20 A-hr, and the magnesium alloys were contained in a 7-mm thick disk of iron Retimet in a cylindrical iron housing (area, 20 cm^2).

The compounds TiS_2, NiS_2, NiO, and FeO were chosen as the positive electrodes because they are solids at cell temperatures and have low free energies of formation (yielding high cell voltages). The positive electrodes consisted of 1 to 5 A-hr of active material in the form of a pellet or a fine powder, which was contained in an 11-cm^2 graphite cup or in a 5- to 10-cm^2 molybdenum housing. The exposed areas of these electrodes were covered by either a porous carbon disk or fine screens and zirconia cloth. The inter-electrode spacing was ~1 cm; this large spacing prevented short circuits due to dendrite growth.

Two electrolytes were initially used in the test cells: 38 mol % LiCl-46 mol % KCl-16 mol % $MgCl_2$ (mp, 336°C) and 30 mol % NaCl-20 mol % KCl-50 mol % $MgCl_2$ (mp, 396°C).

The Mg_2Al_3/TiS_2 cells were operated in both electrolytes. As can be seen in Table IX-3, the cell containing NaCl-KCl-$MgCl_2$ electrolyte achieved a

Table IX-3. Performance of (3.3 A-hr) Mg_2Al_3/TiS_2 (3 A-hr) Cells

Electrolyte	Current Density, mA/cm^2	Utilization,[a] %	Temperature, °C
$NaCl-KCl-MgCl_2$	5	65.5	422
	18	31.0	
	26	25.1	
$LiCl-KCl-MgCl_2$	5	52.3	410
	18	50.0	
	26	43.1	

[a]Assuming the reaction $Mg_2Al_3 + TiS_2 \rightarrow 2MgTi_2S_4 + 3Al$ occurred.

higher electrode utilization at low current density (5 mA/cm^2) than the cell containing $LiCl-KCl-MgCl_2$ electrolyte, but at a high current density (18 and 26 mA/cm^2) the situation was reversed.

Although the utilization of the $Mg_2Al_3/LiCl-KCl-MgCl_2/TiS_2$ cell was good (43% at 26 mA/cm^2), the lithium ions were participating in the cell reaction by forming $LiTiS_2$ in the positive electrode. This undesirable reaction alters the electrolyte composition during cell operation and can cause the salt to solidify. Consequently, this type of cell is impractical.

Figures IX-4 and -5 show the typical utilization *vs.* voltage curves for Mg_2Al_3/TiS_2 cells operated in these two electrolytes. The sloping discharge

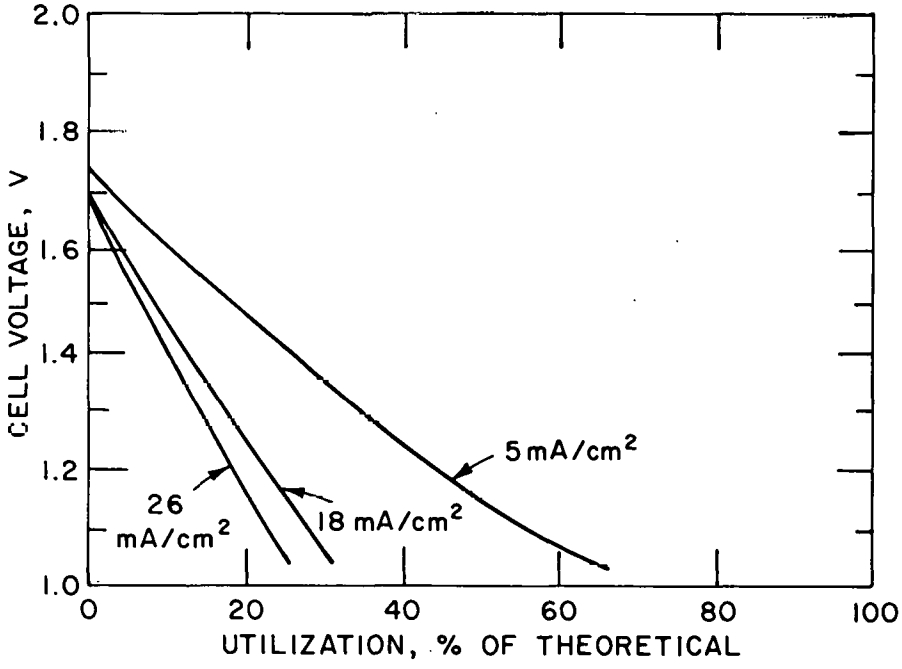

Fig. IX-4. Typical Discharge Curves for $Mg_2Al_3/NaCl-KCl-MgCl_2/TiS_2$ Cell at 422°C

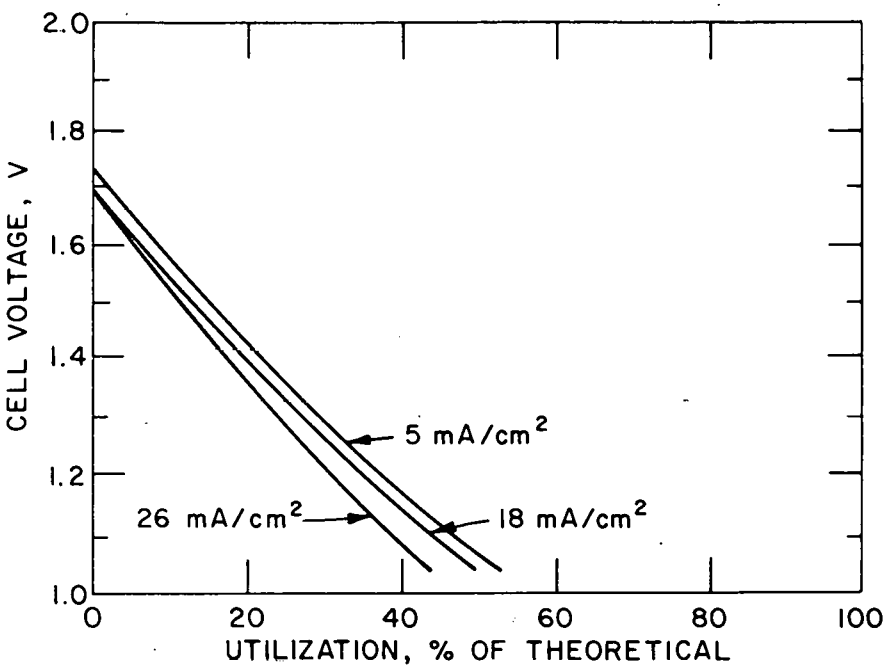

Fig. IX-5. Typical Discharge Curves for $Mg_2Al_3/LiCl-KCl-MgCl_2/TiS_2$ Cell at 410°C

curves obtained using either electrolyte indicate that the reaction mechanism consisted of the formation of an intercalated discharge product in the TiS_2 electrode.

The performance characteristics of the five magnesium cells tested during this period are summarized in Table IX-4. The Mg_2Al_3/NiS_2 cell did not achieve adequate electrode utilization (only 17% at 27 mA/cm).

Table IX-4. Summary of the Performance Characteristics of Magnesium Alloy/Metal Sulfide and Oxide Cells

Cell	Electrolyte	Temp., °C	Open-Circuit Voltage at Full Charge, V	Current Density, mA/cm²	Utilization, %
1) Mg_2Al_3/NiS_2	a	375-425	1.5	27.0	17.0
2) Mg_2Al_3/TiS_2	a	410	1.8	26.0	43.0
	b	422	1.7	26.0	25.0
3) Mg_2Cu/TiS_2	b	417-430	1.3	26.0	22.0
4) $MgCu_2/Ni-MgO$	b	426-465	1.4	20.0	5.6
5) $MgCu_2/Fe-MgO$	b	468	∿1.5	20.0	0

[a] $LiCl-KCl-MgCl_2$

[b] $NaCl-KCl-MgCl_2$

The performance of the $MgCu_2$/Fe-MgO cell (started in the uncharged state) was unsatisfactory because the iron formed a soluble compound, $FeCl_2$, at 1.4 V rather than the desired insoluble compound, FeO, at 1.5 V. Black particles were found in the melt and X-ray diffraction analysis* showed that these particles were α-iron.

The $MgCu_2$/Ni-MgO cell (started in the uncharged state) yielded a very low electrode utilization of 5.6% at a current density of 20 mA/cm^2 and had a coulombic efficiency of only 80.7%. Thus, this cell was also unsatisfactory.

Generally, the cells exhibited rapidly declining capacity with increasing current density. One possible cause of this capacity decline was the slow diffusion of magnesium through the solid phases of the negative electrode. The performance of these cells was not markedly improved by increasing the operating temperature.

The formation of dendrites on the negative electrodes and the unacceptably low utilization of the positive electrodes are the major problems that need to be solved before secondary cells using magnesium as the negative electrode material are successfully developed. The properties of other types of positive electrodes, such as metal halides, may also be of interest in future investigations.

*Conducted by B. S. Tani, Analytical Chemistry Laboratory (ANL).

REFERENCES

1. G. J. Janz, *et al.*, ERDA Publication No. TID-27163 (July 1976).

2. S. J. Preto, L. E. Ross, A. E. Martin, M. F. Roche, *Rechargeable Calcium High-Temperature Cells*, Proc. Symp. and Workshop on Adv. Battery Research and Design, ANL-76-8 (March 1976).

APPENDIX A.

Gould Performance Data on X-Series Cells

Appendix A. Gould Performance Data on X-Series Cells.

Cell No.	Theor. Cap (Ah) Wt. (Kg)	Positive Electrode Disch. Half Thick. (in.) (Porosity)	Additives	Current Collector (Thickness) Density	Negative Electrode	Separator Package (Combined) Face Thick. Fiber Density	Electrolyte (w/o LiCl)	Cell Resistance Operating (mΩ) @ 50% Disch. t = 0	t = 15 sec	Final Frozen (Ω)	Specific Energy, Wh/kg Utilization, (%) @ Current Density 20	40	60	80	Cycle Life (1) Cycles	Hours
GII-03-03 Baseline	168.65 (2.46)	0.192 (40.3%)	10 w/o Fe 1.2 w/o Cu	Fe X-Met Fe Sheet (.005") 1.89 g/Ah	H.P. Powder with Electrolyte 8.18 w/o LiAl (Dis) 17.5 w/o LiAl (Ch)	BN (LiCl-KCl) Cloth Cups ZrO_2 Wrap (0.101") 106 mg/cm^2	LiCl-KCl Eutectic (44.19)	4.5	5.4	700	66 79.8	54 61.3	41 50.0	----	76 L.T.	1729
X-1	190.6 (2.44)	0.197 (37.3)	15 w/o Fe (2) 2.5 w/o Co (3) 5 w/o C	Fe X-Met Fe Sheet (.015") 1.18 g/Ah	H.P. Powder with Electrolyte 5.3 w/o LiAl (Dis) 18.5 w/o LiAl (Ch)	BN (LiCl-KCl) Cloth Cups ZrO_2 Wrap (0.101") 106 mg/cm^2	LiCl-KCl Eutectic (44.19)	----	----	----	----	----	----	----	(1 P.M.	(60
X-2	184.6 (2.30)	0.167 (29.0)	15 w/o Fe (2) 2.5 w/o Co (3) 5 w/o C	Fe X-Met Fe Sheet (.015") 1.28 g/Ah	As X-1	As X-1	LiCl-KCl Eutectic (44.19)	3.5	4.8	35.0	73.4 72.6	50.7 52.2	39.4 41.1	----	25	1133
X-3	119.8 (2.07)	0.114 (33.2)	10 w/o Fe (2) 5 w/o Co (3) 5 w/o C	Fe Sheet (.023") w/buss bar 1.09 g/Ah	H.P. Powder with Electrolyte 4.56 w/o LiAl (Dis) 20 w/o LiAl (Ch)	As X-1	LiCl-KCl Eutectic (44.19)	(4) 3.6	(4) 4.1	2.5	63.8 87.5	53.8 76.2	43.8 64.1	----	10	338
X-4	124.9 (2.03)	0.125 (37.2)	10 w/o Fe (2) 5 w/o Cu (3) 5 w/o C	Fe Sheet (.023") w/buss bar 1.05 g/Ah	H.P. Powder with Electrolyte 5.3 w/o LiAl (Dis) 18.5 w/o LiAl (Ch)	BN (LiCl–KCl) Cloth Cups Carbon Felt Wrap (.080") 106 mg/cm^2	LiCl-KCl Eutectic (44.19)	----	----	1100	50.7 66.5	----	----	----	8	189
X-5	107.4 (1.86)	0.117 (43.2)	10 w/o Fe (2) 5 w/o Cu (3) 5 w/o C	Fe Sheet (.023") w/buss bar 1.23 g/Ah	H.P. Powder with Electrolyte 5.3 w/o LiAl (Dis) 18.4 w/o LiAl (Ch)	As X-4	LiCl-KCl Eutectic (44.19)	----	----	45	57.8 80.7	----	----	----	9-1/2	210

(1) P.M. = Post Mortem (Dissection & analysis after cell failure)
P.O. = Post Operative (Voluntary termination followed by dissection & analysis)
L.T. = Transfer for Life Testing

(2) % of Active Fe

(3) % of (Active Mix Minus Salt)

(4) Data @ 80% Charged

(5) Data @ 88% Charged

(6) For all regions outside local zero shorts

(7) Porosity (By Design)

(8) Measured from Dissected Cells

(9) Operating Temperature = 517°C

(contd)

Appendix A. (contd)

Cell No.	Theor. Cap (Ah) Wt. (Kg)	Positive Electrode Disch. Half Thick. (in.) (Porosity)	Additives	Current Collector (Thickness) Density	Negative Electrode	Separator Package (Combined) Face Thick. Fiber Density	Electrolyte (w/o LiCl)	Cell Resistance Operating (mΩ) @ 50% Disch. t = o	t = 15 sec	Final Frozen (Ω)	Specific Energy, Wh/kg Utilization, (%) @ Current Density 20	40	60	80	Cycle Life (1) Cycles	Hours
X-6	125.1 (1.99)	0.118 (33.1)	10 w/o Fe Flash Cu Plated on C.C. (3) 5 v/o C	Fe Sheet (.023") w/buss bar 1.05 g/Ah	H.P. Powder with Electrolyte 5.3 w/o LiAl (Dis) 18.4 w/o LiAl (Ch)	As X-1	LiCl-KCl Eutectic (44.19)	(4) 3.3	(4) 3.9	900	65.0 82.1	54.0 69.8	43.4 58.5	----	11	338
X-7	124.8 (2.06)	0.137 (40.9)	10 w/o Fe (2) 5 w/o Co (3) ∿5 v/o C	Fe Sheet (.023") w/buss bar 1.11 g/Ah	Machined Ingot 4.56 w/o LiAl (Dis) 18 w/o LiAl (Ch)	BN (LiCl-KCl) Cloth Cups Pre-wetted Carbon Felt (.080") 106 mg/cm^2	LiCl-KCl Eutectic (44.19)	4.4	5.3	----	53.8 71.0	38.1 51.6	22.3 30.9	----	11-1/2 P.O.	279
X-8	132.0 (2.02)	0.133 (38.7)	10 w/o Fe (2) 5 w/o Co	Fe Sheet (.023") w/buss bar 1.04 g/Ah	H.P. Powder with Electrolyte 4.56 w/o LiAl (Dis) 18 w/o LiAl (Ch)	BN (LiCl-KCl) Cloth Cups No Retainer (.030" Compressed) 106 mg/cm^2	LiCl-KCl Eutectic (44.19)	----	----	100	----	----	----	----	⟨1/2 P.M.	⟨60
X-8A	132.0 (2.08)	0.133 (34.2%)	10 w/o Fe (2) 5 w/o Co	Fe Sheet (.023") w/buss bar 1.04 g/Ah	H.P. Powder with Electrolyte 4.56 w/o LiAl (Dis) 18 w/o LiAl (Ch)	BN (LiCl-KCl) Cloth Cups No Retainer (.045") 106 mg/cm^2	LiCl-KCl Eutectic (44.19)	3.2	3.9	102	50 62.5	41 50.0	32 39.5	----	31	459
X-9	129.2 (2.02)	0.129 (37.1%)	10 w/o Fe (2) 5 w/o Co (3) 5 v/o C	Fe Sheet (.023") w/buss bar 1.01 g/Ah	As X-8A	BN (LiCl-KCl) Cloth Cups No Retainer (.050") 106 mg/cm^2	LiCl-KCl Eutectic (44.19)	3.3	3.8	----	69 85.3	59 72.0	50 59.2	----	17-1/2	250
X-10	130.0 (2.17)	0.136 (38.3)	10 w/o Fe (2) 5 w/o Co (3) 5 v/o C	Fe Sheet (.023") w/buss bar 1.00 g/Ah	H.P. Powder with Electrolyte 8.18 w/o LiAl (Dis) 17.9 w/o LiAl (Ch)	BN Felt Cups (LiCl-KCl) No Retainer (0.100") 60 mg/cm^2	LiCl-KCl Eutectic (44.19)	3.9	5.1	4.0	49.8 67.8	41.1 63.7	----	----	6 P.M.	295
X-11	127.8 (2.01)	0.140 (37.5)	10 w/o Fe (2) 5 w/o Co (3) 5 v/o C	Ni Sheet (.013") w/buss bar 0.88 g/Ah	Alcoa Extruded Slabs 5.25 w/o LiAl (Dis) 20.2 w/o LiAl (Ch)	BN Felt Cups (LiCl-KCl) ZrO_2 (0.131") 69 mg/cm^2	LiCl-KCl Eutectic (44.19)	4.9	7.6	4.4	⟨30 ⟨39	----	----	----	4 P.M.	115

(contd)

Appendix A. (contd)

Cell No.	Theor. Cap (Ah) Wt. (Kg)	Positive Electrode Disch. Half Thick. (in.) (Porosity)	Additives	Current Collector (Thickness) Density	Negative Electrode	Separator Package (Combined) Face Thick. Fiber Density	Electrolyte (w/o LiCl)	Cell Resistance Operating (mΩ) @ 50% Disch. t = 0	t = 15 sec	Final Frozen (Ω)	Specific Energy, Wh/kg Utilization, (%) @ Current Density 20	40	60	80	Cycle Life (1) Cycles	Hours
GIII-2 Multi-plate	535.3 (6.50)	0.180 (41.5%)	10 w/o Fe (2) 5 w/o Co (3) 5 v/o C	Ni Sheet (.013") w/buss bar 0.77 g/Ah	H.P. Powder No Salt 8.18 w/o LiAl (Dis) 17.67 w/o LiA (Ch)	BN (LiCl-KCl) Cloth Cups ZrO_2 Sheets (0.101") 106 mg/cm^2	LiCl-KCl Eutectic (44.19)	0.8	1.1	520	90 88.1	58 ----	52 54.9	----	43 P.M.	1150
X-20	185.0 (2.50)	0.200 (36.6%)	50 w/o Fe (2) 5 w/o Co (3) 5 v/o C	Ni Sheet (.013") w/buss bar 0.60 g/Ah	H.P. Powder No Salt 8.18 w/o LiAl (Dis) 17.79 w/o LiA (Ch)	BN Felt (LiCl-KCl) Cups ZrO_2 Sheets (0.201") 51 mg/cm^2	LiCl-KCl Eutectic (44.19)	(5) 2.67	3.3	4.3	----	----	----	----	1-1/2 P.M.	127
X-21	178.7 (2.61)	0.210 (37.0)	100 w/o Fe (2) 5 w/o Co (3) 5 v/o C	Ni Sheet (.013") w/buss bar 0.62 g/Ah	H.P. Powder No Salt 8.18 w/o LiAl (Dis) 17.65 w/o LiAl (Ch)	BN (LiCl-KCl) Cloth Cups ZrO_2 Sheets (0.101") 70 mg/cm^2	LiCl-KCl Eutectic (44.19)	3.0	3.5	>1x10^5	79 92.3	66 80.5	53 66.5	----	32.2 P.O.	1200
X-22	172.7 (2.50)	0.200 (34.1)	100 w/o Fe (2) 5 w/o Co (3) 5 v/o C	Ni Sheet (.013") w/buss bar 0.69 g/Ah	H.P. Powder No Salt 8.18 w/o LiAl (Dis) 17.27 w/o LiAl (Ch)	BN Felt (LiCl-KCl) ZrO_2 Sheets (.040") 60 mg/cm^2	LiCl-KCl (49.48)	2.78	3.29	0.5 5x10^6 (6)	94.3 100	89.6 100	67.7 81.7	----	31 P.M.	744
X-23	166.8 (2.10)	0.216 (35.0) (7)	100 w/o Fe (2) 5 w/o Co (3) 3 v/o C	Ni Sheet (.013") 0.72 g/Ah	LiAl Cast Slabs 6 w/o LiAl (Dis) 19.0 w/o LiAl (Ch)	BN Felt (LiCl-KCl) ZrO_2 Sheets (.040") 126 mg/cm^2	LiCl-KCl (49.0)	3.65	4.43	----	86.5 87.8	----	----	----	3 P.M.	308
X-24	253.6 (2.50)	0.312 (37.1)	100 w/o Fe (2) 5 w/o Co (3) 3 v/o C	Ni Sheet (.013") w/buss bar 0.47 g/Ah	LiAl Cast Slabs 6 w/o LiAl (Dis) 19.5 w/o LiAl (Ch)	BN Felt (LiCl-KCl) ZrO_2 Sheets (.052") (8) 54 mg/cm^2	LiCl-KCl (49.0)	3.4	4.2	3.5 5x10^6 (6)	111.1 87.6	----	----	----	5-1/2 P.M.	439
X-25	160.34 (2.04)	0.200 (38.0) (7)	10 w/o Fe (2) 5 w/o Co (3) 6 v/o C	Ni Sheet (.013") 0.74 g/Ah	LiAl Cast Slabs 6 w/o LiAl (Dis) 17.5 w/o LiAl (Ch)	Y_2O_3 Felt (.050") (8) 157 mg/cm^2	LiCl-KCl (49.0)	---	---	0.6 5x10^6 (6)	----	----	----	----	1/2 P.M.	65
X-26	187.2 (2.095)	0.207 (38.0) (7)	10 w/o Fe (3) 3 v/o Co (3) 3 v/o C	Ni Sheet (.013") 0.64 g/Ah	H.P. Powder No Salt 8 w/o LiAl (Dis) 17.5 w/o LiAl (Ch)	BN Felt (LiCl-KCl) (.050") (8) 61 mg/cm^2 Y_2O_3 40.1 mg/cm^2	LiCl-KCl (50.0)	---	----	0.5 5x10^6 (6)	----	----	----	----	<1/2 P.M.	10

(contd)

Appendix A. (contd)

Cell No.	Theor. Cap (Ah) Wt. (Kg)	Positive Electrode Disch. Half Thick. (in.) (Porosity)	Positive Electrode Additives	Current Collector (Thickness) Density	Negative Electrode	Separator Package (Combined) Face Thick. Fiber Density	Electrolyte (w/o LiCl)	Cell Resistance Operating (mΩ) @ 50% Disch. t = o	Cell Resistance Operating (mΩ) @ 50% Disch. t = 15 sec	Final Frozen (Ω)	Specific Energy, Wh/kg Utilization, (%) @ Current Density 20	40	60	80	Cycle Life (1) Cycles	Hours
X-27	183.43 (1.999)	0.197 (38.0) (7)	10 w/o Fe (3) v/o Cr (3) v/o C	Ni Sheet (.013") 0.65 g/Ah	LiAl Cast Slabs 6 w/o LiAl (Dis) 17.5 w/o LiAl (Ch)	BN Felt (LiCl-KCl) (.062") (8) 55 mg/cm^2 Y_2O_3 40.6 mg/cm^2	LiCl-KCl (50.0)	----	----	0.5 $5x10^6$ (6)	---	----	----	----	<1 P.M.	82
X-28	181.17 (2.09)	0.195 (38.0) (7)	10 w/o Fe (2) 3 v/o Ni (3) 3 v/o C	Ni Sheet (.013") w/buss bar	LiAl Cast Slabs 6 w/o LiAl (Dis) 17.5 w/o LiAl (Ch)	BN Felt Y_2O_3 (LiCl-KCl) (.040")	LiCl-KCl (50.0)	2.8	3.8	0.6 $5x10^6$ (6)	---	----	----	----	2-1/2 P.M.	149
X-29	185.81 (2.054)	0.198 (38.0) (7)	10 w/o Fe (3) 3 v/o V (3) 3 v/o C	Ni Sheet (.013") 0.64 g/Ah	H.P. Powder No Salt 8 w/o LiAl (Dis) 17.5 w/o LiAl (Ch)	BN Felt (LiCl-KCl) ZrO_2 (.040") (8) 67 mg/cm^2	LiCl-KCl (50.0)	3.15	4.04	0.0	---	----	----	----	1-1/2 P.M.	170
X-30	190.24 (2.001)	0.222 (38.0) (7)	10 w/o Fe (3) 3 v/o Mo (3) 3 v/o C	Ni Sheet (.013") 0.63 g/Ah	LiAl Cast Slabs 6 w/o LiAl (Dis) 17.5 w/o LiAl (Ch)	BN Felt (LiCl-KCl) (.080") (8) Y_2O_3 48 mg/cm^2	LiCl-KCl (50.0)	----	----	0.6 $5x10^6$ (6)	----	----	----	----	0 P.M.	10
X-31	174.11 (2.22)	0.225 (35.0) (7)	100 w/o Fe (3) 3 v/o C	Ni Sheet (.013") 0.69 g/Ah	LiAl Cast Slabs 8 w/o LiAl (Dis) 17 w/o LiAl (Ch)	BN Felt (LiCl-KCl) ZrO_2 (.075") (8) 67 mg/cm^2	LiCl-KCl (53.3)	3.63	4.74	1.0 $5x10^6$ (6)	79.0 80.0	53.6 60.2	45.3 48.1	----	9 P.M.	336
X-31A	182.03 (2.099)	0.231 (35.0) (7)	100 w/o Fe (3) 3 v/o C	Ni Sheet (.013") 0.66 g/Ah	LiAl Cast Slabs 8 w/o LiAl (Dis) 20.5 w/o LiAl (Ch)	BN Felt (LiCl-KCl) ZrO_2 (.075") (8) 86 mg/cm^2	LiCl-KCl (53.3)	----	----	0.0	----	----	----	----	<1/2 P.M.	36
X-32	179.62 (2.17)	0.200 (37.0) (7)	50 w/o Fe (3) 3 v/o C	Ni Sheet (.013") 0.67 g/Ah	LiAl Cast Slabs 8 w/o LiAl (Dis) 17 w/o LiAl (Ch)	BN Felt (LiCl-KCl) ZrO_2 (.055") (8) 78 mg/cm^2	LiCl-KCl (53.3)	----	----	0.95	----	----	----	----	<1/2 P.M.	55

(contd)

Appendix A. (contd)

Cell No.	Theor. Cap (Ah) Wt. (Kg)	Positive Electrode Disch. Half Thick. (in.) (Porosity)	Positive Electrode Additives	Current Collector (Thickness) Density	Negative Electrode	Separator Package (Combined) Face Thick. Fiber Density	Electrolyte (w/o LiCl)	Cell Resistance Operating (mΩ) @ 50% Disch. t = 0	Cell Resistance Operating (mΩ) @ 50% Disch. t = 15 sec	Final Frozen (Ω)	Specific Energy, Wh/kg Utilization, (%) @ Current Density 20	40	60	80	Cycle Life (1) Cycles	Cycle Life (1) Hours
X-33	186.08 (2.156)	0.200 (38.0) (7)	25 w/o Fe (3) 3 v/o C	Ni Sheet (.013") 0.65 g/Ah	LiAl Cast Slabs 8 w/o L Al (Dis) 17 w/o LiAl (Ch)	BN Felt (LiCl KCl) ZrO_2 (.045") (8) 82 mg/cm^2	LiCl-KCl (53.3)	----	----	83	----	----	----	----	1 P.M.	42
X-34	175.73 (2.304)	0.211 (37.0) (7)	50 w/o Fe (3) 1.5 w/o Co (3) 3 v/o C	Ni Sheet (.013") 0.68 g/Ah	LiAl Ingot Dust No Salt 8 w/o LiAl (Dis) 17 w/o LiAl (Ch)	Carborundum BN Felt (.025") (8) 46.5 mg/cm^2 4.1g $LiAlCl_4$	LiCl-KCl (53.3)	3.19	4.76	0.0 5×10^6 (6)	----	----	----	----	(1/2 P.M.	65
X-40	164.39 (2.376)	0.206 (35.0) (7)	100 w/o Fe (3) 3 v/o C (3) 1 v/o Co (2) 6.7 w/o Co	Ni Sheet (.013") 0.69 g/Ah	Sawed Powder (20/100 Mesh) No Salt 8 w/o LiAl (Dis) 17.5 w/o LiAl (Ch)	Carborundum BN Felt #D 124 (.040") 58 mg/cm^2 One Side 38 mg/cm^2	LiCl-KCl (49.3)	2.45	3.00	1.4×10^5	81.3 94.0	----	69.8 83.4 (9)	----	)14 L.T.	)528

APPENDIX B.

Rockwell International Performance Data on REVC-Series Cells

Appendix B. Rockwell International Performance Data on REVC-Series Cells

Cell No. REVC-	Positive Electrode	Negative Electrode	Separator	Capacity (Ah)	Energy Density (Wh/kg)	Coulombic Efficiency (%)	Utilization (% at 30 mA/cm^2)	Resistance (Ω-cm^2)	Cycle (No./h)	Objectives	Observations
1	Ni HC* Structure Grounded to Type 304 SS Case	1010 HC	AlN 60 mil	172	70	88→45	76→22	3	218/2500	Test of EV cell based on current state-of-the art Li technology	Poor charge acceptance by UC $FeSi_2$. Shorting at upper plateau of negative electrode.
2	Ni Rib Structure (0.25 mm) Porous Ni Particle Retainer	1010 HC Grounded to Case	Y_2O_3 Felt	-	70	92	69	-	10/200	Evaluate dual face rib structure as + electrode concept	Buckling breakage of bond between negative electrode and copper current collector.
3	Ni Rib Structure (0.25 mm) 3.2-mm Spacing, Porous Ni Brazed to Rib Structure	430 HC	AlN	155	60	96→54	54→20	4	228/2100	Test of inward buckling case design	No swelling. Inability to fully charge negative electrode due to shorting.
4	Ni Rib Structure (0.5 mm) 6-mm Spacing, Porous Ni Diffusion-Bonded to Rib Structure	430 HC	AlN	156	60	96	79	2.4	11/200	Evaluate ribs spaced at larger intervals	Porous nickel ruptured.
5	Ni Rib Structure (0.5 mm) 3-mm Spacing, 100-Mesh Ni Screen Diffusion-Bonded to Rib Structure	430 HC 0.25-mm Cu Conductor	AlN	151	-	100	88	1.07→1.34	141/1800	Evaluate Ni screen as a stronger particle retainer	Good high rate performance. Coulombic efficiency continued to decline with life.
6	Ni Rib Structure (0.25 mm) 3-mm Spacing, Porous Ni Diffusion-Bonded	430 HC 0.25-mm Cu Conductor	AlN	161	-	99→50	83→45	2.3	55/1000	Evaluate structure integrity of diffusion-bonded porous Ni with closer rib spacing	Decline in coulombic efficiency. Large reduction in capacity with cycling at rates above 60 mA/cm^2
7	Split-Rib Structure Reinforced Porous Ni, 1-mm Cu Conductor	430 HC 0.25-mm Cu Conductor	AlN	154	-	98→92	79→43	2.7→2.5	162/2000	Evaluate reinforced porous Ni and central Cu conductor	Highly polarized shorting on charge. Utilization and average voltage declined rapidly as current density was increased.
8	Split-Rib Structure (0.25 mm) Reinforced Porous Ni, 1-mm Cu Conductor	430 HC 0.25-mm Cu Conductor	AlN	-	-	99	79	2.5	8/150	Evaluate partial charge negative electrode	Dead short. Li was electrochemically introduced into the cell.

*Honeycomb structure

(contd)

Appendix B. (contd)

Cell No. REVC-	Positive Electrode	Negative Electrode	Separator	Capacity (Ah)	Energy Density (Wh/kg)	Coulombic Efficiency (%)	Utilization (% at 30 mA/cm^2)	Resistance (Ω-cm^2)	Cycle (No./h)	Objectives	Observations
9	0.48-cm Split-Rib with 100-Mesh Screen Particle Retainer, 0.25-mm Cu Conductor	0.32 cm Cr-Coated 1010 HC 0.25-mm Cu Conductor	AlN	149	62	98	82	1.0	94/1350	Evaluate Li-rich electrolyte (55 wt % LiCl-45 wt % KCl)	Good high rate performance. 73% utilization at 75 mA/cm^2. Declined in coulombic efficiency with time.
10	0.48-cm Split Rib with 100-Mesh Screen Particle Retainer 0.25-mm Cu Conductor	0.32 cm Cr-Coated 1010 HC 0.25-mm Cu Conductor	AlN	151	69	98	83	1.7→2.6	152/1600	Eutectic composition, Lithicoa electrolyte control experiment for REVC-9	56% utilization at 75 mA/cm^2. Accidentally charged at high current (200 A) caused negative electrode to be inoperable. Up to 150 cycles cell operated perfectly.
11	0.48-cm Split-Rib with 25 x 500-Mesh Screen Particle Retainer, 0.25-mm Cu Conductor	0.48 cm 430 HC 0.25-mm Cu Conductor	AlN	140	-	98	75	1.5	78/1350	Evaulate electrochemical introduction of Li into partially charged negative electrode	Only small amount of Li could be introduced before cell shorted.
12	0.48-cm Split-Shelf Structure with Porous Ni Particle Retainer 1-mm Cu Conductor	0.32 mm Cr-Coated 1010 HC 0.1-mm Cu Conductor	AlN	147	-	98	76	2.2	46/900	Evaluate shelf-positive structure	Decline in utilization.
13	0.3-mm Ni Ribs with 200-Mesh Screen Particle Retainer at 3.2-mm Spacing	3.2 mm Cr-Coated 1010 HC 0.25-mm Cu Conductor	AlN	150	98	96	83	1.3	14/300	Evaluate light-weight baseline design. 100 Wh/kg goal. Li Rich electrolyte used.	Shorting occurred. Breakage of weld between rib structure and cap.
14	0.3-mm Ni Ribs with 200-Mesh Screen Particle Retainer at 3.2-mm Spacing	3.2 mm Cr-Coated 1010 HC 0.25-mm Cu Conductor	Y_2O_3 Felt	-	95	79	76	1.6	15/399	Evaluate Y_2O_3 felt. Li rich electrolyte used.	Rib structure-to-cap weld failure.
15	0.3-mm Ni Ribs with 200-Mesh Screen Particle Retainer at 3.2-mm Spacing	3.2 mm Cr-Coated 1010 HC 0.25-mm Cu Conductor	Li_4SiO_4-Li_3PO_3	-	88	-	-	-	-	Evaluate light-weight powder separator. Li rich electrolyte used.	Failure during cell started up. Rib structure-to-weld cap failure due to sulfur sensitization of nickel weld.
16	0.3-mm Ni Ribs with 200-Mesh Screen Particle Retainer at 3.2-mm Spacing 14.3-mm electrode thickness	4.8 mm 430 HC 0.25-mm Cu Conductor	AlN	-	101	-	-	-	-	Evaluate a cell with electrodes 50% thicker. Li rich electrolyte used.	Failure during cell started up. Positive electrode cap broken free. Weld cracks due to sulfur contamination.

THIS PAGE

WAS INTENTIONALLY

LEFT BLANK

APPENDIX C.

ANL Performance Data on Eagle-Picher and Gould Cells

APPENDIX C. ANL Performance Data on Eagle-Picher and Gould Cells.

Cell Description[a]	Max. Performance @ Indicated Rate[b] A-hr	W-hr	Rates, hr Disch.	Charge	Initial Eff.,[c] % A-hr	W-hr	Life Characteristics Days[d]	Cycles[d]	% Decline in[e] Capacity	Energy	A-hr Eff.	W-hr Eff.	Remarks
1A5, Li-Al/FeS-Cu_2S, C, 78/78, 13.5 × 15.6 × 2.3 cm, 1.35 kg	51.7 49.4 48.4	64.9 59.0 55.2	10 4 2.5	10 4 2.5	99	90	19	43	15	18	45	36	EP thin-electrode cell. Restarted to test LiCl-rich electrolyte. Decline in coulombic efficiency after 30 cycles. Terminated.
1B4, Li-Al/FeS-Cu_2S, C, 146/149, 13.5 × 15.6 × 3.8 cm, 2.0 kg	84	93	10	10	85	87	733	1273	34	35	35	32	EP thick-electrode cell. Previously in series with 1B6 as battery. 1339 total cycles. Total operating time 2 yrs 18 days. Tested at 500°C (121 cycles). Terminated.
2B8, Li-Al/FeS_2-CcS_2, C, 149/149, 13.5 × 15.6 × 3.8 cm, 1.9 kg	118 117	159 157	11.8 9.0	11.8 9.0	99	82	378	533	39	41	16	23	Start-up and operation with cell blanketed in Kaowool insulation, exposed to air.
I-3-B-1, Li-Al/FeS-Cu_2S, C, 170/127, 13.5 × 15.6 × 3.8 cm, 2.035 kg	101 88 76	131 108 92	10 5.9 3.8	10 5.9 3.8	99	81	527	896	52	55	45	47	EP cell, with slightly thinner positive and slightly denser negative. Testing terminated.
I-3-B-2, Li-Al/FeS-Cu_2S, C, 193/145, 13.5 × 15.6 × 3.8 cm (shimmed cell), 1.72 kg	85	104	8.5	8.5	99	82	290	505	14	20	23	28	Previously terminated after qualification testing (42 days, 48 cycles). Restarted to study cell operation at 500°C. Testing terminated.
I-3-C-1, Li-Al/FeS-Cu_2S, C, 193/145, 13.5 × 14.5 × 3.8 cm (shimmed cell), 1.72 kg	62	76	6	6	99	84	160	222	7	6	14	15	Cell previously tested for 52 days, 51 cycles. Restarted to study open-circuit voltage as function of discharge state at 450°C and 500°C. Terminated. Cell short-circuited.
I-3-C-2, Li-Al/FeS-Cu_2S, C, 193/145, 13.5 × 15.6 × 3.8 cm (shimmed cell), 1.79 kg	97	112	10	10	98	84	292	527	57	49	46	48	EP cell. Constant current compared to constant voltage charge. Tested at up to 525°C. Terminated due to poor performance.

(Contd)

APPENDIX C. (contd)

Cell Description[a]	Max. Performance @ Indicated Rate[b] A-hr	W-hr	Rates, hr Disch.	Charge	Initial Eff.,[c] % A-hr	W-hr	Life Characteristics Days[d]	Cycles[d]	% Decline in[e] Capacity	Energy	A-hr Eff.	W-hr Eff.	Remarks
I-4-1, Li-Al/FeS_2-CoS_2, C, 170/156, 13.5 × 15.6 × 3.8 cm, 2.18 kg	108	151	11	11	99	83	39	42	31	33	25	44	EP (thick) FeS_2 cell with offset positive terminal rod. Terminated due to declining performance.
I-4-2, Li-Al/FeS_2-CoS_2, C, 170/156, 13.5 × 15.6 × 3.8 cm, 2.21 kg	108 81	150 108	10.8 5.4	10.8 5.4	99	77	69	121	40	40	74	75	EP (thick) FeS_2 cell with offset positive terminal rod. Terminated due to poor efficiency and capacity.
I-4-3, Li/Al/FeS_2-CoS_2, C, 170/156, 13.5 × 15.6 × 3.8 cm, 2.16 kg	85 76	119 102	8.5 5.0	8.5 5.0	99	75	55	91	22	28	4	8	EP (thick) FeS_2 cell with offset positive terminal rod. Terminated because it would not accept charge.
I-6-A-1, Li-Al/FeS_2-CoS_2, C, 199/156, 13.5 × 15.6 × 3.2 cm, 1.66 kg	97	133	10	10	99	82	85	109	15	12	22	18	More compact EP FeS_2 cell, with thinner, less porous electrode (positive) and 55 wt % LiAl negative electrode. Specific energy 72 W-hr/kg at 4-hr rate, peak power 57 W/kg. Terminated, low coulombic efficiency
I-6-A-2, Li-Al/FeS_2-CoS_2, C, 199/156, 13.5 × 15.6 × 3.2 cm, 1.66 kg	97	133	10	10	99	82	99	105	8	18	17	18	More compact EP FeS_2 cell, with thinner, less porous electrode (positive), and 55 at. % LiAl negative electrode. Specific energy of 72 W-hr/kg at 4-hr rate, peak power 57 W/kg. Terminated, low coulombic efficiency.
I-6-B-1, Li-Al/FeS_2-CoS_2, C, 199/156 13.5 × 15.6 × 3.2 cm, 1.61 kg	104	146	10	10	96	80	105	133	33	37	25	28	More compact EP FeS_2 cell, with thinner, less porous electrode (positive), and 55 at. % negative electrode. ZrO_2 retainer cloth removed from negative electrode. Specific energy of 75 W-hr/kg at 4-hr rate. Terminated.

(contd)

APPENDIX C. (contd)

Cell Description[a]	Max. Performance @ Indicated Rate[b] A-hr	W-hr	Rates, hr Disch.	Charge	Initial Eff.,[c] % A-hr	W-hr	Life Characteristics Days[d]	Cycles[d]	% Decline in[e] Capacity	Energy	A-hr Eff.	W-hr Eff.	Remarks
I-6-B-2, Li-Al/FeS_2-CoS_2, C, 199/156, 13.5 × 15.6 × 3.6 cm, 1.61 kg	102	146	10	10	9[illegible]	80	54	65	25	23	30	35	Similar to I-6-B-1, except Mo screen added to positive electrodes. Performance similar to I-6-B-1. Terminated.
I-7-1, Li-Al/FeS_2-CoS_2, C, 230/222, 13.5 × 15.6 × 3.8 cm, ~1.95 kg	95	120	9.5	9.5	9[illegible]	74	67	118	4	3	36	35	Compact EP one-piece positive shimmed cell. Flexible Mo connection. Tested for 4 cycles in glove box at 446°C. Terminated due to poor coulombic efficiency.
I-8-A-1, Li-Al/FeS_2-CoS_2, C, 200/156, 3.5 × 15.6 × 3.2 cm, 1.72 kg	111 89	144 99	9 3.5	12 10	94	68	33	33	12	10	5	5	EP cell. Test of BN felt. Terminated after qualification test. Separator wetting problem.
I-8-A-4, Li-Al/FeS_2-CoS_2, C, 200/156, 13.5 × 15.6 × 3.2 cm, 1.73 kg	102	146	10	12	95	75	20	21	0	0	7	5	EP cell. Test of BN felt. Specific energy of 70 W-hr/kg at 4 hr-rate. Terminated after developing short circuit.
I-8-B-5, Li-Al/FeS_2-CoS_2, C, 200/156, 13.5 × 15.6 × 3.8 cm (shimmed cell), 1.66 kg	110	152	11	11	93	77	46	53	56	60	74	73	EP cell built to study BN felt separator. Terminated, poor coulombic efficiency.
I-8-C-9, Li-Al/FeS_2-CoS_2, C, 200/156, 13.5 × 15.6 × 3.2 cm, 1.65 kg	110	162	10	10	89	65	1	3	0	0	0	0	EP cell. Test of BN felt. Terminated due to short circuit.
I-8-C-10, Li-Al/FeS_2-CoS_2, C, 200/156, 13.5 × 15.6 × 3.2 cm, 1.63 kg	99	137	20	20	78	69	23	18	0	0	50	50	EP cell built to test BN felt. Poor efficiency on initial cycles. Terminated.

(contd)

APPENDIX C. (contd)

Cell Description[a]	Max. Performance @ Indicated Rate[b] A-hr	W-hr	Rates, hr Disch.	Charge	Initial Eff.,[c] % A-hr	W-hr	Life Characteristics Days[d]	Cycles[d]	% Decline in[e] Capacity	Energy	A-hr Eff.	W-hr Eff.	Remarks
I-8-D-13, Li-Al/FeS_2-CoS_2, C, 170/156 13.5 × 15.6 × 3.8 cm, 1.95 kg	115	164	11.6	11.6	99	83	58	72	17	19	0	0	EP cell with additional Mo central plate. Terminated; poor coulombic efficiency.
I-8-E-16, Li-Al/FeS_2-CoS_2, C, 105/156, 13.5 × 15.6 × 3.8 cm, (shimmed cell) 1.9 kg	101 80	148 109	20 8	20 8	99	84	25	22	4	4	58	62	EP cell with Catalyst Research cast negative. Terminated, poor coulombic efficiency.
I-8-F-17, Li-Al/FeS_2-CoS_2, C, 170/71, 13.5 × 15.6 × 3.8 cm, 1.74 kg	58	79	5.8	5.8	99	85	64	251	29	33	0	25	EP cell for study of capacity loading ratio. Terminated.
I-8-G-19, Li-Al/FeS_2- CoS_2, C, 75/156, 13.5 × 15.6 × 3.8 cm, 1.79 kg	62	95	6.2	6.2	96	78	32	85	17	18	0	0	EP cell to study capacity loading ratio. Terminated; poor capacity after temperature controller malfunction.
I-8-G-20, Li-Al/FeS_2-CoS_2, C, 75/150, 13.5 × 15.6 × 3.6 cm, 1.87 kg	40	61	4	4	97.5	78	61	129	0	5.1	0	14	Cycling restricted to 25% of FeS_2 capacity to check lifetime effects. Cell on standby, cycler needed for other test.
I-8-H-027, Li-Al/FeS_2-CoS_2, C, 148/117, 13.5 × 14.8 × 2.2 cm, 1.23 kg	76.0	109.0	7	8	98	80	33	48	21	23	18	16	EP cell. A similar cell examined at EP showed particle loss from the electrodes during electrolyte filling. Terminated, low coulombic efficiency.
I-8-H-040, Li-Al/FeS_2-CoS_2, C, 148/117, 13.5 × 1.56 × 2.3 cm, 1.20 kg	73	100	6	18	>99	84	>153	>174	14	14	0	6	EP cell which will be used to test the effect of low-temperature operation on cell lifetime.

(contd)

APPENDIX C. (contd)

Cell Description[a]	Max. Performance @ Indicated Rate[b] A-hr	W-hr	Rates, hr Disch.	Charge	Initial Eff.,[c] % A-hr	W-hr	Life Characteristics Days[d]	Cycles[d]	% Decline in[e] Capacity	Energy	A-hr Eff.	W-hr Eff.	Remarks
I-8-H-041, Li-Al/FeS_2-CoS_2, C, 148/117, 13.5 × 15.6 × 2.3 cm, 1.22 kg	101	150	10	10	99	76	42	54	41	40	37	43	EP Type I-8-H cell rebuilt with Y_2O_3 felt retainers added to both electrodes. Terminated.
I-8-K-032, Li-Al/FeS_2-CoS_2, C, 289/220, 13.5 × 15.6 × 3.8 cm, 1.87 kg	0	0	0	0	0	0	0	0	0	0	0	0	EP cell. A similar cell examined at EP showed particle loss from electrodes during electrolyte filling. Low frozen resistance. Cell short-circuited on first cycle.
I-8-K-033, Li-Al/FeS_2-CoS_2, C, 289/220, 13.5 × 15.6 × 3.8 cm, 1.87 kg	0	0	0	0	0	0	0	0	0	0	0	0	EP cell. A similar cell examined at EP showed particle loss from electrodes during electrolyte filling. Low frozen resistance. Cell short-circuited on first cycle.
I-8-L-034, Li-Al/FeS_2-CoS_2, C, 289/220, 13.5 × 15.6 × 3.8 cm, 1.71 kg	151	214	12	12	83	62	31	18	35	38	40	36	EP cell. One of cells subject to particle loss during salt filling. Cell qualification tested. Specific energy, 90 W-hr/kg at 4-hr rate. Decline in capacity. Terminated.
I-9-3, Li-Al/FeS_2-CoS_2, C, 106/156 13.5 × 15.6 × 2.61 cm, 1.38 kg	59	91	10	10	96	78	37	56	16	17	26	20	First upper-plateau cell built by EP. Specific energy of 60 W-hr/kg at 4-hr rate and 52 W/kg peak power. Terminated.
G-03-002, Li-Al/FeS-Cu_2S, U, 233/168, 14.0 × 23.5 × 3.2 cm, 2.73 kg	78	92	4	8	99	81	54	98	33	37	29	30	Gould's first baseline cell. Calcium added to negative electrode. Terminated.
G-04-001, Li-Al/FeS_2-CoS_2, U, 95, 14.02 × 21.0 × 3.6 cm, 2.8 kg	89	142	8	8	96	83	30	53	8	8	6	5	Gould FeS_2 upper-plateau cell. Qualification tested. Cell on standby.

(contd)

APPENDIX C. (contd)

Cell Description[a]	Max. Performance @ Indicated Rate[b] A-hr	W-hr	Rates, hr Disch.	Charge	Initial Eff.,[c] % A-hr	W-hr	Life Characteristics Days[d]	Cycles[d]	% Decline in[e] Capacity	Energy	A-hr Eff.	W-hr Eff.	Remarks
G-04-002, Li-Al/FeS_2-CoS_2, U, 139, 14.02 × 21.0 × 3.6 cm. 2.45 kg	116	191	10	10	98	86	20	25	2	4	1	2	Gould upper-plateau cell. Qualification tested. Cell on standby.
G-04-003, Li-Al/FeS_2-CoS_2, U, 96, 14.02 × 21.0 × 3.6 cm, 2.08 kg	73	103	4	12	>99	78	>130	>202	20	22	10	14	Gould FeS_2 upper-plateau cell. Undergoing life test.
G-04-003A, Li-Al/FeS_2-CoS_2, U, 96, 14.02 × 21.0 × 3.6 cm, 2.02 kg	81 81	128 112	5.5 1.8	5.5 5.5	98	82	12	24	1	1	0	0	Gould upper-plateau cell. Cell short-circuited at end of qualification test.
G-04-004, Li-Al/FeS_2 U, 139, 14.02 × 21.0 × 3.6 cm, 2.38 kg	115	187	11	11	99	88	29	37	10	12	2	4	Gould FeS_2 upper-plateau cell. Qualification tested. Cell on standby.
G-04-005, Li-Al/FeS_2-CoS_2, U, 96, 14.02 × 21.0 × 3.8 cm, 2.05 kg	69	114	7	7	92	80	17	39	3	3	6	5	Gould upper-plateau cell, loss of efficiency near end of qualification test. Cell terminated.
G-04-006, Li-Al/FeS_2-CoS_2, U, 140/14.02 × 21.0 × 3.8 cm, 2.33 kg	113	186	10	10	99	86	19	26	12	14	0	3	Gould FeS_2 upper-plateau cell. Qualification testing completed. Cell on standby.
G-04-006A, Li-Al/FeS_2-CoS_2, U, 140, 14.02 × 21.0 × 3.8 cm, 2.33 kg	113	149	6.6	19	100	71	26	53	77	80	0	14	Gould FeS_2 upper-plateau cell. Undergoing life test. Terminated.
G-04-007, Li-Al/FeS_2-CoS_2, U, 78, 14.02 × 21.0 × 3.6 cm, 1.90 kg	66	104	6	6	96	82	20	44	7.5	8.5	4	4	Gould FeS_2 upper-plateau cell. Qualification test completed. Cell on standby.

(contd)

APPENDIX C. (contd)

Cell Description[a]	Max. Performance @ Indicated Rate[b] A-hr	W-hr	Rates, hr Disch.	Charge	Initial Eff.,[c] % A-hr	W-hr	Life Characteristics Days[d]	Cycles[d]	% Decline in[e] Capacity	Energy	A-hr Eff.	W-hr Eff.	Remarks
G-04-008, Li-Al/FeS_2-CoS_2, U, 112, 14.02 × 21.0 × 3.6 cm, 2.14 kg	--	--	--	--	--	--	--	--	--	--	--	--	Gould FeS_2 upper-plateau cell. Cell short-circuited on breakin.
G-04-008A, Li-Al/FeS_2-CoS_2, C, 211/158, 14.02 × 21.0 × 3.2 cm, 2.488 kg	125	188	12	12	97	77	31	130	12	13	11	10	Gould FeS_2 upper-plateau cell. Terminated, cell short-circuited.
G-04-009, Li-Al/FeS_2-CoS_2, U, 180, 14.02 × 21.0 × 3.6 cm, 2.82 kg	153	244	15	15	98	81	41	37	14	14	8	7	Gould FeS_2 upper-plateau cell. Qualification test completed. Cell on standby.
G-04-009A, Li-Al/FeS_2, U, 180, 14.02 × 21.0 × 3.6 cm, 2.83 kg	162	252	11	11	96	80	21	23	0	0	0	0	Gould upper-plateau cell. Matrix testing completed; cell on standby.
G-04-010, Li-Al/FeS_2-CoS_2, U, 180, 14.02 × 21.0 × 3.8 cm, 2.77 kg	161	254	16	16	100	85	17	17	0	0	0	0	Gould upper-plateau cell. Testing completed; cell on standby.
G-04-011A, Li-Al/FeS_2-CoS_2, U, 96.1, 14.02 × 21.0 × 3.8 cm, 2.18 kg	82	127	5.5	6	89	73	19	33	18	13	18	8	Gould upper-plateau cell. Terminated due to poor efficiency.
G-04-012, Li-Al/FeS_2-CoS_2, U, 139, 14.02 × 21.0 × 3.6 cm, 2.5 kg	100	160	10	10	99	82	19	26	0	0	0	0	Gould upper-plateau cell. Terminated after matrix qualification test to make room for next cell.
G-04-013, Li-Al/FeS_2-CoS_2, U, 180, 14.02 × 21.0 × 3.6 cm, 2.85 kg	107	153	5.5	11	97	74	157	214	48	50	62	62	Gould upper-plateau cell. Terminated.

(contd)

APPENDIX C. (contd)

Cell Description[a]	Max. Performance @ Indicated Rate[b] A-hr	W-hr	Rates, hr Disch.	Charge	Initial Eff.,[c] % A-hr	W-hr	Life Characteristics Days[d]	Cycles[d]	% Decline in[e] Capacity	Energy	A-hr Eff.	W-hr Eff.	Remarks
G-04-013A, Li-Al/FeS_2-CoS_2, U, 180, 14.02 × 21.0 × 3.6 cm, 2.92 kg.	134	203	9	11	99	80	16	19	0	0	0	0	Gould FeS_2 upper-plateau cell. Terminated after qualification test to make room for next cell.
G-04-013B, Li-Al/FeS_2-CoS_2, U, 180, 14.02 × 21.0 × 3.6 cm, 2.92 kg	150	229	10	10	100	81	31	47	79	80	84	84	Gould upper-plateau cell terminated due to short circuit.
G-04-014, Li-Al/FeS_2-CoS_2, U, 155, 14.02 × 21.0 × 3.8 cm, 2.55 kg	125	188	8	8	99	80	14	19	0	0	0	0	Gould upper-plateau cell. Testing completed. Cell on standby.
G-04-014A, Li-Al/FeS_2, U, 107, 14.02 × 21.0 × 3.6 cm, 2.55 kg	134	213	12	12	99	85	10	9	-	-	-	-	Gould FeS_2 upper-plateau cell. failed during early cycles due to cycler malfunction.
G-04-014B, Li-Al/FeS_2-CoS_2, U, 146, 14.02 × 21.0 × 3.8 cm, 2.5 kg	111	180	10	10	96	83	13	18	0	0	0	0	Gould upper-plateau cell. Short-circuited.
G-04-015, Li-Al/FeS_2-CoS_2, U, 140, 14.02 × 21.0 × 3.8 cm, 2.44 kg	110 108	148 158	2.5 7	8 7	97	69	21	25	0	0	0	0	Gould FeS_2 upper-plateau cell. Cell totally discharged when power failed during qualification testing. Terminated.
G-04-016, Li-Al/FeS_2-CoS_2, U, 180, 14.02 × 21.0 × 3.8 cm, 2.86 kg	150	240	10	10	94	84	31	30	5	9	6	5	Gould FeS upper-plateau cell. Short-circuited near end of qualification test. Cell terminated.
G-04-017, Li-Al/FeS_2-CoS_2, U, 96, 14.02 × 21.0 × 3.8 cm, 2.12 kg	86 85	132 108	6 1.5	6 6	99	83	15	27	0	0	0	0	Gould upper-plateau cell. Qualification testing finished. Cell on standby.
G-04-019A, Li-Al/FeS_2-CoS_2, U, 130, 14.02 × 21.0 × 3.8 cm, 2.8 kg	129	197	8.5	8.5	70	56	18	17	0	0	0	0	Gould upper-plateau cell. Poor efficiency initially. Cell short-circuited.

(contd)

APPENDIX C. (contd)

Cell Description[a]	Max. Performance @ Indicated Rate[b] A-hr	W-hr	Rates, hr Disch.	Charge	Initial Eff.,[c] % A-hr	W-hr	Life Characteristics Days[d]	Cycles[d]	% Decline in[e] Capacity	Energy	A-hr Eff.	W-hr Eff.	Remarks
G-04-020A, Li-Al/FeS_2-CoS_2, U, 180, 14.02 × 21.0 × 3.6 cm, 2.70 kg	160	257	16	16	98	85	20	15	0	0	0	0	Gould FeS_2 upper-plateau cell. Initial break-in cycles. Cell overcharged by equipment failure; terminated.
G-04-021, Li-Al/FeS_2-CoS_2, U, 164, 14.02 × 21.0 × 3.8 cm, 2.57 kg	113	149	6.6	19	100	71	26	53	77	80	0	14	Gould FeS_2 upper-plateau cell. Capacity low, and resistance high. Terminated.
G-04-021A, Li-Al/FeS_2-CoS_2, U, 168, 14.02 × 21.0 × 3.6 cm, 2.84 kg	91	101	6	6	100	72	6	5	0	0	0	0	Gould FeS_2 upper-plateau cell. Terminated due to unstable resistance
G-04-022, Li-Al/FeS_2, U, 150, 14.02 × 21.0 × 3.6 cm, 2.83 kg	130	195	12	12	>99	76	18	20	0	0	0	0	Gould upper-plateau cell. Qualification tested. Cell on standby.
G-04-022A, Li-Al/FeS_2-CoS_2, U, 160, 14.02 × 21.0 × 3.8 cm, 2.65 kg	--	--	--	--	--	--	--	--	--	--	--	--	Gould FeS_2 upper-plateau cell. Cycling results erratic; cell has high resistance >30 mΩ; terminated.
G-04-023, Li-Al/FeS_2-CoS_2, U, 100, 14.02 × 21.0 × 3.6 cm, 2.45 kg	77	112	5	5	98.5	72	10	20	0	0	0	0	Gould FeS_2 upper-plateau cell. Testing completed. Cell on standby.
G-04-023D, Li-Al/FeS_2-CoS_2, U, 96, 14.02 × 21.0 × 3.8 cm, 1.96 kg	63	98	4	4	92	75	22	46	11	11	5	10	Gould FeS_2 upper-plateau cell. Terminated. Cell on standby.
G-04-024, Li-Al/FeS_2-CoS_2, U, 140, 14.02 × 21.0 × 3.8 cm, 2.44 kg	125	187	8	8	96	75	40	50	20	23	6	6	Gould FeS_2 upper-plateau cell. Qualification tested. Terminated.
G-04-024D, Li-Al/FeS_2-CoS_2, U, 136, 14.02 × 21.0 × 3.6 cm, 2.30 kg	--	--	--	--	--	--	--	--	--	--	--	--	Gould FeS_2 upper-plateau cell. Cell short-circuited on breakin.

(contd)

APPENDIX C. (contd)

Cell Description[a]	Max. Performance @ Indicated Rate[b] A-hr	W-hr	Rates, hr Disch.	Charge	Initial Eff.,[c] % A-hr	W-hr	Life Characteristics Days[d]	Cycles[d]	% Decline in[e] Capacity	Energy	A-hr Eff.	W-hr Eff.	Remarks
G-04-025, Li-Al/FeS_2-CoS_2, U, 180, 14.02 × 21.0 × 3.8 cm, 2.83 kg	120	179	8	8	99	77	20	39	C	0	0	0	Gould FeS_2 upper-plateau cell. Matrix qualification testing completed. Cell on standby.
G-04-025A, Li-Al/FeS_2-CoS_2, U, 114, 14.02 × 21.0 × 3.6 cm, 2.19 kg	68	110	4.5	4.5	98	81	41	102	9	13	4	4	Gould FeS_2 upper-plateau cell. Qualification testing completed. Cell on standby.
G-04-029E, Li-Al/FeS_2-CoS_2, U, 180, 14.02 × 21.0 × 3.6 cm, 2.82 kg	100	138	6.7	6.7	98	70	13	28	9	7	0	0	Gould FeS_2 upper-plateau cell. Qualification test completed. Cell on standby.
G-04-030, Li-Al/FeS_2-CoS_2, U, 140, 14.02 × 21.0 × 3.8 cm, 2.53 kg	119	177	8	8	96	74	21	27	8	8	0	0	Gould FeS_2 upper-plateau cell. Qualification test completed. Cell on standby.

[a]The letters U and C are used to indicate uncharged and charged respectively. The capacity ratio is the number of ampere-hours in the negative electrode over the number of ampere-hours in the positive electrode. In some cases, only the capacity of the limiting electrode is given.

[b]Based on at least five cycles.

[c]Based on at least 10 cycles at the 5-hr discharge rate.

[d]The "greater than" symbols denote continuing operation.

[e]Percent decline from the maximum values at the 5-hr discharge, except where noted.

THIS PAGE

WAS INTENTIONALLY

LEFT BLANK

APPENDIX D.

Post-Test Examinations of Industrial Cells

Appendix D Post-Test Examinations of Industrial Cells

Cell Number and Type[a]	Lifetime		Reason for Termination	Comments
	Days	Cycles		
EP-1A5 Li-Al/FeS-Cu_2S	19	25	Short circuit	Failure located in the positive electrode feedthrough. It was caused by contamination of the feedthrough with salt during handling or electrolyte filling operations. LiCl was added to this cell.
EP-1B4 Li-Al/FeS-Cu_2S	748	1339	Poor coulombic efficiency	This cell was operated longer than any other FeS cell. The short circuit was caused by copper deposition across the entire thickness of the separator in some areas. After more than two years of operation, this cell has shown no evidence of reaction with the BN separator.
EP-1B6 Li-Al/FeS-Cu_2S	512	829	Short circuit	Failure caused by the presence of large iron and copper deposits in the separator.
EP-2B8 Li-Al/FeS_2-CoS_2	377	533	Poor coulombic & energy efficiency	This sealed cell was operated in air without adverse effects. The declining coulombic efficiency was attributed to extrusion of active material from the top and bottom edges of the positive electrode.
EP-I3C-2 Li-Al/FeS-Cu_2S	224	527	Short circuit	Severe localized swelling of the negative electrode compressed one area of the BN separator to approximately one-third of its original thickness. The remainder of the separator contained significant amounts of copper which completed the short circuit. Cell was operated at temperatures to 525°C.
EP-I4-2 Li-Al/FeS_2-CoS_2	68	121	Short circuit	The positive terminal was moved from the center of the cell to a position near one edge of the electrode; this design resulted in nonuniform utilization of the positive electrode. The short circuit was caused by the positive honeycomb current collector cutting through the electrode separator.
EP-I4-3 Li-Al/FeS_2-CoS_2	52	91	Declining coulombic efficiency	The positive terminal design was the same as used in EP-I-4-2, and also resulted in non-uniform utilization of the positive electrode. Cell failure due to the positive honeycomb current collector cutting through the electrode separator and short-circuiting the electrodes.
EP-I5-3 Li-Al/FeS_2-CoS_2	75	130	Poor performance	This cell was operated as part of a six-cell battery. Specific cause of short circuit not identified showed numerous thinned out areas in the BN separator. Also, cell was over discharged to about 0 V.
EP-I5-4 Li-Al/FeS_2-CoS_2	211	247	Short circuit	Failure caused by the positive honeycomb current collector cutting through the electrode separator.
EP-I5-5 Li-Al/FeS_2-CoS_2	227	264	Short circuit	Failure caused by positive active material infiltrating a section of the BN separator that was cut partially through by the positive honeycomb current collector. This cell was operated without restraining plates during its last several cycles. The expansion of the negative electrodes was as much as 115%.

Appendix D. (Cont'd)

Cell Number and Type[a]	Lifetime		Reason for Termination	Comments
	Days	Cycles		
EP-I5-7 Li-Al/FeS_2-CoS_2	211	228	Short circuit	This cell was operated as part of a six-cell battery. The short circuit caused by the positive honeycomb current collector cutting through the separator. Very high temperatures were reached in the shorted area as a result of continued operation of the battery after the cell had short circuited. Corrosion of cell hardware in both the positive and negative electrodes was severe in the shorted area.
EP-I5-8 Li-Al/FeS_2-CoS_2	75	130	Poor performance	This cell operated as part of a six-cell battery. The short circuit was caused by the positive honeycomb current collector cutting through the separator and contacting the negative electrode.
EP-I6A-1 Li-Al/FeS_2-CoS_2	85	109	Poor coulombic efficiency and low capacity	The negative electrodes in this cell utilized 55 at.% LiAl. No differences were noted in the microstructure. Cell failure caused by large amounts of positive active material (Li_2S(Fe), Li_2FeS_2) present in the electrode separator (16 wt % S).
EP-I6A-2 Li-Al/FeS_2-CoS_2	99	105	Poor coulombic efficiency and low capacity	This cell was intermittently heated to 530°C in an attempt to remove Li_2S from the separator. The procedure did not appear to have any effect. Cell failure was attributed to large iron deposits in the separator. The Li-Al alloy was 55 at.% Li.
EP-I7-1 Li-Al/FeS_2-CoS_2	66	113	Short circuit	During operation the usual upper plateau voltage for an FeS_2 cell did not occur. Chemical analysis revealed an Fe:S ratio of approximately 1:1. It was concluded that this cell was assembled using FeS rather than FeS_2. The short circuit was caused by Fe in the separator, presumably from charging the FeS to a charge cut-off potential of 2.0 V.
EP-I7-3 Li-Al/FeS_2-CoS_2	55	50	Short circuit	Failure caused by honeycomb cutting through BN fabric separator.
EP-I8A-001 Li-Al/FeS_2-CoS_2	31	33	Short circuit	These three cells utilized BN felt as the separator material. Cells I-8-A-1 and I-8-A-2 had a cold resistance of 13 Ω and 3 Ω, respectively; and metallographic examination revealed that the short circuit was not too severe because both positive electrodes contained a relatively high amount of FeS_2 (*i.e.*, the highest state charge phase). The separators of these two cells contained minor amounts of Li_2S and Li_2FeS_2, while cell I-8-C-9 (cold resistance, 2 Ω had only Li_2S + Fe. The separator of this last cell contained a minor amount of Li_2S plus bands of very fine metallic particles, which are believed to be the cause of this more severe short circuit.
EP-I8A-002 Li-Al/FeS_2-CoS_2	6	5	Short circuit	
EP-I8C-009 Li-Al/FeS_2-CoS_2	4	5	Short circuit	
EP-I8B-005 Li-Al/FeS_2-CoS_2	45	53	Short circuit	This cell tested a BN-felt separator with a retaining screen over the negative electrode only. Because of non-uniform expansion of the negative electrode some areas of the felt separator were severely compressed. In one area, the expansion ruptured the screen and separator. This permitted direct contact between the electrodes, and a short circuit resulted.

Appendix D. (Cont'd)

Cell Number and Type[a]	Lifetime		Reason for Termination	Comments
	Days	Cycles		
EP-I8C-010 Li-Al/FeS_2-CoS_2	23	18	Poor coulombic efficiency	This cell tested a BN felt separator with retaining screens over both the positive and negative electrodes. Screens over both electrodes gave a more uniform compression of the felt separator and better retention of positive active material. The decline in coulombic efficiency was due to the deposition of $Li_2S(Fe)$ across the thickness of the thin BN felt separator.
EP-I8D-013 Li-Al/FeS_2-CoS_2	55	72	Declining coulombic efficiency	Cell failure caused by the positive honeycomb current collector cutting through the electrode separator and short circuiting the electrodes.
EP-I8E-015 Li-Al/FeS_2-CoS_2	8	11	Short circuit	The short circuit was caused by the positive honeycomb current collector cutting the electrode separator and contacting the negative electrode.
EP-I8E-016 Li-Al/FeS_2-CoS_2	22	22	Short circuit	Short circuit was caused by the positive honeycomb current collector cutting the electrode separator and contacting the negative electrode.
EP-I8F-017 Li-Al/FeS_2-CoS_2	63	251	End of test	This cell had a 2:1 negative-to-positive capacity ratio. As expected, approximately half of the negative electrode was unreacted. The reacted portion had the typical morphology. The relatively low capacity achieved by this cell appeared to be due to incomplete wetting of the negative electrode.
EP-I8G-019 Li-Al/FeS_2-CoS_2	31	86	Low capacity	This cell tested a 1:2 negative-to-positive capacity ratio. The negative electrode was almost completely utilized; negative morphology, however, still indicated less utilization towards the rear of the electrode.
EP-I8L-034 Li-Al/FeS_2-CoS_2	31	18	Short circuit	Failure caused by contact of the positive current collector with the negative electrode frame at the top of the cell. This condition apparently was caused by the upward expansion of the positive electrode.
EP-MP5-001 Li-Al/FeS	5	8	Equipment malfunction	A furnace malfunction resulted in some overheating of this cell. Metallographic examination of the positive electrode buss bar revealed inadequate honeycomb-to-buss bar welds and incomplete brazing of the copper terminal rod to the stainless steel terminal tube.
EP-MP5-003 Li-Al/FeS	39	60	End of test	Good mechanical alignment of all nine electrodes was achieved, and the welds and braze in the positive buss bar were satisfactory. Microscopic examination revealed no significant differences in microstructure between any of the four positive electrodes which were predominantly J-phase. The center portions of the negative electrodes contained large agglomerated areas of Al which is indicative of non-uniform utilization. The entire negative electrode and separator were deficient in electrolyte. This deficiency was probably the major cause of the lower utilization and high cell resistance.

Appendix D. (Cont'd)

Cell Number and Type[a]	Lifetime		Reason for Termination	Comments
	Days	Cycles		
EP-MP7-018 Li-Al/FeS-$CuFeS_2$	38	68	Declining coulombic efficiency and capacity	Failure was caused by a short circuit developing in the positive feedthrough. Declining capacity may have been the result of agglomeration of the negative electrode. This cell exhibited much greater than normal corrosion in both the positive and negative electrodes.
EP-MP7-022 Li-Al/FeS-Cu_2S	6	4	Short circuit	During assembly three electrodes were fractured in several places, with the fractured electrodes cutting through the retaining screens and the BN separator causing the short circuit. Some voids were found in the copper rod to steel tube braze. The BN separator and the negative electrode were both deficient in electrolyte.
GIIX-7 Li-Al/FeS-Co	9	11	Short circuit	This cell utilized a solid plaque negative electrode which was still predominantly a solid piece after 11 cycles. Lithium concentration was non-uniform. The short circuit was located in the positive electrode feedthrough.
G04-014B Li-Al/FeS_2-CoS_2	14	18	Short circuit	Failure caused by positive active material extruding around the insulating BN cloth that surrounds the positive feedthrough.
G04-015 Li-Al/FeS_2-CoS_2	21	25	Short circuit	A cycler malfunction caused an overdischarge of this cell, which deposited aluminum across the thickness of the separator.
G04-029 Li-Al/FeS_2-CoS_2	0	0	Unable to start-up cell	Because of a manufacturing oversight, the cell was not filled with electrolyte.

[a]All of these cells are fabricated either by Eagle-Picher (EP) or Gould (G) and have bicell designs (a single positive electrode with two facing negative electrodes) except for cells EP-MP5-001, EP-MP5-003, EP-MP7-018, and EP-MP7-022 which have multiplate designs.

THIS PAGE

WAS INTENTIONALLY

LEFT BLANK

APPENDIX E.

Performance Data on ANL Cells

APPENDIX E. Performance Data on ANL Cells

Cell Description[a]	Max. Performance @ Indicated Rate[b] A-hr	W-hr	Rates, hr Disch.	Charge	Initial Eff.,[c] % A-hr	W-hr	Life Characteristics Days[d]	Cycles[d]	% Decline in[e] Capacity	Energy	A-hr Eff.	W-hr Eff.	Remarks
R-31, Li-Al/NiS_2-CoS_2, U, 159/132, 13.3 × 15.2 × 3.5 cm, 1.88 kg	83 65	108 79	8 3.5	8 6.5	100	81	378	1025	30	40	30	40	Assembled semicharged with hot-pressed NiS + Li_2S positive. Negative electrode of pressed Al wire partially charged.
R-32, Li-Al/NiS_2, U, 165/127, 13.3 × 15.2 × 3.5 cm, 1.90 kg	85 65	124 79	8 3.5	8 6.5	100	80	95	178	32	31	50	57	Four plateau NiS_2 cell, assembled semicharged with hot-pressed NiS + Li_2S positive. Negative electrode of pressed Al wire, partially charged with Li foil. Terminated.
R-33, Li-Al/NiS_2-FeS_2, U, 159/122, 13.3 × 15.2 × 3.5 cm, 1.90 kg	75	96	5	8	93	71	55	90	20	30	20	30	Four plateau NiS_2-FeS_2 cell, assembled semicharged with hot-pressed NiFe + Li_2S positive. Negative electrode of pressed Al wire, partially charged with Li foil. Heat-treated carbon added to the positive electrode. Terminated.
R-34, Li-Al/FeS-Cu_2S, U, 151/115, 13.3 × 15.2 × 3.5 cm, 2.0 kg	85	101	4	11	98	78	88	144	11	9	15	15	Uncharged FeS cell with 16 mol % Cu_2S additive. Positive has high-temperature carbon. Negative electrode of pressed Al wire partially charged with Li foil. Cold-pressed positive. Terminated.
R-35, Li-Al/FeS_x-NiS_x-CoS_x, U, 144/120, 13.3 × 15.2 × 3.5 cm, 2.2 kg	117	177	15	16	97	81	43	50	44	50	43	50	Similar to R-30, except carbon fiber is added to positive. Terminated.

(contd)

Appendix E. (contd)

Cell Description[a]	Max. Performance @ Indicated Rate[b] A-hr	W-hr	Rates, hr Disch.	Charge	Initial Eff.,[c] % A-hr	W-hr	Life Characteristics Days[d]	Cycles[d]	% Decline in[e] Capacity	Energy	A-hr Eff.	W-hr Eff.	Remarks
R-36, Li-Al/NiS_2-CoS_2, U, 180/150, 13.3 × 15.2 × 3.5 cm, 1.8 kg	100 70	146 84	13.5 3.0	13.5 8.0	99	79	>253	>472	24	24	1	10	Similar to R-31, except high-temperature carbon added to positive electrode.
R-37, Li-Al/FeS, U, 180/150, 13.3 × 15.2 × 3.5 cm, 1.8 kg	64	76	3	8.5	99	78	176	430	15	20	24	23	Baseline FeS cell containing no additive in positive electrode. Terminated.
R-38, Li-Al/FeS, U, 160/125, 13.3 × 15.2 × 3.5 cm, 1.8 kg	83	103	4.5	12	96	82	94	172	23	25	21	22	Similar to R-37 except LiCl-rich electrolyte used. Terminated.
R-39, Li-Al/FeS, U, 129/121, 13.3 × 15.2 × 3.3 cm, 1.73 kg	76	95	8	10	95	84	21	23	18	17	0	0	Similar to R-38 except ZrO_2 powder added to the positive electrode. Terminated.
R-40, Li-Al/FeS-Cu_2S U, 160/137, 13.3 × 15.2 × 3.5 cm, 1.78 kg	76.8	90.5	4	8	100	83	63	108	22	25	22	26	Similar to R-37 except 8 mol % Cu_2S added to positive electrode. Terminated.
R-41, Li-Al/FeS-Cu_2S, U, 180/103, 13.3 × 15.2 × 3.5 cm, 1.7 kg	76	100	3.3	8.8	>99	81	>105	>220	23	30	0	8	FeS cell with BN felt separator treated with $LiAlCl_4$.
R-42, Li-Al/FeS-Cu_2S, U, 160/113, 13.3 × 15.2 × 3.5 cm, 1.7 kg	61	75	3.0	6.0	92	75	>93	>216	4	8	0	4	Similar to R-41 but with $LiAlCl_4$ in positive electrode.
T-1, Li-Al/FeS-Cu_2S, U, 35/27, 13.2 × 12.8 × 1.01 cm, 0.34 kg	22	26	4	8	85	74	23	48	50	50	35	31	FeS cell with BN felt separator treated with $LiAlCl_4$. Terminated.
R-43, Li-Al/FeS, U, 180/134, 13.3 × 15.2 × 3.5 cm, 1.8 kg	65	96	5	8	98	80	>48	>78	0	0	0	0	FeS cell with BN felt separator (treated with $LiAlCl_4$), LiCl-rich electrolyte and high-temperature carbon additive. Pos. contains $LiAlCl_4$.

(contd)

Cell Description[a]	Max. Performance @ Indicated Rate[b] A-hr	W-hr	Rates, hr Disch.	Charge	Initial Eff.,[c] % A-hr	W-hr	Life Characteristics Days[d]	Cycles[d]	% Decline in[e] Capacity	Energy	A-hr Eff.	W-hr Eff.	Remarks
R-44, Li-Al/FeS, U, 180/133, 17.7 × 15.2 × 3.5 cm, 1.8 kg	73	84	4	10	97	82	>32	>39	0	0	0	0	FeS cell with BN felt separator (treated with $LiAlCl_4$), LiCl-rich electrolyte and high-temperature carbon added to positive electrode.
M-4, Li-Al/FeS_2-NiS-Mo-Fe, C, 165/267, 13.3 × 13.3 × 3.3 cm, 1.8 kg	135 112	187 159	9 4	9 8	99	81	172	300	17	21	13	22	EP cold-pressed negative and ANL hot-pressed positive. Y_2O_3 felt separator/retainer. Cell resistance: 2.8-3.6 mΩ: specific energy: 70 W-hr/kg at the 2-hr rate. Terminated.
M-5, Li-Al/FeS-NiS-Fe, C, 139/105, 13.3 × 14.6 × 2.8 cm, 1.62 kg	73	96	7	10	97	85	83	80	16	19	<1	35	Positive electrode was hot-pressed into current collector of Ni and Mo (no iron present). Hot-pressed negative of 55 at. % Li-Al. Y_2O_3 felt separator. Cell resistance: 3.3-5.7 mΩ: specific energy: 59 W-hr/kg at 7-hr rate. Terminated.
M-6, Li-Al/FeS-Cu_2S, U, 158/128, 13.9 × 13.6 × 1.1 cm, 1.8 kg	111 75 68	135 81 78	11 4 2	15 11 8	100	82	44	64	16	4.5	0	0	Hot-pressed electrodes. Negative electrode is 55 at. % LiAl. Pre-wet BN felt separator/retainer. Welded positive terminal. Cell resistance: 3.9-4.9 mΩ. Terminated.
M-7, Li-Al/FeS_2-NiS-Mo-Fe, C, 233/194, 13.3 × 13.5 × × 2.7, 1.6 kg	118	173	8	9	96	84	87	138	20	24	12	20	Hot-pressed negative and positive. Y_2O_3 felt separator/retainer. Cell resistance of 2.4 mΩ and specific energy of 78 W-hr/kg at 2-hr rate. Peak specific power, 200 W/kg. Terminated.
M-8, Li-Al/FeS, C, 155/113, 13.3 × 13.5 2.8 cm, 1.55 kg	33 74	101 68	8 3.8	8.5 7.5	97	84	>112	>180	3	2	0	0	Hot-pressed electrodes and BN felt separator/retainer. LiCl-rich electrolyte (Anderson) used throughout. Positive theor. cap. density of 1.41 Ahr/cm^3. Cell resistance, 3.5 mΩ.

(contd)

Appendix E. (contd)

Cell Description[a]	Max. Performance @ Indicated Rate[b] A-hr	W-hr	Rates, hr Disch.	Charge	Initial Eff.,[c] % A-hr	W-hr	Life Characteristics Days[d]	Cycles[d]	% Decline in[e] Capacity	Energy	A-hr Eff.	W-hr Eff.	Remarks
M-9, Li-Al/FeS-Cu_2S, C, 174/143, 13.3 × 13.5 × 2.8 cm, 1.52 kg	76 65.6	92 77.4	4 2	8 6.5	99	85	132	240	25	25	0	0	Hot-pressed electrodes and BN-felt separator/retainer. Wishbone positive-terminal design. High theoretical capacity density (1.62 A-hr/cm^3). Cell resistance: 3.4 mΩ. Terminated.
M-10, Li-Al/FeS, C, 155/115, 13.3 × 13.5 × 2.8 cm, 1.56 kg	56 43	65 50	2.8 1.4	5.5 4.5	99 99	83 83	>44	>105	0	0	0	0	Hot-pressed electrodes and BN-felt separator/retainer. Electrolyte, LiCl-KCl eutectic. Positive theor. cap. density of 1.40 A-hr/cm^3.
M-11, Li-Al/FeS, C, 174/132, 13.3 × 13.5 × 2.8 cm, 1.52 kg	71 60	80 67	3.5 2	7 6	99 99	79 77	>45	>90	0	0	0	0	Hot-pressed electrodes and BN-felt separator/retainer. LiCl-rich electrolyte (Anderson). Positive theor. cap. density of 1.61 A-hr/cm^3. Cell resistance, 3.5 mΩ.
M-12, Li-Al/FeS-Cu_2S, C, 155/121, 13.3 × 13.5 × 2.8 cm, 1.55 kg	67	80	3.3	6.8	98	83.6	>25	>40	12	10	6	6	Hot-pressed electrodes and BN-felt separator/retainer. LiCl-KCl eutectic. Positive theor. cap. density of 1.40 A-hr/cm^3. Cell resistance: 3.6 mΩ.
KK-12, Li-Al/FeS_2-CoS_2-TiS_2, C, 150/95, 13.3 × 12.4 × 3.5 cm, 1.8 kg	90	126	8	10	98	81	35	45	0	0	0	0	Carbon-bonded positive electrode with facial TiS_2 layer (ANL); hot-pressed LiAl (EP) electrodes. Cell rebuilt with BN-felt separator. Terminated--non-wetting BN felt.
KK-13, Li-Al/NiS_2-CoS_2, C, 210/160, 13.3 × 13.6 × 3.6 cm, 1.7 kg	120 100	177 140	10 4	12 10	99+	82	171	315	12	15	25	25	Carbon-bonded positive and LiAl pressed + Al wire negative. Welded Mo molybdenum current collector. Y_2O_3 felt separator. Specific energy, 78 W-hr/kg at 4-hr rate. Terminated after overcharge.

(contd)

Appendix E. (contd)

Cell Description[a]	Max. Performance @ Indicated Rate[b] A-hr	W-hr	Rates, hr Disch.	Charge	Initial Eff.,[c] % A-hr	W-hr	Life Characteristics Days[d]	Cycles[d]	% Decline in[e] Capacity	Energy	A-hr Eff.	W-hr Eff.	Remarks
KK-14, Li-Al/FeS-Cu_2S, C, 160/135, 13.3 × 13.3 × 3.1 cm, 1.55 kg	102 93 79.5	122 107 82	10 5 2	10 9 8	99	81	162	301	20	22	25	28	Carbon-bonded positive and hot-pressed negative electrode. BN-felt separator. Cell operated through four thermal cycles and two corrected short circuits in the feedthrough. Terminated, longest BN-felt test.
KK-15, Li-Al/FeS, C, 150/113, 13.3 × 13.3 × 2.8 cm, 1.54 kg	101 87 77.5	128 108 93.5	10 4.5 2.5	10 8 7	99	89	>20	>35	0	0	0	0	Carbon-bonded positive, hot-pressed negative electrodes, LiCl-rich electrolyte, BN-felt separator. Resistance, 2.9 mΩ; specific energy, 70 W-hr/kg at 4-hr rate.
PW-8, Li-Al/FeS, 1/2 C, 190/115, 13.65 × 13.02 × 4.9 cm, 2.0 kg	63 35	78 39.7	12.6 2.3	12.6 4.7	99	86	280	687	0	0	0	9.0	MgO powder separator, vibratory loaded. Screens & frames on positive and negative electrodes. Use of M-series cell design. No FeS additives. Resistance, 8-10 mΩ. Voluntarily terminated.
PW-9, Li-Al/FeS, 1/2 C, 216/144, 13.65 × 13.02 × 4.2 cm, 1.94 kg	94 69 55.8	114 82.6 65.84	18.4 6.9 3.7	18.4 9.3 7.4	99	82	>301	>481	0	0	0	0	Hot-Pressed MgO powder separator. Screen and frames on negative electrodes. M-series cell design. Resistance 8-10 mΩ.
PW-10, Li-Al/FeS, 1/2 C, 190/131, 14.63 × 13.97 × 2.8 cm, 1.6 kg	49.7	60.6	5	6.7	99	83	172	470	43	43	0	0	MgO powder separator. Vibratory loaded 2-mm thick separator layer. M-series design. Frames and screens on negative and positive electrodes. Resistance 5-7 mΩ. Temporarily terminated.

(contd)

Appendix E. (contd)

Cell Description[a]	Max. Performance @ Indicated Rate[b]		Rates, hr		Initial Eff.,[c] %		Life Characteristics						Remarks
									% Decline in[e]				
	A-hr	W-hr	Disch.	Charge	A-hr	W-hr	Days[d]	Cycles[d]	Capacity	Energy	A-hr Eff.	W-hr Eff.	
PW-11, Li-Al/FeS, 1/2 C, 190/150, 13.97 × 14.63 × 2.9 cm, 1.59 kg	76.5	89.3	8.5	10	95	79	22	28	8.5	10.4	53	60	Vibratory loaded MgO powder (2-mm thick, 70 vol % salt). Powder cost, 9.5¢/#. Resistance is 2.9-5 mΩ. Cell short-circuited.
PW-12, Li-Al/FeS, 1/2 C, 109/134, 14.53 × 13.97 × 2.69 cm, 1.6 kg	65	79.3	8.5	97	87	87	>73	> 99	30	8	23	23	Hot-pressed MgO powder separator (2-mm thick, 70 vol % salt). Powder cost is 9.5¢/#. Resistance is 4.6-6.4 mΩ.
PW-13, Li-Al/FeS, 1/2 C, 175/144, 14.63 × 13.97 × 2.6 cm, 1.7 kg	83	96.6	11	11	99	80	>74	>111	34	33	0	0	MgO powder separator. Similar in design to PW-10. Cell short circuited in early stages of cycling but was repaired. Resistance is 5 mΩ.
PW-14, Li-Al/FeS-Cu_2S, 1/2 C, 177/151, 2.94 × 13.97 × 14.6 cm, 1.9 kg	100	122	13	13	98	85	21	22	0	0	0	0	MgO powder separator. Vibratory loaded (2-mm thick) separator. Operating at 1.55-charge voltage cutoff. Internal resistance 4.9 to 6.5 mΩ. After power bump, a short circuit developed. Terminated.
PW-16, Li-Al/FeS, 1/2 C, 173/131, 14.63 × 13.97 × 2.69 cm, 1.8 kg	106 83 65	129 96 71	12 4.2 2.1	14 11 8.7	99	78	>41	>67	0	0	0	0	Vibratory loaded MgO powder separator. LiCl-rich electrolyte (Anderson) used throughout cell. Positive loading density, 1.1 A-hr/cm^3. Internal resistance is 5 mΩ.

(contd)

Appendix E. (contd)

Cell Description[a]	Max. Performance @ Indicated Rate[b] A-hr	W-hr	Rates, hr Disch.	Charge	Initial Eff.,[c] % A-hr	W-hr	Life Characteristics Days[d]	Cycles[d]	% Decline in[e] Capacity	Energy	A-hr Eff.	W-hr Eff.	Remarks
PFC-3-01, Li-Al/FeS_2-CoS_2, C, 150/159, 13.5 × 15.6 × 3.8 cm, 1.92 kg	109	133	10	10	98	66	44	58	34	37	8	6	Pellet cell not sealed. First pellet cell built with no center plate in positive. Cell has high resistance thought to be due to broken Mo rod-electrode weld. Terminated.
PCM-2-01, Li-Al/FeS_2-Mo, C, 156/164, 13.5 × 13.5 × 3.75 cm, 2.7 kg	85	108	5.5	8	95	70	50	92	10	10	14	11	Pellet cell. Test FeS_2-Mo electrode mix. Terminated, declining coulombic efficiency.

[a]The letters U and C are used to indicate uncharged and charged respectively. The capacity ratio is the number of ampere-hours in the negative electrode over the number of ampere-hours in the positive electrode. In some cases, only the capacity of the limiting electrode is given.

[b]Based on at least five cycles.

[c]Based on at least 10 cycles at the 5-hr discharge rate.

[d]The "greater than" symbols denote continuing operation.

[e]Percent decline from the maximum values at the 5-hr discharge, except where noted.

APPENDIX F.

Post-Test Examinations of ANL Cells

Cell Number and Type	Lifetime		Reason for Termination	Comments
	Days	Cycles		
A-4 Li-Al/FeS_2-CoS_2	119	188	Short circuit	The short circuit was a reoccurrence of a problem with misalignment of components that occurred in the initial cell assembly and allowed contact between the negative and positive electrodes. The positive and negative electrodes were very nonuniform in thickness and probably contributed to the reoccurrence of the short circuit.
TiSp-1 Li-Al/TiS_2	21	20	Short circuit	Although Li_2S is normally observed in separators of FeS_2 cells, no Li_2S was observed in the BN separator of these two cells. The positive electrode contained a layered-type structure (a particle-like structure normally observed in FeS_2 electrodes). The short circuit in TiSp-1 was isolated to a small area near the top BN keeper, where a thinned area of BN cloth had been infiltrated with a large amount of metallic particles. The short circuit in TiSp-2 was attributed to the honeycomb current collector of the positive electrode cutting through the BN separator near the bottom edge of the cell. The negative electrodes had a skeletal-type microstructure. The positive electrode of TiSp-1 had excessive swelling (30-40%).
TiSp-2 Li-Al/TiS_2	11	15	Short circuit	
CA-12 $Mg_2Si/Ca_{1.5}$-$NiS_{1.5}$	48	76	Declining capacity	Very large (0.2 mm) cubic crystals of CaO were observed throughout the BN separator, and considerable ZrO_2 fabric had been reduced to Zr_3C. The conductive ZrO_2 cloth was contacting both electrodes, causing a partial short circuit.
R-30 Li-Al/FeS_2-CoS_2 (M/S=1.6)	48	71	Short circuit	Examination of the upper portion of the cell showed the short circuit was caused by the rupture of the Hastelloy B picture frames at the bent corners; this rupture allowed positive electrode material to extrude and make contact with the negative electrode. The Hastelloy B should be annealed after forming.
R-32 Li-Al/NiS_2 -C	94	178	Short circuit	Cell failure caused by the absence of separator just above the bottom picture frame which permitted positive electrode material to contact the negative electrode. A band of Li_2S was deposited in separator. The separator contained 8.5 wt % sulfur; nickel was not observed. Spherical Li-Al particles near the electrode face indicated lithium enrichment.
R-33 Li-Al/FeS_2-NiS_2-C	69	118	Short circuit	Cell failure caused by positive electrode material extending past the end of the BN fabric separator and contacting the top retainer frame (at negative potential). A band of Li_2S and Fe particles was deposited in the separator, which also contained 16.7 wt % sulfur. The negative electrodes showed considerable expansion; the positive electrode was compressed.
R-34 Li-Al/FeS-Cu_2S-C	88	144	Short circuit	Cell failure caused by the ZrO_2 cloth of the positive electrode contacting the frame at negative electrode potential. The ZrO_2 becomes conductive when reacted with lithium. The electrolyte in the negative electrode was mostly primary crystals of KCl.
R-35 Li-Al/$FeS_{1.75}$ -C-Co	43	50	Short circuit	The lower metal-to-sulfur ratio in this cell reduced the amount of Li_2S normally deposited in FeS_2 cells. The short circuit was caused by extrusion of positive electrode material through a rupture in the screen retainer and BN-fabric separator adjacent to the retainer frame. This rupture was probably caused by the severe swelling of the positive electrode. The electrolyte in the negative electrode appeared to be mostly primary crystals of KCl.

Appendix F. (Cont'd)

Cell Number and Type	Lifetime		Reason for Termination	Comments
	Days	Cycles		
M-6 Li-Al/FeS-Cu_2S-C	44	64	Loss of capacity	Resistance of the as-received cell >3 MΩ. The cause of the declining capacity was not identified. This cell was operated to evaluate the effects of a high-temperature carbon additive on cell performance. Chemical analysis showed 0.16 wt % carbon in the negative electrode. The current collectors showed excessive corrosion, which was attributed to cell operation at 500°C.
M-4 Li-Al/FeS_2-NiS-Mo-Fe (M/S = 1.44)	172	300	End of test	Room-temperature resistance of this cell was 3 Ω, indicating the existence of a partial short circuit. Metallographic examination and X-ray diffraction analyses[a] show that the molybdenum powder has participated in the cell cycling reactions. The Y_2O_3 separator contained considerable metallic particulate and Y_2O_3S, with minor amount of Li_2S.
PMC-1-01 Li-Al/FeS_2-MoS_2	67	234	Declining performance	These two cells were fabricated using the pellet method of forming electrodes. Cell PMC-1-01 contained FeS_2, $Li_3Fe_2S_4$, FeS, and MoS_2 in the positive electrode. The MoS_2 particles retained their original angular form, indicating that they did not enter into the cell reaction. Cell PMC-2-01 contained FeS_2, FeS, MoS_2, with no evidence of the original molybdenum metal particles remaining. Both negative electrodes exhibited the typical Li-Al structure, except for some agglomeration in Cell PMC-2-01.
PMC-2-01 Li-Al/FeS_2-Mo	50	92	Declining performance	
A-5 Li-Al/NiS_2	92	115	Poor utilization	The objective of this cell was to establish a NiS_2 baseline for future additive studies. Lack of electrolyte in the upper one-third of the positive electrode caused poor utilization; Li_2S was deposited in the separator. Also, unreacted aluminum wire was observed in the negative electrode.
A-6 Li-Al/$FeS_{1.5}$-C	146	214	Short circuit	This cell was operated to evaluate the performance of a positive electrode with a sulfur-to-metal ratio of 1.5 while cycling at the same charge-and discharge-cutoff voltages as an FeS_2 cell. A 1.6 Ω resistance between electrodes (short circuit) was caused by the conductive ZrO_2 cloth contacting both electrodes. No Li_2S was observed in the separator, but extensive corrosion of the Hastelloy B positive-current collector lowered the overall sulfur-to-metal ratio to an estimated value of 1.2. The positive electrode was severely compressed by the excessive expansion of the negative electrode.
R-39 Li-Al/FeS + ZrO_2-C	21	23	Short circuit	Examination showed that the short circuit was located in the lower Y_2O_3 insulator of the feedthrough. The chopped ZrO_2 fibers and carbon powder added to the positive electrode were well distributed. This cell used a LiCl-rich electrolyte.
Ca-14 $Ca_x(Mg_2Si)$/NiS_2-C	70	120	End of test	Examination revealed that the positive electrode contained a mixture of CaS and Ni-S particles with a very dense layer of CaS at the front face of the electrode. The high density of this layer and its location probably caused a substantial reduction in cell performance by impeding ionic transport. The negative electrode contained primarily Mg_2Si.

[a] B. Tani, Analytical Chemistry Laboratory, ANL.

Distribution for ANL-78-94

Internal:

M. V. Nevitt
R. V. Laney
P. R. Fields
S. A. Davis
B. R. T. Frost
G. T. Garvey
D. C. Price
K. E. Anderson
J. D. Arntzen
J. Barghusen
D. L. Barney (50)
L. Bartholme
J. E. Battles
E. C. Berrill
C. A. Boquist
L. Burris
F. A. Cafasso
A. A. Chilcnskas
K. Choi
P. Cunningham
D. Day
W. DeLuca
R. Dunne
R. Elliott
A. K. Fischer
W. R. Frost
E. C. Gay
J. Harmon
F. Hornstra
A. A. Jonke
R. W. Kessie
G. M. Kesser
V. M. Kolba
W. Kremsner
M. L. Kyle
W. W. Lark
S. Lawroski
R. F. Malecha
A. E. Martin
F. J. Martino
C. A. Melendres
A. Melton
W. E. Miller
F. Mrazek
K. M. Myles
T. Olszanski
P. A. Nelson (50)
E. G. Pewitt
E. R. Proud
S. Preto
G. Redding
M. F. Roche
L. E. Ross
M. Saboungi
W. W. Schertz
J. L. Settle
H. Shimotake
J. A. Smaga
R. K. Steunenberg
B. Swaroop
C. A. Swoboda
Z. Tomczuk
R. Varma
D. R. Vissers
S. Vogler
W. J. Walsh
D. S. Webster
S. E. Wood
N. P. Yao
P. Eshman
J. E. A. Graae
J. L. Hamilton
P. A. Eident
T. D. Kaun
J. E. Kincinas
K. Kinoshita
Z. Nagy
K. A. Reed
M. A. Slawecki
N. Otto
C. Sy
R. B. Poeppel
B. Bandyopadhyay
A. B. Krisciunas
ANL Contract File
ANL Libraries (5)
TIS Files (6)

External:

DOE-TIC, for distribution per UC-94cb (354)
Chief, Office of Patent Counsel, CH
V. Hummel, DOE-CH
President, Argonne Universities Association
Chemical Engineering Division Review Committee:
C. B. Alcock, U. Toronto
R. C. Axtmann, Princeton Univ.
R. E. Balzhiser, Electric Power Research Institute
J. T. Banchero, Univ. Notre Dame
T. Cole, Ford Motor Corp.
P. W. Gilles, Univ. Kansas
R. I. Newman, Allied Chemical Corp.
G. M. Rosenblatt, Pennsylvania State Univ.
J. G. Ahlen, Illinois Legislative Council, Springfield
J. W. Alpha, Corning Glass Works
J. Ambrus, Naval Surface Weapons Center
J. N. Anand, Dow Chemical Co., Walnut Creek, Calif.
F. Anson, California Inst. Technology

P. Auh, Brookhaven National Laboratory
B. S. Baker, Energy Research Corp.
H. Balzan, Tennessee Valley Authority
K. F. Barber, Div. Transportation Energy Conservation, USDOE
H. J. Barger, Jr., U. S. Army MERDC, Fort Belvoir
R. W. Barnes, Lithium Corp. of America, Gantonia, N.C.
T. R. Beck, Electrochemical Technology Corp., Seattle
J. A. Belding, Div. Conservation Research & Technology, USDOE
M. Benedict, Massachusetts Institute of Technology
D. N. Bennion, Univ. California, Los Angeles
J. Birk, Electric Power Research Inst.
J. Braunstein, Oak Ridge National Laboratory
M. Breiter, GE Research & Development Center
J. O. Brittain, Northwestern U.
R. Brodd, Parma Technical Center, Union Carbide Corp.
J. J. Brogan, Div. Transportation Energy Conservation, USDOE
E. Brooman, Battelle Memorial Institute, Columbus
B. D. Brummet, McGraw-Edison Co., Bloomfield, NJ
D. M. Bush, Sandia Laboratories
E. Buzzelli, Westinghouse Electric Corp., Pittsburgh
E. J. Cairns, Lawrence Berkeley Lab.
E. Carr, Eagle-Picher Industries, Joplin
P. Carr, Energy Development Associates, Madison Heights, Mich.
Chloride Systems (U. S. A.) Inc., North Haven, Conn.
C. Christenson, Gould Inc.
C. A. Clemons, PPG Industries, Pittsburgh
M. Cohen, Univ. of Chicago
A. R. Cook, Int'l Lead Zinc Research Organization, Inc., New York City
G. Coraor, E. I. duPont de Nemours & Co., Wilmington
D. R. Craig, Hooker Chemical Corp.
G. Cramer, Southern California Edison, Rosemead
F. M. Delnick, Sandia Labs.
H. Dietrich, Fiber Materials, Inc., Biddeford, Mass.
D. L. Douglas, Gould Inc., Rolling Meadows
E. Dowgiallo, MERADCOM, Ft. Belvoir
J. Dunning, General Motors Research Lab., Warren, Mich.
P. Eggers, Battelle Memorial Institute, Columbus
M. Eisenberg, Electrochimica Corp.
R. P. Epple, Div. Physical Research, USDOE
P. L. Fleischner, National Beryllia Corp.
J. H. B. George, Arthur D. Little, Inc.
J. Giner, Giner, Inc., Waltham, Mass.
G. Goodman, Globe-Union, Inc., Milwaukee
G. Gorten, Gorten and Associates, Sherman Oaks, Calif
H. Grady, Foote Mineral Co., Exton, Pa.
S. Gratch, Birmingham, Mich.
D. Gregory, Institute of Gas Technology, Chicago
N. Gupta, Ford Motor Co.
N. Hackerman, Rice U.
G. Hagey, Div. of Technology Overview, USDOE
C. Halpin, Halpin Engrs., Grosse Point, Mich.
R. Hamilton, Carborundum Co., Niagara Falls
W. Hassenzahl, Los Alamos Scientific Laboratory
L. A. Heredy, Atomics International
B. Higgins, Eagle-Picher Industries, Joplin

R. Hudson, Eagle-Picher Industries, Joplin
J. R. Huff, U. S. Army Mobility Equipment R&D Center, Fort Belvoir
R. A. Huggins, Stanford U.
R. A. Huse, Public Service Electric & Gas Co., Newark, N.J.
S. D. James, U. S. Naval Surface Weapons Center
M. A. Jansen, Allegheny Power Service Corp., Greensburgh, Pa.
G. Janz, Rensselaer Polytechnic Inst.
H. Jensen, C&D Batteries, Plymouth Meeting, Pa.
F. Kalhammer, Electric Power Research Institute
M. Katz, Div. Energy Storage Systems, USDOE
K. Kinsman, Ford Motor Co.
R. Kirk, Div. of Transportation Energy Conservation, USDOE
K. W. Klunder, Div. of Energy Storage Systems, USDOE
J. Lagowski, Detroit Edison Utility Co.
J. J. Lander, Air Force Aero Propulsion Lab., Wright-Patterson AFB
A. Landgrebe, Div. of Energy Storage Systems, USDOE (6)
C. E. Larson, Bethesda, Md.
S. H. Law, Northeast Utilities, Hartford, Conn.
H. Leribaux, Texas A&M U.
D. Linden, U. S. Army Electronics Command, Fort Monmouth, N.J.
R. Llewellyn, Indiana State U.
P. S. Lykoudis, Purdue Univ.
G. Mamantov, U. Tennessee
J. Mathers, U. Maryland
C. J. Mazac, PPG Industries, Corpus Christi
J. McKeown, Office of Program Administration, USDOE
C. McMurty, Carborundum Co., Niagara Falls
R. McRae, ILC Technology, Sunnyvale, Calif.
D. Meighan, C&D Batteries, Plymouth Meeting, Pa.
R. C. Miller, Kawecki Berylco Industries, Inc., Boyertown, Pa.
R. Minck, Ford Motor Co.
F. Moore, Div. of Energy Storage Systems, USDOE
R. Murie, General Motors Corp., Warren, Mich.
G. Murray, Detroit Edison Utility Co.
J. Newman, U. California, Berkeley
J. Nowabilski, Union Carbide Co., Tonawanda
C. Pax, Div. Transportation Energy Conservation, USDOE
G. F. Pezdirtz, Div. of Energy Storage Systems, USDOE
R. K. Quinn, Sandia Labs.
R. Rightmire, Standard Oil of Ohio, Cleveland
P. F. Ritterman, TRW Inc., Redondo Beach
R. Rizzo, Globe-Union, Inc., Milwaukee
N. Rosenberg, Transportation Systems Center, Cambridge, Mass.
R. Rubischko, Gould Inc.
A. Salkind, ESB Inc., Yardley, Pa.
W. Schaefer, Commonwealth Edison, Maywood, Ill.
G. Scharbach, American Motors General Corp., Wayne, Mich.
T. Schneider, Public Service Electric & Gas Co., Newark, N.J.
R. I. Schoen, National Science Foundation
J. R. Schorr, Battelle Memorial Institute, Columbus
D. R. Schramm, Public Service Electric & Gas Co., Newark, N.J.
H. J. Schwartz, NASA Lewis Research Center
J. R. Selman, Illinois Institute of Technology
A. I. Snow, Atlantic Richfield Co., Harvey, Ill.

S. Srinivasan, Brookhaven National Laboratory
D. Stakem, Catalyst Research Corp., Baltimore
E. Steeve, Commonwealth Edison Co., Chicago
R. H. Strange II, National Science Foundation
R. L. Strombotne, U. S. Dept. Transportation, Washington
S. Sudar, Atomics International
R. H. Swoyer, Pennsylvania Power and Light Co., Allentown
R. Szwarc, General Electric Co., St. Petersburg
F. Tepper, Catalyst Research Corp., Baltimore
L. Thaller, NASA Lewis Research Center
G. M. Thur, Div. Transportation Energy Conservation, USDOE
C. W. Tobias, U. California, Berkeley
W. Towle, Globe-Union, Inc., Milwaukee
A. A. Uchiyama, Jet Propulsion Lab.
J. Vanderryn, Office of Intern, R&D Programs, USDOE
J. V. Vinciguerra, Eagle-Picher Industries, Joplin
R. D. Walker, Jr., U. Florida
C. O. Wanvig, Jr., Globe-Union, Inc., Milwaukee
S. A. Weiner, Ford Motor Co.
J. Werth, ESB Inc., Yardley, Pa.
C. Wienlein, Globe-Union, Inc., Milwaukee
F. Will, General Electric R&D Center, Schenectady
J. Withrow, Chrysler Corp., Detroit
S. E. Wood, El Paso, Tex.
T. Wydeven, NASA Ames Research Center
O. Zimmerman, Portland General Electric Co., Portland, Ore.
M. Zlotnick, Div. Conservation Research and Technology, USDOE
Chloride Technical Limited, Manchester, England
L. Pearce, Admiralty Materials Lab., Holten Heath, England
E. Voss, Varta Batterie A.G., Kelkhern, Germany
E. Aiello, U. of Chicago
W. J. Argersinger, Jr., U. of Kansas
J. T. Banchero, U. of Notre Dame
K. J. Bell, Oklahoma State U.
R. Blanco, Oak Ridge Nat. Lab.
C. F. Bonilla, Columbia U.
W. Brandt, U. of Wisconsin-Milwaukee
A. E. Dukler, U. of Houston
W. J. Frea, Michigan Tech. U.
J. E. Linehan, Marquette U.
Maine Univ., Prof. in charge of Chem. Engr. Lib.
Marquette U., Dept. of Chemistry
Michigan Tech. U., Library
N. R. Miller, United Nuclear Industries, Richland
G. Murphy, Iowa State U.
E. A. Peretti, U. of Notre Dame
G. W. Preckshot, U. of Missouri
H. Rosson, U. of Kansas
C. Sanathanan, U. of Illinois–Chicago Circle
A. Sesonske, Purdue U.
USDOE, Director, Div. of Safeguards and Security
B. W. Wilkinson, Michigan State U.
Comision Nacional de Energia Atomica, Library, Argentina

J. A. Sabato, Com. Nac. de Energia Atomica, Buenos Aires, Argentina
C. H. Cheng, Nat'l Tsing Hau Univ., China
National Radiological Protection Board, Library, Harwell, England
L. Kemmerich, Ges. fur Kernforschung, Karlsruhe, Germany
F. Weigel, Inst. fur Anorganische Chemie der U. Munich, Germany
N. Saratchandran, Bhabha Atomic Research Centre, Bombay, India
K. Fujimiya, U. of Tokyo, Japan
Japan Atomic Energy Research Inst., Tokai-mura, Japan
K. Matsuda, Inst. of Physical & Chemical Res., Yamato-machi, Japan
Sang-Soo Lee, Korea Advanced Institute of Science, Korea
Korean Atomic Energy Research Institute, Korea
Ragnar Nordberg, Sahlgren's Hospital, Göteborg, Sweden

☆ U.S. GOVERNMENT PRINTING OFFICE: 1979—651-044